TESTING THE ROLE OF ASYMMETRIC MIGRATORY BEHAVIORS FOUND IN A NOVEL POPULATION OF MESENDODERMAL CELLS

CATARINA MARTA GONÇALVES BOTA

A thesis submitted in partial fulfillment of the requirements for the Doctoral Degree in Biomedicine

PhD in Association:
Universidade NOVA de Lisboa (Faculdade de Ciências Médicas | NOVA Medical School)
Universidade de Aveiro

March, 2023

TESTING THE ROLE OF ASYMMETRIC MIGRATORY BEHAVIORS FOUND IN A NOVEL POPULATION OF MESENDODERMAL CELLS

Catarina Marta Gonçalves Bota
Susana Lopes, Principal Investigator at Faculdade de Ciências Médicas | NOVA Medical School
Moisés Mallo, Principal Investigator at Instituto Gulbenkian de Ciência

A thesis submitted in partial fulfillment of the requirements for the Doctoral Degree in Biomdicine

PhD in Association:
Universidade NOVA de Lisboa (Faculdade de Ciências Médicas | NOVA Medical School)
Universidade de Aveiro

March, 2023

Table of Contents

Acknowledgements

Em primeiro lugar quero agradecer à Susana Lopes, a minha orientadora. Foi ela quem me introduziu aos primórdios deste projeto durante a minha tese de mestrado e aceitou-me no laboratório em 2016 para este desafio. Mais tarde deu-me a possibilidade de continuar este estudo numa tese de doutoramento, depositando em mim a confiança que eu muitas vezes não tive. Agora em retrospetiva, vejo que sempre acreditaste que eu estava à altura para todos os desafios que me deste. O meu mais sincero agradecimento por todo o conhecimento e sabedoria, entusiasmo pela ciência, gosto em questionar e colocar hipóteses que partilhaste comigo ao longo destes quase 7 anos. Além disso, tenho também a agradecer-te a liberdade para poder seguir os caminhos que te propus para este projeto, mas sobretudo por me teres ajudado a manter numa estrutura coerente, pois quando há tantas coisas giras para estudar é fácil perdermo-nos pelo caminho. Seja qual for o meu caminho na ciência, uma coisa é certa, vais ser sempre a minha referência pois foste tu que me mostraste o que é fazer ciência ao longo destes anos. Obrigada! E prometo-te que um dia vou aprender a relaxar.

Tenho também a agradecer ao Moises Mallo por ter aceite ser meu co-orientador e desta forma ter tornado possível que eu fizesse este doutoramento.

Um agradecimento especial será sempre para o Gabriel Martins, por tudo o que me ensinou quando fui sua aluna, e por ter estado sempre disposto a ajudar-me mesmo já neste doutoramento e sobretudo por sempre explorar todas as hipóteses às quais o apresentei. Foi ele quem me fez gostar de imagens bonitas e *imaging*, e se algum dia trabalhar numa unidade de microscopia, já sabemos quem é o culpado.

Agradeço a todos da Fish Facility do CEDOC, ao Telmo da Microscopia e ao staff da Microscopia do IGC.

E agora chega a parte em que vou ter de me conter, pois prometi a mim mesma que esta seção de agradecimentos não ia ser demasiado lamechas! Quero agradecer a todos que passaram pelo grupo, pois cada um ensinou-me sempre algo. Em especial agradeço à Sara, obrigada por tudo o que me ensinaste quando 'migrei' para o CEDOC e ao longo destes anos também. Pelas conversas, risadas e cafés e às vezes companhia nas noitadas no lab. À Margarida, não só pelo conhecimento que partilhou comigo no lab, pela companhia por todos esses restaurantes de Ramen (e não só) por Lisboa, por me ter apresentado aos patins e sobretudo por tentar me ensinar que a vida pode ser levada com mais calma. Agradeço a todos os alunos que passaram pelo lab e os quais tive o prazer de ensinar o que sabia, mostraram-me que o conhecimento só é valioso quando o podemos partilhar. Em especial à Raquel, foi um prazer acompanhar parte do teu mestrado. Além dos cílios, terei sempre de agradecer à Andreia, tanto por me inspirar enquanto cientista, como pela boa amiga que encontrei. Obrigada por todo o apoio e por tudo, vamos manter isto curto, mas sabes que sem ti estes anos de CEDOC teriam sido muito mais difíceis! Um obrigada à Petra, por toda a ajuda e pelas conversas sobre tudo o que se passa pelos nossos cérebros! Não posso deixar de agradecer à minha *cheerleader*, a Mariana, prometo-te que vou tentar ver-me como tu me vês!

Agradeço a todos os meus amigos que já me acompanham há muito tempo apesar de estarmos meio que separados ao longo do mapa. Em especial ao Mauro, obrigada por tudo mesmo! Mesmo quando me pedes para não agradecer porque não fazes 'fretes', sem dúvida estiveste sempre lá e vou sempre agradecer-te por zelares pela minha sanidade mental. 😊 Agradeço também a quem não foi um azar, mas sim uma sorte conhecer na fase mais difícil.

Ao Daniel, que acompanhou uma tese de mestrado e logo a seguir uma de doutoramento.

O meu maior agradecimento será sempre aos meus pais, Paula e Rogério, sem os quais nunca teria chegado aqui. Obrigada por me apoiarem incondicionalmente em todas as minhas escolhas, mesmo que tenham de me ouvir queixar delas.

Abstract

During vertebrate development, symmetry breaking occurs in the left-right (LR) organizer (LRO). The transfer of asymmetric molecular information to the lateral plate mesoderm is essential for the precise patterning of asymmetric internal organs, such as the heart. However, it is also necessary to maintain symmetry at the somite level for correct musculature and vertebrae specification. In this study, we investigated the effects of LR signals on the behavior of zebrafish somite cell precursors.

Here, we demonstrate how LR signals affect the behavior of zebrafish somite cell precursors. We describe a population of cells in the vicinity of the LRO, named Non-KV Sox17:GFP^{+} Tailbud Cells (NKSTCs), which migrate anteriorly and contribute to future somites. We showed that NKSTCs originate in a cluster of cells aligned with the midline, posterior to the LRO, and leave that cluster in an LR alternating manner, primarily from the left side. Fate mapping revealed that more NKSTCs integrated into somites on the left side of the embryo. To investigate the role of asymmetric cues from the LRO, we used *dand5*$^{-/-}$ mutant embryos and found that NKSTCs no longer displayed asymmetric patterns. Cell exit from the posterior cluster became bilaterally synchronous in *dand5*$^{-/-}$ embryos, revealing a new link between somite specification and Dand5 function. Moreover, we observed compromised anterior movement and reduced *myoD* expression in the absence of the KV, indicating its role in tailbud cell movement and somite specification. Our findings demonstrate the asymmetric behavior of somite precursor cells in response to LR signals *in vivo*, which requires Dand5, and suggest an additional role for the KV in tailbud cell movement and somite specification.

Additionally, using single-molecule fluorescence *in situ* hybridization (smFISH), we quantified the number of *dand5* mRNA transcripts in 3D in the KV over time. We found that *dand5* asymmetry is already established at 6 ss, which is one hour earlier than previously reported by less sensitive methods, and primarily occurs on the anterior side of the KV.

Overall, our findings demonstrate the asymmetric behavior of somite precursor cells in response to LR signals *in vivo*, which requires Dand5, and suggest an additional role for the KV in tailbud cell movement and somite specification. This study provides new insights into *dand5* asymmetric expression in zebrafish and sets the foundation for studying the involvement of other genes of the LR cascade in this context. Our results have implications for understanding the role of asymmetric cues in the formation of symmetric structures and provide insights into the mechanisms underlying embryonic development.

Resumo

Externamente, o corpo dos vertebrados é simétrico bilateralmente, no entanto, órgãos como o coração, intestino, pâncreas e fígado, pulmões e a vasculatura apresentam uma assimetria relativamente ao eixo Esquerda-Direita (ED), no que diz respeito ao seu posicionamento e/ou morfologia, numa disposição conservada denominada de *situs solitus*. O estabelecimento do eixo ED ocorre durante a embriogénese num processo coordenado após o estabelecimento dos eixos Antero-Posterior (AP) e Dorso-Ventral (DV). Esta assimetria é estabelecida durante o desenvolvimento embrionário por meio de um processo altamente regulado que envolve o organizador esquerda-direita (OED). O OED é responsável pela quebra da simetria bilateral através de um fluxo de fluido assimétrico que é gerado por cílios móveis. Este fluxo assimétrico leva a uma diminuição na expressão do mRNA de *Dand5,* um potente inibidor de sinalização Nodal*,* no lado esquerdo do OED, o que permite que Nodal, uma proteína envolvida no estabelecimento e transdução da assimetria ED, persista apenas no lado esquerdo da placa mesodérmica lateral (PML). Desta forma, uma cascata de eventos de expressão genética é desencadeada que resultam no desenvolvimento de órgãos internos com assimetria ED.

No peixe-zebra, o OED é chamado de Vesícula de Kupffer (VK), esta é uma estrutura esférica e monociliada dentro da qual está presente um fluído e que se desenvolve durante os primeiros estadios de segmentação no final posterior da notocorda. A VK é derivada de um agregado de células superficiais localizadas perto do escudo embrionário, conhecidas como Células Percursoras Dorsais (CPD). As CPDs formam um padrão de roseta plana e circular, que depois coalesce numa estrutura tridimensional com uma cavidade central preenchida com fluido. À medida que a VK se forma, o influxo de fluido e a ciliogénese coincidem, resultando na expansão do lúmen e de cada célula da VK origina um único cílio que se estende para o lúmen. Subsequentemente, a VK passa por uma remodelação estrutural ao longo do eixo AP, levando a uma distribuição assimétrica das células ciliadas. Este processo depende de uma complexa interação de vários fatores, incluindo rearranjos no citoesqueleto induzidos pela notocorda, acúmulo de matriz extracelular, a função da Rho quinase Rock2b, Miosina não-muscular II e forças mecânicas de arrasto sobre a VK provocadas pelo movimento das células da cauda.

A expressão do gene *dand5* na VK é inicialmente simétrica, no entanto, no estadio de 8 sómitos (ss), a sua expressão passa a ser assimétrica, estando mais expresso no lado direito, num processo que é dependente do fluxo assimétrico no sentido anti-horário. O fluxo é gerado pelos cílios móveis e detetado pelo complexo de policistinas Pkd1l1 e Pkd2, no entanto o exato

mecanismo de deteção do fluxo ainda não é completamente conhecido. Todavia, recentes descobertas sugerem que o Bicc1 tem um papel importante na desestabilização e inibição da tradução de *dand5*, tanto em ratos quanto em sapos, no lado esquerdo do OED, de uma maneira que é dependente do fluxo. Esse processo envolve a ação conjunta de Dicer1 e Pkd2, embora ainda não esteja claro se Bicc1 e Dicer cooperam na regulação de microRNAs para mediar a diminuição de *dand5*. Além disso, o mecanismo preciso pelo qual o Bicc1 interage com a região 3'-UTR de *dand5* no peixe-zebra ainda não é conhecido, portanto, mais estudos são necessários.´

O gene *nodal* do peixe-zebra *southpaw* (*spaw*) desempenha um papel crucial no estabelecimento e transdução da assimetria ED. Inicialmente, *spaw* é expresso bilateralmente num padrão simétrico nas células adjacentes à VK por volta dos 4-6 ss. Por volta dos 10-12 ss, a expressão de *spaw* torna-se assimétrica no lado esquerdo da PML devido à remoção da inibição Dand5-Southpaw. Tal mecanismo permite que Spaw induza a expressão de seu mRNA, que subsequentemente se espalha da região posterior para a anterior do lado esquerdo da PML até aos 22 ss. O confinamento de Spaw no lado esquerdo é alcançado por meio de diferentes fatores secretados da família TGF-β. Lefty1 fornece uma barreira na linha média, Lefty2 cria uma barreira anterior no campo cardíaco esquerdo e a sinalização BMP forma uma barreira posterior. Juntos, estes processos coordenam o estabelecimento e a manutenção da assimetria ED no peixe-zebra que se traduz numa organogénese assimétrica posteriormente.

Tão crucial como a quebra da simetria durante o desenvolvimento embrionário, é manter a simetria em estruturas como os sómitos que são a base para a musculatura simétrica, vertebras e inervação. Os sómitos formam-se de forma periódica e simétrica a partir da mesoderme pre-somítica que não é segmentada num processo chamado de somitogénese. Este processo ocorre por meio de um mecanismo de *clock* de segmentação e frente de onda. O comprimento de cada somito é regulado por uma combinação do período do *clock* e da velocidade da frente de onda, regulado por gradientes morfogénicos de FGF, Wnt e ácido retinóico (RA). Embora a via de padronização ED instrua o desenvolvimento embrionário para a formação de padrões assimétricos, existem pistas moleculares compartilhadas para formar estruturas tanto simétricas quanto assimétricas. Nomeadamente, é sugerido que a sinalização por RA contraria os efeitos de dessincronização da via ED nos sómitos.

No Capítulo 2, o nosso objetivo foi testar a presença de assimetrias in vivo no movimento das células precursoras durante a formação dos sómitos. Através da utilização de *live imaging* e da linha transgénica Tg(sox17:GFP), observámos que um grupo de células próximas à VK apresenta assimetrias ao adquirir posições cada vez mais anteriores sucessivamente no lado esquerdo,

bem como em número. Ao seguir estas células até às 24 horas pós-fertilização, confirmámos que estas células integram os sómitos e de uma forma alternada, contudo mais proeminente no lado esquerdo. Confirmámos também que estas assimetrias são dependentes das pistas moleculares ED, pois embriões mutantes homozigotas para *dand5* não apresentam assimetrias tanto na posição como no número de células e a sua integração nos sómitos é simétrica. Assim, os nossos resultados sugerem que as células precursoras dos sómitos exibem um comportamento assimétrico *in vivo* em resposta a sinais ED e que requerem a presença da proteína Dand5, secretada pelas células da VK.

No Capítulo 3, investigámos o papel da VK nas células adjacentes. Descrevemos que a partir dos 10 ss, a presença da VK afeta uma população de células localizadas posteriormente à mesma. Observámos que essas células passam de um estado agregado para um estado migratório após entrarem em contato com a VK e migram em direção à região anterior, contribuindo para a formação dos sómitos. Para avaliar esta interação, examinámos o comportamento das células adjacentes no botão caudal em embriões sem VK, a fim de compreender melhor a sua função. Para isso, recorremos à ablação a laser das células precursoras da VK. Os nossos resultados mostraram que a ausência de VK comprometeu o movimento anterior e reduziu a expressão de *myoD*, sugerindo a sua importância no movimento das células do botão caudal e na especificação dos sómito. Estes resultados fornecem evidências preliminares de que a VK desempenha um papel crítico na especificação dos sómitos, tanto por meio de sinalização quanto possivelmente por um mecanismo mecânico. Portanto, descrevemos um papel adicional da VK no desenvolvimento embrionário do peixe-zebra.

Por fim, o Capítulo 4 apresenta a implementação de um novo protocolo de hibridação *in situ* de fluorescência de *single molecule* (smFISH) em embriões *wholemount* de peixe-zebra com o objetivo de fornecer dados de maior resolução para uma melhor compreensão da dinâmica temporal e espacial da diminuição do lado esquerdo da expressão de *dand5* durante a quebra de simetria. Este estudo identificou padrões de expressão assimétricos mais precoces de mRNA *dand5* no polo anterior esquerdo da VK, sugerindo que as células anteriores do lado esquerdo são as primeiras a detetar o fluxo, e é nestas onde a maquinaria por trás da degradação do mRNA *dand5* pode ser ativada. Assim, mostrámos que a assimetria do *dand5* é estabelecida aos 6 ss, uma hora antes do que estava previamente descrito por métodos menos sensíveis. Os nossos resultados são congruentes com estudos prévios acerca da mecânica do fluxo na VK e da dinâmica de mRNA, contribuindo para uma melhor compreensão dos mecanismos subjacentes à quebra de simetria no peixe-zebra.

Em conclusão, o nosso estudo relata a ligação entre o primeiro gene assimétrico no estabelecimento do eixo ED, *dand5*, e do OED nos movimentos da cauda de embriões de peixe-zebra, estabelecendo assim a base para estudar o envolvimento de outros genes da cascata ED neste contexto. Os resultados apresentados nesta tese têm implicações para a compreensão do papel de sinais assimétricos na formação de estruturas simétricas e fornecem informações sobre os mecanismos subjacentes ao desenvolvimento embrionário. Além disso, esclarecemos o momento em que a assimetria de *dand5* é estabelecida no peixe-zebra, proporcionando novas perspetivas para a compreensão do estabelecimento da assimetria ED em vertebrados.

List of Publications

Part of the work shown in this thesis is included in the following publications:

Bota, C., Martins, G. G., and Lopes, S. S. (2023). Dand5 is involved in zebrafish tailbud cell movement. Frontiers in Cell and Developmental Biology 10.

Sampaio, P., Pestana, S., Bota, C., Guerrero, A., Telley, I. A., Smith, D. J., and Lopes, S. S. (2023). Fluid extraction from the left-right organizer uncovers mechanical properties needed for symmetry breaking. (under submission)

During the course of this PhD the author has contributed to the following publication:

Pinto, A. L., Rasteiro, M., Bota, C., Pestana, S., Sampaio, P., Hogg, C., et al. (2021). Zebrafish motile cilia as a model for primary ciliary dyskinesia. International Journal of Molecular Sciences 22, 8361.

List of Abbreviations

AP - Antero-Posterior

BMP - Bone morphogenetic protein

LPM - Lateral plate mesoderm

LR - Left-Right

LRO - Left-right organizer

KV - Kupffer's Vesicle

Dand5 – DAN family member 5

DAPI - 4',6-diamidino-2-phenylindole

DFC - Dorsal forerunner cells

DV - Dorso-Ventral

ECM - Extracellular matrix

E3 - embryonic medium

EMT – epithelial to mesenchymal transition

Fgf – Fibroblast Growth Factor

FRAP - fluorescence recovery after photobleaching

hpf – hours post-fertilization

ICOs – Intracilliary calcium oscillations

LMA - low-melting agarose

MZ - Maturation zone

N - sample size

Oep – One-eyed pinhead (protein)

PCD – Primary ciliary dyskinesia

PCP – Planar Cell Polarity

PFA - paraformaldehyde

PSM – Presomitic Mesoderm

ROI - Region of interest

ss - somite stage

smFISH - single molecule Fluorescent *in situ* Hybridization

Spaw - Southpaw

TGF-β – Transforming Growth Factor Beta

Wnt – Wingless/Integrated Family Members

WT - wild type

2p - two-photon

3D - three-dimensional

List of Figures

Supplementary Figures

List of videos

List of Tables

CHAPTER 1:

Introduction

Left-right asymmetry

Symmetry is a fundamental pattern in nature and is characterized by the exact similarity of parts around an axis. However, morphological asymmetries exist in many organisms concerning the left-right (LR) axis. Organisms display three primary forms of asymmetry. The first is known as fluctuating asymmetry, which occurs due to minor deviations from perfect LR symmetry during development in a process called developmental noise. The second form is called antisymmetry, in which structures consistently exhibit asymmetry, but the direction of this asymmetry is random between individuals. Finally, there are directional asymmetries, in which structures consistently show a particular direction of asymmetry that is the same in all individuals (Grimes, 2019). In vertebrates, the positioning and patterning of visceral organs and vasculature exhibit directional LR asymmetry while displaying a bilaterally symmetric external body plan (Grimes and Burdine, 2017; Blum and Ott, 2018; Grimes, 2019; Hamada and Tam, 2020).

For instance, during development, the heart loops asymmetrically and ultimately takes a leftward position in the chest cavity. Additionally, the gut coils asymmetrically, and in the abdomen, the stomach and pancreas are positioned on the left side, whereas the liver is positioned on the right side. In addition, the right and left lungs have different number of lobes and morphological and functional asymmetries are present in the brain (Grimes and Burdine, 2017; Blum and Ott, 2018; Grimes, 2019; Hamada and Tam, 2020). This typical asymmetric arrangement of organs is referred to as *situs solitus* (Figure 1.1). Disruption of the developmental processes responsible for establishing organ laterality during embryogenesis leads to changes in the placement and/or morphology of the affected organs (Ramsdell, 2005; Peeters and Devriendt, 2006; Sutherland and Ware, 2009; Gabriel and Lo, 2020).

Regarding organ position, anomalies in LR asymmetry can be classified as *situs inversus*, which involves perfect mirror-image of all organs with respect to the other two body axes. Alternatively, *situs ambiguous*, also known as heterotaxy, is characterized by an abnormal arrangement of thoracic and/or abdominal organs, where some develop normal LR asymmetry while others do not. This disorder may also involve isomerism, in which organs develop symmetrically, such as in left or right atrial isomerism (Figure 1.1). This condition is highly associated with health problems and prenatal death. Heterotaxy is estimated to occur in 1 in 10,000 births in humans (Lin et al., 2000) and is associated with significant fetal and perinatal mortality in both humans and other vertebrates, mainly because of its implications in complex cardiovascular malformations. Situs *inversus* is associated with lower mortality; however, affected individuals may still suffer from respiratory, kidney, and reproductive dysfunctions,

because defects in motile cilia are usually associated with this condition (Fliegauf et al., 2007; Wallmeier et al., 2020). The Physicians Siewert and Kartagener first observed the connection between cilia motility and LR defects in patients showing bronchiectasis and *situs inversus*. Further investigation has revealed that approximately half of individuals with primary ciliary dyskinesia (PCD) also exhibit *situs inversus* or heterotaxy, indicating that cilia play a crucial role in establishing normal LR (Kennedy et al., 2007; Shapiro et al., 2014; Li et al., 2016). PCD is also characterized by respiratory dysfunction and infertility, and it was discovered that these conditions are due to the loss of cilia motility (Afzelius, 1976; Pedersen and Mygind, 1976). Many studies have identified mutations in numerous genes responsible for proper cilia motility in patients with laterality defects (Knowles et al., 2013; Praveen et al., 2015; Nöthe-Menchen et al., 2019; Lucas et al., 2020; Wallmeier et al., 2020).

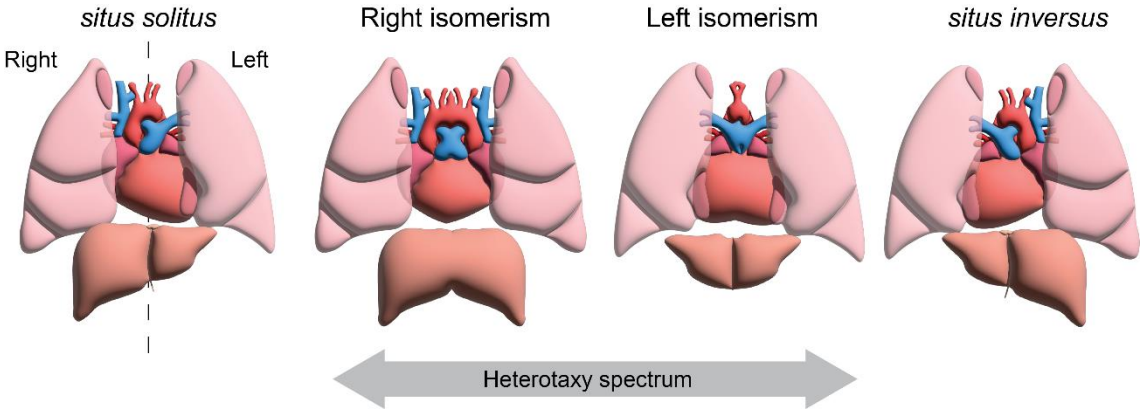

Figure 1.1. The human anatomy of *situs* disorders. *Situs solitus* is the typical arrangement, where the cardiac apex is oriented leftward, the right lung has three lobes, the left lung has two lobes, and the liver is on the right. Heterotaxy is a group of disorders that result in the abnormal arrangement of internal organs. Right atrial isomerism is a type of heterotaxy where both lungs have three lobes, the liver is midline, and the orientation of the heart apex is random. Left atrial isomerism is another type of heterotaxy where both lungs have two lobes, the liver is midline, and the orientation of the heart apex is random. Finally, *situs inversus* is a rare condition where the internal organs mirror the normal arrangement. In *situs inversus*, the cardiac apex is oriented rightward, the right lung has two lobes, the left lung has three lobes, and the liver is on the left.

The asymmetrical arrangement of organs along the LR axis is a fundamental aspect of the vertebrate body plan and is also present in some invertebrate species (Namigai et al., 2014; Blum and Ott, 2018; Hamada and Tam, 2020). Over the last three decades, three main vertebrate models have been established to study the mechanisms underlying LR patterning during embryonic development: mouse, *Xenopus* frogs and zebrafish (Blum and Ott, 2018, 2019; Hamada and Tam, 2020; Little and Norris, 2021; Forrest et al., 2022). The prevailing model implies that in these vertebrates, the initial step in LR asymmetry occurs in a specialized organ

known as the LR organizer (LRO). The LRO is enabled by polarized cilia, which create an asymmetric fluid flow that is considered to be the primary driving force behind symmetry breaking. Body asymmetry is then established by the asymmetric expression of Nodal on the left side of the lateral plate mesoderm (LPM).

The Nodal signaling pathway: key components and function on vertebrate LR

Nodal, a highly conserved member of the transforming growth factor-beta (TGF-β) family, was initially considered to be restricted to deuterostomes. However, research has demonstrated its presence in the hydra, which is essential for establishing an axial asymmetry along the main body axis (Watanabe et al., 2014). Additionally, Grande and Patel, (2009) showed that Nodal signaling is involved in specifying left-right asymmetry in snails. The major roles of Nodal signaling (Figure 1.2) in vertebrates include mesoderm and endoderm specification and in controlling LR asymmetry (Shen, 2007; Zinski et al., 2017).

In vertebrates, it was first established that LR patterning involves the expression of *Nodal,* only in the LPM (Levin et al., 1995a; Collignon et al., 1996; Lowe et al., 1996; Meno et al., 1996a; Long, 2003). More specifically, during LR patterning, Nodal is involved in establishing the LRO and transmitting LR information to the LPM. Despite the phylogenetic features; for simplicity, here, all nodal and nodal-related genes will be referred to simply as nodal, which include mouse Nodal; Cyclops, Squint, and Southpaw in zebrafish; Xnr1, 2, 3, 4, 5 and 6 in *Xenopus* (Schier, 2003; Shen, 2007; Zinski et al., 2017; Opazo et al., 2019).

The Nodal protein is initially expressed as a precursor that includes a long N-terminal prodomain. The mature domain of the protein is then separated from the prodomain by proteases belonging to the proprotein convertase family (Beck et al., 2002; Shen, 2007). Nodal seems to require the formation of heterodimers with Gdf1/3 proteins, encoded by another member of the TGF-β family, to activate the signaling pathway. Gdf3 is needed in zebrafish (Bisgrove et al., 2017; Montague and Schier, 2017; Pelliccia et al., 2017; Montague et al., 2018a) and Gdf1 and Gdf3 in frogs and mammals (Andersson et al., 2007; Tanaka et al., 2007; Fuerer et al., 2014; Opazo and Zavala, 2018; Opazo et al., 2019). Notably, Gdf1/3 in amphibians are independently originated copies (Opazo and Zavala, 2018). Nodal binds to a complex of serine/threonine kinase receptors,

including a type II receptor (Acvr2a and Acvr2b) and a type I receptor (ALK4 and ALK7) (Attisano and Wrana, 2002; Shen, 2007). Type II receptors phosphorylate and activate type I receptors, which in turn phosphorylate cytoplasmic Smad2 and/or Smad3. Phosphorylated Smads then interact with Smad4 and accumulate in the nucleus (Hill, 2016, 2018). Once in the nucleus, Smads bind to transcription factors such as FoxH1 and Mixer, leading to the transcriptional activation of downstream target genes such as *lefty1/2*, *nodal*, and *pitx2*, as well as other genes (Whitman, 2001; Shen, 2007). Nodal signaling is also dependent on EGF-CFC co-receptors, which are extracellular and GPI-linked proteins, including zebrafish One-eyed pinhead (Oep) (Gritsman et al., 1999), frog (Xcr) (Kinoshita et al., 1995), and mouse/human Cripto/Cryptic (Shen et al., 1997; Foley et al., 2003).

Some proteins, including Cerberus/Dand5 and Lefty, act as inhibitors of Nodal signaling (Meno et al., 1996a; Branford et al., 2000; Cheng et al., 2000; Hashimoto et al., 2004a; Marques et al., 2004; Wang and Yost, 2008; Schweickert et al., 2010). Lefty, for instance, is an extracellular antagonist of Nodal signaling that binds directly to Nodal ligands and co-receptors (Chen and Shen, 2004). Its action is EGF-CFC-dependent, as it interacts with EGF-CFC proteins and competes with Nodal to bind to these coreceptors to block the formation of a functional ligand-receptor complex (Chen and Shen, 2004; Cheng et al., 2004). In the context of LR development, EGF-CFC is expressed in both the right and left LPM and notochord, where it interacts with Nodal to induce Nodal signaling and physically binds to Lefty1 to antagonize Nodal signaling (Yan et al., 1999; Cheng et al., 2004).

Dand5, a member of the DAN family, is a potent secreted inhibitor of Nodal proteins (Bachiller et al., 2000; Bell et al., 2003; Hashimoto et al., 2004; Marques et al., 2004; Aykul et al., 2015). The Dand5 overall architecture is similar to other cystine-knot-containing proteins, including BMP, another signalling pathway via Smad phosphorylation belonging to the TGFβ family (Nolan and Thompson, 2014). More precisely, in zebrafish, overexpressing *dand5* in one-cell stage embryos antagonized the function of all three *nodal* genes: *cyclops*, *squint*, and *spaw*, which are crucial for dorsal-ventral patterning during embryonic development. Conversely, suppression *of dand5* resulted in distinct defects in laterality, such as the bilateral expression of *spaw*, *lefty1*, *lefty2*, and *pitx2*, which caused organ *situs* defects (Hashimoto et al., 2004).

Pitx2 is a downstream target of the Nodal signalling pathway and is involved in the final step of LR patterning, instructing asymmetric visceral organogenesis. Asymmetric P*itx2* expression is induced by nodal expression in left LPM in various organisms, including Xenopus, mice and

zebrafish (Logan et al., 1998; Piedra et al., 1998; Ryan et al., 1998; Yoshioka et al., 1998; Campione et al., 1999; Long, 2003; Shiratori et al., 2006). *Pitx2*-expressing cells typically develop a left-sided morphology, and ectopic or defective/symmetrical expression can alter the laterality of organs, including the heart, lungs, gut, and brain in *Xenopus* and mice (Ryan et al., 1998; Campione et al., 1999; Lin et al., 1999; Okada et al., 1999). However, unlike other vertebrates, zebrafish *pitx2* is not required for normal organ laterality despite being expressed in the left LPM in response to Nodal signalling (Ji et al., 2016).

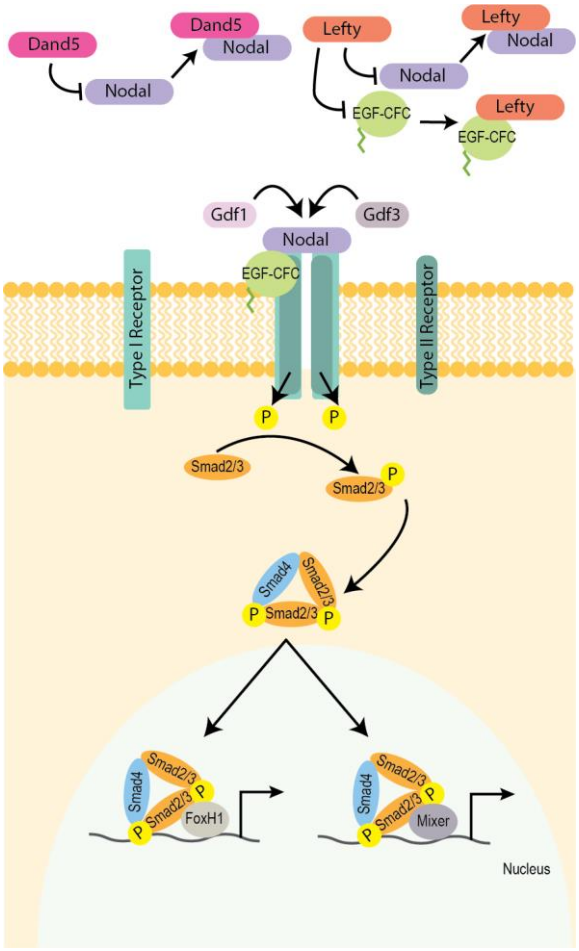

Figure 1.2. Simplified schematic diagram of the Nodal signaling pathway, depicting the critical components required for the activation and regulation of the pathway. The Nodal pathway is a part of the TGFβ family of ligands, with various species-specific ligands such as Nodal, Cyclops, Squint, Southpaw, and Xnr1, 2, 4, 5, and 6. The EGF-CFC family of coreceptor proteins, including one-eyed pinhead (*oep*), Cripto, and Cryptic proteins, play crucial roles in Nodal signaling. Nodal ligands bind to type I and type II serine-threonine kinase receptors, leading to phosphorylation of the type I receptor by type II kinase, followed by phosphorylation of Smad2/3. Activated Smad2/3-Smad4 complexes translocate to the nucleus, where they interact with the transcription factor FoxH1 or Mixer on target promoters. The transcription factors FoxH1 and Mixer, which contain Smad-interaction motifs, play a vital role in regulating the function of the Nodal pathway. Antagonists, such as Dand5 and Lefty proteins, can interact with Nodal ligands and Lefty proteins can bind to EGF-CFC coreceptors and inhibit their function. This diagram is adapted from Schier and Shen (2000), Shen (2007), and Hill (2018)**.**

The LROs: Cilia and flow

The role of motile cilia in LR patterning was initially linked to a specific embryonic structure in the mouse embryo, called the 'ventral node' or simply 'node' (Sulik et al., 1994; Nonaka et al., 1998). This transient structure appears during the early somite stages and is composed of epithelial cells that extend a single cilium into a concave cavity filled with extraembryonic fluid (Sulik et al., 1994; Lee and Anderson, 2008). In mice, cells located at the core of the node, commonly referred to as 'pit cells,' are predominantly characterized by the presence of motile cilia. Conversely, the neighboring cells bordering the left and right edges, known as 'crown cells', possess primarily immotile cilia (McGrath et al., 2003; Yoshiba et al., 2012).

Several studies in the mouse embryo led to the establishment that motile cilia produce an asymmetrical fluid flow at the node, 'the nodal flow,' which is the driving force for the asymmetrical expression of Nodal in the LPM. These seminal studies include those on *inversus viscerum* mutants (*iv*), in which the Left-right dynein gene (also known as Dnah11) is affected and showed immotile cilia and randomized organ position (Supp et al., 1997, 1999; Okada et al., 1999). The studies on *inversion of embryonic turning* (*inv*) mutants, where the *Inversin* gene was targeted, showed defective fluid flow and *situs inversus* (Morgan et al., 1998; Okada et al., 1999). The knockout of Kif3b, a motor protein necessary for intraflagellar transport, that abolished the leftward flow in the node due to the loss of cilia. The absence of cilia disrupted asymmetric Nodal signaling, resulting in defects in organ laterality (Nonaka et al., 1998). Moreover, employing artificial flow, using a peristaltic chamber in cultured mouse embryos, provided conclusive evidence that nodal flow was the basis for symmetry breaking. Reversing the flow altered gene expression, such as *Pitx2*, and caused a reversal of heart looping. Conversely, applying a leftward

flow to *iv/iv* mutants normalized left *Pitx2* expression and subsequent heart placement (Nonaka et al., 2002). In addition, the flow is now well characterized, as planar cell polarity cues have been shown to cause posterior tilting of motile cilia (Hashimoto et al., 2010; Song et al., 2010), producing a leftward flow of fluid across the node through vortex-like unidirectional motion (Nonaka et al., 1998, 2005). This asymmetrical flow is crucial for the asymmetric Nodal expression (Cartwright et al., 2004; Nonaka et al., 2005; Okada et al., 2005).

After discovering transient monociliated structures in amniotes, such as the node (Levin et al., 1995b; Collignon et al., 1996), and in other vertebrate embryos, including zebrafish (Essner et al., 2005), frog (Schweickert et al., 2007), and chicken, it has been suggested that a cilia-based mechanism conserved across vertebrates regulates LR patterning. These structures, the LROs, were identified as the gastrocoel roof plate (GRP) in amphibians (Schweickert et al., 2007) and Kupffer's vesicle (KV) in teleost fish (Essner, 2005; Hojo et al., 2007). The presence of motile cilia and asymmetric fluid flow has also been demonstrated in the KV in zebrafish (Essner et al., 2005; Kramer-Zucker et al., 2005; Sampaio et al., 2014) and the GRP in the frog (Schweickert et al., 2007). Genetic or embryological perturbation of these ciliated structures disrupted asymmetric Nodal pathway expression and organ laterality, confirming their essential role in LR patterning.

While the asymmetric expression of *Nodal* is conserved across vertebrates, the upstream events that establish LR asymmetry differ among species (Schröder and Weizbauer, 2016). For instance, in chick mutants with cilia defects, normal LR asymmetry still develops (Yin et al., 2009; Bangs et al., 2011; Stephen et al., 2013), and the left-sided asymmetric expression of Nodal in the LPM is dependent on the asymmetrical migration of cells expressing Shh around Hensen's node, which results in asymmetrical Shh expression (Gros et al., 2009). Similarly, the LRO in pig and cow embryos lack cilia and exposure to embryonic fluid (Gros et al., 2009; Schröder and Weizbauer, 2016). These studies collectively challenge the concept of a single conserved mechanism responsible for breaking LR symmetry in vertebrates. Thus, in addition to cilia-driven flows, LR positional information can bypass the requirement for cilia (Blum et al., 2014; Dasgupta and Amack, 2016; Inaki et al., 2016; Hamada and Tam, 2020; Rahman et al., 2020) .

In vertebrates with ciliated LROs, the asymmetrical fluid flow precedes the degradation of *Dand5* mRNA on the left side (Marques et al., 2004; Lopes et al., 2010; Schweickert et al., 2010). Recent research has revealed that Bicc1 and Dicer mediate the left-sided *Dand5* mRNA decay (Maerker et al., 2021; Minegishi et al., 2021). In addition, a recent evo-devo study comparing vertebrates with motile cilia in their LRO to those without, identified five missing proteins in animals lacking ciliated LROs. One of these proteins is CIROP (ciliated left-right organizer metallopeptidase), a

metalloprotease expressed exclusively in the LRO of zebrafish, *Xenopus*, and mice. Knockdown of *Cirop* in zebrafish and *Xenopus* resulted in laterality defects, bilateral *dand5* expression and absent *nodal* expression. Additionally, in *Xenopus*, left-sided lineage-restricted gene inactivation demonstrated that *Cirop* is required for proper LR asymmetry patterning only on the left side of the embryo. Thus, the study suggests that Cirop acts upstream of Dand5, enhancing Nodal signaling, to establish correct LR asymmetry in vertebrate embryos possessing an LRO with motile cilia. Furthermore, the authors report mutations in *CIROP* in humans with laterality disorders (Szenker-Ravi et al., 2022).

However, it is still unclear how directional fluid flow translates into molecular asymmetry. Two hypotheses (Figure 1.3) have been proposed for sensing cilia-driven asymmetric fluid flow in the LRO. The first, the chemosensing mechanism, suggests that the flow transports either a secreted morphogen into the extracellular liquid of the node (Nonaka et al., 1998; Okada et al., 2005) or extracellular vesicles, called nodal vesicular parcels (NVPs) carrying Sonic Hedgehog (Shh) or Retinoic Acid (RA) (Tanaka et al., 2005) to the left side of the LRO to induce asymmetric $Ca2^{+}$ flux and downstream signaling events (Figure 1.3A). Furthermore, Tanaka et al. (2005) showed that ciliary motility is crucial for breaking these vesicles, as they take longer to break in mutants lacking cilia. However, this hypothesis was deemed unlikely as NVPs could not be broken by either the force of the flow or the action of motile cilia, owing to the biophysical properties of the fluid, such as its high viscosity (Cartwright et al., 2007).

Alternatively, the mechanosensing hypothesis posited that immotile cilia in the LROs (located in peri-nodal cells in the mouse node and *Xenopus* GRP, and intermingled with motile cilia in zebrafish, due to architectural differences in the KV (Amack et al., 2007; Sampaio et al., 2014; Tavares et al., 2017)) were suggested to sense fluid flow and contribute to LR patterning (McGrath et al., 2003; Tabin and Vogan, 2003). It has been proposed that these cilia act as mechanosensors, bending in response to fluid flow and opening stretch-activated ion channels composed of subunits of Pkd2 and Pkd1l1 in the ciliary membrane, which then initiate asymmetric Ca^{2+} signaling (Figure 1.3B). This mechanism is supported by evidence that Pkd1l1-Pkd2 complexes are involved in LR patterning (Pennekamp et al., 2002; Bisgrove et al., 2005; Field et al., 2011; Kamura et al., 2011). Moreover, Ca^{2+} transients were reported to initiate in immotile cilia and then preferentially propagate to the left side of the mouse LRO to instruct the Nodal cascade on the left LPM (Mizuno et al., 2023). In further support of this mechanism, Katoh et al. (2023) recently demonstrated that directional fluid flow imposes different bending angles on the immotile cilia in the crown cells of mice. Specifically, the cilia on the left side bend towards the ventral side, and the cilia on the right side bend towards the dorsal side. Mechanical stimuli

applied to these cilia triggered a reduction in *Dand5* mRNA and Ca^{2+} transients; however, this response was not observed in *Pkd2* mutants, confirming that this mechanism is Pkd2-dependent. Furthermore, the mouse study showed that Pkd2 is preferentially localized on the dorsal side of the immotile cilia, suggesting that Pkd2 activation depends on the bending angle imposed by directional fluid flow. In zebrafish, Yuan et al. (2015) showed that left sided biased calcium transients are present in motile and immotile cilia. Recently, Djenoune et al., (2023) showed that KV cilia function as mechanosensors, converting mechanical forces into calcium signals that direct LR asymmetry. Mechanical manipulation of KV cilia by using optic tweezers induced intraciliary calcium transients (ICOS), and the study confirmed the requirement of Pkd2 for these transients to happen. Furthermore, mechanical force applied to KV cilia rescued and reversed the cardiac *situs* in zebrafish lacking directional fluid flow. Additionally, the location of cilia within the KV did not affect intraciliary calcium transients upon ciliary bending, suggesting that endogenous left-sided ICOs are generated in response to the counterclockwise flow force. Thus, with these last and very recent developments, the mechanical hypothesis seems to be favored over the chemical hypothesis.

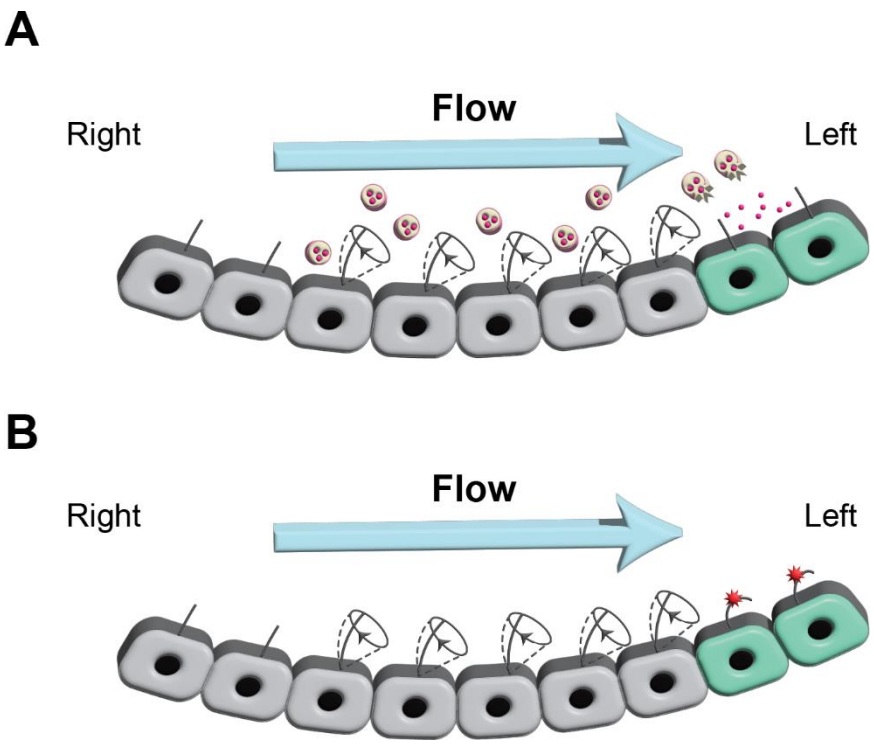

Figure 1.3. Figure 1.3 Two models for flow-sensing mechanism in mice. **(A)** The first model, known as the chemical hypothesis, suggests that ciliary movement transports NVPs toward the left side of the node. This triggers the release of NVPs and an asymmetric calcium signal in the left node crown cells (highlighted in green). **(B)** The second model, referred to as the mechanical hypothesis, proposes that immotile cilia detect fluid flow generated by motile cilia on the left perinodal crown cilia via a Pkd2-dependent mechanism. Adapted from Sampaio (2021).

Nevertheless, ongoing research in the field is still actively exploring the involvement of chemosensing, mechanosensing, or possibly both mechanisms in the process of fluid flow sensing in the LROs. At least in zebrafish it is not clear what enhances the calcium signals on the left side or restricts the *dand5* mRNA reduction to the left side.

The zebrafish LRO, Kupffer's vesicle: from specification to asymmetric fluid flow

In zebrafish, symmetry-breaking events occur within the Kupffer's vesicle (KV), which is equivalent to the LRO of the mouse, node, and GRP of *Xenopus* (Essner et al., 2005). This transient organ, found across teleost fish, has a more intricate microarchitecture than that of other species (Amack et al., 2007). The KV is an ellipsoidal fluid-filled organ enveloped by curved epithelium lined with cilia that emerges during the initial segmentation phase at the posterior end of the notochord (Essner et al., 2000; Amack and Yost, 2004).

The current understanding of the development of the KV shows that a group of mesenchymal cells, without any polarization, come together to form a flat, circular pattern resembling a rosette. This pattern then consolidates into a spherical three-dimensional structure with a central cavity filled with fluid. Fluid influx and ciliogenesis coincide during lumen expansion, with each KV cell producing a single cilium that extends into the lumen (Figure 1.4) (Amack et al., 2007; Oteíza et al., 2008). Consequently, disturbance of any of these steps will lead to defects in LR patterning. The KV emerges from the dorsal forerunner cells (DFCs), a cluster derived from a group of 20–30 dorsal surface epithelial cells (Cooper and D'amico, 1996; Oteíza et al., 2008). The formation of the DFCs depends on the transition of epithelial enveloping layer cells to mesenchymal DFCs (EMT), which is also instructed by Nodal signaling (Oteíza et al., 2008). DFC specification is completed at 50% epiboly prior to the formation of the embryonic shield (6 hpf) (D'Amico and Cooper, 1997; Oteíza et al., 2008). Choi et al., (2007) first reported that DFC specification relies on Nodal signaling. Specifically, it was shown that upregulation of the nodal

gene *squint* (*sqt*) led to an increase in the number of DFCs, while an increase in the levels of the nodal antagonist *lefty2* (*lft2*) resulted in a decrease in the number of DFCs. The critical role of Nodal signaling in DFC formation was demonstrated by DFC absence in maternal-zygotic *one-eyed-pinhead* mutants. Moreover, ectopic DFC formation through cell ingression has been observed in *cyclops* (*cyc*) overexpression sites, confirming the involvement of Nodal signaling in DFC specification (Oteíza et al., 2008). Lin et al., (2017) proposed that Krüppel-like factor 8 (Klf8) may play a role in regulating the number of DFCs. The authors observed a decrease in the number of DFCs in *klf8* morphants during 75% epiboly, which affected the number and length of the KV cilia. However, the study did not establish whether Klf8 has a direct regulatory function in the established signaling pathways that govern DFC cluster formation.

The clustering and collective migration of DFCs at the leading edge of the dorsal blastodermal layer towards the vegetal pole is governed by various genes and signaling pathways. DFCs express *cadherin1* and *cadherin2* (*E-cadherin* and *N-cadherin* in zebrafish, respectively) (Babb and Marrs, 2004; Esguerra et al., 2007; Harrington et al., 2007; Warga and Kane, 2007), and cadherin-based adherens junctions mediate their interactions (Matsui et al., 2011; Warga and Kane, 2018; Kim et al., 2019). While the attachment of DFCs to the EVL is maintained by tight junctions (Oteíza et al., 2008). Furthermore, Integrins αV and β1b promote both DFC cell-to-cell and cell-to-extracellular matrix adhesions (Ablooglu et al., 2010). Tight junctions between DFCs and EVL during epiboly are thought to facilitate vegetal migration. However, live imaging has shown that DFCs located at the front of the cluster often extend cell protrusions (such as filopodia and lamellipodia) towards the vegetal pole (Ablooglu et al., 2010). These findings suggest that DFCs may not only rely on tight junctions for passive migration but also can actively migrate towards the vegetal pole. A recent study by Stark et al., (2022) demonstrated that Carmil3, which plays a role in regulating the activity of capping protein during actin polymerization, is essential for the proper migration of endodermal cells, as well as the migration and clustering of DFCs. It has also been shown that migrasomes are newly discovered chemoattractants that position DFCs correctly next to the embryonic shield, essential for both DFC clustering and migration (Jiang et al., 2019). Migrasomes are large oval-shaped extracellular vesicles, up to 3000 nm, that contain smaller vesicles and are involved in cell migration. They are released through a mechanism called "migracytosis" derived from retraction fibers at the rear edge of migrating cells (Ma et al., 2015).

The proper organization and movement of DFCs during gastrulation are also governed by intercellular signaling mechanisms. One such mechanism is the Ephrin signaling pathway, which maintains the border between DFCs and adjacent cells. Through Ephb4b-Efnb2b interactions, a

repulsive signal is provided that ensures the clustering state of DFCs during gastrulation cell movements (Zhang et al., 2016). DFC migration is also regulated by Wnt signaling. Canonical Wnt signaling activates downstream target genes in DFCs (Lin and Xu, 2009), but during migration, β-catenin nuclear translocation must be inhibited by endogenous $Ca2^{+}$ waves or Naked Cuticle 1 activity (Schneider et al., 2008, 2010). In addition, non-canonical Wnt ligands control planar cell polarity (PCP), and inhibition of both *wnt11* and *prickle1a* impairs DFC cluster adhesion at late gastrulation stages (9-10 hpf), resulting in dysmorphic KV formation (Oteiza et al., 2010).

Furthermore, Arrington et al., (2013) have shown that Syndecan 2 (Sdc2) activity also regulates the proliferation and coalescence of DFCs during epiboly, which in turn affects their incorporation into the forming KV. The authors observed that *sdc2* morphants exhibited dispersed DFCs, reduced cell proliferation, and loose adhesion. Additionally, downstream of Sdc2, Tbx16 and Fgf2 were found to be involved in this regulatory pathway.

During the final stages of epiboly, the DFC cluster changes and detaches from the dorsal marginal EVL. At the early somitogenesis, by the bud stage (9 hpf), the apices of bottle-shaped DFCs in the cluster turn inward, forming three-dimensional rosette structures enriched in tight junction components such as zonula occludens-1 (ZO-1). Over time, the multiple rosette structures are rearranged into a single focal point in the shape of a flattened sphere and undergo mesenchymal to epithelial transition (MET) to form epithelial KV cells regulated by No tail (Ntl) and Tbx16 (Amack et al., 2007), ultimately forming an inner ZO-1-lined lumen sphere (Oteíza et al., 2008; Oteiza et al., 2010). *claudin5a* is also abundantly expressed on the apical surface of KV epithelial cells, where it forms a strong barrier that seals the lumen allowing proper KV inflation with liquid (Kim et al., 2017).

Current understanding indicates that three main processes are involved in the expansion of the spherical KV lumen. The first step involves Myosin1d directing vacuolar trafficking towards the apical surface of KV cells, which allows for efficient expulsion of intracellular fluid from epithelial cells into the lumen. This is crucial for correct KV lumen formation and expansion, as described by Saydmohammed et al., (2018). During cell division, Rathbun et al., (2020) demonstrated that mitotic cells in the KV position cytokinetic bridges to guide the delivery of cystic fibrosis transmembrane conductance regulator (CFTR) protein by Rab11 vesicles to the center of the rosette. CFTR is necessary for proper lumen establishment and, at approximately 2 ss, becomes the primary driver of fluid secretion and KV lumen expansion (Navis et al., 2013; Roxo-rosa et al., 2015). By regulating the flow of chloride ions, CFTR creates an osmotic gradient that facilitates the movement of water into the KV lumen. Impairment of KV lumen inflation and

subsequent development of LR defects result from the absence or suppression of CFTR activity (Navis et al., 2013; Roxo-rosa et al., 2015; Gokey et al., 2016). Additionally, Roxo-rosa et al. (2015) showed that reduced Polycystin-2 (Pkd2) levels lead to CFTR-mediated over-inflation of the KV, resulting in larger KVs in pkd2-morphants than in WT embryos. This KV enlargement is due to increased fluid secretion into the lumen and not cell proliferation.

During lumen expansion in the KV, fluid influx coincides with ciliogenesis. This process involves the formation and elongation of a single cilium from the apical surface of each KV cell, which then extends into the lumen. Even before lumen expansion, DFCs express ciliary genes that promote ciliogenesis and ciliary motility (Essner et al., 2005; Yu et al., 2008).

The transcription factor Forkhead box J1a (Foxj1a) is considered a master regulator of motile cilia, as it regulates a group of genes required for motile cilia formation and function (Yu et al., 2008). Knockdown of Foxj1a in zebrafish leads to the absence of motile cilia in the KV (Stubbs et al., 2008; Yu et al., 2008) and in other motile ciliated structures, such as the floor plate and pronephric ducts, as well as the lack of expression of genes required for the development and activity of motile cilia such as *dynein axonemal heavy chain 9* (*dnah9*), *centrin*, *EF-hand protein 2* (*cent2*). Conversely, ectopic *foxj1a* expression induces ectopic motile cilia-like cilia and the ectopic expression of motility cilia genes (Yu et al., 2008). The expression of *foxj1a* in the DFCs/KV is induced by the fibroblast growth factor (FGF) signaling (Neugebauer et al., 2009; Li et al., 2018), whereas canonical Wnt signaling acts downstream of FGF to directly control *foxj1a* expression through TCF/LEF transcription factor-binding sites located within the *foxj1a* promoter (Caron et al., 2012). This was demonstrated by the inhibition of *foxj1a* transcription in DFCs and downregulation of cilia length and number in the KV upon depletion of Lef1 and Tcf7 (Zhu et al., 2015). In addition to that, overexpression of *wnt8a* in a single cell at the 128-cell stage of zebrafish development induced the formation of an ectopic protrusion with ectopic *foxj1a* expression and ectopic cilia-like structures (Zhu et al., 2015). Foxj1 is expressed in both the mouse node and *Xenopus* GRP, and its inactivation results in a randomized LR patterning and defects in ciliogenesis (Stubbs et al., 2008; Alten et al., 2012).

Related to motile ciliogenesis, Dutta et al., (2015) have shown that Nlz1, a zinc-finger-containing protein is also essential for motile cilia formation in zebrafish embryos, as its knockdown results in motile cilia depletion. Furthermore, Nlz1 acts downstream of Foxj1a and canonical Wnt signaling (Wnt8a) and positively regulates non-canonical Wnt signaling (Wnt11), contributing to ciliary formation.

As the motile cilia extend from the KV cells, their length and motility progressively increases, resulting in the generation of a fluid flow within the KV (Sampaio et al 2014, Yuan et al., 2015; Ferreira and Vermot, 2017; Tavares et al., 2017).

Cilia length is regulated by Notch signaling via the DeltaD ligand. Specifically, a reduction in Notch signaling is associated with shorter cilia, while hyperactivation of Notch leads to longer cilia. (Lopes et al., 2010). Additionally, the decreased cilia length observed in *dld*$^{-/-}$ mutants led to slower fluid flow velocity and affected LR patterning (Lopes et al., 2010; Sampaio et al., 2014). In contrast, Pintado et al., (2017) showed that overexpression of Arl13b increased cilia length but did not strongly affect the flow pattern and intensity. The authors inferred that a ciliary length between 5-7 µm is optimal for producing LR symmetry breaking and that cilia length is more strictly regulated for shorter cilia than for longer cilia. Jacinto et al., (2021) reported that the knockdown of Pkd2 resulted in a decrease in cilia length and, subsequently, a reduction in KV flow speed. However, the authors did not conclude on the cause of the decrease in cilia length because in zebrafish, Pkd2 does not act upstream of Foxj1a, as reported in *Xenopus* embryos (Vick et al., 2018). Jászai et al., (2020) also demonstrated that Prominin3 morphants showed reduced cilia number and length in the KV and suggested a Prominin-Arl13b interaction in ciliated structures, due to the observation of similar L-R asymmetry defects in zebrafish Arl13b mutants and morphants (Duldulao et al., 2009), such as decreased cilia length.

In addition, Notch signaling also plays a role in the acquisition of motility in KV cilia. It has been demonstrated that Notch signaling modulates the ratio of motile to immotile cilia (Sampaio et al., 2014; Tavares et al., 2017). Using electron microscopy, Tavares et al., (2017) demonstrated that all cilia in the KV exhibit the required ultrastructure for motility. However, live imaging confirmed that 20% of these cilia remained immotile. The authors also discovered that overexpression of *hairy-related 12* (*her12*) or Notch intracellular domain (NICD) increased the number of immotile cilia while decreasing motile cilia by acting downstream of Foxj1a. Notably, the first link between Notch signaling and the number of motile cilia was reported by (Boskovski et al., 2013). The authors showed that GALNT11, implicated in human heterotaxy, activates Notch signaling and controls the ratio of motile to immotile cilia in *Xenopus* LRO. Further, they found that Galnt11-mediated Notch1 signaling regulates the distribution of cilia, and depletion of *galnt11* or *notch1* leads to an increase in motile cilia at the expense of immotile cilia, causing defects in left-right patterning downstream.

As ciliary motility progressively increases, the KV undergoes an asymmetric cell shape rearrangement along the anteroposterior axis, resulting in thin and elongated anterior cells, and

flattened and wide posterior cells (Wang et al., 2011; Dasgupta et al., 2018). The process of KV reshaping occurs between 4-6 ss and is vital in creating an uneven distribution of cilia by constraining more ciliated cells in the anterior dorsal zone (AD) than in the posterior cells, resulting in increased ciliary density in the anterior region as originally seen by Kreilling et al. (2007) and mechanistically explained by (Wang et al., 2011). As a result, this restructuring guarantees the production of a directional fluid flow (Kreiling et al., 2007; Sampaio et al., 2014).

Although not fully understood, evidence suggests that the KV reshaping process is regulated by a complex interplay of mechanical, genetic, and biochemical factors. It has been shown to be dependent on the function of the Rho kinase gene *rock2b* and *non-muscle myosin II* (Wang et al., 2011, 2012). The authors suggested that the actin-myosin pathway modulates interfacial tension between cells during KV reshaping. This is accomplished by the regulation of cell contractility and adhesion (Wang et al., 2012). Inhibition of Rock2b function or Non-muscle myosin II prevents AP asymmetric cell remodeling, without affecting KV lumen expansion or ciliary length. This disruption leads to impaired LR patterning by affecting the asymmetric cilia-driven flow.

An additional role in this process was demonstrated to be orchestrated by an AP asymmetric deposition of the extracellular matrix (ECM) produced and assembled at the notochord (Compagnon et al., 2014). The ECM accumulation limits the apical expansion of cells in the anterior dorsal region, indicating that only cells on the posterior ventral side undergo apical development as the lumen inflates (Compagnon et al., 2014). In fact, the increase of the KV lumen during the lumen expansion process, seems to directly contribute to the observed cellular changes. As shown by Compagnon et al., (2014) inhibition of lumen growth or expansion beyond the maximum volume observed in unperturbed embryos resulted in a reduction in the cell density ratio between the anterodorsal (AD) and posteriordosal (PV) regions of the KV, whereas the tissue architecture or molecular composition adjacent to the KV remained unchanged. This suggests that local cell shape variations within the KV are dependent on the interaction between intraluminal pressure and regional changes in contractility of the contiguous epithelium. In contrast, Dasgupta et al., (2018) showed that during the KV reshaping process, the volume of KV anterior cells increased, while that of KV posterior cells decreased, in a mechanism mediated by ion channel activity but independent of KV lumen expansion. Inhibition of the sodium-potassium pump and CFTR without perturbing lumen expansion eliminated the asymmetric volume changes in KV cells, indicating that ion flux drives these changes along the AP axis.

Besides, Sanematsu et al., (2021) recently investigated the pressure and shear stress generated by tailbud cells on the KV reshaping process as the KV travels through the tailbud tissue from 2 ss to 8 ss. Using 3D simulations and PIV analyses of live images of the KV development, the authors showed notable velocity gradients surrounding the KV. These observations suggest that the tailbud tissue exerts mechanical drag forces on KV during the 2-4 ss and 4-6 ss stages and aids in the KV reshaping process. However, further experimental studies are required to test the predictions made by these models and to understand the extent to which drag forces impact the morphogenesis of KV.

As architectural changes in KV cells occur and the proportion of motile *vs.* immotile cilia increases, a directional cilia-driven fluid flow is established, in a circular counterclockwise direction (Kramer-Zucker et al., 2005). To specify more exactly, the measurement of flow velocities in various regions of the KV demonstrated that the anterior region exhibited higher velocities compared to the posterior region. This difference in AP velocities causes a robust leftward flow across the KV's anterior pole, whereas the rightward return flow across the posterior end is slower (Sampaio et al., 2014).

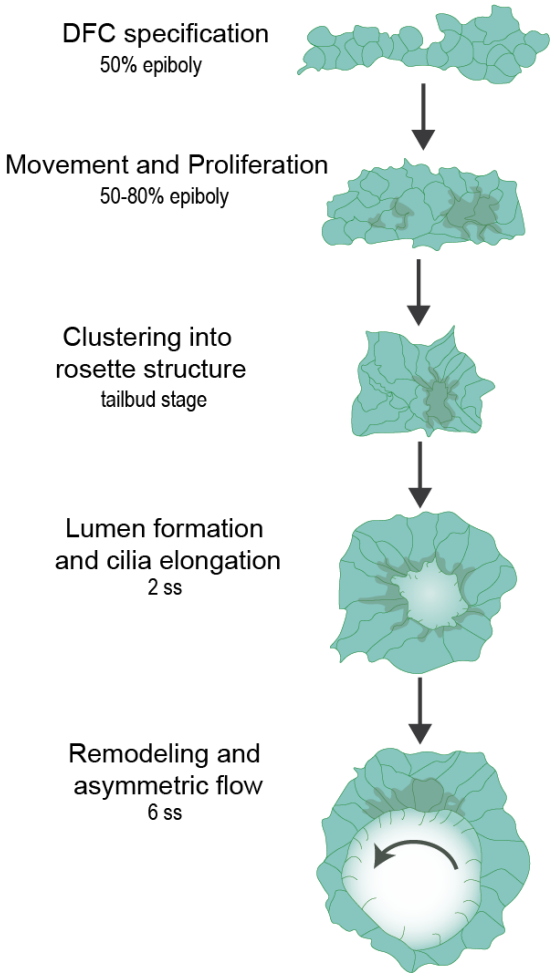

Figure 1.4. KV Morphogenesis. Mesenchymal DFCs are specified during the 50% epiboly stage, migrate posteriorly, and proliferate between the 50% and 80% epiboly stages. During EMT at the end of epiboly, the DFCs cluster to form a rosette-like structure. In the early somite stages, a fluid-filled lumen expands, and cilia elongate into the lumen. At 2 ss, the anterior and posterior KV cells have similar morphology. Between 4 and 6 ss, KV cells undergo an asymmetric cell shape change along the anterior-posterior axis, referred to as KV remodeling. This enables tight packing of cilia in the anterior region of the KV, driving a robust counterclockwise fluid flow (indicated by the black arrow). Adapted from Forrest et al., (2022).

A robust directional cilia-driven fluid flow in the KV requires proper orientation of cilia. Precisely, cilia must be tilted posteriorly, a process that requires the PCP signaling pathway component Van gogh-like 2 (Vangl2) (Borovina et al., 2010), as also shown in mice (Hashimoto et al., 2010; Song et al., 2010). This was determined by the observation of defective cilia orientation due to the loss of Vangl2 disrupting cilia-driven fluid flow and LR patterning. (Borovina et al., 2010; May-Simera et al., 2010). Myo1d was also reported to interact with Vangl2, indicating that they jointly regulate the polarization of cilia in the KV (Juan et al., 2018) for zebrafish *myo1d* mutants showed a decrease in flow angular velocity. Furthermore, in a theoretical simulation analysis of the ciliary angle and its relationship with the plasma membrane, Ferreira and Vermot, (2017) proposed that in order to generate effective unidirectional flow, most motile cilia require a meridional tilt.

While the mouse node can break symmetry with only two motile cilia to establish a normal organ *situs* regardless of their position (Shinohara et al., 2012) , in the zebrafish KV, a minimum of approximately 30 motile cilia are required for *situs solitus* (Sampaio et al., 2014; Tavares et al., 2017). This discrepancy is attributed to differences in organ morphology, cilia number, and topological distribution. Specifically, the node is a flat invagination where all motile cilia are located on the floor, whereas the KV is a spherical, enclosed organ with cilia distributed all around, with some cilia at the ventral pole generating a flow that opposes the desired flow (Smith et al., 2014).

Symmetry breaking and asymmetry establishment in zebrafish

Although the exact mechanism of fluid flow detection in LROs is not yet fully understood, current evidence suggests that the initial response to fluid flow sensing involves an influx of calcium ions (Yuan et al., 2015). This influx was shown to be dependent on the function of the Pkd2 cation

channel. Pkd2, a TRIP2 cation channel protein, is expressed in various locations, including KV-lining cells, intracellularly and along the KV cilia of zebrafish (Roxo-rosa et al., 2015). Additionally, Pkd2 was found in the basal body of the KV cilia (Roxo-rosa et al., 2015), and its crucial involvement in calcium signaling regulation has been demonstrated in previous studies (Koulen et al., 2002; Nauli et al., 2003; Qian et al., 2003; Paavola et al., 2013).

While not yet functionally validated in zebrafish, previous studies have identified Pkd1l1 as a sensory partner of Pkd2 in the LRO of mouse and medaka (Field et al., 2011; Kamura et al., 2011). Studies have shown that in medaka, both Pkd1l1 and Pkd2 are present in all KV cilia (Kamura et al., 2011), while in zebrafish, *pkd1l1* is also expressed in the KV (England et al., 2017) and its protein has been detected along KV cilia (Roxo-Rosa and Lopes, 2019).

Furthermore, weekly transient activation of Ca2+/Calmodulin-dependent protein kinase (CaMK-II) was shown at 3-6 ss along the left anterior wall of the KV, which reached its peak at 10-12 ss (Francescatto et al., 2010). In addition to that, CaMKII knockdown leads to the disruption of asymmetric gene expression and randomization of organ situs (Francescatto et al., 2010).

Bisgrove et al., (2005) showed that *pkd2* is expressed in the DFCs from gastrulation to the early somite stages in the KV-ciliated cells. The absence of Pkd2 in *pkd2* morphants and *pkd2*$^{-/-}$ embryos leads to defects in LR patterning, leading to the loss of *dand5* asymmetric expression, thereby leading to randomization of the nodal cascade genes on the LPM (Bisgrove et al., 2005; Schottenfeld et al., 2007; Yuan et al., 2015; Jacinto et al., 2021).

More specifically, Yuan et al. (2015) reported that during the early stages of somitogenesis, 1-4 ss, asymmetric intraciliary calcium oscillations (ICOs) are predominantly observed at the anterior left quadrant of the KV and play a crucial role in symmetry breaking, possibly involved in fluid flow sensing. These ICOs initiate in cilia and then form cytosolic calcium waves that spread to neighboring KV cells and culminate in a rapid wave of calcium on the left side, extending beyond the KV. The resulting calcium transients lead to a stable elevation of mesendodermal calcium on the left domain beyond the KV, which persists for a 2-hour window (around 6ss to 10 ss). Also, the authors demonstrated that intraciliary calcium signaling depends on Pkd2 since, in *pkd2* morphants and mutants, both ICOs and cytoplasmic calcium waves were remarkably suppressed. Suggesting that in the KV the onset of flow triggers Pkd2-dependent ICOs, which induce secondary calcium waves in the surrounding mesendodermal cells. These waves activate the Nodal signaling cascade, thereby establishing LR asymmetry. In addition to that, ICOs were reported to peak earlier than cytosolic waves, indicating that their cumulative effect is required for robust signaling. These findings were corroborated by Djenoune et al. (2023) by providing

evidence that cilia in the KV act as mechanosensors and can convert mechanical forces into calcium signals to instruct LR asymmetry. This was shown by intraciliary calcium transients being activated when KV cilia were mechanically manipulated. The recent study further validated the requirement of Pkd2 in intraciliary calcium oscillations, as observed by the loss of intraciliary calcium transients in *pkd2* mutant embryos when cilia were mechanically bent. Additionally, Dejoune et al. (2023) findings showed that the mechanical force applied to KV cilia was sufficient to rescue and reverse cardiac *situs* in zebrafish lacking directional fluid flow. In addition to that, ciliary bending with intraciliary calcium transients could occur regardless of the location of the cilia within the KV, suggesting that the endogenous left-sided ICOs are generated in response to the force exerted by the directional flow. Sampaio et al. (2014) had also shown that flow is instructive by selecting immotile cilia morphant embryos with only a few right sided motile cilia, and showed that these embryos resulted in situs inversus. Although the activation of CaMKII in left-anterior KV cells was found to reach its peak between 10 and 12 ss (Francescatto et al., 2010), indicating that CaMKII could be targeted by Ca^{2+} fluxes triggered by ICOs, there is currently no established link between these occurrences. Overall, it appears that the anterior region of the KV, which is subjected to the strongest flow, is also where the initial molecular asymmetries occur, more precisely on the left-anterior side.

Thus, based on current understanding in zebrafish embryos, it is suggested that mechanosensing is the primary sensing mechanism for perceiving asymmetrical fluid flow, rather than chemosensing, although the latter cannot be completely ruled out.

The *dand5* asymmetry in the zebrafish

As observed in mouse and frog (Schweickert et al., 2010; Nakamura et al., 2012), the asymmetric flow precedes the downregulation of *dand5* gene mRNA on the left side of the KV, which removes the Dand5-Southpaw (Spaw) inhibition (Sampaio et al., 2014).

The *dand5* expression in zebrafish is restricted to the KV cells and its transcripts first appear at 1 ss (White et al., 2017), just before the lumen formation of the KV. Next, transcripts are detected through *in situ* hybridization at 2-3 ss (Hashimoto et al., 2004). The expression of *dand5* is initially symmetrical on the left and right sides of the KV and forms a horseshoe-shaped zone with an open anterior side until approximately 7 ss. However, by 8 ss, *in situ* hybridization reveals that *dand5* expression becomes asymmetrical due to a decrease in the detection of expression on the left-side cells of the KV. This is the first asymmetric gene reported in the LR patterning

(Lopes et al., 2010). Later, *dand5* expression persists in KV cells throughout somitogenesis and disappears by 24 hpf (Hashimoto et al., 2004; White et al., 2017) in the KV-derived cells (Ikeda et al., 2022). It has been shown that *dand5* expression is dependent on the presence of the Ntl protein (Hashimoto et al., 2004; Amack et al., 2007; Gourronc et al., 2007), and that there is a T-box-rich region near the *dand5* transcription start site (Gourronc et al., 2007). Three potential binding sites for the CSL/RBP-J protein were found upstream of the transcription start site of *dand5*. Notch signaling was indeed shown to be necessary for *dand5* expression by treating zebrafish embryos with a Notch signaling inhibitor (Gourronc et al. 2007). Lopes et al. (2010) also showed that *deltaD* mutants have very little *dand5* mRNA expression.

Nakamura et al., (2012) first established that the destabilization of *Dand5* mRNA on the left side of the mouse LRO was flow-dependent, explicitly targeting the 3-'UTR region of *Dand5*. Moreover, recent findings in mouse and *Xenopus* have revealed that the destabilization and translation inhibition of *dand5* on the left side is mediated in a flow-dependent manner by Bicc1, a member of the BicC family of RNA-binding proteins, that acts through the 3'-UTR of *dand5* (Maerker et al., 2021; Minegishi et al., 2021). More precisely, it has been reported that the possible degradation of mouse *Dand5* mRNA on the left side of the node depends on the first 200 nucleotides of its 3'-UTR. Bicc1 recognizes a specific sequence motif consisting of eight nucleotides that is conserved in this region (Minegishi et al., 2021). In *Xenopus* LRO, the Bicc1 responsive element was described as a segment of approximately 139 nucleotides in the proximal 3'-UTR of *dand5*. This region is both necessary and sufficient for translational repression mediated by Bicc1 (Maerker et al., 2021). Still, the mechanism by which Bicc1 interacts with the 3'-UTR of *dand5* in zebrafish has yet to be determined and we must conceive that the same outcome could be achieved in a different manner.

Nevertheless, evidence from studies in mouse, frog, and zebrafish suggests that Bicc1, along with Dicer1 (an endonuclease enzyme critical for the biosynthesis of microRNAs) and Pkd2, all contribute to the repression of *dand5* (Maerker et al., 2021). In mouse *Dicer* mutants and Xenopus *dicer1* morphants, the left-sided downregulation of *Dand5* mRNA levels during the post-flow stages was compromised. In zebrafish, also no left-sided *dand5* repression was observed in 10 ss maternal-zygotic (MZ) *dicer* mutants, suggesting that Dicer has a specific function in *dand5* regulation. However, it remains unclear whether Bicc1 and Dicer cooperate in regulating miRNAs to mediate the left-sided decrease of *dand5* expression.

In addition, Szenker-Ravi et al., (2022) recently demonstrated the involvement of Cirop in *dand5* left-sided decrease and the Nodal cascade in the LPM. The authors reported that *cirop* is

exclusively expressed in the DFCs and initial KV stages downstream of Foxj1a, but Foxj1a alone was insufficient to activate *cirop* DFC expression. Also, it was shown that *MZcirop*$^{-/-}$ embryos exhibited heterotaxy and *situs inversus*, likely due to the absence or posterior-restricted expression of *spaw* in the LPM. The expression of *lefty1* and *lefty2* in the left diencephalon and left cardiac field, respectively, was also abolished in the absence of Cirop. Furthermore, *dand5* expression in *MZcirop*$^{-/-}$ embryos was maintained bilateral, not being repressed on the left side at 8 ss. However, this effect was shown not to be due to the disruption of KV morphogenesis or asymmetric fluid flow within the KV. These findings suggest that while the loss of Cirop does not impact the process of ciliogenesis and motile cilia-driven flow, it does play a significant role downstream cilia-driven cascade that controls LR patterning, specifically in the *dand5* left-sided downregulation.

The Nodal Signaling Pathway in the zebrafish LR Asymmetry

In zebrafish, the nodal ligand Southpaw (Spaw) is responsible for breaking and transducing LR asymmetry (Long et al., 2003). Unlike in mice, where *Nodal* expression occurs in the node crown cells, in zebrafish, the expression of *spaw* is first detected in a symmetric bilateral shape in the cells surrounding the KV cells at 4-6 ss, rather than in the KV cells themselves. Expression of *tbx16* and *ntl* overlaps in the vicinity of the KV and likely regulates peri-KV *spaw* expression, as demonstrated by the absence or delay of *spaw* expression when both genes are absent (Gourronc et al., 2007).

During somite stages 10-12, *spaw* expression becomes asymmetrical in the left LPM (Long et al., 2003) due to the release of Dand5 inhibition via *dand5* left-sided downregulation (Lopes et al., 2010; Maerker et al., 2021b). Gdf3 (Vg1/Dvr1) is essential for Nodal signaling in the LPM, as knockdown of Gdf3 reduces the expression of *spaw* (Peterson et al., 2013), with Spaw and Gdf3 known to form heterodimers (Bisgrove et al., 2017; Montague and Schier, 2017; Pelliccia et al., 2017; Montague et al., 2018). Spaw induces its own amplification and expression through a positive feedback, starting at the posterior end of the LPM and spreading along the AP axis in a posterior-to-anterior direction, covering the entire left side of the LPM in a distinct stripe of expression until 22 ss (Wang and Yost, 2008).

The expression of l*efty* genes, which restrict the extent of Nodal signaling, is also activated by Spaw. The expression of *lefty1* and *lefty2* is lost in *spaw* morphants and mutants (Long et al.,

2003; Montague et al. 2018). *lefty1* is expressed in the midline at approximately 10 ss, before *spaw* expression in the left LPM. It starts propagating anteriorly at 15 ss, reaching the anterior end of the midline at approximately 20-22 ss (Wang and Yost, 2008). In the absence of *lefty1*, *spaw* is expressed in both the left and right LPM, but left LPM *spaw* expression precedes the right even in a premature manner compared to WT embryos (Montague et al., 2018). This suggests that Spaw later leaks to the right side, stimulating its own expression in the right LPM (Long, 2003; Montague et al., 2018). Furthermore, in *lefty1* mutants, *spaw* expression was already present around the KV 1-2 hours earlier than in WT embryos, indicating that premature LPM *spaw* expression was caused by earlier initiation of *spaw* (Montague et al., 2018). Thus, Lefty1 regulates Spaw activity, both spatially and temporally.

The absence of *dand5* expression also leads to premature *spaw* initiation in the LPM but without a left bias, which indicates cooperation with Lefty1 to spatially and temporally restrict Spaw (Wang and Yost, 2008; Montague et al., 2018).

In contrast to other vertebrates, which express *lefty2* throughout the left LPM (Meno et al., 1996; Cheng et al., 2000), in zebrafish, *lefty2* is only expressed in the left cardiac field (Long et al., 2003), preventing *spaw* expression from propagating from the anterior left LPM to the anterior right LPM and then spreading to the posterior region (Lenhart et al., 2011). Therefore, Lefty2 acts as an anterior barrier during the left-sided Spaw constrain.

The left-sided constrain of Spaw activity is also achieved by cooperation of additional players. Explicitly, it is suggested that BMP signaling limits the response of cells in the LPM to Nodal by setting a threshold for Nodal activation that low concentrations of Spaw cannot overcome. Thus, BMP signaling acts as a gatekeeper, ensuring that Nodal signaling is only activated in the left sided LPM, where Spaw levels are consistently higher (Lenhart et al., 2011). On the other hand, the physical interaction between Lefty1 and the zebrafish EGF-CFC receptor Oep in the midline results in a partial repression of Lefty1. This leads to a decrease in the amount of free Lefty1, which in turn reduces its ability to repress Nodal signaling in the LPM. As a result, the threshold for Spaw to activate the Nodal cascade in the LPM is lowered (Burdine and Grimes, 2016). In addition, Smith et al., (2011) showed that BMP signaling also regulates *lefty1* expression. Maintaining *lefty1* expression in the midline requires both Spaw and BMP activities in two mechanistically parallel ways. More precisely, the authors showed that even in the absence of Nodal activity, ectopic BMP signaling can induce *lefty1* expression in the midline when BMP

signaling is sufficiently high. Therefore, suggesting that *lefty1* expression in the midline is initiated by BMP signaling independent of Spaw activity.

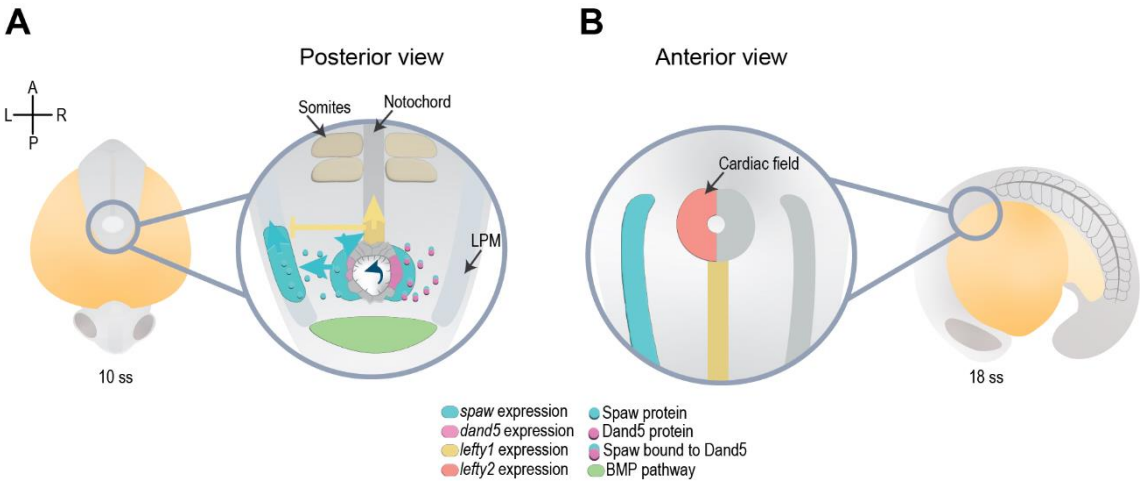

Figure 1.5. Nodal pathway components during LR axis symmetry breaking and patterning in zebrafish embryos. **(A)** Initially, *spaw* is expressed symmetrically around the Kupffer's vesicle (KV) and the expression of *dand5* becomes asymmetric in the KV cells, decreasing on the left side in a flow-dependent manner. Dand5 binds to Spaw and inhibits its diffusion to the right lateral plate mesoderm (LPM). This leads to the asymmetric expression of *spaw* and its downstream targets. Spaw induces its own expression in the left LPM and its antagonist, *lefty1*, which is already expressed at the posterior notochord. *spaw* expression propagates posteriorly and then anteriorly in the LPM, along with *lefty1* that extends anteriorly in the notochord. Both *spaw* and *lefty1* are expressed throughout the LPM and notochord, respectively. BMP signaling in the posterior tailbud domain represses Nodal activation. **(B)** As *spaw* reaches the anterior region, Nodal antagonism by Lefty2 in the left cardiac field blocks its transfer to the right LPM. Abbreviations: A, Anterior; P, Posterior; L, Left; R, Right.

Although the nodal pathway in the LPM is well established as playing a crucial role in asymmetry and is conserved among vertebrates, the mechanisms that control asymmetric organogenesis remain poorly characterized. This lack of understanding presents a significant challenge in LR patterning. Moreover, recent studies in zebrafish have proposed alternative pathways and factors that may also influence heart and gut LR morphogenesis in addition to the Nodal-Pitx2 signaling axis, further highlighting the need for a deeper understanding of the mechanisms that regulate asymmetric organogenesis.

Pitx2, a conserved homeodomain transcription factor, is a target of nodal signalling (Yoshioka et al., 1998); hence, *pitx2* expression in the left LPM is dependent on Spaw and mimics *spaw* propagation along the AP axis (Wang and Yost, 2008). Although mutations in *spaw* can modify LR asymmetry in the heart (Montague et al., 2018) and gut (Noël et al., 2013), it was found that

in zebrafish, *pitx2* is not required for normal heart and gut laterality (Ji et al., 2016). This finding contrasts with knowledge from other vertebrates, such as the mouse, in which *pitx2* expression translates into the proper orientation of asymmetric organs (Piedra et al., 1998; Yonei-tamura et al., 1998; Campione et al., 1999). Ji et al., (2016) suggested that *elovl6*, a fatty acid elongase, expressed at the left side of the LPM around 18 ss, dependent on KV function and Nodal signalling, may be involved in organ laterality in zebrafish instead of *pitx2*. However, further studies are needed to investigate the extent of Elovl6 contribution to asymmetric organogenesis through gain/loss-of-function experiments in zebrafish.

BMP signaling has also been found to trigger the activation of Prrx1a, an EMT inducer, and *snail*-related gene, in the LPM, and the activation of this pathway appears to be stronger on the right side of the LPM. Prrx1a-positive cells undergo EMT via an actomyosin-dependent mechanism, leading to displacement of the posterior cardiac pole towards the left side (Ocaña et al., 2017). In the study, Ocaña et al., (2017) demonstrated that the downregulation of *prrx1a* led to central heart development in embryos. Furthermore, Rago et al., (2019) showed that while *prrx1a* transcription in the LPM is symmetrical on both sides during development, its transient right-sided expression is regulated through a post-transcriptional mechanism that involves miRNAs induced by Nodal within a specific period. However, Tessadori et al., (2020) reported that different *prrx1a* mutants exhibited normal heart development and that the absence of cardiac phenotypes was not due to compensation by *prrx1b* or the maternal contribution of *prrx1a*. The laterality phenotypes previously observed were likely off-target effects produced by the morpholinos. On the other hand, Castroviejo et al., (2020) refuted that newly generated *prrx1a*-crispant embryos still showed the same heart phenotype and that other EMT transcription factors, such as *twist1a* and *snail1b*-crispants, which also exhibited mesocardia, suggesting compensatory interactions. Consequently, further research is needed to fully understand the role of *prrx1a* in zebrafish LR cardiac development.

Other partial laterality phenotypes are worth investigating; according to Derrick et al., (2022), *MZjnk3* mutant embryos, a proposed downstream component of PCP signalling, can establish a normal left-right axis and midline, and show no significant deviation in heart jogging. However, a significant proportion of these embryos develop bilateral guts, similar to the phenotype observed in *deltaD* (Lopes et al., 2010) and *lamb1a* (Hochgreb-Hägele et al., 2013) mutants. These findings suggest that a KV-dependent, *spaw*-independent mechanism may be at play in promoting gut looping morphogenesis.

Grimes et al., (2020) proposed a mechanism where left jogging increases the effectiveness of the heart's intrinsic ability to generate dextral loops, even without Spaw asymmetries. The positioning of the heart tube to the left of the midline initially, driven by left-sided Nodal/Spaw signals, enhances the robustness of dextral looping. Nodal-independent mechanisms proposed to control heart looping include actin cytoskeletal dynamics. This is supported by observations of cultured explanted hearts, which maintain correct chiral looping behavior even without the influence of Spaw signals. Furthermore, directional heart looping is maintained in most embryos through a tissue-intrinsic mechanism that involves actin polymerization and myosin II activity (Noël et al., 2013). Nodal-independent mechanisms on cardiac looping have also been reported. Specifically, Lombardo et al.(2019) showed that heart tube bending depends on BMP signaling, the activity of which is stronger at the upper AVC than at the lower AVC, producing a lopsided distribution of BMP signaling. This seems to induce myocardial cells to assume conical and bottlenecked forms, which aid in the bending of the heart during S-looping.

As well, according to a recent study by Kidokoro et al., (2022), Nodal signaling was reported play a crucial role in heart rotation by boosting cell rearrangement and shape change in the peripheral region of heart primordia. This results in an asymmetric deformation of the left and right halves of the heart tube, creating critical asymmetry during heart formation. The study found that knocking down Spaw only reduced convergence in the peripheral region of the left primordium, indicating that Nodal signaling does not trigger different types of morphogenesis but instead modulates the magnitude of morphological changes.

Symmetry *vs.* asymmetry: LR patterning and zebrafish somite formation

Symmetrical features of the body, such as the muscles, skeleton, and limbs, surround and support asymmetrical internal organs. During embryonic development, the precursors of symmetric somites and limb buds are formed in an embryo that is instructed for asymmetric patterning via the LR pathway. For instance, somites develop from the presomitic mesoderm (PSM), which is situated between the LRO and the LPM; therefore, owing to their proximity, they may be subjected to asymmetric signals. However, symmetrical and asymmetrical structures are formed using shared molecular cues, suggesting that protective mechanisms exist to shield the symmetric structures from the asymmetric signals (Grimes, 2019).

The somites are a critical morphological feature of chordate development, comprising paired epithelial blocks of the mesoderm on either side of the neural tube. In vertebrates, somites are crucial precursor tissues for the developing vertebrae, ribs, skeletal muscles, and dermis associated with each vertebra (Dequéant and Pourquié, 2008), forming the developmental basis of segmented adult bodies. Somitogenesis is the process by which an unsegmented PSM forms somites and occurs bilaterally symmetrically, starting from the anterior region and progressing posteriorly until all the PSM is segmented.

The combined segmentation clock and wavefront mechanism (Cooke and Zeeman, 1976) is the prevailing conceptual framework for somitogenesis regulation. In zebrafish, extensive work by many groups has studied the segmentation clock that comprises intracellular genetic oscillators. The Notch target genes *her1* and *her7* generate oscillations through a delayed negative feedback loop, in which their own protein products directly inhibit their own expression and the Notch ligand Delta. Thus, Notch signaling synchronizes oscillations between neighboring cells through Delta-Notch coupling, thereby minimizing the effects of noise to maintain a consistent oscillation (Holley et al., 2000; Jiang et al., 2000; Lewis, 2003; Horikawa et al., 2006; Lewis et al., 2009; Delaune et al., 2012; Keskin et al., 2018).

The wavefront represents the spatial location in the PSM where clock oscillations stop and segment boundary positions are established; subsequently, regression of the wavefront towards the posterior side of the PSM occurs as new somites form (Cooke and Zeeman, 1976). The size of each somite is determined by the number of PSM cells that pass through the determination front during each cycle of the segmentation clock. Somites form bilaterally symmetrically, with a combination of clock period and wavefront velocity regulating the length of each somite. The three morphogen gradients in the PSM that control wavefront velocity are FGF, Wnt, and RA (Oates et al., 2012; Mallo, 2016; Naganathan and Oates, 2020).

Both FGF and Wnt morphogens create a posterior-to-anterior gradient, with higher expression levels on the posterior side. Evidence has shown that FGF signaling activity is maximal in the tailbud and decreases anteriorly, in accordance with the expression of *fgf3* and *fgf8* ligands (Sawada et al., 2001). Wnt signaling activity is also maximal in the tailbud and decreases anteriorly, with overlapping expression of *wnt3a* and *wnt8* ligands (Bajard et al., 2014). Decreasing the activity of FGF or Wnt signaling leads to an increase in somite length, whereas increasing their activity corresponds to a decrease in somite length (Sawada et al., 2001; Dequéant and Pourquié, 2008). In contrast, RA forms an inverse gradient from anterior to posterior as the production of RA peaks in the somites and anterior PSM and decreases

posteriorly (Kawakami et al., 2005) as the catabolic enzyme *cyp26a1*, which breaks down RA, holds greater expression levels in the tailbud and decreases anteriorly (Mandal et al., 2013; Shimozono et al., 2013). Altering RA levels also changes somite length, with the knockdown of *cyp26a1* leading to smaller somites (Echeverri and Oates, 2007).

Furthermore, it has been suggested that RA signals counteract a desynchronizing effect on somites from the LR pathway (Kawakami et al., 2005; Vermot and Pourquié, 2005). In zebrafish, *raldh2* (*aldehyde dehydrogenase 1, A2*) morphants and *nls* mutants (lacking RALDH2 activity) showed that lack of RA signaling disrupts the synchronicity of somite formation by increasing the number of latest-formed somites on the left side between the 6^{th} and 13^{th} somites (Kawakami et al., 2005). The timing of asymmetric somite formation in the absence of RA signaling is consistent with the time at which LR cues are transmitted to the LPM (Long, 2003). Kawakami et al. indicated that the asymmetric phenotype was due to the desynchronization of Notch activity on the left side, where cyclic genes, such as *deltaC*, *her1*, and *her7*, were out of phase between the left and right sides and showed an extension of *fgf8* expression on the right side (Kawakami et al., 2005). While the exact mechanism by which RA buffers asymmetric cues remains unclear, studies conducted in mice have shown that the expansion of *Fgf8* expression in *Rere* mutants lacking the transcriptional co-regulator RERE may be a direct effect of RA. This is because the *Fgf8* locus contains an RA-responsive element, at which RERE localizes in the absence of RA and acts as a co-repressor (Kumar and Duester, 2014).

In addition, previous studies have demonstrated that suppressor of hairless (*su(H)*) genes, which encode critical transcriptional mediators of Notch signaling, are required for the expression of *cyp26a1*. This gene is essential for cyclic bilaterality of *deltaC* expression, and increasing levels of exogenous RA can induce asymmetries in cyclic gene expression in embryos that lack RA degradation. Consequently, it has been suggested that Notch signaling via Su(H) may play an unexpected role upstream of RA-dependent mechanisms that both generate the determination front and buffer LR asymmetrical signaling cues (Echeverri and Oates, 2007). Furthermore, targeting both zebrafish *su(H)* genes during the early embryo led to the randomization of heart positioning (Echeverri and Oates, 2007). In fact, Notch signaling has been shown to be involved in LR development in zebrafish. For instance, *deltaD*$^{-/-}$ embryos have shorter cilia, which leads to reduced flow in the KV (Lopes et al., 2010). These results are consistent with the observation that early inhibition of Notch signaling during epiboly causes visceral asymmetries, whereas later treatment during segmentation stages leads to somitic defects in embryos with normal *situs*, as LR asymmetry has already been established in the LPM (Kawakami et al., 2005), showing that

Notch involvement on LR patterning occurs prior to disruption of symmetrical gene oscillation during somitogenesis.

Furthermore, the transcription factor Dmrt2 is involved in both somitogenesis and LR patterning of visceral organs in zebrafish and *Xenopus*. Knockdown of Dmrt2a in zebrafish resulted in desynchronization of *deltaC*, *her1*, and *her7* expression, as well as randomization of *spaw* and *pitx2* expression in the LPM, leading to heart position defects (Saúde et al., 2005). Dmrt2a is expressed on the anterior side of the KV (Lourenço et al., 2010), and its precise expression is controlled by the RNA-binding protein Celf1. Celf1 promotes *dmrt2a* mRNA decay by interacting with the 3'UTR of *dmrt2a* mRNA. Overexpression of *celf1* reduced the levels of *dmrt2a* mRNA, leading to asymmetric somitogenesis and laterality defects (Matsui et al., 2012). However, the mechanistic details of how Celf1 controls symmetry and asymmetry remain unknown. In Xenopus, Dmrt2 regulates the formation of ciliated LRO and sensory LRO cells, as well as the patterning of the paraxial mesoderm. Dmrt2 is required for *foxj1* expression for ciliogenesis in the LRO, and it is essential for sensory LRO formation due to its function in paraxial mesodermal patterning. In embryos where *dmrt2* was suppressed, there was a misregulation of the myogenic transcription factors *tbx6* and *myf5* during the early gastrula stages. This was followed by a misspecification of sensory LRO cells during neurula stages (Tingler et al., 2022). However, there were no reported asymmetry effects on somites in Xenopus (Tingler et al., 2022) and mouse embryos lacking Dmrt2 do not exhibit any LR defects (Lourenço et al., 2010).

Despite the presence of buffering mechanisms to shield somite precursors from LR cues originating in the LRO (Kawakami et al., 2005) and the Notch signaling mechanism to counteract the significant genetic noise during somite specification via the segmentation clock (Horikawa et al., 2006; Keskin et al., 2018), several somite pairs initially form LR asymmetrically in zebrafish, with variations in position and length (Naganathan et al., 2022). These imprecisions are subsequently corrected by the somite surface tension (Naganathan et al., 2022). This highlights the importance of several known and possibly unknown mechanisms in ensuring symmetry in symmetrical structures at various checkpoints during embryo patterning.

Somite precursors originate from a dorsal tailbud population of neuromesodermal progenitor cells (Kanki and Ho, 1997; Martin and Kimelman, 2012) that commit to the mesoderm fate, move ventrally to the maturation zone (MZ), migrate (Kanki and Ho 1997; Griffin and Kimelman 2002; Fior et al. 2012; Manning and Kimelman 2015), and generate cell flows towards the PSM, where cell motility decreases to form the somites (Kanki and Ho, 1997; Lawton et al., 2013; Banavar et

al., 2021). However, the existence of LR asymmetries in somite precursors at cellular resolution during somite formation *in vivo* has not been previously reported.

Aims

In this study, our objective was to investigate the behavior of cells located in close proximity to zebrafish LRO, which might be exposed to asymmetric signals. Our aim was to gain insights into their behavior and the impact on zebrafish embryonic development by examining how these cells respond to the LRO signals. Furthermore, we sought to analyze the spatial and temporal dynamics of the left-sided downregulation of *dand5*, which is the first asymmetric gene known to date and it is already asymmetric in the KV cells . Our findings will contribute to a better understanding of the complex processes involved in zebrafish embryonic development, such as the interplay between LR signals and adjacent symmetric structures and may have implications for the study of other vertebrate developmental systems.

In Chapter 2 of this PhD thesis, our objective was to investigate the behavior of a specific population of tailbud cells located near the KV. To achieve this goal, we used live imaging techniques and a transgenic line that allowed us to label a mesoderm tailbud migratory population, enabling us to track their migration patterns. To delineate the fate of these cells, which exhibit asymmetric behavior, we traced the Kaede-photoconverted cells and recorded their positions. Subsequently, we assessed the impact of LR asymmetric signals generated at the KV on the asymmetric behaviors of these cells using mutant embryos with absent *dand5* expression and examined how their behaviors and fate were altered.

In Chapter 3, we sought to test the role of the KV as an organ, and as a mechanical presence, by generating embryos lacking the whole KV and observing the consequent behavior of the referred tailbud adjacent cells. For this section we used laser ablation of KV cells during DFC stages.

In Chapter 4, our objective was to implement a high-resolution *in situ* hybridization technique in the KV to analyze *dand5* mRNA transcripts both spatially and temporally. Our aim was to obtain a more precise quantification of the number of *dand5* transcripts over time and correlate this cell resolution information with the current understanding of cilia-driven flow and the consequent *dand5* downregulation.

References

Ablooglu, A. J., Tkachenko, E., Kang, J., and Shattil, S. J. (2010). Integrin αV is necessary for gastrulation movements that regulate vertebrate body asymmetry. Development 137, 3449–3458.

Alten, L., Schuster-Gossler, K., Beckers, A., Groos, S., Ulmer, B., Hegermann, J., et al. (2012). Differential regulation of node formation, nodal ciliogenesis and cilia positioning by Noto and Foxj1. Development 139, 1276–1284. doi: 10.1242/dev.072728.

Amack, J. D., Wang, X., and Yost, H. J. (2007). Two T-box genes play independent and cooperative roles to regulate morphogenesis of ciliated Kupffer's vesicle in zebrafish. Developmental biology 310, 196–210.

Amack, J. D., and Yost, H. J. (2004). The T box transcription factor no tail in ciliated cells controls zebrafish left-right asymmetry. Current biology 14, 685–690.

Andersson, O., Bertolino, P., and Ibáñez, C. F. (2007). Distinct and cooperative roles of mammalian Vg1 homologs GDF1 and GDF3 during early embryonic development. Developmental Biology 311, 500–511. doi: https://doi.org/10.1016/j.ydbio.2007.08.060.

Arrington, C. B., Peterson, A. G., and Yost, H. J. (2013). Sdc2 and Tbx16 regulate Fgf2-dependent epithelial cell morphogenesis in the ciliated organ of asymmetry. Development 140, 4102–4109. doi: 10.1242/dev.096933.

Attisano, L., and Wrana, J. L. (2002). Signal transduction by the TGF-β superfamily. Science 296, 1646–1647.

Aykul, S., Ni, W., Mutatu, W., and Martinez-Hackert, E. (2015). Human Cerberus prevents nodal-receptor binding, inhibits nodal signaling, and suppresses nodal-mediated phenotypes. PLoS One 10, e0114954.

Babb, S. G., and Marrs, J. A. (2004). E-cadherin regulates cell movements and tissue formation in early zebrafish embryos. Developmental dynamics: an official publication of the American Association of Anatomists 230, 263–277.

Bachiller, D., Agius, E., Kemp, C., Borges, A. C., Marques, S., Piccolo, S., et al. (2000). Cerberus-like Is a Secreted BMP and Nodal Antagonist Not Essential for Mouse Development. 270, 265–270.

Bajard, L., Morelli, L. G., Ares, S., Pécréaux, J., Jülicher, F., and Oates, A. C. (2014). Wnt-regulated dynamics of positional information in zebrafish somitogenesis. Development 141, 1381–1391.

Bangs, F., Antonio, N., Thongnuek, P., Welten, M., Davey, M. G., and Briscoe, J. (2011). Generation of mice with functional inactivation of talpid3 , a gene first identified in chicken. 3272, 3261–3272. doi: 10.1242/dev.063602.

Beck, S., Le Good, J. A., Guzman, M., Haim, N. Ben, Roy, K., Beermann, F., et al. (2002). Extraembryonic proteases regulate Nodal signalling during gastrulation. Nature cell biology 4, 981–985.

Bell, E., Muñoz-Sanjuán, I., Altmann, C. R., Vonica, A., and Brivanlou, A. H. (2003). Cell fate specification and competence by Coco, a maternal BMP, TGFβand Wnt inhibitor.

Bisgrove, B. W., Snarr, B. S., Emrazian, A., and Yost, H. J. (2005). Polaris and Polycystin-2 in dorsal forerunner cells and Kupffer's vesicle are required for specification of the zebrafish left-right axis. Developmental Biology 287, 274–288. doi: 10.1016/j.ydbio.2005.08.047.

Bisgrove, B. W., Su, Y.-C., and Yost, H. J. (2017). Maternal Gdf3 is an obligatory cofactor in Nodal signaling for embryonic axis formation in zebrafish. Elife 6, e28534.

Blum, M., Feistel, K., Thumberger, T., and Schweickert, A. (2014). The evolution and conservation of left-right patterning mechanisms. Development 141, 1603–1613. doi: 10.1242/dev.100560.

Blum, M., and Ott, T. (2018). Animal left–right asymmetry. Current Biology 28, R301–R304. doi: 10.1016/j.cub.2018.02.073.

Blum, M., and Ott, T. (2019). Mechanical strain, novel genes and evolutionary insights: news from the frog left-right organizer. Current opinion in genetics & development 56, 8–14.

Borovina, A., Superina, S., Voskas, D., and Ciruna, B. (2010). Vangl2 directs the posterior tilting and asymmetric localization of motile primary cilia. Nature cell biology 12, 407–412.

Boskovski, M. T., Yuan, S., Pedersen, N. B., Goth, C. K., Makova, S., Clausen, H., et al. (2013). The heterotaxy gene GALNT11 glycosylates Notch to orchestrate cilia type and laterality. Nature 504, 456–459. doi: 10.1038/nature12723.

Branford, W. W., Essner, J. J., and Yost, H. J. (2000). Regulation of gut and heart left–right asymmetry by context-dependent interactions between Xenopus lefty and BMP4 signaling. Developmental biology 223, 291–306.

Burdine, R. D., and Grimes, D. T. (2016). Antagonistic interactions in the zebrafish midline prior to the emergence of asymmetric gene expression are important for left–right patterning. Philosophical Transactions of the Royal Society B: Biological Sciences. doi: 10.1098/rstb.2015.0402.

Campione, M., Steinbeisser, H., Schweickert, A., Deissler, K., Bebber, F. Van, Lowe, L. A., et al. (1999). The homeobox gene Pitx2 : mediator of asymmetric left-right signaling in vertebrate heart and gut looping. 1234, 1225–1234.

Cartwright, J. H. E., Piro, N., Piro, O., and Tuval, I. (2007). Embryonic nodal flow and the dynamics of nodal vesicular parcels. Journal of the Royal Society, Interface / the Royal Society 4, 49–55. doi: 10.1098/rsif.2006.0155.

Cartwright, J. H. E., Piro, O., and Tuval, I. (2004). Fluid-dynamical basis of the embryonic development of left-right asymmetry in vertebrates. Proceedings of the National Academy of Sciences 101, 7234–7239. doi: 10.1073/pnas.0402001101.

Castroviejo, N., Ocaña, O. H., Rago, L., Coskun, H., Arcas, A., Galcerán, J., et al. (2020). Reply to: Zebrafish prrx1a mutants have normal hearts. Nature 585, E17–E19.

Chen, C., and Shen, M. M. (2004). Two modes by which Lefty proteins inhibit nodal signaling. Current Biology 14, 618–624.

Cheng, A. M. S., Thisse, B., Thisse, C., and Wright, C. V. E. (2000). The lefty-related factor Xatv acts as a feedback inhibitor of Nodal signaling in mesoderm induction and L-R axis development in Xenopus. 1061, 1049–1061.

Cheng, S. K., Olale, F., Brivanlou, A. H., and Schier, A. F. (2004). Lefty blocks a subset of TGFβ signals by antagonizing EGF-CFC coreceptors. PLoS Biology 2. doi: 10.1371/journal.pbio.0020030.

Choi, W.-Y., Giraldez, A. J., and Schier, A. F. (2007). Target protectors reveal dampening and balancing of Nodal agonist and antagonist by miR-430. Science 318, 271–274.

Collignon, J., Varlet, I., and Robertson, E. J. (1996). Relationship between asymmetric nodal expression and the direction of embryonic turning. Nature 381, 155–158. doi: 10.1038/381155a0.

Compagnon, J., Barone, V., Rajshekar, S., Kottmeier, R., Pranjic-Ferscha, K., Behrndt, M., et al. (2014). The notochord breaks bilateral symmetry by controlling cell shapes in the zebrafish laterality organ. Developmental cell 31, 774–783.

Cooke, J., and Zeeman, E. C. (1976). A clock and wavefront model for control of the number of repeated structures during animal morphogenesis. Journal of theoretical biology 58, 455–476.

Cooper, M. S., and D'amico, L. A. (1996). A cluster of noninvoluting endocytic cells at the margin of the zebrafish blastoderm marks the site of embryonic shield formation. Developmental biology 180, 184–198.

D'Amico, L. A., and Cooper, M. S. (1997). Spatially distinct domains of cell behavior in the zebrafish organizer region. Biochemistry and cell biology 75, 563–577.

Dasgupta, A., and Amack, J. D. (2016). Cilia in vertebrate left?right patterning. Philosophical Transactions of the Royal Society B: Biological Sciences 371, 20150410. doi: 10.1098/rstb.2015.0410.

Dasgupta, A., Merkel, M., Clark, M. J., Jacob, A. E., Dawson, J. E., Manning, M. L., et al. (2018). Cell volume changes contribute to epithelial morphogenesis in zebrafish Kupffer's vesicle. eLife 7, e30963. doi: 10.7554/eLife.30963.

Delaune, E. A., François, P., Shih, N. P., and Amacher, S. L. (2012). Single-cell-resolution imaging of the impact of Notch signaling and mitosis on segmentation clock dynamics. Developmental cell 23, 995–1005.

Dequéant, M.-L., and Pourquié, O. (2008). Segmental patterning of the vertebrate embryonic axis. Nature Reviews Genetics 9, 370–382. doi: 10.1038/nrg2320.

Derrick, C. J., Santos-Ledo, A., Eley, L., Paramita, I. A., Henderson, D. J., and Chaudhry, B. (2022). Sequential action of JNK genes establishes the embryonic left-right axis. Development 149, dev200136.

Djenoune, L., Mahamdeh, M., Truong, T. V, Nguyen, C. T., Fraser, S. E., Brueckner, M., et al. (2023). Cilia function as calcium-mediated mechanosensors that instruct left-right asymmetry. Science 379, 71–78.

Duldulao, N. A., Lee, S., and Sun, Z. (2009). Cilia localization is essential for in vivo functions of the Joubert syndrome protein Arl13b/Scorpion. Development 136, 4033–4042.

Dutta, S., Sriskanda, S., Boobalan, E., Alur, R. P., Elkahloun, A., and Brooks, B. P. (2015). nlz1 is required for cilia formation in zebrafish embryogenesis. Developmental Biology 406, 203–211. doi: https://doi.org/10.1016/j.ydbio.2015.08.019.

Echeverri, K., and Oates, A. C. (2007). Coordination of symmetric cyclic gene expression during somitogenesis by Suppressor of Hairless involves regulation of retinoic acid catabolism. Developmental biology 301, 388–403.

England, S. J., Campbell, P. C., Banerjee, S., Swanson, A. J., and Lewis, K. E. (2017). Identification and expression analysis of the complete family of zebrafish pkd genes. Frontiers in Cell and Developmental Biology 5, 5.

Esguerra, C. V, Nelles, L., Vermeire, L., Ibrahimi, A., Crawford, A. D., Derua, R., et al. (2007). Ttrap is an essential modulator of Smad3-dependent Nodal signaling during zebrafish gastrulation and left-right axis determination.

Essner, J. J., Amack, J. D., Nyholm, M. K., Harris, E. B., and Yost, H. J. (2005). Kupffer's vesicle is a ciliated organ of asymmetry in the zebrafish embryo that initiates left-right development of the brain, heart and gut. Development 132 (6), 1247–1260. doi: https://doi.org/10.1242/dev.01663.

Essner, J. J., Branford, W. W., Zhang, J., and Yost, H. J. (2000). Mesendoderm and left-right brain , heart and gut development are differentially regulated by pitx2 isoforms. 1093, 1081–1093.

Ferreira, R. R., and Vermot, J. (2017). The balancing roles of mechanical forces during left-right patterning and asymmetric morphogenesis. Mechanisms of Development 144, 71–80. doi: 10.1016/j.mod.2016.11.001.

Field, S., Riley, K.-L., Grimes, D. T., Hilton, H., Simon, M., Powles-Glover, N., et al. (2011). Pkd1l1 establishes left-right asymmetry and physically interacts with Pkd2. Development 138, 1131–1142. doi: 10.1242/dev.058149.

Fliegauf, M., Benzing, T., and Omran, H. (2007). When cilia go bad : cilia defects and ciliopathies. 8. doi: 10.1038/nrm2278.

Foley, S. F., van Vlijmen, H. W. T., Boynton, R. E., Adkins, H. B., Cheung, A. E., Singh, J., et al. (2003). The CRIPTO/FRL-1/CRYPTIC (CFC) domain of human Cripto: Functional and structural insights through disulfide structure analysis. European journal of biochemistry 270, 3610–3618.

Forrest, K., Barricella, A. C., Pohar, S. A., Hinman, A. M., and Amack, J. D. (2022). Understanding laterality disorders and the left-right organizer: Insights from zebrafish. Frontiers in cell and developmental biology 10, 1035513. doi: 10.3389/fcell.2022.1035513.

Francescatto, L., Rothschild, S. C., Myers, A. L., and Tombes, R. M. (2010). The activation of membrane targeted CaMK-II in the zebrafish Kupffer's vesicle is required for left-right asymmetry. Development 137, 2753–2762.

Fuerer, C., Nostro, M. C., and Constam, D. B. (2014). Nodal· Gdf1 heterodimers with bound prodomains enable serum-independent nodal signaling and endoderm differentiation. Journal of Biological Chemistry 289, 17854–17871.

Gabriel, G. C., and Lo, C. W. (2020). Left–right patterning in congenital heart disease beyond heterotaxy. American Journal of Medical Genetics Part C: Seminars in Medical Genetics 184, 90–96. doi: https://doi.org/10.1002/ajmg.c.31768.

Gokey, J. J., Ji, Y., Tay, H. G., Litts, B., and Amack, J. D. (2016). Kupffer's vesicle size threshold for robust left-right patterning of the zebrafish embryo. Developmental Dynamics 245, 22–33. doi: 10.1002/dvdy.24355.

Gourronc, F., Ahmad, N., Nedza, N., Eggleston, T., and Rebagliati, M. (2007). Nodal activity around Kupffer's vesicle depends on the T-box transcription factors notail and spadetail and on notch signaling. Developmental dynamics: an official publication of the American Association of Anatomists 236, 2131–2146.

Grande, C., and Patel, N. H. (2009). Nodal signalling is involved in left–right asymmetry in snails. Nature 457, 1007–1011.

Grimes, D. T. (2019). Making and breaking symmetry in development, growth and disease. doi: 10.1242/dev.170985.

Grimes, D. T., and Burdine, R. D. (2017). Left–right patterning: breaking symmetry to asymmetric morphogenesis. Trends in Genetics 33, 616–628.

Grimes, D. T., Patterson, V. L., Luna-Arvizu, G., Schottenfeld-Roames, J., Irons, Z. H., and Burdine, R. D. (2020). Left-right asymmetric heart jogging increases the robustness of dextral heart looping in zebrafish. Developmental biology 459, 79–86.

Gritsman, K., Zhang, J., Cheng, S., Heckscher, E., Talbot, W. S., and Schier, A. F. (1999). The EGF-CFC Protein One-Eyed Pinhead Is Essential for Nodal Signaling. 97, 121–132.

Gros, J., Feistel, K., Viebahn, C., Blum, M., and Tabin, C. J. (2009). Cell movements at Hensen's node establish left/right asymmetric gene expression in the chick. Science 324, 941–944.

Hamada, H., and Tam, P. (2020). Diversity of left-right symmetry breaking strategy in animals. F1000Research 9. doi: 10.12688/f1000research.21670.1.

Harrington, M. J., Hong, E., Fasanmi, O., and Brewster, R. (2007). Cadherin-mediated adhesion regulates posterior body formation. BMC Developmental Biology 7, 1–19.

Hashimoto, H., Rebagliati, M., Ahmad, N., Muraoka, O., Kurokawa, T., Hibi, M., et al. (2004). The Cerberus/Dan-family protein Charon is a negative regulator of Nodal signaling during left-right patterning in zebrafish. Development 131, 1741–1753. doi: 10.1242/dev.01070.

Hashimoto, M., Shinohara, K., Wang, J., Ikeuchi, S., Yoshiba, S., Meno, C., et al. (2010). Planar polarization of node cells determines the rotational axis of node cilia. Nature Cell Biology 12, 170–176. doi: 10.1038/ncb2020.

Hill, C. S. (2016). Transcriptional control by the SMADs. Cold Spring Harbor perspectives in biology 8, a022079.

Hill, C. S. (2018). Spatial and temporal control of NODAL signaling. Current Opinion in Cell Biology 51, 50–57. doi: https://doi.org/10.1016/j.ceb.2017.10.005.

Holley, S. A., Geisler, R., and Nüsslein-Volhard, C. (2000). Control of her1 expression during zebrafish somitogenesis by a delta-dependent oscillator and an independent wave-front activity. Genes & development 14, 1678–1690.

Horikawa, K., Ishimatsu, K., Yoshimoto, E., Kondo, S., and Takeda, H. (2006). Noise-resistant and synchronized oscillation of the segmentation clock. Nature 441, 719–723.

Inaki, M., Liu, J., and Matsuno, K. (2016). Cell chirality: its origin and roles in left–right asymmetric development. Philosophical Transactions of the Royal Society B: Biological Sciences 371, 20150403. doi: 10.1098/rstb.2015.0403.

Jacinto, R., Sampaio, P., Roxo-Rosa, M., Pestana, S., and Lopes, S. S. (2021). Pkd2 affects cilia length and impacts LR flow dynamics and dand5. Frontiers in Cell and Developmental Biology 9, 624531.

Jászai, J., Thamm, K., Karbanová, J., Janich, P., Fargeas, C. A., Huttner, W. B., et al. (2020). Prominins control ciliary length throughout the animal kingdom: New lessons from human prominin-1 and zebrafish prominin-3. Journal of Biological Chemistry 295, 6007–6022.

Ji, Y., Buel, S. M., and Amack, J. D. (2016). Mutations in zebrafish pitx2 model congenital malformations in Axenfeld-Rieger syndrome but do not disrupt left-right placement of visceral organs. Developmental Biology 416, 69–81. doi: 10.1016/j.ydbio.2016.06.010.

Jiang, D., Jiang, Z., Lu, D., Wang, X., Liang, H., Zhang, J., et al. (2019). Migrasomes provide regional cues for organ morphogenesis during zebrafish gastrulation. Nature Cell Biology 21, 966–977. doi: 10.1038/s41556-019-0358-6.

Jiang, Y.-J., Aerne, B. L., Smithers, L., Haddon, C., Ish-Horowicz, D., and Lewis, J. (2000). Notch signalling and the synchronization of the somite segmentation clock. Nature 408, 475–479.

Juan, T., Géminard, C., Coutelis, J., Cerezo, D., Polès, S., Noselli, S., et al. (2018). Myosin1D is an evolutionarily conserved regulator of animal left–right asymmetry. Nature Communications. doi: 10.1038/s41467-018-04284-8.

Kamura, K., Kobayashi, D., Uehara, Y., Koshida, S., Iijima, N., Kudo, A., et al. (2011). Pkd1l1 complexes with Pkd2 on motile cilia and functions to establish the left-right axis. Development 138, 1121–1129. doi: 10.1242/dev.058271.

Kawakami, Y., Raya, Á., Raya, R. M., Rodríguez-Esteban, C., and Belmonte, J. C. I. (2005). Retinoic acid signalling links left–right asymmetric patterning and bilaterally symmetric somitogenesis in the zebrafish embryo. Nature 435, 165–171. doi: 10.1038/nature03512.

Kennedy, M. P., Omran, H., Leigh, M. W., Dell, S., Morgan, L., Molina, P. L., et al. (2007). Congenital heart disease and other heterotaxic defects in a large cohort of patients with primary ciliary dyskinesia. Circulation 115, 2814–2821. doi: 10.1161/CIRCULATIONAHA.106.649038.

Keskin, S., Devakanmalai, G. S., Kwon, S. Bin, Vu, H. T., Hong, Q., Lee, Y. Y., et al. (2018). Noise in the vertebrate segmentation clock is boosted by time delays but tamed by notch signaling. Cell reports 23, 2175–2185.

Kidokoro, H., Saijoh, Y., and Schoenwolf, G. C. (2022). Nodal signaling regulates asymmetric cellular behaviors, driving clockwise rotation of the heart tube in zebrafish. Communications Biology 5, 996. doi: 10.1038/s42003-022-03826-7.

Kim, J., Bae, S., Lee, H. S., Park, J., and Kim, K. (2017). Claudin5a is required for proper inflation of Kupffer ' s vesicle lumen and organ laterality. 1–18.

Kim, J., Kim, H.-H., and Bae, S.-J. (2019). Akap12beta supports asymmetric heart development via modulating the Kupffer's vesicle formation in zebrafish. BMB reports 52, 526.

Kinoshita, N., Minshull, J., and Kirschner, M. W. (1995). The identification of two novel ligands of the FGF receptor by a yeast screening method and their activity in Xenopus development. Cell 83, 621–630.

Knowles, M. R., Daniels, L. A., Davis, S. D., Zariwala, M. A., and Leigh, M. W. (2013). Primary ciliary dyskinesia. Recent advances in diagnostics, genetics, and characterization of clinical disease. American journal of respiratory and critical care medicine 188, 913–922.

Koulen, P., Cai, Y., Geng, L., Maeda, Y., Nishimura, S., Witzgall, R., et al. (2002). Polycystin-2 is an intracellular calcium release channel. Nature cell biology 4, 191–197.

Kramer-Zucker, A. G., Olale, F., Haycraft, C. J., Yoder, B. K., Schier, A. F., and Drummond, I. A. (2005). Cilia-driven fluid flow in the zebrafish pronephros, brain and Kupffer's vesicle is required for normal organogenesis.

Kumar, S., and Duester, G. (2014). Retinoic acid controls body axis extension by directly repressing Fgf8 transcription. Development 141, 2972–2977.

Lee, J. D., and Anderson, K. V (2008). Morphogenesis of the node and notochord: The cellular basis for the establishment and maintenance of left–right asymmetry in the mouse. Developmental Dynamics 237, 3464–3476. doi: https://doi.org/10.1002/dvdy.21598.

Lenhart, K. F., Lin, S., Titus, T. A., Postlethwait, J. H., and Burdine, R. D. (2011). Two additional midline barriers function with midline lefty1 expression to maintain asymmetric Nodal signaling during left-right axis specification in zebrafish INTRODUCTION. 4410, 4405–4410. doi: 10.1242/dev.071092.

Levin, M., Johnson, R. L., Sterna, C. D., Kuehn, M., and Tabin, C. (1995). A molecular pathway determining left-right asymmetry in chick embryogenesis. Cell 82, 803–814. doi: 10.1016/0092-8674(95)90477-8.

Lewis, J. (2003). Autoinhibition with Transcriptional Delay: A Simple Mechanism for the Zebrafish Somitogenesis Oscillator. Current Biology 13, 1398–1408. doi: https://doi.org/10.1016/S0960-9822(03)00534-7.

Lewis, J., Hanisch, A., and Holder, M. (2009). Notch signaling, the segmentation clock, and the patterning of vertebrate somites. Journal of biology 8, 1–7.

Li, J., Gao, F., Zhao, Y., He, L., Huang, Y., Yang, X., et al. (2018). Zebrafish znfl1s regulate left-right asymmetry patterning through controlling the expression of fgfr1a. Journal of Cellular Physiology, 1–9. doi: 10.1002/jcp.27564.

Li, Y., Yagi, H., Onuoha, E. O., Damerla, R. R., Francis, R., Furutani, Y., et al. (2016). DNAH6 and Its Interactions with PCD Genes in Heterotaxy and Primary Ciliary Dyskinesia. PLoS Genetics 12, 1–20. doi: 10.1371/journal.pgen.1005821.

Lin, A. E., Ticho, B. S., Houde, K., Westgate, M.-N., and Holmes, L. B. (2000). Heterotaxy: Associated conditions and hospital-based prevalence in newborns. Genetics in Medicine 2, 157–172. doi: 10.1097/00125817-200005000-00002.

Lin, C. R., Kioussi, C., O'Connell, S., Briata, P., Szeto, D., Liu, F., et al. (1999). Pitx2 regulates lung asymmetry, cardiac positioning and pituitary and tooth morphogenesis. Nature 401, 279–282. doi: 10.1038/45803.

Lin, C., Tsai, M., Liu, Y., Lu, Y., Chen, Y., Lai, Y., et al. (2017). Klf8 regulates left-right asymmetric patterning through modulation of Kupffer ' s vesicle morphogenesis and spaw expression. 1–14. doi: 10.1186/s12929-017-0351-y.

Lin, X., and Xu, X. (2009). Distinct functions of Wnt/β-catenin signaling in KV development and cardiac asymmetry.

Little, R. B., and Norris, D. P. (2021). Right, left and cilia: How asymmetry is established. Seminars in Cell & Developmental Biology 110, 11–18. doi: https://doi.org/10.1016/j.semcdb.2020.06.003.

Logan, M., Pagán-Westphal, S. M., Smith, D. M., Paganessi, L., and Tabin, C. J. (1998). The Transcription Factor Pitx2 Mediates Situs-Specific Morphogenesis in Response to Left-Right Asymmetric Signals. Cell 94, 307–317. doi: https://doi.org/10.1016/S0092-8674(00)81474-9.

Lombardo, V. A., Heise, M., Moghtadaei, M., Bornhorst, D., Männer, J., and Abdelilah-Seyfried, S. (2019). Morphogenetic control of zebrafish cardiac looping by Bmp signaling. Development 146, dev180091.

Long, S., Ahmad, N., and Rebagliati, M. (2003). The zebrafish nodal-related gene southpaw is required for visceral and diencephalic left-right asymmetry. Development 130, 2303–2316.

Lopes, S. S., Lourenco, R., Pacheco, L., Moreno, N., Kreiling, J., and Saude, L. (2010). Notch signalling regulates left-right asymmetry through ciliary length control. Development 137, 3625–3632. doi: 10.1242/dev.054452.

Lourenço, R., Lopes, S. S., and Saúde, L. (2010). Left-right function of dmrt2 genes is not conserved between zebrafish and mouse. PLoS One 5, e14438.

Lowe, L. A., Supp, D. M., Sampath, K., Yokoyama, T., Wright, C. V. E., Potter, S. S., et al. (1996). Conserved left–right asymmetry of nodal expression and alterations in murine situs inversus. Nature 381, 158–161. doi: 10.1038/381158a0.

Lucas, J. S., Davis, S. D., Omran, H., and Shoemark, A. (2020). Primary ciliary dyskinesia in the genomics age. The Lancet Respiratory Medicine 8, 202–216. doi: https://doi.org/10.1016/S2213-2600(19)30374-1.

Ma, L., Li, Y., Peng, J., Wu, D., Zhao, X., Cui, Y., et al. (2015). Discovery of the migrasome, an organelle mediating release of cytoplasmic contents during cell migration. Cell research 25, 24–38.

Maerker, M., Getwan, M., Dowdle, M. E., McSheene, J. C., Gonzalez, V., Pelliccia, J. L., et al. (2021). Bicc1 and Dicer regulate left-right patterning through post-transcriptional control of the Nodal inhibitor Dand5. Nature Communications 12, 5482. doi: 10.1038/s41467-021-25464-z.

Mallo, M. (2016). Revisiting the involvement of signaling gradients in somitogenesis. FEBS Journal 283, 1430–1437. doi: 10.1111/febs.13622.

Mandal, A., Rydeen, A., Anderson, J., Sorrell, M. R. J., Zygmunt, T., Torres-Vázquez, J., et al. (2013). Transgenic retinoic acid sensor lines in zebrafish indicate regions of available embryonic retinoic acid. Developmental Dynamics 242, 989–1000.

Marques, S., Borges, A. C., Silva, A. C., Freitas, S., Cordenonsi, M., and Belo, J. A. (2004). The activity of the Nodal antagonist Cerl-2 in the mouse node is required for correct L/R body axis. Genes & development 18, 2342–2347.

Matsui, T., Sasaki, A., Akazawa, N., Otani, H., and Bessho, Y. (2012). Celf1 regulation of dmrt2a is required for somite symmetry and left-right patterning during zebrafish development. Development 139, 3553–3560.

Matsui, T., Thitamadee, S., Murata, T., Kakinuma, H., Nabetani, T., Hirabayashi, Y., et al. (2011). Canopy1, a positive feedback regulator of FGF signaling, controls progenitor cell clustering during Kupffer's vesicle organogenesis. Proceedings of the National Academy of Sciences 108, 9881–9886.

May-Simera, H. L., Kai, M., Hernandez, V., Osborn, D. P. S., Tada, M., and Beales, P. L. (2010). Bbs8, together with the planar cell polarity protein Vangl2, is required to establish left–right asymmetry in zebrafish. Developmental biology 345, 215–225.

McGrath, J., Somlo, S., Makova, S., Tian, X., and Brueckner, M. (2003). Two populations of node monocilia initiate left-right asymmetry in the mouse. Cell 114, 61–73. doi: 10.1016/S0092-8674(03)00511-7.

Meno, C., Saijoh, Y., Fujii, H., Ikeda, M., Yokoyama, T., Yokoyama, M., et al. (1996). Left–right asymmetric expression of the TGFβ-family member lefty in mouse embryos. Nature 381, 151–155. doi: 10.1038/381151a0.

Minegishi, K., Rothé, B., Komatsu, K. R., Ono, H., Ikawa, Y., Nishimura, H., et al. (2021). Fluid flow-induced left-right asymmetric decay of Dand5 mRNA in the mouse embryo requires a Bicc1-Ccr4 RNA degradation complex. Nature Communications 12, 4071. doi: 10.1038/s41467-021-24295-2.

Mizuno, K., Shiozawa, K., Katoh, T. A., Minegishi, K., Ide, T., Ikawa, Y., et al. (2023). Role of Ca2+ transients at the node of the mouse embryo in breaking of left-right symmetry. Science Advances 6, eaba1195. doi: 10.1126/sciadv.aba1195.

Montague, T. G., Gagnon, J. A., and Schier, A. F. (2018). Conserved regulation of Nodal-mediated left-right patterning in zebrafish and mouse. Development 145, dev171090.

Montague, T. G., and Schier, A. F. (2017). Vg1-Nodal heterodimers are the endogenous inducers of mesendoderm. Elife 6, e28183.

Morgan, D., Turnpenny, L., Goodship, J., Dai, W., Majumder, K., Matthews, L., et al. (1998). Inversin, a novel gene in the vertebrate left-right axis pathway, is partially deleted in the inv mouse. Nature Genetics 20, 149–156. doi: 10.1038/2450.

Naganathan, S. R., and Oates, A. C. (2020). Patterning and mechanics of somite boundaries in zebrafish embryos. Seminars in Cell & Developmental Biology 107, 170–178. doi: https://doi.org/10.1016/j.semcdb.2020.04.014.

Naganathan, S. R., Popović, M., and Oates, A. C. (2022). Left–right symmetry of zebrafish embryos requires somite surface tension. Nature 605, 516–521.

Nakamura, T., Saito, D., Kawasumi, A., Shinohara, K., Asai, Y., Takaoka, K., et al. (2012). Fluid flow and interlinked feedback loops establish left–right asymmetric decay of Cerl2 mRNA. Nature communications 3, 1322.

Namigai, E. K. O., Kenny, N. J., and Shimeld, S. M. (2014). Right across the tree of life: The evolution of left–right asymmetry in the Bilateria. genesis 52, 458–470. doi: https://doi.org/10.1002/dvg.22748.

Nauli, S. M., Alenghat, F. J., Luo, Y., Williams, E., Vassilev, P., Li, X., et al. (2003). Polycystins 1 and 2 mediate mechanosensation in the primary cilium of kidney cells. Nature genetics 33, 129–137.

Navis, A., Marjoram, L., and Bagnat, M. (2013). Cftr controls lumen expansion and function of Kupffer ' s vesicle in zebrafish. 1712, 1703–1712. doi: 10.1242/dev.091819.

Neugebauer, J. M., Amack, J. D., Peterson, A. G., Bisgrove, B. W., and Yost, H. J. (2009). FGF signalling during embryo development regulates cilia length in diverse epithelia. Nature 458, 651–654.

Noël, E. S., Verhoeven, M., Lagendijk, A. K., Tessadori, F., Smith, K., Choorapoikayil, S., et al. (2013). A Nodal-independent and tissue-intrinsic mechanism controls heart-looping chirality. Nature communications 4, 2754.

Nolan, K., and Thompson, T. B. (2014). The DAN family: Modulators of TGF-β signaling and beyond. Protein Science 23, 999–1012. doi: https://doi.org/10.1002/pro.2485.

Nonaka, S., Shiratori, H., Saijoh, Y., and Hamada, H. (2002). Determination of left–right patterning of the mouse embryo by artificial nodal flow. Nature 418, 96–99. doi: 10.1038/nature00849.

Nonaka, S., Tanaka, Y., Okada, Y., Takeda, S., Harada, A., Kanai, Y., et al. (1998). Randomization of Left–Right Asymmetry due to Loss of Nodal Cilia Generating Leftward Flow of Extraembryonic Fluid in Mice Lacking KIF3B Motor Protein. Cell 95, 829–837. doi: https://doi.org/10.1016/S0092-8674(00)81705-5.

Nonaka, S., Yoshiba, S., Watanabe, D., Ikeuchi, S., Goto, T., Marshall, W. F., et al. (2005). De novo formation of left-right asymmetry by posterior tilt of nodal cilia. PLoS Biology 3. doi: 10.1371/journal.pbio.0030268.

Nöthe-Menchen, T., Wallmeier, J., Pennekamp, P., Höben, I. M., Olbrich, H., Loges, N. T., et al. (2019). Randomization of Left-Right Asymmetry and Congenital Heart Defects. Circulation: Genomic and Precision Medicine 12, e002686. doi: 10.1161/CIRCGEN.119.002686.

Oates, A. C., Morelli, L. G., and Ares, S. (2012). Patterning embryos with oscillations: structure, function and dynamics of the vertebrate segmentation clock. Development 139, 625–639.

Ocaña, O. H., Coskun, H., Minguillón, C., Murawala, P., Tanaka, E. M., Galcerán, J., et al. (2017). A right-handed signalling pathway drives heart looping in vertebrates. Nature 549, 86–90. doi: 10.1038/nature23454.

Okada, Y., Nonaka, S., Tanaka, Y., Saijoh, Y., Hamada, H., and Hirokawa, N. (1999). Abnormal Nodal Flow Precedes Situs Inversus in iv and inv mice. Molecular Cell 4, 459–468. doi: https://doi.org/10.1016/S1097-2765(00)80197-5.

Okada, Y., Takeda, S., Tanaka, Y., Belmonte, J. C. I., and Hirokawa, N. (2005). Mechanism of nodal flow: A conserved symmetry breaking event in left-right axis determination. Cell 121, 633–644. doi: 10.1016/j.cell.2005.04.008.

Opazo, J. C., Kuraku, S., Zavala, K., Toloza-Villalobos, J., and Hoffmann, F. G. (2019). Evolution of nodal and nodal-related genes and the putative composition of the heterodimers that trigger the nodal pathway in vertebrates. Evolution & development 21, 205–217.

Opazo, J. C., and Zavala, K. (2018). Phylogenetic evidence for independent origins of GDF1 and GDF3 genes in anurans and mammals. Scientific Reports 8, 1–7.

Oteíza, P., Köppen, M., Concha, M. L., and Heisenberg, C.-P. (2008). Origin and shaping of the laterality organ in zebrafish. Development (Cambridge, England) 135, 2807–13. doi: 10.1242/dev.022228.

Oteiza, P., Köppen, M., Krieg, M., Pulgar, E., Farias, C., Melo, C., et al. (2010). Planar cell polarity signalling regulates cell adhesion properties in progenitors of the zebrafish laterality organ. Development 137, 3459–3468.

Paavola, J., Schliffke, S., Rossetti, S., Kuo, I. Y.-T., Yuan, S., Sun, Z., et al. (2013). Polycystin-2 mutations lead to impaired calcium cycling in the heart and predispose to dilated cardiomyopathy. Journal of molecular and cellular cardiology 58, 199–208.

Peeters, H., and Devriendt, K. (2006). Human laterality disorders. European Journal of Medical Genetics 49, 349–362. doi: 10.1016/j.ejmg.2005.12.003.

Pelliccia, J. L., Jindal, G. A., and Burdine, R. D. (2017). Gdf3 is required for robust nodal signaling during germ layer formation and left-right patterning. eLife 6, 1–23. doi: 10.7554/eLife.28635.

Pennekamp, P., Karcher, C., Fischer, A., Schweickert, A., Skryabin, B., Horst, J., et al. (2002). The ion channel polycystin-2 is required for left-right axis determination in mice. Current Biology 12, 938–943. doi: 10.1016/S0960-9822(02)00869-2.

Peterson, A. G., Wang, X., and Yost, H. J. (2013). Dvr1 transfers left – right asymmetric signals from Kupffer â€TM s vesicle to lateral plate mesoderm in zebra fi sh. Developmental Biology 382, 198–208. doi: 10.1016/j.ydbio.2013.06.011.

Piedra, M. E., Icardo, J. M., Albajar, M., Rodriguez-rey, J. C., and Ros, M. A. (1998). Pitx2 Participates in the Late Phase of the Pathway Controlling Left-Right Asymmetry. 94, 319–324.

Pintado, P., Sampaio, P., Tavares, B., Smith, D. J., and Lopes, S. S. (2017). Dynamics of cilia length in left – right development.

Praveen, K., Davis, E. E., and Katsanis, N. (2015). Unique among ciliopathies: primary ciliary dyskinesia, a motile cilia disorder. F1000prime reports 7.

Qian, Q., Hunter, L. W., Li, M., Marin-Padilla, M., Prakash, Y. S., Somlo, S., et al. (2003). Pkd2 haploinsufficiency alters intracellular calcium regulation in vascular smooth muscle cells. Human molecular genetics 12, 1875–1880.

Rago, L., Castroviejo, N., Fazilaty, H., Garcia-Asencio, F., Ocaña, O. H., Galcerán, J., et al. (2019). MicroRNAs establish the right-handed dominance of the heart laterality pathway in vertebrates. Developmental cell 51, 446–459.

Rahman, T., Zhang, H., Fan, J., and Wan, L. Q. (2020). Cell chirality in cardiovascular development and disease. APL Bioengineering 4, 31503. doi: 10.1063/5.0014424.

Ramsdell, A. F. (2005). Left-right asymmetry and congenital cardiac defects: Getting to the heart of the matter in vertebrate left-right axis determination. Developmental Biology 288, 1–20. doi: 10.1016/j.ydbio.2005.07.038.

Rathbun, L. I., Colicino, E. G., Manikas, J., O'Connell, J., Krishnan, N., Reilly, N. S., et al. (2020). Cytokinetic bridge triggers de novo lumen formation in vivo. Nature communications 11, 1269.

Roxo-rosa, M., Jacinto, R., Sampaio, P., and Lopes, S. S. (2015). The zebrafish Kupffer ' s vesicle as a model system for the molecular mechanisms by which the lack of Polycystin-2 leads to stimulation of CFTR. 1356–1366. doi: 10.1242/bio.014076.

Roxo-Rosa, M., and Lopes, S. S. (2019). "The zebrafish kupffer's vesicle: a special organ in a model organism to study human diseases," in Zebrafish in Biomedical Research (IntechOpen).

Ryan, A. K., Blumberg, B., Rodriguez-Esteban, C., Yonei-Tamura, S., Tamura, K., Tsukui, T., et al. (1998). Pitx2 determines left–right asymmetry of internal organs in vertebrates. Nature 394, 545–551. doi: 10.1038/29004.

Sampaio, P., Ferreira, R. R., Guerrero, A., Pintado, P., Tavares, B., Amaro, J., et al. (2014). Left-right organizer flow dynamics: how much cilia activity reliably yields laterality? Developmental cell 29, 716–728.

Sampaio, P. R. M. de A. (2021). Uncoupling heart and liver laterality events during embryogenesis.

Sanematsu, P. C., Erdemci-Tandogan, G., Patel, H., Retzlaff, E. M., Amack, J. D., and Manning, M. L. (2021). 3D viscoelastic drag forces contribute to cell shape changes during organogenesis in the zebrafish embryo. Cells & Development 168, 203718. doi: https://doi.org/10.1016/j.cdev.2021.203718.

Saúde, L., Lourenço, R., Gonçalves, A., and Palmeirim, I. (2005). terra is a left–right asymmetry gene required for left–right synchronization of the segmentation clock. Nature cell biology 7, 918–920.

Sawada, A., Shinya, M., Jiang, Y.-J., Kawakami, A., Kuroiwa, A., and Takeda, H. (2001). Fgf/MAPK signalling is a crucial positional cue in somite boundary formation.

Saydmohammed, M., Yagi, H., Calderon, M., Clark, M. J., Feinstein, T., Sun, M., et al. (2018). Vertebrate myosin 1d regulates left–right organizer morphogenesis and laterality. Nature Communications 9, 3381.

Schier, A. F. (2003). Nodal Signaling in Vertebrate Development. Annual Review of Cell and Developmental Biology 19, 589–621. doi: 10.1146/annurev.cellbio.19.041603.094522.

Schier, A. F., and Shen, M. M. (2000). Nodal signalling in vertebrate development. Nature 403, 385–389. doi: 10.1038/35000126.

Schneider, I., Houston, D. W., Rebagliati, M. R., and Slusarski, D. C. (2008). Calcium fluxes in dorsal forerunner cells antagonize β-catenin and alter left-right patterning.

Schneider, I., Schneider, P. N., Derry, S. W., Lin, S., Barton, L. J., Westfall, T., et al. (2010). Zebrafish Nkd1 promotes Dvl degradation and is required for left–right patterning. Developmental biology 348, 22–33.

Schottenfeld, J., Sullivan-brown, J., and Burdine, R. D. (2007). Zebrafish curly up encodes a Pkd2 ortholog that restricts left-side-specific expression of southpaw. Development 134, 1605–1615. doi: 10.1242/dev.02827.

Schröder, S. S., and Weizbauer, A. (2016). Paraxial Nodal Expression Reveals a Novel Conserved Structure of the Left-Right Organizer in Four Mammalian Species. 77–87. doi: 10.1159/000440951.

Schweickert, A., Vick, P., Getwan, M., Weber, T., Schneider, I., Eberhardt, M., et al. (2010). The nodal inhibitor Coco is a critical target of leftward flow in Xenopus. Current Biology 20, 738–743.

Schweickert, A., Weber, T., Beyer, T., Vick, P., Bogusch, S., Feistel, K., et al. (2007). Report Cilia-Driven Leftward Flow Determines Laterality in Xenopus. 60–66. doi: 10.1016/j.cub.2006.10.067.

Shapiro, A. J., Davis, S. D., Ferkol, T., Dell, S. D., Rosenfeld, M., Olivier, K. N., et al. (2014). Laterality Defects Other Than Situs Inversus Totalis in Primary Ciliary Dyskinesia: Insights Into Situs Ambiguus and Heterotaxy. Chest 146, 1176–1186. doi: https://doi.org/10.1378/chest.13-1704.

Shen, M. M. (2007). Nodal signaling: developmental roles and regulation. Development 134, 1023–1034. doi: 10.1242/dev.000166.

Shen, M. M., Wang, H., and Leder, P. (1997). A differential display strategy identifies Cryptic, a novel EGF-related gene expressed in the axial and lateral mesoderm during mouse gastrulation. Development 124, 429–442.

Shimozono, S., Iimura, T., Kitaguchi, T., Higashijima, S., and Miyawaki, A. (2013). Visualization of an endogenous retinoic acid gradient across embryonic development. Nature 496, 363–366.

Shiratori, H., Yashiro, K., Shen, M. M., and Hamada, H. (2006). Conserved regulation and role of Pitx2 in situs-specific morphogenesis of visceral organs. Development 133, 3015–3025. doi: 10.1242/dev.02470.

Smith, K. A., Noël, E., Thurlings, I., Rehmann, H., Chocron, S., and Bakkers, J. (2011). Bmp and nodal independently regulate lefty1 expression to maintain unilateral nodal activity during left-right axis specification in zebrafish. PLoS genetics 7, e1002289.

Solowiej-Wedderburn, J., Smith, D. J., Lopes, S. S., and Montenegro-Johnson, T. D. (2019). Wall stress enhanced exocytosis of extracellular vesicles as a possible mechanism of left-right symmetry-breaking in vertebrate development. Journal of Theoretical Biology 460, 220–226. doi: https://doi.org/10.1016/j.jtbi.2018.10.015.

Song, H., Hu, J., Chen, W., Elliott, G., Andre, P., Gao, B., et al. (2010). Planar cell polarity breaks bilateral symmetry by controlling ciliary positioning. Nature 466, 378–382. doi: 10.1038/nature09129.

Stark, B. C., Gao, Y., Sepich, D. S., Belk, L., Culver, M. A., Hu, B., et al. (2022). CARMIL3 is important for cell migration and morphogenesis during early development in zebrafish. Developmental Biology 481, 148–159. doi: https://doi.org/10.1016/j.ydbio.2021.09.008.

Stephen, L. A., Davis, G. M., Katie, E. M. C., James, J., Lynn, M. C., Kierans, M., et al. (2013). Failure of Centrosome Migration Causes a Loss of Motile Cilia in talpid 3 Mutants. 923–931. doi: 10.1002/dvdy.23980.

Stubbs, J. L., Oishi, I., Izpisúa Belmonte, J. C., and Kintner, C. (2008). The forkhead protein Foxj1 specifies node-like cilia in Xenopus and zebrafish embryos. Nature Genetics 40, 1454–1460. doi: 10.1038/ng.267.

Sulik, K., Dehart, D. B., Inagaki, T., Carson, J. L., Vrablic, T., Gesteland, K., et al. (1994). Morphogenesis of the murine node and notochordal plate. Developmental Dynamics 201, 260–278. doi: https://doi.org/10.1002/aja.1002010309.

Supp, D. M., Brueckner, M., Kuehn, M. R., Witte, D. P., Lowe, L. A., McGrath, J., et al. (1999). Targeted deletion of the ATP binding domain of left-right dynein confirms its role in specifying development of left-right asymmetries. Development 126, 5495–5504. doi: 10.1242/dev.126.23.5495.

Supp, D. M., Witte, D. P., Potter, S. S., and Brueckner, M. (1997). Mutation of an axonemal dynein affects left–right asymmetry in inversus viscerum mice. Nature 389, 963–966. doi: 10.1038/40140.

Sutherland, M. J., and Ware, S. M. (2009). Disorders of left-right asymmetry: Heterotaxy and situs inversus. American Journal of Medical Genetics, Part C: Seminars in Medical Genetics 151, 307–317. doi: 10.1002/ajmg.c.30228.

Szenker-Ravi, E., Ott, T., Khatoo, M., Moreau de Bellaing, A., Goh, W. X., Chong, Y. L., et al. (2022). Discovery of a genetic module essential for assigning left–right asymmetry in humans and ancestral vertebrates. Nature Genetics 54, 62–72. doi: 10.1038/s41588-021-00970-4.

Tabin, C. J., and Vogan, K. J. (2003). A two-cilia model for vertebrate left-right axis specification. 1–6. doi: 10.1101/gad.1053803.Tabin.

Tanaka, C., Sakuma, R., Nakamura, T., Hamada, H., and Saijoh, Y. (2007). Long-range action of Nodal requires interaction with GDF1. Genes & development 21, 3272–3282.

Tanaka, Y., Okada, Y., and Hirokawa, N. (2005). FGF-induced vesicular release of Sonic hedgehog and retinoic acid in leftward nodal flow is critical for left–right determination. Nature 435, 172–177. doi: 10.1038/nature03494.

Tavares, B., Jacinto, R., Sampaio, P., Pestana, S., Pinto, A., Vaz, A., et al. (2017). Notch/Her12 signalling modulates, motile/immotile cilia ratio downstream of Foxj1a in zebrafish left-right organizer. Elife 6, e25165.

Tessadori, F., de Bakker, D. E. M., Barske, L., Nelson, N., Algra, H. A., Willekers, S., et al. (2020). Zebrafish prrx1a mutants have normal hearts. Nature 585, E14–E16.

Tingler, M., Brugger, A., Feistel, K., and Schweickert, A. (2022). dmrt2 and myf5 link early somitogenesis to left-right Axis determination in Xenopus laevis. Frontiers in Cell and Developmental Biology 10.

Vermot, J., and Pourquié, O. (2005). Retinoic acid coordinates somitogenesis and left–right patterning in vertebrate embryos. Nature 435, 215–220.

Vick, P., Kreis, J., Schneider, I., Tingler, M., Getwan, M., Thumberger, T., et al. (2018). An early function of polycystin-2 for left-right organizer induction in Xenopus. IScience 2, 76–85.

Wallmeier, J., Nielsen, K. G., Kuehni, C. E., Lucas, J. S., Leigh, M. W., Zariwala, M. A., et al. (2020). Motile ciliopathies. Nature Reviews Disease Primers 6, 77. doi: 10.1038/s41572-020-0209-6.

Wang, G., Cadwallader, A. B., Jang, D. S., Tsang, M., Yost, H. J., and Amack, J. D. (2011). The Rho kinase Rock2b establishes anteroposterior asymmetry of the ciliated Kupffer ' s vesicle in zebrafish. 54, 45–54. doi: 10.1242/dev.052985.

Wang, G., Manning, M. L., and Amack, J. D. (2012). Regional cell shape changes control form and function of Kupffer ' s vesicle in the zebrafish embryo. Developmental Biology 370, 52–62. doi: 10.1016/j.ydbio.2012.07.019.

Wang, X., and Yost, H. J. (2008). Initiation and propagation of posterior to anterior (PA) waves in zebrafish left–right development. Developmental Dynamics 237, 3640–3647.

Warga, R. M., and Kane, D. A. (2007). A role for N-cadherin in mesodermal morphogenesis during gastrulation. Developmental biology 310, 211–225.

Warga, R. M., and Kane, D. A. (2018). Probing Cadherin Interactions in Zebrafish with E-and N-Cadherin Missense Mutants. Genetics 210, 1391–1409.

Watanabe, H., Schmidt, H. A., Kuhn, A., Höger, S. K., Kocagöz, Y., Laumann-Lipp, N., et al. (2014). Nodal signalling determines biradial asymmetry in Hydra. Nature 515, 112–115.

White, R. J., Collins, J. E., Sealy, I. M., Wali, N., Dooley, C. M., Digby, Z., et al. (2017). A high-resolution mRNA expression time course of embryonic development in zebrafish. eLife, 1–32.

Whitman, M. (2001). Nodal Signaling in Early Vertebrate Embryos: Themes and Variations. Developmental Cell 1, 605–617. doi: 10.1016/S1534-5807(01)00076-4.

Yan, Y.-T., Gritsman, K., Ding, J., Burdine, R. D., Corrales, J. D., Price, S. M., et al. (1999). Conserved requirement for EGF–CFC genes in vertebrate left–right axis formation. Genes & Development 13, 2527–2537. Available at: http://genesdev.cshlp.org/content/13/19/2527.abstract.

Yin, Y., Bangs, F., Paton, I. R., Prescott, A., James, J., Davey, M. G., et al. (2009). The Talpid3 gene (KIAA0586) encodes a centrosomal protein that is essential for primary cilia formation. 664, 655–664. doi: 10.1242/dev.028464.

Yonei-tamura, S., Tamura, K., Ryan, A. K., Blumberg, B., Sabbagh, W., Greenwald, J., et al. (1998). Pitx2 determines left – right asymmetry of internal organs in vertebrates. 545–551.

Yoshiba, S., Shiratori, H., Kuo, I. Y., Kawasumi, A., Shinohara, K., Nonaka, S., et al. (2012). Cilia at the node of mouse embryos sense fluid flow for left-right determination via Pkd2. Science 338, 226–231.

Yoshioka, H., Meno, C., Koshiba, K., Sugihara, M., Itoh, H., Ishimaru, Y., et al. (1998). Pitx2, a bicoid-type homeobox gene, is involved in a lefty-signaling pathway in determination of left-right asymmetry. Cell 94, 299–305. doi: 10.1016/S0092-8674(00)81473-7.

Yu, X., Ng, C. P., Habacher, H., and Roy, S. (2008). Foxj1 transcription factors are master regulators of the motile ciliogenic program. Nature Genetics 40, 1445–1453. doi: 10.1038/ng.263.

Yuan, S., Zhao, L., Brueckner, M., and Sun, Z. (2015). Intraciliary calcium oscillations initiate vertebrate left-right asymmetry. Current Biology 25, 556–567. doi: 10.1016/j.cub.2014.12.051.

Zhang, J., Jiang, Z., Liu, X., and Meng, A. (2016). Eph/ephrin signaling maintains the boundary of dorsal forerunner cell cluster during morphogenesis of the zebrafish embryonic left-right organizer. Development 143, 2603–2615.

Zhu, P., Xu, X., and Lin, X. (2015). Both ciliary and non-ciliary functions of Foxj1a confer Wnt/β-catenin signaling in zebrafish left-right patterning. Biology open 4, 1376–1386.

Zinski, J., Tajer, B., and Mullins, M. C. (2017). TGF-β Family Signaling in Early Vertebrate Development. Cold Spring Harbor Perspectives in Biology, a033274.

CHAPTER 2:

The zebrafish Dand5 beyond left-right asymmetry: the role in somite precursor specification and tailbud movements

The zebrafish Dand5 beyond left-right asymmetry: the role in somite precursor specification and tailbud movements

Catarina Bota[1], Gabriel Martins[2] and Susana S. Lopes[1*]

1 iNOVA4Health, NOVA Medical School|Faculdade de Ciências Médicas, NMS|FCM, Universidade Nova de Lisboa; Lisboa, Portugal.

2. Instituto Gulbenkian de Ciência, Fundação Calouste Gulbenkian, 2780-156 Oeiras, Portugal.

Keywords: *dand5*; Kuppfer's vesicle; somites; asymmetry; symmetry; left-right development; cell migration; zebrafish

Abstract

During vertebrate development, symmetry breaking occurs in the left-right organizer (LRO). The transfer of asymmetric molecular information to the lateral plate mesoderm is essential for the precise patterning of asymmetric internal organs, such as the heart. However, at the same developmental time, it is crucial to maintain symmetry at the somite level for correct musculature and vertebrae specification. Here, we demonstrate how left-right signals affect the behavior of zebrafish somite cell precursors. We describe a population of cells in the vicinity of the LRO, named Non-KV Sox17:GFP^{+} Tailbud Cells (NKSTCs), which migrate anteriorly and contribute to future somites. We show that NKSTCs originate in a cluster of cells aligned with the midline, posterior to the LRO, and leave that cluster in a left-right alternating manner, primarily from the left side. Fate mapping revealed that more NKSTCs integrated somites on the left side of the embryo. We then abolished the asymmetric cues from the LRO using *dand5*$^{-/-}$ mutant embryos and verified that NKSTCs no longer displayed asymmetric patterns. Cell exit from the posterior cluster became bilaterally synchronous in *dand5*$^{-/-}$ mutants. Our study revealed a new link between somite specification and Dand5 function. The gene *dand5* is well known as the first asymmetric gene involved in vertebrate LR development. Furthermore, we observed compromised anterior movement and reduced *myoD* expression in the absence of the KV, indicating its role in tailbud cell movement and somite specification. Our findings demonstrate the asymmetric behavior of somite precursor cells in response to LR signals in vivo, which require Dand5, and suggest an additional role of the KV in tailbud cell movement and somite specification.

Introduction

Despite having a bilaterally symmetric body plan in vertebrates, visceral organs display left-right (LR) asymmetry in position and pattern. Symmetry breaking occurs at the LR organizer (LRO), where polarized cilia produce an asymmetric fluid flow, leading to the degradation of *Dand5* mRNA on the left side (Bachiller et al., 2000; Lopes et al., 2010; Schweickert et al., 2010). Recent studies have shown that Bicc1 and Dicer mediate the degradation of *Dand5* mRNA (Maerker et al., 2021; Minegishi et al., 2021). As Dand5 is a Nodal inhibitor, Nodal persists only on the left side of the lateral plate mesoderm (LPM), establishing an asymmetric gene expression cascade. Nodal proteins activate the nodal pathway and target promoters by forming complexes with the type II and type I Activin receptors serine/threonine kinases (reviewed in (Schier, 2003; Shen, 2007)). Subsequent activation of the transcription factor Pitx2 on the left LPM leads to asymmetric organogenesis. The detailed mechanisms underlying the establishment and transduction of LR asymmetry have been extensively reviewed in previous studies (Grimes and Burdine, 2017; Schweickert et al., 2017; Zinski et al., 2017).

The LROs vary across different vertebrate species, and are known as node in amniotes (Levin et al., 1995b; Collignon et al., 1996), gastrocoel roof plate in amphibians (Schweickert et al., 2007), and Kupffer's vesicle (KV) in teleost fish (Essner et al., 2005; Hojo et al., 2007). The zebrafish KV is a spherical fluid-filled structure that appears during the initial segmentation phase at the posterior end of the notochord (Essner et al., 2000; Amack and Yost, 2004). It is a transient structure composed of a monociliated epithelium that emerges from the dorsal forerunner cells (DFCs), a group of 20-30 dorsal surface epithelial cells controlled by Nodal signaling (Cooper and D'amico, 1996).

Initially, the expression of *dand5* is symmetric; however, it becomes biased towards the right side of the KV at 8 ss (Lopes et al., 2010) in a flow-dependent process. This highly regulated counterclockwise fluid flow (Sampaio et al., 2014; Tavares et al., 2017) is generated by motile cilia in the KV (Essner et al., 2005; Supatto et al., 2008) and perceived by the polycystin complex composed of Pkd1l1 and Pkd2 (Pennekamp et al., 2002; Schottenfeld et al., 2007; Field et al., 2011; Kamura et al., 2011; Yoshiba et al., 2012; Yuan et al., 2015). However, the exact mechanism of flow sensing remains to be determined and may involve either mechanosensing or chemosensing processes.

Meanwhile, *southpaw* (*spaw),* the zebrafish nodal gene involved in establishing and transducing LR asymmetry, is initially expressed bilaterally in a symmetric pattern in cells adjacent to the KV at 4-6 ss (Long et al., 2003). Later, *spaw* expression becomes asymmetric on the left side of the LPM at 10-12 ss through the release of Dand5-Southpaw inhibition, which allows Spaw to induce its mRNA expression. Then, the expression of Spaw spreads from the posterior to the anterior range of the left LPM until 22 ss (Wang and Yost, 2008). The confinement of Spaw to the left side is achieved through different secreted factors from the TGF-β family: Lefty1 provides a midline barrier (Wang and Yost, 2008), Lefty2 (Long et al., 2003) in the left cardiac field creates an anterior barrier, and BMP signaling forms a posterior (Lenhart et al., 2011).

The correct placement of internal organs depends on breaking symmetry, whereas maintaining symmetry is essential for producing symmetrical somites, which serve as the foundation for developing symmetrical musculature, vertebrae, and innervation (Grimes, 2019a). Somites are formed in a symmetrical periodic fashion through the genetic oscillations of a segmentation clock (Oates et al., 2012) from the unsegmented presomitic mesoderm (PSM). To achieve somitic symmetry, the PSM must be actively shielded from the LR signals of the LRO and LPM (Kawakami et al., 2005; Vermont and Pourquié, 2005). A recent study reported that zebrafish somites initially form with asymmetric differences in length and position but are corrected by somite surface tension (Naganathan et al., 2022). Somite precursors originate from a dorsal tailbud population of neuromesodermal progenitor cells (Kanki and Ho, 1997; Martin and Kimelman, 2012) that commit to the mesoderm fate, move ventrally to the maturation zone (MZ), migrate (Kanki and Ho 1997; Griffin and Kimelman 2002; Fior et al. 2012; Manning and Kimelman 2015), and generate cell flows towards the PSM, where cell motility decreases to form the somites (Kanki and Ho, 1997; Lawton et al., 2013; Banavar et al., 2021).

Numerous studies in zebrafish have examined cell movement during posterior elongation (Lawton et al., 2013; Mongera et al., 2018; Das et al., 2019; Banavar et al., 2021) or tailbud exit of somite precursors (Fior et al., 2012a; O'Neill and Thorpe, 2013; Manning and Kimelman, 2015; Goto et al., 2017). However, the existence of LR asymmetries in somite precursor cell movement during somite formation *in vivo* has not been previously reported.

To address this question, we used live imaging and a transgenic line that labeled a mesoderm tailbud population. We identified a group of cells that displayed asymmetry by acquiring successive anterior positions on the left side of the embryo, beginning with an asymmetric cell exit from a cluster of cells posterior to the KV in the MZ region. Furthermore, fate mapping confirmed that the asymmetric cells were somite precursors and demonstrated that they

integrated the somites in a left-biased alternating manner in WT embryos but not in *dand5*$^{-/-}$ embryos. We also observed compromised anterior movement and reduced *myoD* expression in the absence of the KV, indicating its role in tailbud cell movement and somite specification. Our findings demonstrate the asymmetric behavior *in vivo* of somite precursor cells in response to LR signals, which require *dand5*, and suggest that the KV plays an additional role in tailbud cell movement and somite specification.

Materials and Methods

Zebrafish lines and embryo manipulation

The zebrafish strains used in this study were wild type (AB strain—ZFIN), transgenic Tg(sox17:GFP)^{s870Tg} (Sakaguchi et al., 2006), Tg(-6.3drl:mCherry)^{zh705Tg} (Sánchez-Iranzo et al., 2018), Tg(act2b:LIFEACT-RFP) ^{e115Tg} (Behrndt et al., 2012) and mutant dand5$^{a204/a204}$ (Montague et al., 2018). Adult zebrafish were kept in a recirculating water treatment unit system at 28.0°C, pH 7, and 950 µS/m conductivity under a 10h dark/14h light cycle. They were spawned by pair mating, and eggs were collected and staged according to standard protocols (Kimmel et al., 1995; Dahm and Nüsslein-Volhard, 2002). Embryos were raised in E3 medium (5 mM NaCl, 0.17 mM KCl, 0.33 mM CaCl2, 0.33 mM MgSO4, with 0.0001% methylene blue at early stages) at 28.0°C.

Embryo microinjections

For Kaede photoconversion, 100 pg of *Kaede* mRNA were injected into one-cell stage WT and Tg(sox17:GFP) embryos.

Immunostaining and *in situ* Hybridization

Whole-mount immunostaining was performed as described previously (Lopes et al., 2010) using the following antibodies: anti-MF20 (1:100; DSHB), anti-fibronectin (1:100;Sigma), anti-acetylated α-tubulin (1:300; Sigma), anti-GFP (1:500; Invitrogen), anti-rabbit Alexa Fluor 488 (Invitrogen; 1:500), anti-mouse Alexa Fluor 647 (Invitrogen; 1:500), and anti-mouse Alexa Fluor 546 (Invitrogen; 1:500). Flat-mounted 13-16 ss embryos and 24 hpf embryos mounted in 1% low-melting agarose (LMA) with the dorsal side facing the glass bottom of the dish were imaged using a Zeiss LSM 980 Airyscan confocal microscope. The DFC-ablated 14 ss embryos were mounted in 1% LMA, with the tail facing the bottom of the glass-bottom dish, and images were

acquired using a Zeiss LSM 980 Airyscan confocal microscope. Individual sox17, *myoD*, double *myoD* and *dand5* whole-mount *in situ* hybridization was performed as previously described (Thisse and Thisse, 2014). The embryos were photographed using a Zeiss Axio Imager Z2 upright microscope. Gene expression for *myoD* and double staining for *myoD* and *dand5* were scored blindly for the different genotypes and analyzed by either Fisher's exact test or the chi-square test using Prism 8 (GraphPad).

Live imaging and photoconversion

For live imaging of sox17:GFP^{+} cells in whole zebrafish embryos, 10 ss embryos were mounted in 1% LMA (low melting agarose) in a petri dish with the dorsal side facing the objective and fully submerged in E3. Images of the KV and adjacent cells were acquired using a Praire Ultima two-photon system mounted on an Olympus BX60 upright microscope. Z-stacks were obtained at 2 µm intervals at 28°C and time cycles of 3 and 6 min for 3-6 hours. 10 ss *dand5*$^{-/-}$ embryos were mounted in 1% LMA, with the tail facing the bottom of the dish, and images were acquired using a Zeiss LSM 980 Airyscan confocal microscope. 10 ss *Tg(sox17:GFP);Tg(act2b:LIFEACT-RFP)* double-transgenic embryos were mounted in 1% LMA, with the tail facing the bottom of the dish, and images were acquired using a Zeiss LSM 980 Airyscan confocal microscope. Z-stacks were acquired at 0.35 µm step size at 1 s intervals. Z-stacks were obtained at 2 µm intervals at 28°C for 2 min for 60-90 min. Kaede photoconversion was performed using a Leica TCS SP5 confocal laser scanning microscope with the FRAP module. *Kaede* mRNA-injected 8 ss embryos were mounted in 1% LMA and the targeted cluster of sox17:GFP^{+} cells localized posterior to the KV was subjected to a 9 s exposure to a 50% 405 nm UV laser. Images of the entire tail and targeted region were acquired before, during, and post-UV exposure. After photoconversion, the embryos were released into the E3 medium at 28°C until 14ss or 24 hpf. 14 ss embryos were fixed in 4% PFA ON, and 24 hpf embryos were mounted in 1% LMA in a dorsal position for tail z-stack acquisition using a two-photon microscope.

Body Length Measurement

To measure body length, 3 days post-fertilization (dpf), WT (AB), and *dand5*$^{-/-}$ larvae were mounted in 2% methylcellulose and photographed using a Zeiss Axio Observer. Larvae were measured using the Fiji software.

Imaging of fixed embryos

For imaging of sox17:GFP+ cells, WT 10 ss, WT, and *dand5*$^{-/-}$ 13 and 14 ss embryos were fixed in 4% PFA and stored in PBS at 4°C. To preserve uniformity between analyses, embryos were

mounted in 1% LMA at the same position as described here for live imaging. Z-stacks were acquired on a Praire Ultima two-photon system at 1 µm intervals. Co-localization evaluation of Sox17 and Draculin was performed in 18 ss, 20ss, and 24 hpf embryos fixed in PFA 4% ON and imaged using a Zeiss LSM 710 confocal microscope. The embryos were mounted with the dorsal side facing the glass bottom of the dish, and z-stacks were acquired at 0.7-1 µm intervals. Kaede photoconverted WT 14 ss embryos were imaged using a Zeiss LSM 980 Airyscan confocal microscope.

To evaluate KV morphology, 8 ss sox17:GFP and *dand5*$^{-/-}$ embryos raised in the sox17:GFP background were fixed in 4% PFA ON, and z-stacks of the KV were acquired using a Zeiss LSM 980 Airyscan confocal microscope.

Image analysis

Datasets were first processed using the FIJI/ImageJ software (Schindelin et al., 2012). Imaris v9.8.1 (Bitplane) was used to render Z-stacks of live-imaged sox17:GFP^{+} cells and produce accelerated 3D movies from which we manually tracked NKSTC cells (on both the left and right sides) and the KV centroid. The number of tracks and spots, anterior position (µm), anterior track distance (µm), the shortest distance to KV (µm), the shortest distance to nearest neighbor (µm), and track speed (µm.s-1) were computed with Imaris v9.8.1 (Bitplane) and extracted. KV 3D surfaces were acquired by manual drawing in every slice, where KV cells were always visible when the KV was still open. For fixed embryos, z-stacks of sox17:GFP^{+} cells were reconstructed in 3D using Imaris v9.8.1 (Bitplane), and x, y, and z coordinates for Left and Right cells plus the center point of the lumen of the KV were extracted. These coordinates were then imported into a MATLAB 2019a script written to calculate the number of cells on both the left and right sides, the distance of cells to the KV lumen (µm), and the anterior distance of cells to the KV (µm) (or y distance) as a measure of the displacement along the AP axis of the embryos. The number of Kaede-photoconverted cells was scored using the Fiji software. The somite height and width were measured in Fiji. The morphology of the KV lumen was assessed by 3D projections using IMARIS v9.8.1 (Bitplane) and manually tracing the KV lumen to produce representative 3D surfaces. The calculated volume (µm^3), area (µm^2), and sphericity were extracted. All paired and unpaired comparisons were performed using the t-test in Prism 8 (GraphPad).

Results

We used the Tg(sox17:GFP) line, first described by Sakaguchi et al. (2006), as a KV reporter to investigate the migratory behavior of cells in the vicinity of the KV. We observed a distinct group of cells that were positive for sox17:GFP and presented several unique properties: i) asymmetric pattern of anterior migration along the midline axis (Figure 2.1A); ii) cell protrusions, denoting potential anterior migratory behavior; and iii) shape, size, and position distinct from those of the gut precursors.

The most striking characteristic of these migratory cells is that they reach more anterior positions on the left side of the embryo. Therefore, we investigated whether sox17:GFP+ cells are affected by the laterality pathway. To identify the tracked cells, we compared the expression pattern of sox17 mRNA using whole-mount in situ hybridization with sox17:GFP^{+} cells from the bud stage to 14 ss. We concluded that *sox17* mRNA is strongly expressed in DFCs at the bud stage. However, we did not find cells expressing *sox17* mRNA in the KV at 8 ss or close to the KV at 8 or 13-14 ss (as shown in Supplementary Figure 2.1). Therefore, we inferred that the cells of interest were likely to be labeled by *sox17* promoter leakage (outside the KV), GFP perdurance (such as in the KV cells), or both. Nevertheless, this transgenic line inadvertently highlights a group of cells close to and in the same focal plane as the KV, displaying an intriguing asymmetric pattern along the midline axis. As a result, we decided to use the sox17:GFP transgenic line as a tailbud cell reporter and named the cells of interest Non-KV Sox17:GFP^{+} Tailbud Cells, or NKSTCs, for simplicity.

NKSTC asymmetric migration regarding the LR axis

We observed that NKSTCs exhibited migratory behavior towards the anterior side with an asymmetric trend towards the left side (Figure 2.1A; Supplementary Video 2.1). Using 3D tracking to monitor these cells over time (Supplementary Video 2.2), we found that the number of tracks on each side of the KV was asymmetrical (Figure 2.1D; p-value = 0.0024), with more cells on the left side (Figure 2.1E; p-value = 0.0006). We concluded that the first asymmetric pattern was the presence of more cells on the left side, moving towards the anterior side of the embryo. As time progressed, the cells on the left side acquired more anterior positions than those on the right side (Figure 2.1B, C), as shown by their larger average and maximum anterior

positions (y) (Figure 2.1F; p-value = 0.0006; Figure 2.1G; p-value = 0.0045) and the increased average and maximum track anterior displacement (y) (Figure 2.1H; p-value = 0.0215; Figure 2.1I; p-value = 0.0016), at the final time point.

We also analyzed the distance of the cells to the center of the KV, as a reference point, and found that at the last time point, the cells on the left side showed a higher maximum shortest distance to the KV than those on the right (Figure 2.1J; p-value = 0.0360). This observation indicated that in each embryo analyzed in 3D space, the cells on the left side were farther away from the KV than those on the right side. We also measured the minimum distance to the nearest neighbor at the last time point imaged and found that this distance was more significant on the left side than on the right (Figure 2.1K; p-value = 0.0263).

To determine whether NKSTCs were actively migrating, we used the Tg(sox17:GFP);Tg(act2b:LIFEACT-RFP) double transgenic and observed F-actin dynamics and found the presence of lamellipodia and filopodia characteristics of migratory cells (Figure 2.1L). In addition, we evaluated the migration speed of NKSTCs and found no differences in the average track speed (Figure 2.1M; p-value = 0.5304). Consequently, we concluded that different rates of motion were not the cause for the left-sided cells to reach more anterior positions.

Next, we imaged NKSTCs at earlier developmental stages to determine whether we could track the establishment of the asymmetric pattern mentioned above. At 9-10 ss, we observed a cluster of NKSTCs localized posterior to the KV (Figure 2.2A) (Supplementary Video 2.3) and confirmed this at 10 ss in fixed embryos for better image resolution (Figure 2.2B). The cell morphology in the cluster differed from that of the larger, highly dispersed endodermal cells that later will form the gut tube. We determined that the aggregate, which we named the 'posterior cluster,' comprised an average of 42 NKSTCs ($\bar{x}$ = 42.33; σ = 8.41; N = 9). We observed that during tail extension, the KV aligns with the 'posterior cluster' (Supplementary Video 2.4), causing cells from the cluster to start leaving it in an alternating manner, either from the left or right side, towards the anterior of the embryo when approaching the location of the cluster. We again observed that NKSTCs acquired more anterior positions on the left side (Figure 2.2A,B), matching our first observation (Figure 1A). Therefore, the KV, the zebrafish LRO, appeared to be the driving force for the NKSTCs' departure from the 'posterior cluster' (Supplementary Video 2.4). Whether the cue triggered by the KV is mechanic or molecular is yet to be tested. Next, we manipulated the LR pathway and tested whether the migratory behavior of NKSTCs was affected.

The asymmetric localization of NKSTCs is lost in *dand5*$^{-/-}$ embryos

To investigate how NKSTCs respond to the manipulation of LR cues, we examined *dand5*$^{-/-}$ embryos raised on a *Tg(sox17:GFP)* background. In these mutants, the absence of *dand5* mRNA and secreted protein in the KV abolishes its inhibitory effect on Southpaw, resulting in free movement of this Nodal-related signal to both sides of the embryo, as shown in the diagram (Figure 2.3A), and confirmed in our laboratory (data not shown) and by Montague et al., (2018). We predicted that if the *sox17:GFP* transgenic reporter line is Nodal-dependent, pronounced NKSTCs anterior migration would be observed bilaterally.

We compared the behavior of NKSTCs in *dand5*$^{-/-}$ and WT embryos at 14 ss by quantifying the 3D positions of each cell detached from the posterior cluster. Consistent with our previous live imaging data (Figure 2.1), WT fixed embryos showed a left-sided asymmetry in cell distribution at 14 ss (Figure 3B, p-value = 0.0262). In contrast, *dand5*$^{-/-}$ embryos exhibited a more symmetrical pattern, with similar numbers of cells on both the left and right sides at 14 ss (Figure 2.3B, p-value = 0.4605). We also found that WT embryos displayed a greater average anterior distance to the KV on the left side than the right (Figure 2.3D, p-value = 0.0162). In contrast, in *dand5*$^{-/-}$ mutants, there was no significant difference in the distance of cells to the KV between the two sides.

Paired comparisons of left-right differences in anterior migration distance showed no evidence of the expected bilateral migration or a right-sided bias in *dand5*$^{-/-}$ embryos (Figure 2.3D). These results suggest that, in the absence of Dand5-mediated inhibition, NKSTCs migration is randomized.

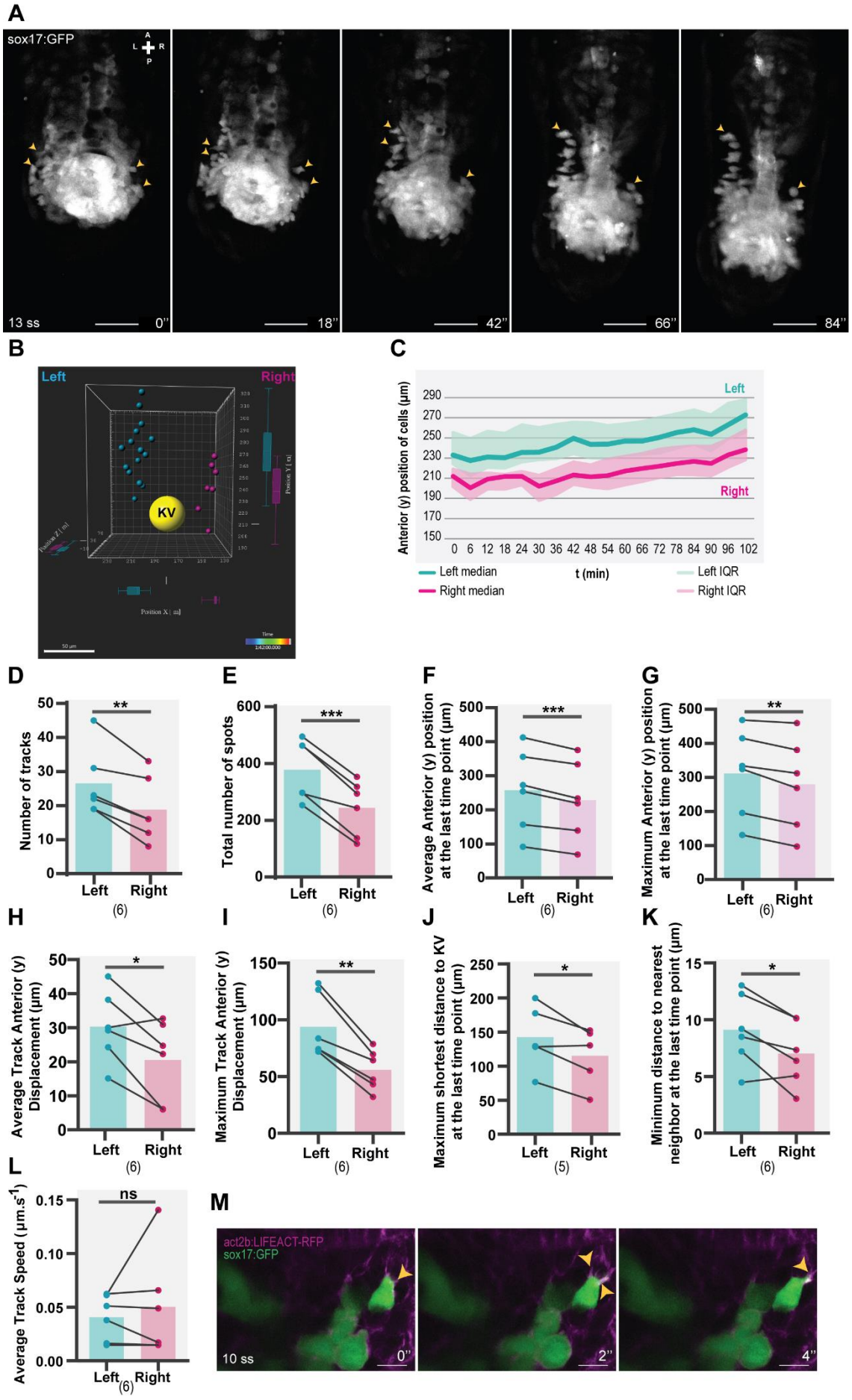
A
sox17:GFP
A
L
R
P
13 ss
0''
18''
42''
66''
84''
B
Left
Right
KV
C
Left
Right
Anterior (y) position of cells (µm)
290
270
250
230
210
190
170
150
0 6 12 18 24 30 36 42 48 54 60 66 72 78 84 90 96 102
t (min)
Left median
Right median
Left IQR
Right IQR
D
Number of tracks
50
40
30
20
10
0
**
Left
Right
(6)
E
Total number of spots
600
400
200
0
***
Left
Right
(6)
F
Average Anterior (y) position at the last time point (µm)
500
400
300
200
100
0
***
Left
Right
(6)
G
Maximum Anterior (y) position at the last time point (µm)
500
400
300
200
100
0
**
Left
Right
(6)
H
Average Track Anterior (y) Displacement (µm)
50
40
30
20
10
0
*
Left
Right
(6)
I
Maximum Track Anterior (y) Displacement (µm)
150
100
50
0
**
Left
Right
(6)
J
Maximum shortest distance to KV at the last time point (µm)
250
200
150
100
50
0
*
Left
Right
(5)
K
Minimum distance to nearest neighbor at the last time point (µm)
15
10
5
0
*
Left
Right
(6)
L
Average Track Speed (µm.s-1)
0.15
0.10
0.05
0.00
ns
Left
Right
(6)
M
act2b:LIFEACT-RFP
sox17:GFP
10 ss
0''
2''
4''

Figure 2.1. Asymmetric patterns of NKSTCs in WT embryos. **(A)** Time-lapse images of a *Tg(sox17:GFP)* embryo at selected time points, starting at 13 ss and ending at 18 ss. Yellow arrowheads indicate the more anterior positions on the left and right sides, respectively. The elapsed time is indicated in minutes (') at the bottom-right. **(B)** 3D distribution of manually tracked cells at the last time point. Left spots are shown in cyan, right in magenta, and the KV lumen in yellow. **(C)** Dynamics of the anterior positions on the left (cyan) and right (magenta) sides at consecutive time points. The thick lines represent medians and the interquartile range is lighter. **(D-L)** Left *vs.* right parameters extracted from cell tracking data, with cyan representing the left side and magenta representing the right side. t-test paired comparisons were used, and the bars represent the mean values, whereas the dots represent individual embryos. *corresponds to a p-value <0,05; ** to a p-value <0,005 and *** to a p-value <0,0005. **(M)** Lamellipodium-like (yellow arrowheads) structures in NKSTCs were observed in Tg(act2b:LIFEACT-RFP);Tg(sox17:GFP). The axes indicate A for the anterior, P for the posterior, L for the left, and R for the right. The number of embryos (N) is shown in parentheses. Scale bars: 50 µm in **(A)** and 10 µm in **(M)**.

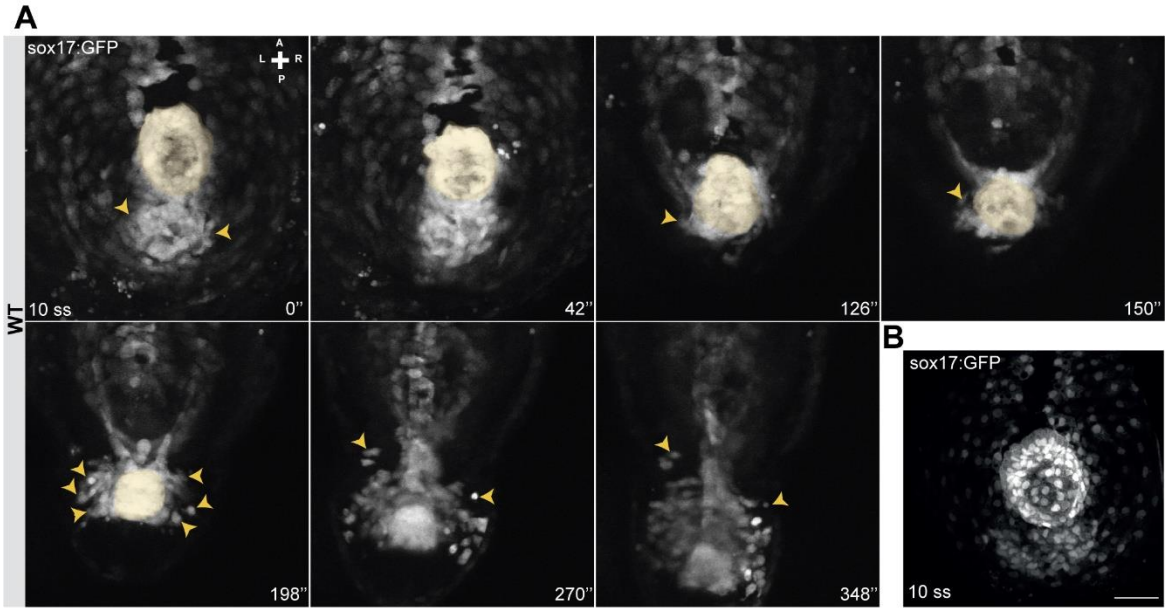

Figure 2.2. Dynamic movement of NKSTCs from a posterior cluster aligned with the KV towards the anterior side. **(A)** Time-lapse images of a *Tg(sox17:GFP)* embryo starting at 10 ss, displaying the first NKSTCs exiting the cluster and migrating towards the anterior side from the left and right sides. Yellow arrowheads firstly indicate NKSTCs in the cluster. In the following snapshots, the yellow arrowheads show the first cells that exit the cluster and migrate towards the anterior side from either the left or the right side. **(B)** The maximum intensity projection of a 10 ss *Tg(sox17:GFP)* fixed embryo showing the posterior cluster aligned with the KV. The elapsed time is indicated in minutes (') at the right and axes are indicated: A, anterior; P, posterior; L, left; R, right. N is shown in parentheses. The scale bar = 50 µm.

To further validate the use of the *Tg(sox17:GFP)* line, we tested for asymmetries in tailbud cell movement using a method independent of the reporter line. We repeated the experiments by photoconverting the region of the 'posterior cluster' at 8 ss in *Kaede*-injected embryos and assessed the positions of the photoconverted cells on the left and right sides at 14 ss, as shown in the diagram (Figure 2.4A). Again, we observed a more significant number of cells on the left side (p-value = 0,0266) (Figure 2.4B-D). However, the number of Kaede photoconverted cells in

the tails of 14 ss embryos was higher than that of sox17:GFP^{+} cells (NKSTCs) (p-value = 0,0068) (Figure 2.4E). We acknowledge that there might have been photoconverted cells above and below the proximity of the KV (*i.e.*, along the z-axis), since we used a conventional confocal microscopy system to perform the photoconversion which effectively creates an axial cone of illumination rather than a confined volume (Figure 2.4B). However, we could not efficiently use a two-photon system to improve the photoconversion volume.

Although we could not determine the degree of left anterior bias with statistical significance by using the Kaede photoconversion method, the observed left-sided prevalence was consistent with our previous results. In Kaede photoconverted embryos, we observed that 9 of 15 embryos (60%) reached more anterior cell positions on the left side (Figure 2.4F; p-value = 0.2148). Therefore, our Kaede photoconversion experiments provide additional support for the higher numbers of cells on the left side observed using the *sox17:GFP* reporter line, but failed to provide statistical significance to the left anterior bias.

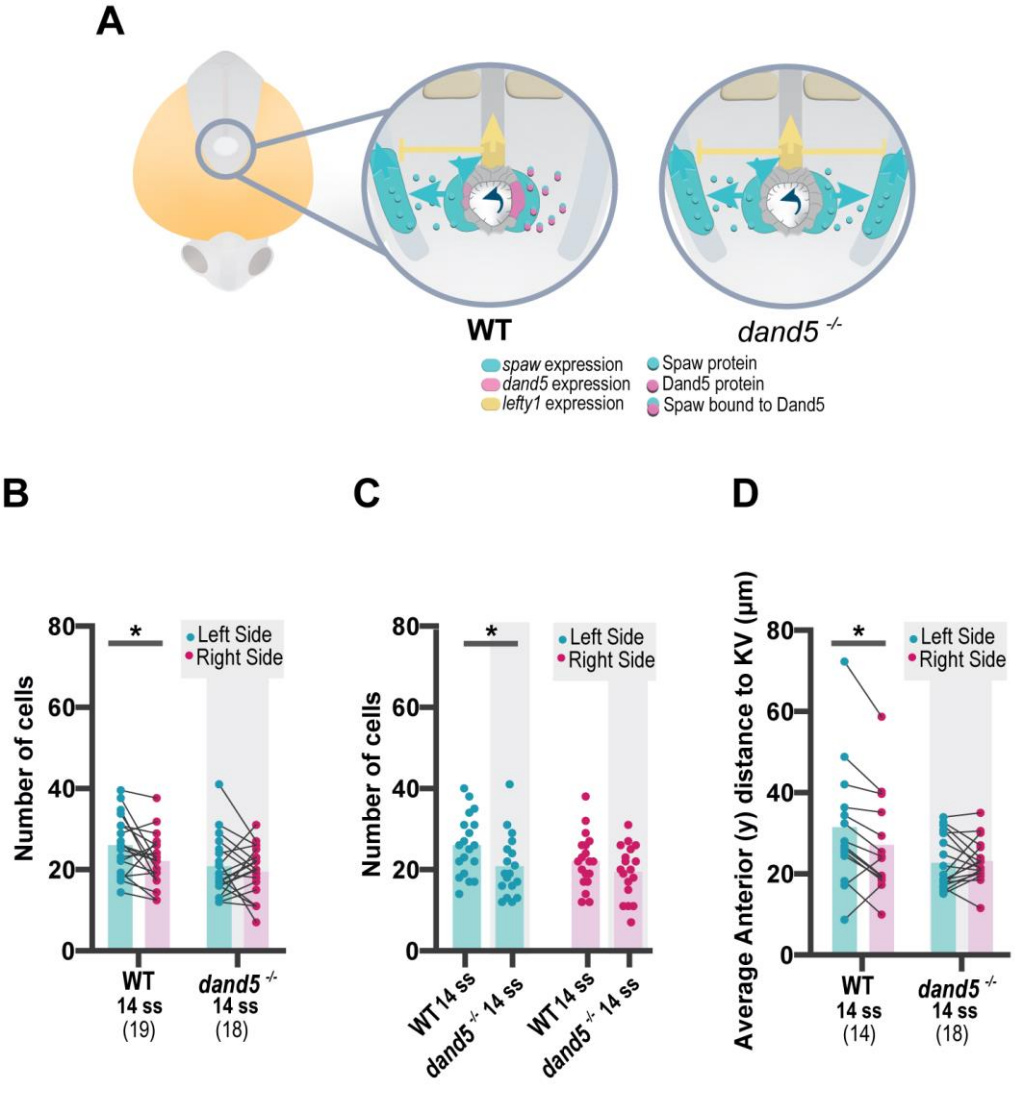

Figure 2.3. Quantification of NKSTCs distribution patterns in WT and *dand5*$^{-/-}$ embryos. **(A)** Schematic representation of early asymmetric establishment in WT and *dand5*$^{-/-}$ embryos. In the absence of *dand5* expression, Spaw freely travels to both sides of the LPM, where it activates its own expression and its inhibitor *lefty1* at the midline. **(B)** Quantification of left-right differences in the number of NKSTCs at 14 ss in WT and *dand5*$^{-/-}$ embryos. **(C)** Quantification of differences in the number of NKSTCs observed on each side of the embryos at 14 ss in WT and *dand5*$^{-/-}$ embryos. **(D)** Quantification of left-right differences observed in the anterior distance to the KV based on the 3D coordinates of NKSTCs at 14 ss in WT and *dand5*$^{-/-}$ embryos. Cyan represents the left side, and magenta represents the right side. t-test paired and unpaired comparisons were used to analyze data. Bars represent mean values, and dots represent individual embryos. Asterisks indicate significant differences with * corresponding to a p-value <0.05.

dand5$^{-/-}$ mutant NKSTCs migrate bilaterally synchronized from the posterior cluster

Next, having established that the NKSTCs come from the 'posterior cluster,' we quantified if the asymmetry seen in their destination at 14 ss was first visualized by an asymmetric departure from the 'posterior cluster.' We found that in 50% of the analyzed WT embryos (N = 12), the first cells to depart from the posterior cluster were from the left side, 25% from the right side, and 25% from both sides simultaneously. However, in *dand5*$^{-/-}$ embryos (Figure 2.5A), 67% of NKSTCs departed simultaneously from both sides, 22% left first from the right side, and 11% from the left side (Supplementary Video 5; N=9; Figure 2.5B). These results showed that cell behavior differed between WT and *dand5*$^{-/-}$ embryos.

As cells in the 'posterior cluster' appear to respond to the KV position to exit towards the anterior side of the embryo, we evaluated whether the symmetric cell behavior in *dand5*$^{-/-}$ embryos was due to changes in KV morphology. Therefore, we examined the KV lumen morphology in WT and *dand5*$^{-/-}$ embryos raised in a *sox17:GFP* background at 8 ss (Supplementary Figure 2.2A, B). Our analysis revealed no significant difference in the volume or area of the KV lumen between WT and *dand5*$^{-/-}$ embryos (Supplementary figure 2.2C, D). Nevertheless, *dand5*$^{-/-}$ embryos had more spherical KVs (Supplementary Figure 2.2E). Thus, we conclude that the symmetric cell exit in *dand5*$^{-/-}$ embryos is not triggered by differences in the KV volume.

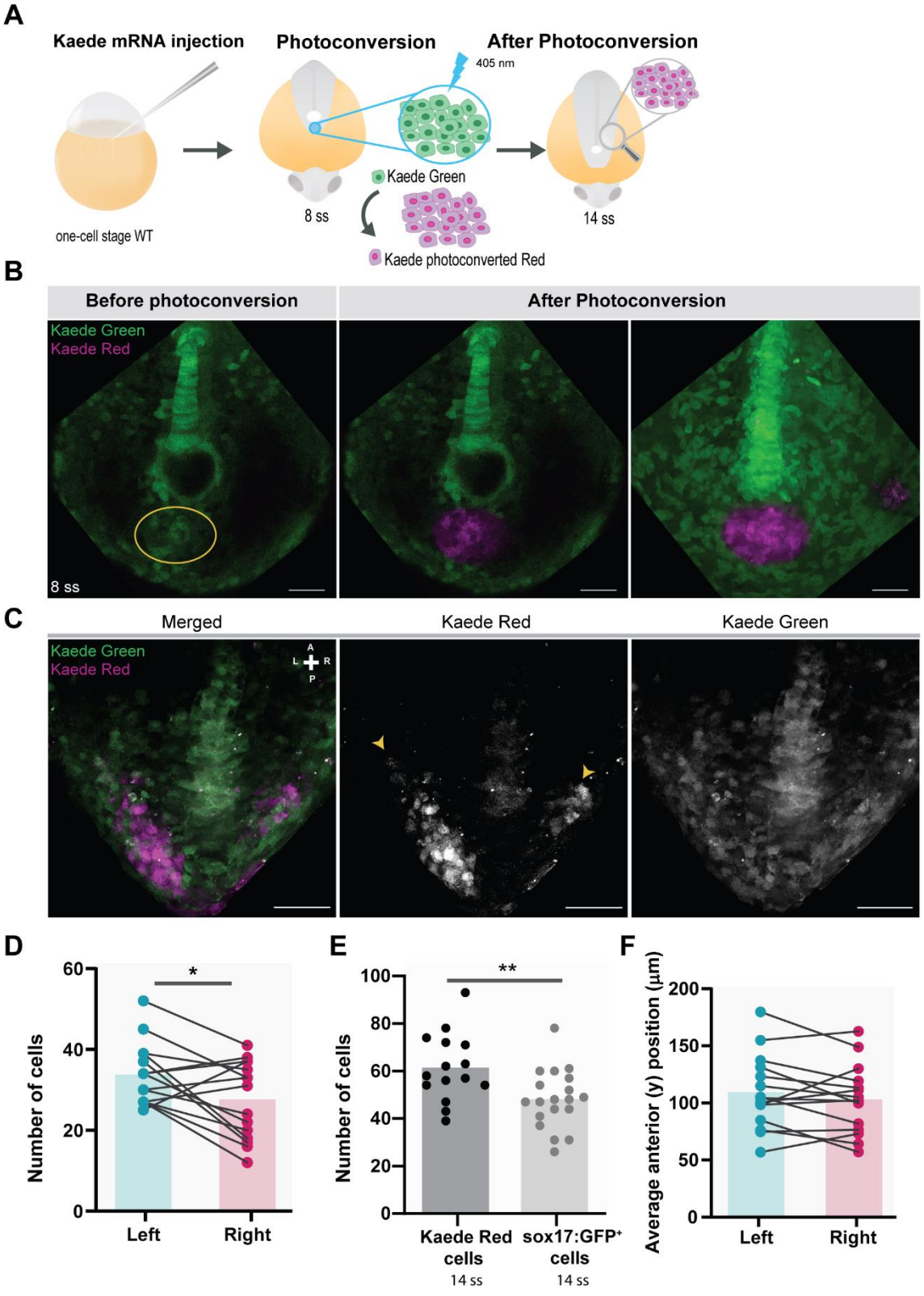
A
Kaede mRNA injection
Photoconversion
After Photoconversion
405 nm
Kaede Green
8 ss
14 ss
one-cell stage WT
Kaede photoconverted Red
B
Before photoconversion
After Photoconversion
Kaede Green
Kaede Red
8 ss
C
Merged
Kaede Red
Kaede Green
Kaede Green
Kaede Red
A
L
R
P
D
Number of cells
60
40
20
0
*
Left
Right
E
Number of cells
100
80
60
40
20
0
**
Kaede Red cells
14 ss
sox17:GFP+ cells
14 ss
F
Average anterior (y) position (µm)
200
150
100
50
0
Left
Right

Figure 2.4. Testing for left-right asymmetries independent of the *Tg(sox17:GFP)* reporter line. **(A)** Schematic representation of the photoconversion setup using Kaede to track specific tailbud cells. *Kaede* mRNA was injected into one-cell stage WT embryos, and the 'posterior cluster' region was blindly photoconverted at 8 ss using UV light. At 14 ss, embryos were screened for the location of Kaede photoconverted cells. (**B**) Before and after Kaede photoconversion of the 'posterior cluster' region at 8 ss in the WT embryos. The KV middle focal plane was used as a reference (note that photoconversion can occur along the axial cone of illumination of the confocal system). The maximum intensity projection shows the total area of the photoconverted cells, with Kaede green cells in green and photoconverted cells in magenta. Scale bar = 50 µm. **(C)** Positions of Kaede photoconverted cells in the dorsal view of a 14 ss WT embryo, with yellow arrowheads indicating the more anterior positions of the photoconverted cells on both sides. Scale bar = 100 µm. **(D)** Paired comparison of the number of photoconverted cells on the left and right side at 14ss. **(E)** Quantification of differences in the total number of photoconverted cells and NKSTCs at 14 ss. Dark gray represents photoconverted cells, and light gray represents NKSTCs. **(F)** Paired comparison of the average anterior positions of the photoconverted cells on the left and right sides at 14 ss, with cyan representing the left side and magenta representing the right side. The bars show the mean values and the dots indicate individual embryos. Asterisks indicate significance levels: * corresponds to a p-value <0,05 and ** corresponds to a p-value <0,005.

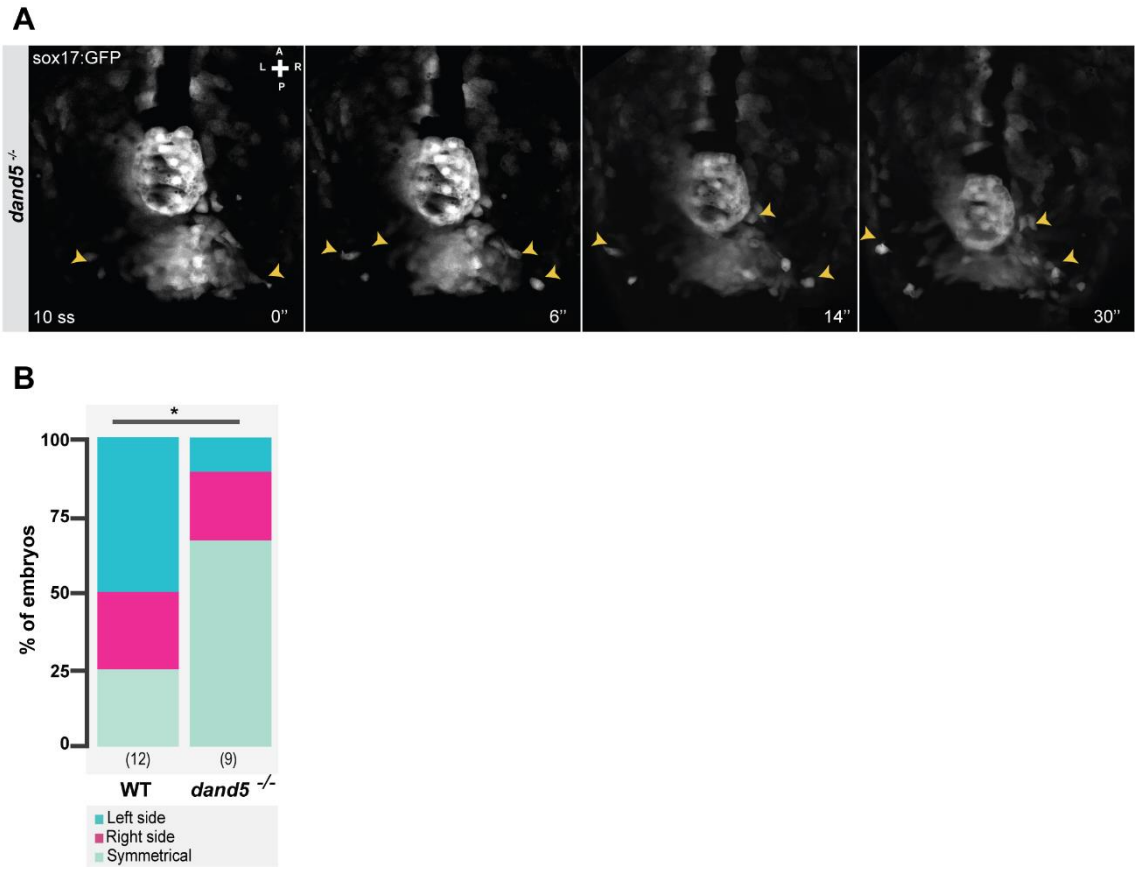

Figure 2.5. Snapshots from live imaging of NKSTCs leaving the posterior cluster. **(A)** Time-lapse imaging of NKSTCs leaving the posterior cluster in a *dand5*$^{-/-}$ embryo raised on a *Tg(sox17:GFP)* background, starting at 10 ss. The elapsed time is indicated in minutes (') at the bottom right, and the axes are indicated as A, anterior; P, posterior; L, left; R, right. N is shown in parentheses. **(B)** Quantification of the first side from which NKSTCs departed from the posterior cluster in WT and *dand5*$^{-/-}$ embryos using chi-square test. The significance level is indicated by asterisks; * corresponds to a p-value <0,05.

NKSTCs have a somitic fate

Given the proximity of NKSTCs and the LPM, we aimed to investigate whether any *sox17:GFP*$^{+}$ cells co-localize with Draculin, a pan-LPM marker (Prummel et al., 2019), in later developmental stages. To this end, we used the double transgenic line *Tg(sox17:GFP); Tg(-6.3drl:mCherry)* to test whether NKSTCs can integrate LPM-derived structures. However, we observed no co-localization of *sox17:GFP*$^{+}$ cells with *drl:mCherry* at 18 ss, 20 ss, and 24 hours post-fertilization (hpf) embryos, except some cells in the gut tube (Supplementary Figure 2.3A,B), which were likely not NKSTCs because of their posterior location at the tailbud. Our findings show that NKSTCs do not integrate into the LPM and highlight the challenges of co-localization studies on NKSTCs without a reliable marker to track these cells.

To map the fate of NKSTCs, we photoconverted the 'posterior cluster' at 8 ss prior to NKSTC migration (Figure 2.6A, B) using *Tg(sox17:GFP)* embryos in both WT and *dand5* mutants. We tracked the double-labeled sox17:GFP^{+} and Kaede photoconverted cells at 24 hpf (white cells) and scored their fate (Figure 2.6A, B, C, and D). In WT embryos, 88% of the photoconverted cells were located in the tail somites, whereas the remaining 12% were categorized as 'other fates' (N = 10; Ncells = 241), including the notochord and nearby structures (Figure 2.6E).

In *dand5*$^{-/-}$ embryos, we found that photoconverted NKSTCs were also integrated into somites (94,9 %; N=13; N cells =198; Figure 2.6D, E). However, the proportion of acquired fates differed significantly between *dand5*$^{-/-}$ and WT embryos (Figure 2.6E; p-value = 0,0009). When considering LR cell fates within somites, we observed that in WT embryos, 53% of photoconverted NKSTCs were located on the left and 35% on the right somites. Therefore, in a pairwise comparison, we determined that left-sided somites received more photoconverted cells (p-value = 0.0457). In contrast, in *dand5*$^{-/-}$ mutants, 44% of NKSTCs were found on the left somites and 50.5% on the right somites, which was not significantly different in pairwise comparison (p = 0.4688). Moreover, in *dand5*$^{-/-}$embryos, the number of cells that integrated into the left somites was lower than that in WT embryos (Figure 6F; p-value = 0,0031). Thus, we concluded that in WT embryos, NKSTCs tend to incorporate more left-sided somites than right-sided somites. In contrast, this incorporation was mainly symmetric in *dand5*$^{-/-}$embryos, despite a tendency towards right-sided somites. These findings highlight the important role of Dand5 in establishing asymmetry in NKSTC fate and LR bias in somite incorporation by these cells in WT embryos.

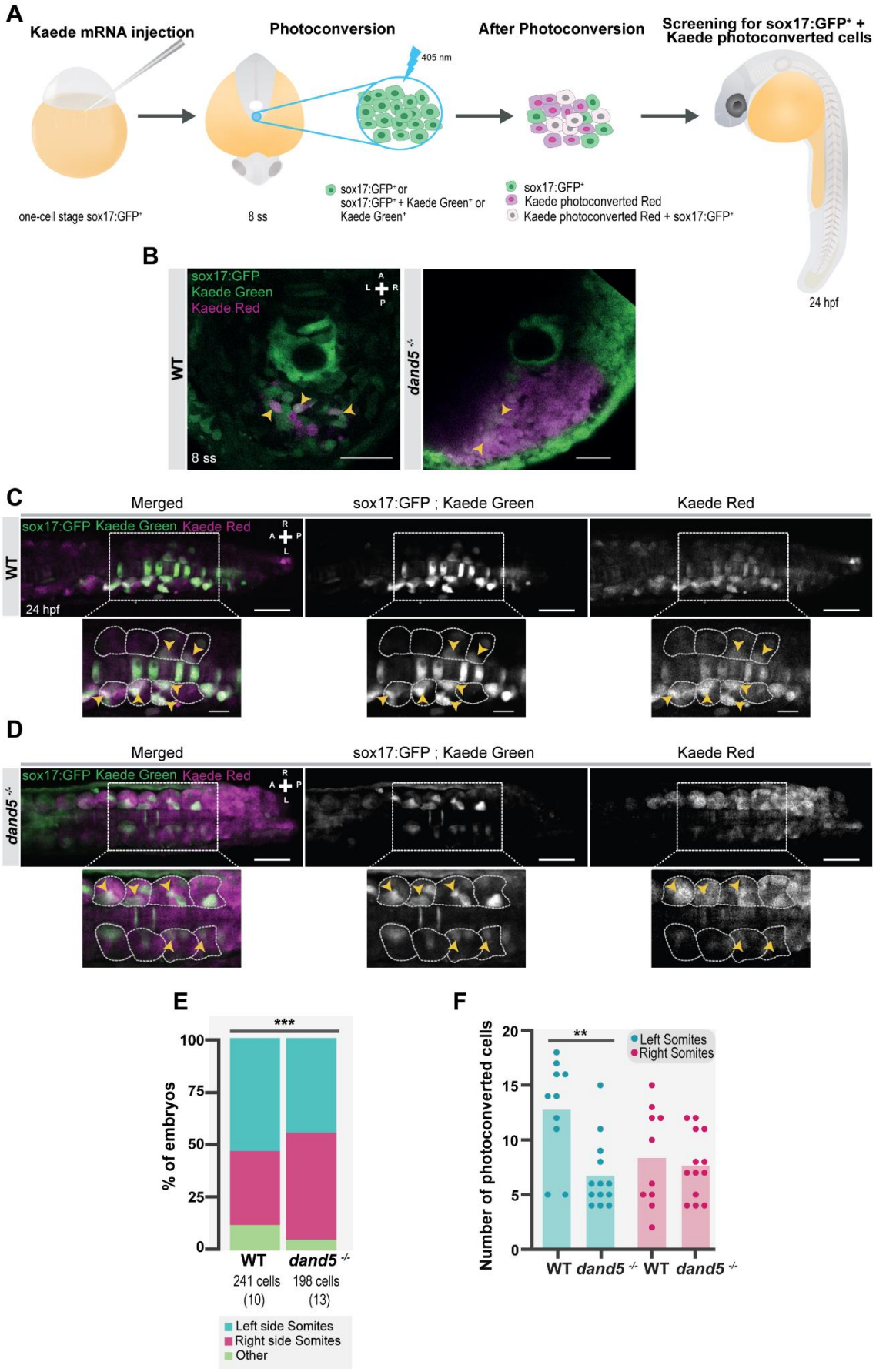
A
Kaede mRNA injection
Photoconversion
After Photoconversion
Screening for sox17:GFP+ + Kaede photoconverted cells
405 nm
one-cell stage sox17:GFP+
8 ss
sox17:GFP+ or sox17:GFP+ + Kaede Green− or Kaede Green+
sox17:GFP+
Kaede photoconverted Red
Kaede photoconverted Red + sox17:GFP+
24 hpf
B
sox17:GFP
Kaede Green
Kaede Red
WT
dand5 -/-
8 ss
C
Merged
sox17:GFP ; Kaede Green
Kaede Red
WT
24 hpf
D
dand5 -/-
E
***
% of embryos
100
75
50
25
0
WT
dand5 -/-
241 cells (10)
198 cells (13)
Left side Somites
Right side Somites
Other
F
**
Number of photoconverted cells
20
15
10
5
0
Left Somites
Right Somites
WT
dand5 -/-
WT
dand5 -/-

Figure 2.6. Fate mapping of NKSTCs. **(A)** Schematic representation of the fate map setup using the photoconvertible protein, Kaede. One-cell-stage Tg(sox17:GFP) embryos were injected with kaede mRNA. The 'posterior cluster' was photoconverted at 8 ss embryos using UV light. After photoconversion, three populations of cells were observed in the region of interest: sox17:GFP^{+} (green), Kaede photoconverted (magenta), and Kaede photoconverted colocalized with sox17:GFP^{+} (white). At 24 hpf, the embryos were screened for the location of Kaede photoconverted colocalized with sox17:GFP^{+} cells. The same procedure was used for *dand5*$^{-/-}$ embryos on *a Tg(sox17:GFP)* background. (**B**) Kaede photoconversion of the 'posterior cluster' at 8ss in WT and *dand5*$^{-/-}$ embryos. Kaede photoconverted is in magenta; sox17:GFP^{+} and Kaede not photoconverted are in green, and Kaede photoconverted colocalized with sox17:GFP^{+} cells are shown in white. Scale bar = 50 µm. (C) Dorsal view of a *Tg(sox17:GFP)* 24 hpf Kaede photoconverted embryo. Scale bar = 50 µm. Magnification shows the region of interest where NKSTCs (yellow arrowheads) are located at both the left and right somites (yellow arrowheads). The somites are outlined by light grey dashed lines. Scale bar = 20 µm. (**D**) Dorsal view of a *dand5*$^{-/-}$; *Tg(sox17:GFP)* 24 hpf Kaede photoconverted embryo. Scale bar = 50 µm. Magnification shows the region of interest where NKSTCs (yellow arrowheads) are located at both the left and right somites (yellow arrowheads). The somites are outlined by light grey dashed lines. Scale bar = 20 µm. **(E)** Quantification and comparison of the proportion of cells that incorporated somites and 'other fates' in both WT and *dand5*$^{-/-}$ 24 hpf embryos. Chi-square test. * corresponds to a p-value <0,05. **(F)** Quantification of differences in the number of NKSTCs per somite side. Cells on the left and right sides of WT vs. *dand5*$^{-/-}$. t-test paired and unpaired comparisons. Bars represent mean values and dots individual embryos. * corresponds to a p-value <0,05 and ** to a p-value <0,005. N is shown in parentheses.

Additionally, we investigated whether NKSTCs integrate somites in an anterior asymmetric manner. To test this hypothesis, we compared the maximum anterior positions of photoconverted NKSTCs with the anterior positions of Kaede photoconverted cells alone at 24 hpf (Supplementary Figure 2.4A) in the same embryos. We observed a left-sided bias in photoconverted NKSTCs (Supplementary Figure 2.4C) that was not evident when scoring all Kaede photoconverted cells (Supplementary Figure 2.4B). As photoconversion potentially reaches more cells along the axial cone of illumination of the confocal microscope (labeled magenta cells), it may make it more difficult to ascertain the subtle asymmetries found by observing only photoconverted NKSTCs (labeled both green and magenta).

To further understand the effects of NKSTCs on somite formation, we investigated whether early somite specification differed between WT and *dand5*$^{-/-}$ embryos. We aimed to score the expression of *myoD*, an early marker of myogenic commitment (Weinberg et al., 1996), and *dand5* using double staining in whole-mount in situ hybridization (WISH). In WT embryos, we could easily distinguish the mRNA of both genes in the tailbud because of the distinct 3D localization of the adaxial cells (dorsal) and the KV (ventral) (Supplementary Figure 2.5A). Moreover, in *dand5*$^{-/-}$ embryos, *dand5* mRNA is absent (Supplementary Figure 2.5B). Our first observation in WT embryos was that *myoD* expression in the presumptive somites was symmetrical on each side of the adaxial cells in 48% of the embryos (N = 27), indicating that we observed the same number of segments labeled by *myoD* on each side of the embryo.

However, in the remaining 52% of the embryos, *myoD* expression was asymmetrical (Figure 2.7A, B). We then scored the *dand5* expression in combination with the *myoD* expression. In most *dand5*$^{-/-}$ embryos, symmetrical myoD expression (82.8 %) was observed, which differed significantly from the WT expression pattern (Figure 2.7B; p-value = 0,0064).

Additionally, we found that 12% of *the dand5*$^{-/-}$ embryos exhibited fused somites at the midline at 15-16 ss (Supplementary Figure 2.5D, E), revealing a midline specification defect in a small portion of the embryos. We subsequently scored *dand5* expression at 15-16 ss and, as expected, found that in WT embryos, the expression was right-sided (85,19%, N=27; Figure 2.7C). This suggests that the absence of *dand5* is associated with symmetric *myoD* expression.

We also examined the impact of *dand5* heterozygosity on the expression patterns of both *dand5* and *myoD*. We analyzed 15-16 ss *dand5*$^{+/-}$ embryos and observed that 57.78% (N=45) exhibited dand5 right-sided expression, while 24.44% and 6.67% displayed bilateral and left-sided expression, respectively (Supplementary Figure 2.5D). Interestingly, 11.11% of the embryos showed no *dand5* mRNA expression. Although the rescue of right-sided *dand5* mRNA in *dand5*$^{+/-}$ was moderate, the expression pattern in 15-16 ss embryos was still different from that in WT (p-value = 0.0256). Our initial observations in WT embryos revealed that *myoD* expression in the presumptive somites was symmetrical on each side of the adaxial cells in 48% of the embryos (N = 27), indicating the same number of segments labeled by *myoD* on each side of the embryo. Furthermore, we observed symmetrical *myoD* expression in the majority of *dand5*$^{+/-}$embryos (68.3%), which differed from the WT expression pattern (Supplementary Figure 2.5E; p-value = 0.0080)

Furthermore, we observed that the width of the *myoD*-labelled segments was smaller in *dand5*$^{-/-}$ embryos than in WT embryos at 15 ss (p-value <0.0001) and 16 ss (Figure 2.7D; p-value = 0.0010). Therefore, the absence of Dand5 affects early somite specification, which may have resulted in smaller somites.

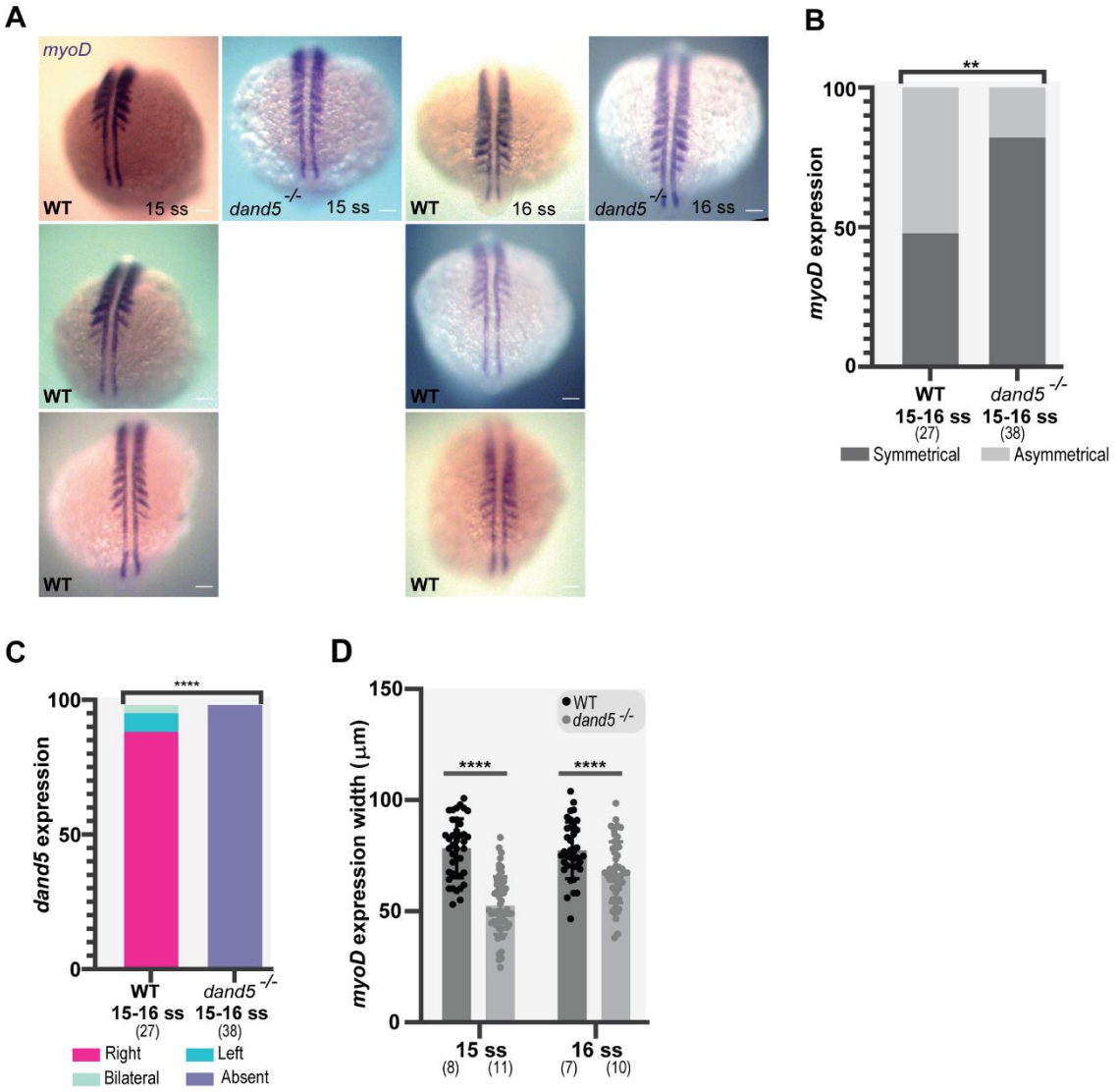

Figure 2.7. Whole-mount *in situ* hybridization reveals expression patterns of *myoD* and *dand5*. **(A-B)** Expression of *myoD* (purple) in WT and *dand5*$^{-/-}$ embryos, with side scoring. **(C)** Quantification of differences in *dand5* expression between WT and *dand5*$^{-/-}$ embryos. The chi-square test was used for statistical analysis. **(D)** Quantification of *myoD* expression width in WT and *dand5*$^{-/-}$ embryos at 15-16 ss. Bars represent mean values, and dots represent individual embryos. Statistical significance is indicated by asterisks: *p < 0.05, **p < 0.005, ***p < 0.0005, and ****p < 0.00005. Scale bar = 100 µm. The anterior region is at the top, and the posterior region is at the bottom. The N values are shown in parentheses.

The absence of the Dand5 function affects body size but not somite symmetry

Finally, to analyze the effect of the absence of Dand5 on somite morphology, we measured somite size in *dand5*$^{-/-}$ embryos using a different approach. We performed immunostaining for fibronectin (FN), which labels somite borders at 14 ss (Figure 2.8A). The results showed that body length was shorter in *the dand5*$^{-/-}$ mutants (Figure 2.8B; p-value <0,0001). Somite dimensions were measured and normalized to body length (Supplementary Figure 2.6A-C). We

established that Dand5 is essential for a regular somite size and body length at 14 ss. We also tested the differences between left and right somite sizes. We found a randomized distribution of left vs. right differences in both WT (Supplementary Figure 2.7A, B, and C) and *dand5*$^{-/-}$ embryos (Supplementary Figure 2.7D, E, and F). Therefore, we concluded that somite symmetry was not altered in WT or *dand5*$^{-/-}$ embryos. To test whether the smaller body length found in *dand5*$^{-/-}$ embryos could affect later zebrafish size, we compared the body length of WT and *dand5*$^{-/-}$ in 3 dpf larvae. We observed that 3 dpf *dand5*$^{-/-}$ larvae were slightly smaller than WT (Figure 2.7C, D; p-value = 0,0220). However, the difference at 3 dpf was less pronounced than that at 14 ss, indicating that the first observed difference in body size is likely transient. Thus, we concluded that body size could be rectified later, without affecting adult fish size.

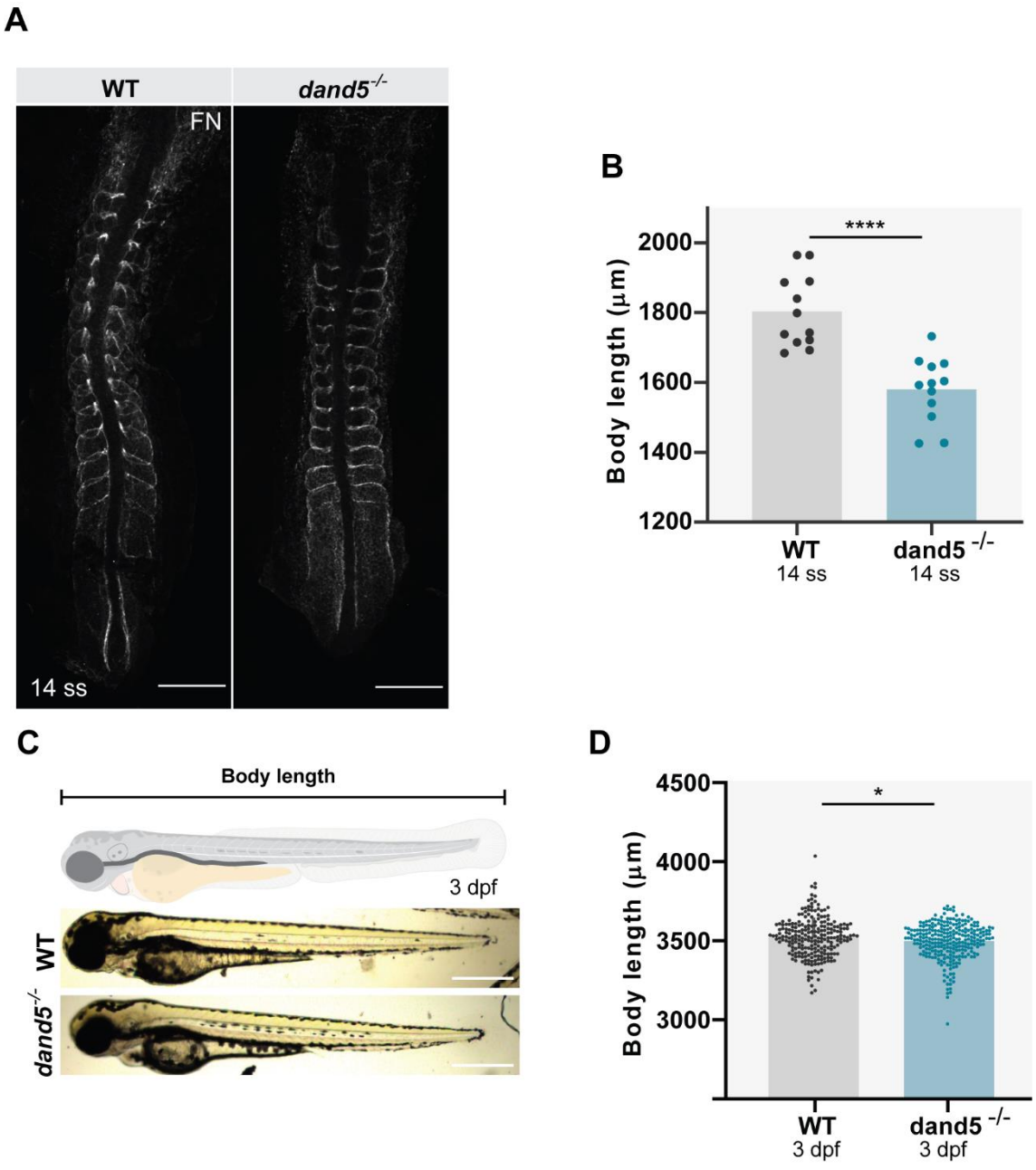

Figure 2.8. Body size and somite morphology in WT and *dand5*$^{-/-}$ embryos. **(A)** Fibronectin (FN) immunostaining showing somite borders in WT and *dand5*$^{-/-}$ embryos at 14 ss. Scale bar = 100 µm. The top is anterior, and the bottom is posterior. **(B)** Comparison of WT and *dand5*$^{-/-}$ body length at 14 ss. **(C)** WT and *dand5*$^{-/-}$ 3 dpf larvae and a schematic representation of body length measurements. Scale bar = 500 µm. **(D)** Comparison of body length measurements between WT (N = 234) and *dand5*$^{-/-}$ (N = 271) 3 dpf larvae. Gray represents WT embryos, and blue represents *dand5*$^{-/-}$ embryos. t-test unpaired comparison. Bars represent mean values, and dots represent individual embryos. * corresponds to a p-value <0,05; **** corresponds to a p-value <0,00005.

Discussion

In this study, we described a population of tailbud cells (NKSTCs) that exhibits LR asymmetric features in cell number and migration patterns. Our findings show that the majority of NKSTCs contribute to somites with a left-sided bias, and we have established that these cells respond to LR cues by losing their migratory asymmetries in the absence of Dand5.

As previously reviewed, symmetric structures must be protected from asymmetric cues in order to maintain bilateral synchronicity of the segmentation clock and wavefront, which involves two opposing gradients acting at the wavefront (Brend and Holley, 2009; Grimes, 2019). In zebrafish, *raldh2* (aldehyde dehydrogenase 1, A2) morphants and *nls* mutants (lacking RALDH2 activity) showed that a lack of RA signaling disrupted the synchronicity of somite formation by increasing the number of latest-formed somites on the left side between the 6th and 13th somites (Kawakami et al., 2005).

The timing of asymmetric somite formation in the absence of RA signaling is consistent with the time at which LR cues are transmitted to the LPM (Long et al., 2003). Kawakami *et al.* indicated that the asymmetric phenotype was due to the desynchronization of Notch activity on the left side, where cyclic genes, such as *deltaC*, *her1,* and *her7*, were out of phase between the left and right sides and showed an extension of *fgf8* expression on the right side (Kawakami et al., 2005). In the present study, we showed that 52% of WT embryos exhibited asymmetric *myoD* expression in the last-formed somites. Our findings suggest that asymmetries in somite formation may be common and result from early events that are resolved during development without impacting final somite differentiation. Using live imaging, we demonstrated that NKSTCs move asymmetrically from the posterior side of the embryo towards the anterior side and are biased to the left side in 50% of the embryos. We also confirmed by Kaede photoconversion and

fate mapping that these cells are somite precursors that eventually incorporate somites in a left-sided biased manner although somites later become symmetrical structures.

In addition, we showed that cell asymmetries in somite incorporation are due to the function of Dand5. In mutants homozygous for *dand5*, NKSTCs do not assume asymmetric positions and incorporate somites in a randomized manner.

In conclusion, our study reveals the existence of a tailbud population of cells with LR asymmetric features that contribute to somite formation, shedding light on the mechanisms underlying LR patterning and symmetry maintenance during embryonic development. Our findings also have implications for the understanding of the role of asymmetric cues in the formation of symmetric structures.

myoD expression patterns are affected by Dand5

In this study, we investigated the role of *dand5* in the expression patterns of *myoD* during embryonic segmentation. *dand5* is reported to be expressed throughout the segmentation period from 1-25 ss (White et al., 2017), with higher expression peaks observed between 14-19 ss (White et al., 2017) when asymmetry is already established at the LPM (Long et al., 2003). Moreover, its expression is limited to KV-derived cells (Ikeda et al., 2022). These findings suggest that Dand5 secreted by KV cells, besides breaking embryonic symmetry may play an important role in a yet unknown process. On the other hand, *myoD* expression is first detected from 75% epiboly closer to the organizer and starts in the adaxial cells on each side of the future notochord before somite formation. Immediately after somite formation, *myoD* is expressed bilaterally in the posterior most region of the somites. In this study, we observed that in WT embryos, *myoD* expression fluctuates, as it is not perfectly aligned bilaterally in 50% of the cases, with one side of the embryo showing one extra presumptive somite marked by *myoD* expression. However, in *dand5*$^{-/-}$ embryos, *myoD* expression was always symmetric. Therefore, the absence of Dand5 may prevent fluctuations in a LR manner during myogenic differentiation.

Here, we showed that there is noise in the process of myogenesis , with the left and right sides not always perfectly aligned. Dand5 secreted protein, encoded by the first known asymmetric gene, seems to be responsible for generating some asymmetry in presumptive somites from the 13 to 15 somite stage. To understand the extent to which Dand5 interacts with myogenic differentiation and somite specification, further evaluation of the expression patterns of other myogenic differentiation factors and clock genes in the absence of *dand5* expression is required.

Embryos are smaller in the absence of Dand5

The flow of cells through the PSM has been proposed to control somite size (Fior et al., 2012). The differentiation and movement of mesoderm progenitor cells from the tailbud to the PSM are regulated by the expression of *tbx16* and *msgn1* (Fior et al., 2012; Yabe and Takada, 2012; Manning and Kimelman, 2015). In the absence of *msgn1,* somites are consequently smaller due to decreased cell flow (Fior et al., 2012) and *tbx16* and *msgn1* mutants show deficient exit from the mesodermal progenitor zone due to unproductive lamellipodia and loss of directed movement to the anterior side (Manning and Kimelman, 2015). Such publications support our results because, despite being transient, *dand5*$^{-/-}$ embryos showed smaller somites proportional to their shorter body length. Additionally, we observed that *dand5*$^{-/-}$ embryos showed fewer cells exiting from the posterior cluster, and fewer photoconverted cells were found in somites at 24 hpf.

The tailbud is an overly complex region of diverse molecular interactions: Wnt and FGF signaling cooperate to induce mesodermal commitment from the neuromesodermal population, thereby positively regulating *tbx16* and *msgn1* (Goto et al., 2017). Controlled levels of BMP signaling in the zebrafish tail are also vital for the correct exit of cells from the tailbud and differentiation into tail somites, with high levels of BMP inhibiting cell exit from the tailbud (O'Neill and Thorpe, 2013). Nodal is also essential for tailbud cell exit, since *oep;tbx16* mutants lack somites (Griffin and Kimelman, 2002), but not by inhibiting BMP signaling (O'Neill and Thorpe, 2013). In zebrafish, Dand5 was shown to inhibit all three Nodals: *sqnt*, *cyc*, and *spaw*, and to exert weak BMP inhibition given the absence of a dorsalized phenotype upon *dand5* overexpression (Hashimoto et al., 2004). Therefore, we hypothesize that Dand5 could be regulating tailbud cell exit to the PSM by inhibiting Nodal or BMP signaling. Furthermore, Dand5 could inhibit BMP locally in cells close to the KV and KV-derived cells, where *dand5* expression persists; therefore, we suggest Dand5 could maintain optimal levels of BMP signaling and cooperate with *chordin* and *noggin* (Dal-Pra et al., 2006; Von Der Hardt et al., 2007) controlling cell exit from the tailbud.

Alternatively, in *dand5*$^{-/-}$ embryos, earlier *spaw* expression, seen in KV adjacent cells (Montague et al., 2018), could affect the induction of somite precursors to leave the tailbud, accelerating the initial cell flow into the PSM and consequently reducing the number of cells in the tailbud niche. These interpretations, here formulated as two hypotheses, highlight the potential role of Dand5 in somite precursor specification, in addition to LR establishment. Thus, to verify how tailbud cell exit is affected, we highlight the need for further studies regarding BMP and Wnt

signaling and assessing *msgn1* and *tbx16* expression in the zebrafish tailbud under the manipulation of *dand5* expression.

Conclusions

Our report on the link between the first asymmetric gene in LR establishment, *dand5*, in zebrafish tailbud movements sets the foundation for studying the involvement of other genes of the LR cascade in this context. Since, *spaw* is asymmetrically expressed in the LPM due to inhibition by Dand5, further studies on tailbud cell movement, myogenic differentiation, and tail size in *spaw*$^{-/-}$ and *dand5*$^{-/-}$;*spaw*$^{-/-}$ (Montague et al., 2018) embryos would aid in evaluating the link between LR patterning and tailbud events. The findings have implications for the understanding of the role of asymmetric cues in the formation of symmetric structures and provide insights into the mechanisms underlying embryonic development.

As a final illustrative summary, we describe the different steps affected by the absence of Dand5 and the KV without inferring a causal relationship (Figure 2.9).

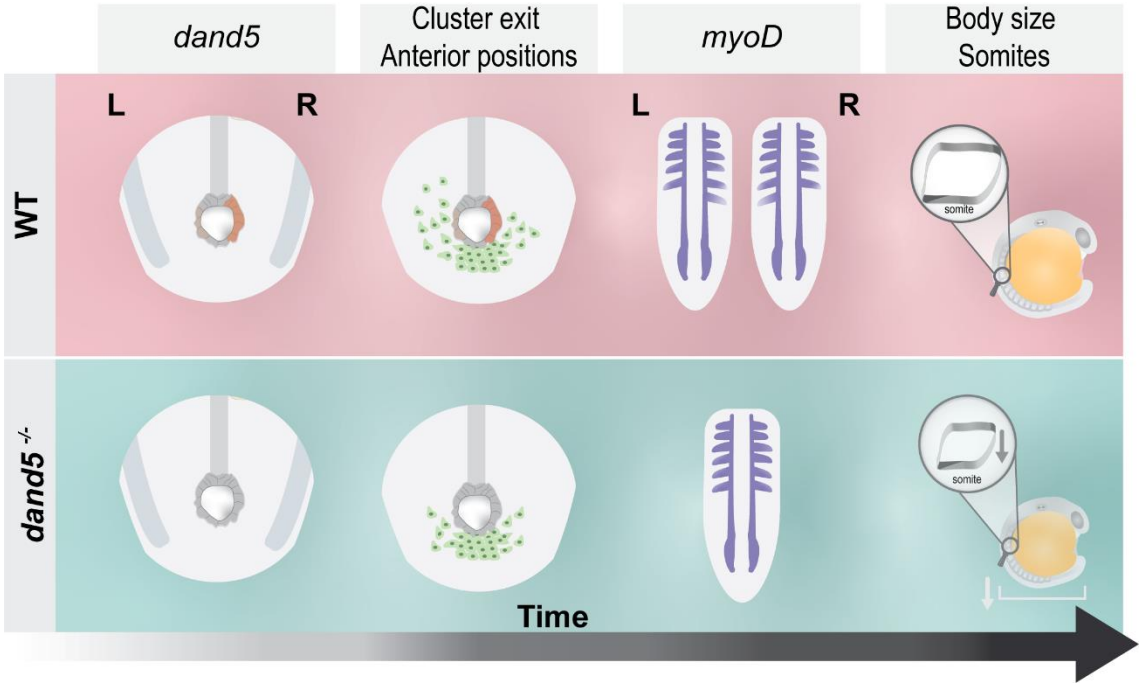

Figure 2.9. Schematic illustration of the main findings of this study. In WT embryos, *dand5* is expressed on the right side of the LRO, NKSTCs exit the posterior cluster first from the left side in 50% of the embryos, and *myoD* is symmetrical in the same proportion of embryos. In *dand5*$^{-/-}$ mutants, which lack *dand5* expression, NKSTCs simultaneously depart from the posterior cluster from the left and right sides and acquire symmetrical positions. Later, *myoD* presumptive somite expression becomes symmetric, accordingly. In addition, in *dand5* mutants, the width of the *myoD* segments was significantly shorter and the body length was decreased.

References

Amack, J. D., and Yost, H. J. (2004). The T box transcription factor no tail in ciliated cells controls zebrafish left-right asymmetry. Current biology 14, 685–690.

Bachiller, D., Agius, E., Kemp, C., Borges, A. C., Marques, S., Piccolo, S., et al. (2000). Cerberus-like Is a Secreted BMP and Nodal Antagonist Not Essential for Mouse Development. 270, 265–270.

Banavar, S. P., Carn, E. K., and Rowghanian, P. (2021). Mechanical control of tissue shape and morphogenetic flows during vertebrate body axis elongation. Scientific Reports, 1–14. doi: 10.1038/s41598-021-87672-3.

Behrndt, M., Salbreux, G., Campinho, P., Hauschild, R., Oswald, F., Roensch, J., et al. (2012). Forces driving epithelial spreading in zebrafish gastrulation. Science 338, 257–260.

Brend, T., and Holley, S. A. (2009). Balancing segmentation and laterality during vertebrate development. in Seminars in cell & developmental biology (Elsevier), 472–478.

Callol-massot, C., and Izpisu, J. C. (2006). Regulation of primary cilia formation and left-right patterning in zebrafish by a noncanonical Wnt signaling mediator , duboraya. 38, 1316–1322. doi: 10.1038/ng1892.

Collignon, J., Varlet, I., and Robertson, E. J. (1996). Relationship between asymmetric nodal expression and the direction of embryonic turning. Nature 381, 155–158. doi: 10.1038/381155a0.

Compagnon, J., Barone, V., Rajshekar, S., Kottmeier, R., Pranjic-Ferscha, K., Behrndt, M., et al. (2014). The notochord breaks bilateral symmetry by controlling cell shapes in the zebrafish laterality organ. Developmental cell 31, 774–783.

Cooper, M. S., and D'amico, L. A. (1996). A cluster of noninvoluting endocytic cells at the margin of the zebrafish blastoderm marks the site of embryonic shield formation. Developmental biology 180, 184–198.

Dahm, R., and Nüsslein-Volhard, C. (2002). Zebrafish: A practical approach. Oxford University Press doi: 10.1017/S0016672303216384.

Dal-Pra, S., Fürthauer, M., Van-Celst, J., Thisse, B., and Thisse, C. (2006). Noggin1 and Follistatin-like2 function redundantly to Chordin to antagonize BMP activity. Developmental biology 298, 514–526.

Das, D., Jülich, D., Schwendinger-Schreck, J., Guillon, E., Lawton, A. K., Dray, N., et al. (2019). Organization of embryonic morphogenesis via mechanical information. Developmental cell 49, 829–839.

Dasgupta, A., Merkel, M., Clark, M. J., Jacob, A. E., Dawson, J. E., Manning, M. L., et al. (2018). Cell volume changes contribute to epithelial morphogenesis in zebrafish Kupffer's vesicle. eLife 7, e30963. doi: 10.7554/eLife.30963.

Devoto, S. H., Melançon, E., Eisen, J. S., and Westerfield, M. (1996). Identification of separate slow and fast muscle precursor cells in vivo, prior to somite formation. Development 122, 3371–3380.

Essner, J. J., Amack, J. D., Nyholm, M. K., Harris, E. B., and Yost, H. J. (2005). Kupffer's vesicle is a ciliated organ of asymmetry in the zebrafish embryo that initiates left-right development of the brain, heart and gut. Development 132 (6), 1247–1260. doi: https://doi.org/10.1242/dev.01663.

Essner, J. J., Branford, W. W., Zhang, J., and Yost, H. J. (2000). Mesendoderm and left-right brain , heart and gut development are differentially regulated by pitx2 isoforms. 1093, 1081–1093.

Ferreira, R. R., and Vermot, J. (2017). The balancing roles of mechanical forces during left-right patterning and asymmetric morphogenesis. Mechanisms of Development 144, 71–80. doi: 10.1016/j.mod.2016.11.001.

Field, S., Riley, K.-L., Grimes, D. T., Hilton, H., Simon, M., Powles-Glover, N., et al. (2011). Pkd1l1 establishes left-right asymmetry and physically interacts with Pkd2. Development 138, 1131–1142. doi: 10.1242/dev.058149.

Fior, R., Maxwell, A. A., Ma, T. P., Vezzaro, A., Moens, C. B., Amacher, S. L., et al. (2012). The differentiation and movement of presomitic mesoderm progenitor cells are controlled by Mesogenin 1. 4665, 4656–4665. doi: 10.1242/dev.078923.

Gokey, J. J., Ji, Y., Tay, H. G., Litts, B., and Amack, J. D. (2016). Kupffer's vesicle size threshold for robust left-right patterning of the zebrafish embryo. Developmental Dynamics 245, 22–33. doi: 10.1002/dvdy.24355.

Goto, H., Kimmey, S. C., Row, R. H., Matus, D. Q., and Martin, B. L. (2017). FGF and canonical Wnt signaling cooperate to induce paraxial mesoderm from tailbud neuromesodermal progenitors through regulation of a two-step epithelial to mesenchymal transition. Development 144, 1412–1424.

Griffin, K. J. P., and Kimelman, D. (2002). One-Eyed Pinhead and Spadetail are essential for heart and somite formation. Nature Cell Biology 4, 821–825.

Grimes, D. T. (2019a). Making and breaking symmetry in development, growth and disease. Development 146, dev170985.

Grimes, D. T. (2019b). Making and breaking symmetry in development , growth and disease. doi: 10.1242/dev.170985.

Grimes, D. T., and Burdine, R. D. (2017). Left-Right Patterning: Breaking Symmetry to Asymmetric Morphogenesis. Trends in Genetics 33, 616–628. doi: 10.1016/j.tig.2017.06.004.

Hashimoto, H., Rebagliati, M., Ahmad, N., Muraoka, O., Kurokawa, T., Hibi, M., et al. (2004). The Cerberus/Dan-family protein Charon is a negative regulator of Nodal signaling during left-right patterning in zebrafish. Development 131, 1741–1753. doi: 10.1242/dev.01070.

Hojo, M., Takashima, S., Kobayashi, D., Sumeragi, A., Shimada, A., Tsukahara, T., et al. (2007). Right-elevated expression of charon is regulated by fluid flow in medaka Kupffer ' s vesicle. 395–405. doi: 10.1111/j.1440-169x.2007.00937.x.

Ikeda, T., Inamori, K., Kawanishi, T., and Takeda, H. (2022a). Reemployment of Kupffer's vesicle cells into axial and paraxial mesoderm via transdifferentiation. Development, Growth & Differentiation 64, 163–177.

Ikeda, T., Inamori, K., Kawanishi, T., and Takeda, H. (2022b). Reemployment of Kupffer ' s vesicle cells into axial and paraxial mesoderm via transdifferentiation. 1–15. doi: 10.1111/dgd.12774.

Kamura, K., Kobayashi, D., Uehara, Y., Koshida, S., Iijima, N., Kudo, A., et al. (2011). Pkd1l1 complexes with Pkd2 on motile cilia and functions to establish the left-right axis. Development 138, 1121–1129. doi: 10.1242/dev.058271.

Kanki, J. P., and Ho, R. K. (1997). The development of the posterior body in zebrafish. Development 124, 881–893.

Kawakami, Y., Raya, Á., Raya, R. M., Rodríguez-Esteban, C., and Belmonte, J. C. I. (2005). Retinoic acid signalling links left–right asymmetric patterning and bilaterally symmetric somitogenesis in the zebrafish embryo. Nature 435, 165–171. doi: 10.1038/nature03512.

Kim, J., Bae, S., Lee, H. S., Park, J., and Kim, K. (2017). Claudin5a is required for proper inflation of Kupffer ' s vesicle lumen and organ laterality. 1–18.

Kimmel, C. B., Ballard, W. W., Kimmel, S. R., Ullmann, B., and Schilling, T. F. (1995). Stages of embryonic development of the zebrafish. Developmental Dynamics 203, 253–310. doi: 10.1002/aja.1002030302.

Kreiling, J. A., Prabhat, Williams, G., and Creton, R. (2007). Analysis of Kupffer's vesicle in zebrafish embryos using a cave automated virtual environment. Developmental Dynamics 236, 1963–1969. doi: 10.1002/dvdy.21191.

Lawton, A. K., Nandi, A., Stulberg, M. J., Dray, N., Sneddon, M. W., Pontius, W., et al. (2013). Regulated tissue fluidity steers zebrafish body elongation. Development 140, 573–582.

Lenhart, K. F., Lin, S., Titus, T. A., Postlethwait, J. H., and Burdine, R. D. (2011). Two additional midline barriers function with midline lefty1 expression to maintain asymmetric Nodal signaling during left-right axis specification in zebrafish INTRODUCTION. 4410, 4405–4410. doi: 10.1242/dev.071092.

Levin, M., Johnson, R. L., Sterna, C. D., Kuehn, M., and Tabin, C. (1995). A molecular pathway determining left-right asymmetry in chick embryogenesis. Cell 82, 803–814. doi: 10.1016/0092-8674(95)90477-8.

Lin, C., Tsai, M., Liu, Y., Lu, Y., Chen, Y., Lai, Y., et al. (2017). Klf8 regulates left-right asymmetric patterning through modulation of Kupffer ' s vesicle morphogenesis and spaw expression. 1–14. doi: 10.1186/s12929-017-0351-y.

Long, S. (2003). The zebrafish nodal-related gene southpaw is required for visceral and diencephalic left-right asymmetry. Development 130, 2303–2316. doi: 10.1242/dev.00436.

Long, S., Ahmad, N., and Rebagliati, M. (2003). The zebrafish nodal-related gene southpaw is required for visceral and diencephalic left-right asymmetry. Development 130, 2303–2316.

Lopes, S. S., Lourenco, R., Pacheco, L., Moreno, N., Kreiling, J., and Saude, L. (2010). Notch signalling regulates left-right asymmetry through ciliary length control. Development 137, 3625–3632. doi: 10.1242/dev.054452.

Maerker, M., Getwan, M., Dowdle, M. E., McSheene, J. C., Gonzalez, V., Pelliccia, J. L., et al. (2021). Bicc1 and Dicer regulate left-right patterning through post-transcriptional control of the Nodal inhibitor Dand5. Nature communications 12, 1–15.

Manning, A. J., and Kimelman, D. (2015). Tbx16 and Msgn1 are required to establish directional cell migration of zebra fi sh mesodermal progenitors. Developmental Biology 406, 172–185. doi: 10.1016/j.ydbio.2015.09.001.

Martin, B. L., and Kimelman, D. (2012). Canonical Wnt signaling dynamically controls multiple stem cell fate decisions during vertebrate body formation. Developmental cell 22, 223–232.

Matsui, T., Ishikawa, H., and Bessho, Y. (2015). Cell collectivity regulation within migrating cell cluster during Kupffer's vesicle formation in zebrafish. Frontiers in cell and developmental biology 3, 27. doi: 10.3389/fcell.2015.00027.

Minegishi, K., Rothé, B., Komatsu, K. R., Ono, H., Ikawa, Y., Nishimura, H., et al. (2021). Fluid flow-induced left-right asymmetric decay of Dand5 mRNA in the mouse embryo requires a Bicc1-Ccr4 RNA degradation complex. Nature Communications 12, 1–17.

Mongera, A., Rowghanian, P., Gustafson, H. J., Shelton, E., Kealhofer, D. A., Carn, E. K., et al. (2018). vertebrate body axis elongation. Nature. doi: 10.1038/s41586-018-0479-2.

Montague, T. G., Gagnon, J. A., and Schier, A. F. (2018a). Conserved regulation of Nodal-mediated left-right patterning in zebrafish and mouse. Development 145, dev171090.

Montague, T. G., Gagnon, J. A., and Schier, A. F. (2018b). Conserved regulation of Nodal-mediated left-right patterning in zebrafish and mouse Development • Accepted manuscript. 3. doi: 10.1242/dev.171090.

Naganathan, S. R., Popović, M., and Oates, A. C. (2022). Left–right symmetry of zebrafish embryos requires somite surface tension. Nature 605, 516–521.

Navis, A., Marjoram, L., and Bagnat, M. (2013). Cftr controls lumen expansion and function of Kupffer ' s vesicle in zebrafish. 1712, 1703–1712. doi: 10.1242/dev.091819.

O'Neill, K., and Thorpe, C. (2013). BMP signaling and spadetail regulate exit of muscle precursors from the zebrafish tailbud. Developmental biology 375, 117–127.

Oates, A. C., Morelli, L. G., and Ares, S. (2012). Patterning embryos with oscillations: structure, function and dynamics of the vertebrate segmentation clock. Development 139, 625–639.

Oteíza, P., Köppen, M., Concha, M. L., and Heisenberg, C.-P. (2008). Origin and shaping of the laterality organ in zebrafish. Development (Cambridge, England) 135, 2807–13. doi: 10.1242/dev.022228.

Pennekamp, P., Karcher, C., Fischer, A., Schweickert, A., Skryabin, B., Horst, J., et al. (2002). The ion channel polycystin-2 is required for left-right axis determination in mice. Current Biology 12, 938–943. doi: 10.1016/S0960-9822(02)00869-2.

Pownall, M. E., Gustafsson, M. K., and Emerson Jr, C. P. (2002). Myogenic regulatory factors and the specification of muscle progenitors in vertebrate embryos. Annual review of cell and developmental biology 18, 747–783.

Prummel, K. D., Hess, C., Nieuwenhuize, S., Parker, H. J., Rogers, K. W., Kozmikova, I., et al. (2019). A conserved regulatory program initiates lateral plate mesoderm emergence across chordates. Nature Communications, 1–15. doi: 10.1038/s41467-019-11561-7.

Rathbun, L. I., Colicino, E. G., Manikas, J., O'Connell, J., Krishnan, N., Reilly, N. S., et al. (2020). Cytokinetic bridge triggers de novo lumen formation in vivo. Nature communications 11, 1269.

Roxo-rosa, M., Jacinto, R., Sampaio, P., and Lopes, S. S. (2015). The zebrafish Kupffer ' s vesicle as a model system for the molecular mechanisms by which the lack of Polycystin-2 leads to stimulation of CFTR. 1356–1366. doi: 10.1242/bio.014076.

Sakaguchi, T., Kikuchi, Y., Kuroiwa, A., Takeda, H., and Stainier, D. Y. R. (2006). The yolk syncytial layer regulates myocardial migration by influencing extracellular matrix assembly in zebrafish. Development 133, 4063–4072. doi: doi.org/10.1242/dev.02581.

Sampaio, P., Ferreira, R. R., Guerrero, A., Pintado, P., Tavares, B., Amaro, J., et al. (2014). Left-right organizer flow dynamics: How much cilia activity reliably yields laterality? Developmental Cell 29, 716–728. doi: 10.1016/j.devcel.2014.04.030.

Sánchez-Iranzo, H., Galardi-Castilla, M., Minguillón, C., Sanz-Morejón, A., González-Rosa, J. M., Felker, A., et al. (2018). Tbx5a lineage tracing shows cardiomyocyte plasticity during zebrafish heart regeneration. Nature communications 9, 428.

Sanematsu, P. C., Erdemci-Tandogan, G., Patel, H., Retzlaff, E. M., Amack, J. D., and Manning, M. L. (2021). 3D viscoelastic drag forces contribute to cell shape changes during organogenesis in the zebrafish embryo. Cells & Development 168, 203718. doi: https://doi.org/10.1016/j.cdev.2021.203718.

Saydmohammed, M., Yagi, H., Calderon, M., Clark, M. J., Feinstein, T., Sun, M., et al. (2018). Vertebrate myosin 1d regulates left–right organizer morphogenesis and laterality. Nature Communications 9, 3381.

Schier, A. F. (2003). Nodal Signaling in Vertebrate Development. Annual Review of Cell and Developmental Biology 19, 589–621. doi: 10.1146/annurev.cellbio.19.041603.094522.

Schindelin, J., Arganda-Carreras, I., Frise, E., Kaynig, V., Longair, M., Pietzsch, T., et al. (2012). Fiji: an open-source platform for biological-image analysis. Nature methods 9, 676–682.

Schottenfeld, J., Sullivan-brown, J., and Burdine, R. D. (2007). Zebrafish curly up encodes a Pkd2 ortholog that restricts left-side-specific expression of southpaw. Development 134, 1605–1615. doi: 10.1242/dev.02827.

Schweickert, A., Ott, T., Kurz, S., Tingler, M., Maerker, M., Fuhl, F., et al. (2017). Vertebrate Left-Right Asymmetry: What Can Nodal Cascade Gene Expression Patterns Tell Us? Journal of Cardiovascular Development and Disease 5, 1. doi: 10.3390/jcdd5010001.

Schweickert, A., Vick, P., Getwan, M., Weber, T., Schneider, I., Eberhardt, M., et al. (2010). The nodal inhibitor Coco is a critical target of leftward flow in Xenopus. Current Biology 20, 738–743.

Schweickert, A., Weber, T., Beyer, T., Vick, P., Bogusch, S., Feistel, K., et al. (2007). Report Cilia-Driven Leftward Flow Determines Laterality in Xenopus. 60–66. doi: 10.1016/j.cub.2006.10.067.

Shen, M. M. (2007). Nodal signaling: developmental roles and regulation. Development 134, 1023–1034. doi: 10.1242/dev.000166.

Supatto, W., Fraser, S. E., and Vermot, J. (2008). An All-Optical Approach for Probing Microscopic Flows in Living Embryos. Biophysical Journal 95, L29–L31. doi: 10.1529/biophysj.108.137786.

Tavares, B., Jacinto, R., Sampaio, P., Pestana, S., Pinto, A., Vaz, A., et al. (2017). Notch/Her12 signalling modulates, motile/immotile cilia ratio downstream of Foxj1a in zebrafish left-right organizer. Elife 6, e25165.

Vermot, J., and Pourquié, O. (2005). Retinoic acid coordinates somitogenesis and left–right patterning in vertebrate embryos. Nature 435, 215–220.

Von Der Hardt, S., Bakkers, J., Inbal, A., Carvalho, L., Solnica-Krezel, L., Heisenberg, C.-P., et al. (2007). The Bmp gradient of the zebrafish gastrula guides migrating lateral cells by regulating cell-cell adhesion. Current Biology 17, 475–487.

Wang, G., Cadwallader, A. B., Jang, D. S., Tsang, M., Yost, H. J., and Amack, J. D. (2011). The Rho kinase Rock2b establishes anteroposterior asymmetry of the ciliated Kupffer ' s vesicle in zebrafish. 54, 45–54. doi: 10.1242/dev.052985.

Wang, G., Manning, M. L., and Amack, J. D. (2012). Regional cell shape changes control form and function of Kupffer's vesicle in the zebrafish embryo. Developmental biology 370, 52–62.

Wang, X., and Yost, H. J. (2008). Initiation and propagation of posterior to anterior (PA) waves in zebrafish left–right development. Developmental Dynamics 237, 3640–3647.

White, R. J., Collins, J. E., Sealy, I. M., Wali, N., Dooley, C. M., Digby, Z., et al. (2017). A high-resolution mRNA expression time course of embryonic development in zebrafish. eLife, 1–32.

Yabe, T., and Takada, S. (2012). Mesogenin causes embryonic mesoderm progenitors to differentiate during development of zebrafish tail somites. Developmental Biology 370, 213–222. doi: 10.1016/j.ydbio.2012.07.029.

Yoshiba, S., Shiratori, H., Kuo, I. Y., Kawasumi, A., Shinohara, K., Nonaka, S., et al. (2012). Cilia at the node of mouse embryos sense fluid flow for left-right determination via Pkd2. Science 338, 226–231.

Yuan, S., Zhao, L., Brueckner, M., and Sun, Z. (2015). Intraciliary calcium oscillations initiate vertebrate left-right asymmetry. Current biology 25, 556–567.

Zinski, J., Tajer, B., and Mullins, M. C. (2017). TGF-β Family Signaling in Early Vertebrate Development. Cold Spring Harbor Perspectives in Biology, a033274.

Supplementary Material

Supplementary videos

Supplementary Video 2.1. Time-lapse imaging of asymmetric NKSTC positions from two-photon z-stacks of a Tg(sox17:GFP) embryo starting at 13 ss**.** On the left side, sox17:GFP+ cells are shown in green as a composite with transmitted light, and on the right side, in grayscale. NKSTCs reach more anterior positions on the left side of the KV. Dorsal view: The anterior is to the top, and the left is to the left.

Supplementary Video 2.2. NKSTCs migration is characterized by live imaging. Representative tracking of individual cells. Migrating cells near the KV were manually tracked in a time-lapse of two-photon z-stacks of a Tg(sox17:GFP) embryo starting at 11 ss using Imaris (Bitplane). Frames were acquired every 3 min. The tracked cells are marked by cyan and magenta spots on the left and right sides, respectively. At the starting point, spots marked the cells that started migrating at consecutive time points. The associated tracks are displayed in a heatmap color scheme for

the elapsed time. Tracked cells on the left side acquired more anterior positions over time than those on the right side. Dorsal view: The anterior is to the top, and the left is to the left.

Supplementary Video 2.3. An unreported cluster of NKSTCs posterior to the KV. Time-lapse imaging from two-photon z-stacks of a Tg(sox17:GFP) embryo starting at 10 ss. Frames were acquired every 6 min. NKSTCs are present posterior to the KV. During tail elongation, the KV moves through the posterior cluster. Immediately after the KV reached the NKSTCs cluster, a few cells started leaving the left side. Soon, more cells were seen performing the same behavior on both the left and right sides, displaying asymmetric positions. Dorsal view: The anterior is to the top, and the left is to the left.

Supplementary Video 2.4. Time-lapse imaging from confocal z-stacks of a *dand5*$^{-/-}$ embryo raised on the Tg(sox17:GFP) background, starting at 10 ss. Frames were acquired every 2 min. A posterior NKSTCs cluster is present posterior to the KV. As the KV progresses posteriorly, cells leave the cluster simultaneously from the left and right sides. Dorsal view: The anterior is to the top, and the left is to the left.

Supplementary Figures

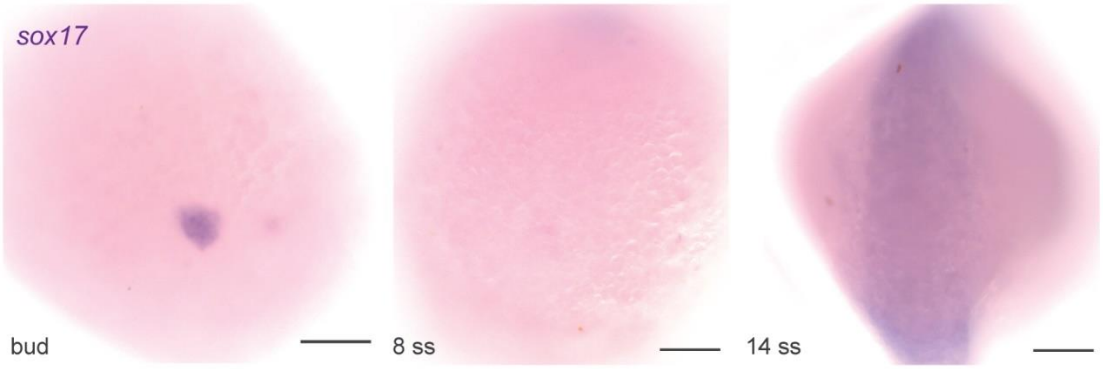

Supplementary Figure 2.1. sox17:GFP^{+} cells in the vicinity of the KV do not express *sox17* .WISH showed that *sox17* is expressed at the bud stage in DFCs but not in the KV and cells outside the KV from the 8 ss onwards. Scale bar = 30 µm. The top of the image is anterior, the bottom is posterior, the left is left, and the right is right.

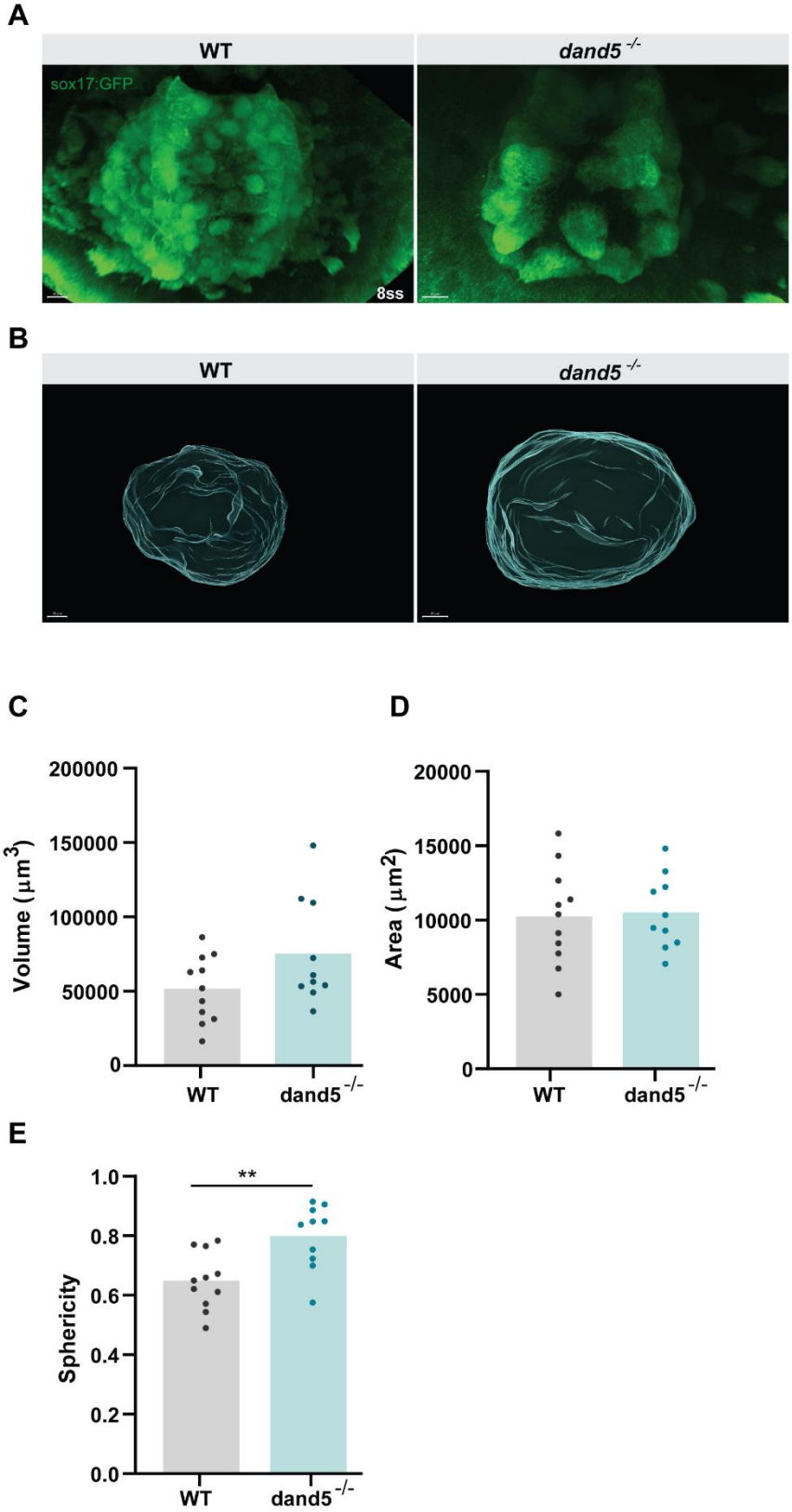

Supplementary Figure 2.2. Effect of *dand5* absence on KV morphology. **(A)** 3D visualization of the KV in Tg(sox17:GFP) and *dand5*$^{-/-}$ raised on Tg(sox17:GFP) background embryos at 8 ss. **(B)** 3D surfaces from the KV lumen in Tg(sox17:GFP) and *dand5*$^{-/-}$ on Tg(sox17:GFP) background embryos at 8 ss. Comparison of volume **(C)**, area **(D)**, and sphericity **(E)** between WT and *dand5*$^{-/-}$ embryos. Scale bar = 30 µm. The top of the image is anterior, the bottom is posterior, the left is left, and the right is right.

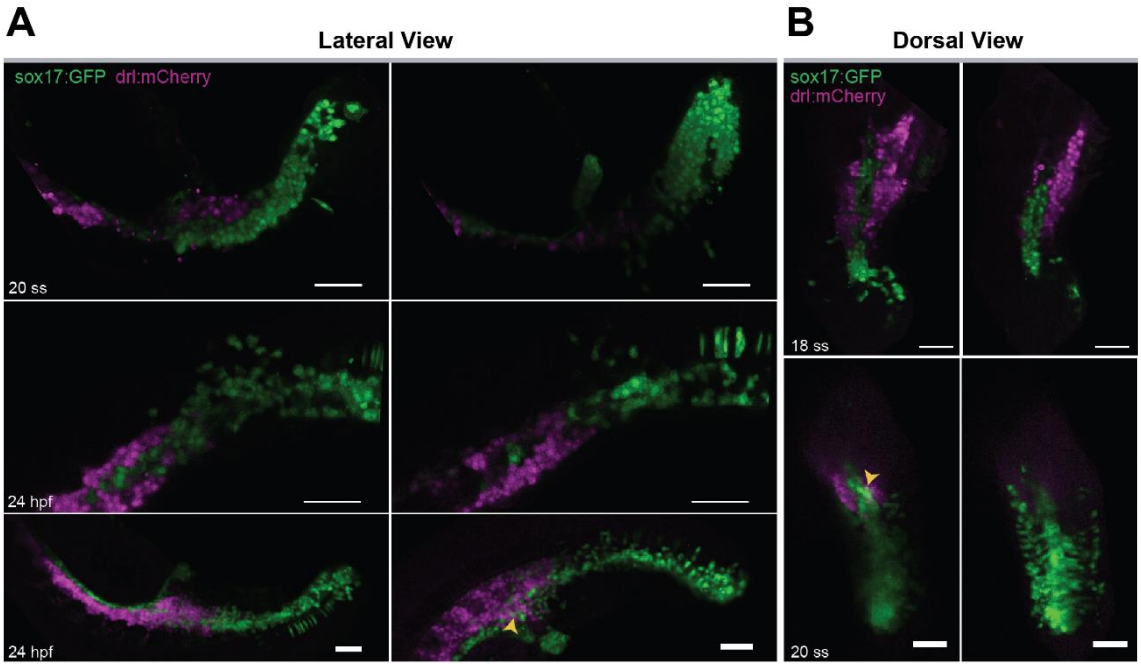

Supplementary Figure 2.3. sox17:GFP^{+} cells do not colocalize with drl:mCherry. **(B-C)** 18 ss, 20 ss, or 24 hpf, except for some gut tube cells (yellow arrowheads**).** Scale bar = 30 µm. **(B)** Lateral view of single z-planes of *T(sox17:GFP);Tg(drl:mCherry)* embryos. Left, anterior; right, posterior. **(C)** Dorsal view of single z-planes of T(sox17:GFP);Tg(drl:mCherry) embryos. The top is anterior, and the left is left.

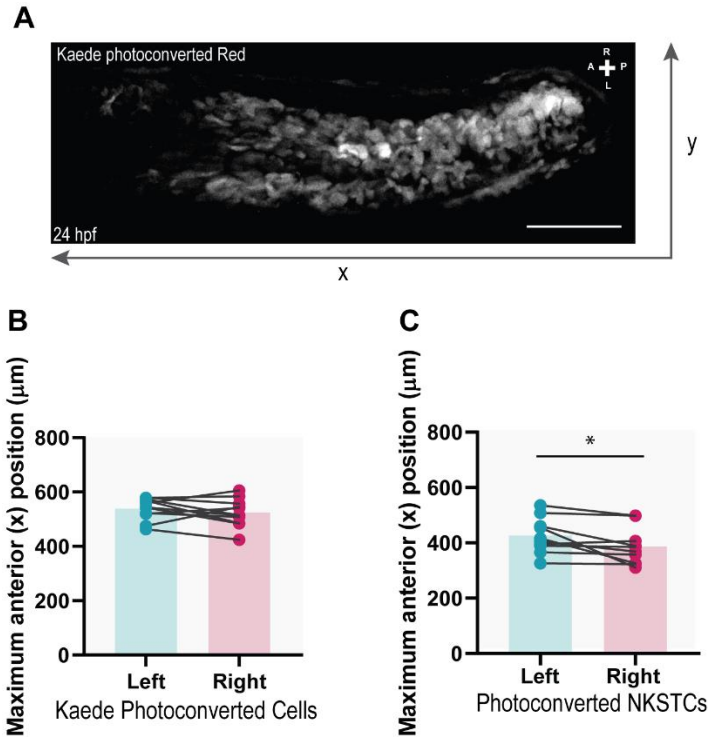

Supplementary Figure 2.4. Assessment of left-right asymmetry of cell position in somites. **(A)** Maximum intensity projection of a 24 hpf embryo showing the anterior (x-axis) position of the photoconverted cells. Dorsal view: The anterior is to the right, and the left is to the bottom. Scale bar = 100 µm. **(B-C)** Quantification of the differences in the more anterior distances occupied by photoconverted cells **(B)** and NKSTCs co-labeled with photoconverted cells **(C)** per somite side. t-test paired comparisons. Bars represent mean values, and dots represent individual embryos. * corresponds to a p-value <0,05.

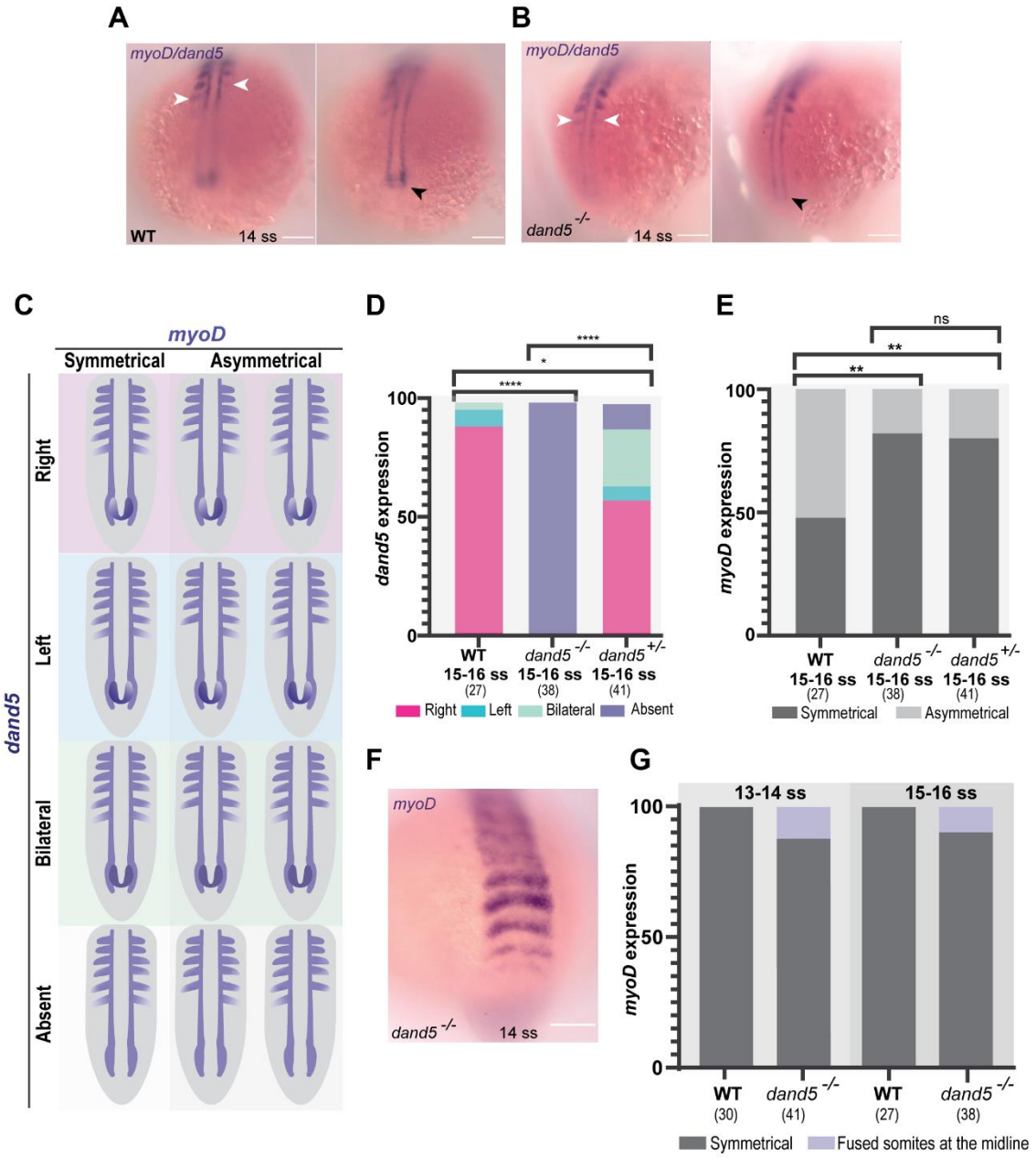

Supplementary Figure 2.5. *myoD* and *dand5* expression in *dand5* mutants. Double WISH for *myoD* and *dand5* expression in WT **(A)** and *dand5*$^{-/-}$ **(B)**, where *dand5* is absent. **(C)** Schematic representation of all different combinations found for the expression of both *myoD* and *dand5.* **(D)** Quantification of differences in *dand5* expression patterns in WT, *dand5* homozygous mutants and *dand5* heterozygous mutants. **(E)** *myoD* expression and side scoring in WT, *dand5* homozygous mutants and *dand5* heterozygous mutants. **(E-D)** The chi-squared test was used for statistical analysis. **(F-G)** Fused somites at the midline are shown by *myoD* WISH in 13-14ss and 15-16 ss *dand5*$^{-/-}$ embryos **(D)** but not in WT embryos **(E)**. Scale bar = 30 µm. The top is anterior, and the left is left.

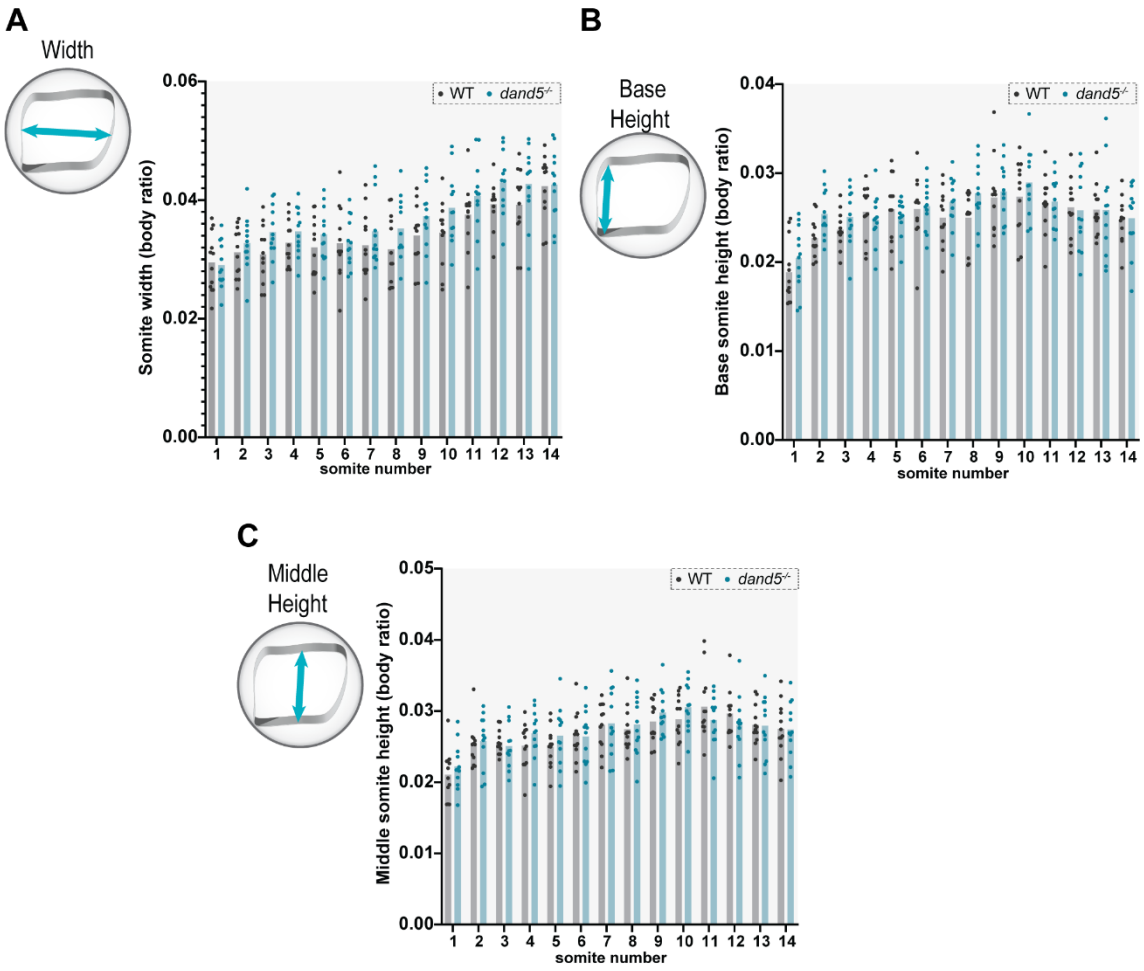

Supplementary Figure 2.6. Morphological measurements of somites in WT and *dand5*$^{-/-}$ embryos. **(A-C)** Comparison of somite width **(A)**, base height **(B)**, and middle height **(C)** of every 14 somites in both WT and *dand5*$^{-/-}$ embryos normalized to the embryo body length.

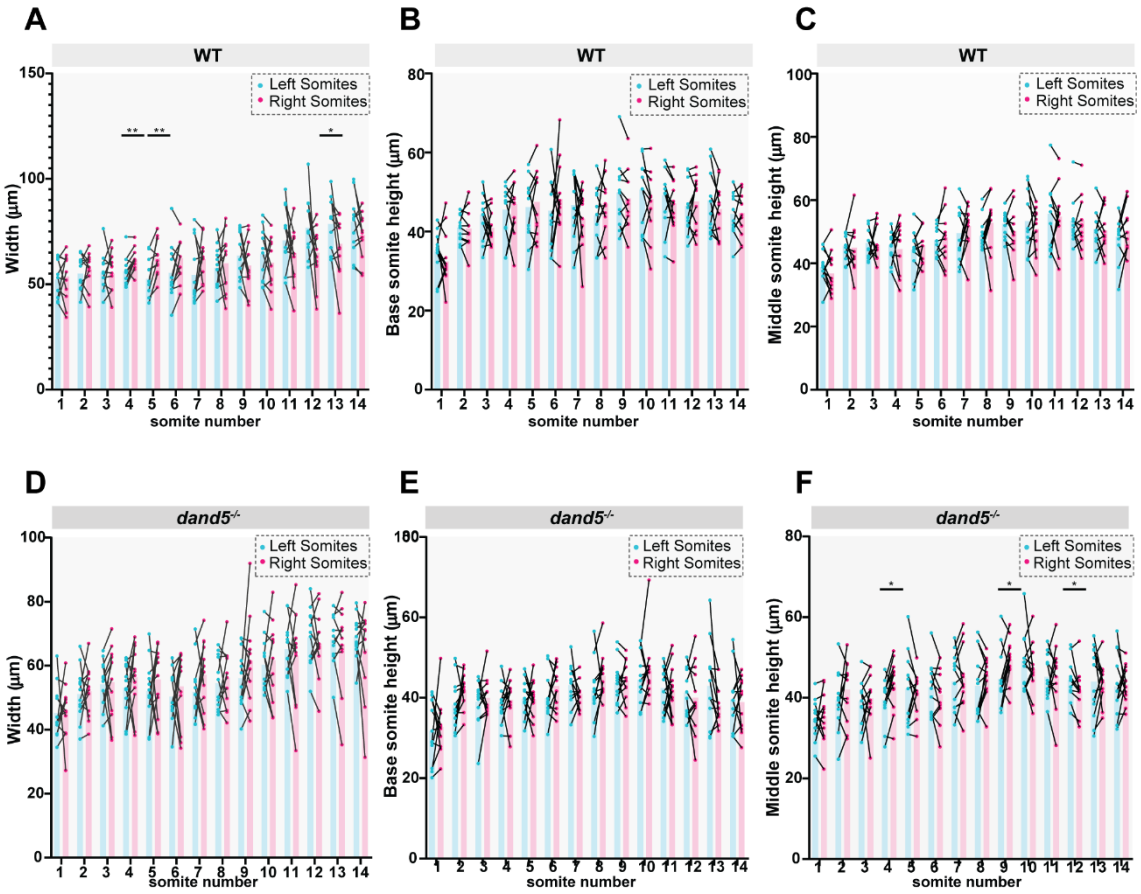

Supplementary Figure 2.7. Comparison of morphological somite measurements between the left and right sides of the embryo. **(A-F)** Pairwise comparisons between the left and right somites of somite width in WT **(A)** and *dand5*$^{-/-}$ embryos **(D)**; somite base height of WT **(B)** and *dand5*$^{-/-}$ **(E)** and somite middle height in WT **(C)** and *dand5*$^{-/-}$ embryos **(F)** of every 14 somites. Bars represent mean values, and dots represent individual embryos. * corresponds to a p-value <0,05 and ** to a p-value <0,005.

CHAPTER 3:

The Kupffer's Vesicle: A Multifunctional Structure in Zebrafish Embryonic Development?

The Kupffer's Vesicle: A Multifunctional Structure in Zebrafish Embryonic Development?

Catarina Bota[1], Susana S. Lopes[1]

1 iNOVA4Health, NOVA Medical School|Faculdade de Ciências Médicas, NMS|FCM, Universidade Nova de Lisboa; Lisboa, Portugal.

Abstract

In this study, we aimed to investigate whether the spheroid structure of the KV promotes tailbud movements beyond *dand5* expression. In addition, we hypothesized that the KV could exert mechanical forces on the tailbud cell population as it travels through it. To test this, we generated embryos without KV, evaluated the behavior of the previously described tailbud population, and assessed somite morphology. Our results indicate that in the absence of the KV, non-KV sox17:GFP+ cells failed to move towards the anterior side of the embryo, and posterior *myoD* expression was substantially reduced or absent in severe cases. Therefore, we propose that the KV plays a significant role in the initiation of tailbud cell movements, which are essential for proper somite development, in addition to its role as the LRO in zebrafish.

Keywords: kupffer's vesicle, tailbud, zebrafish, somites,

Introduction

Bilaterally symmetric body plans are a hallmark of vertebrates, but their visceral organs and vasculature exhibit left-right (LR) asymmetry in their position and pattern. Failure to correctly establish the LR axis during development can lead to a range of congenital disorders affecting the arrangement and morphology of visceral organs. In vertebrates, LR asymmetry is established by the expression of Nodal in the left Lateral Plate Mesoderm (LPM). Symmetry-breaking events occur in a specialized structure known as the LR organizer (LRO), which is a transient structure that forms during early embryogenesis and is enabled by polarized cilia, generating an asymmetric fluid flow that acts as the driving force. The LROs vary across different vertebrate species, and are known as node in amniotes (Levin et al., 1995b; Collignon et al., 1996),

gastrocoel roof plate in amphibians (Schweickert et al., 2007), and Kupffer's vesicle (KV) in teleost fish (Essner et al., 2005; Hojo et al., 2007).

The zebrafish KV is a transient fluid-filled, monociliated, epithelial, and spherical structure that emerges during the initial segmentation phase at the posterior end of the notochord (Essner et al., 2000; Amack and Yost, 2004). The current understanding of the development of the KV suggests that a group of mesenchymal cells, without any polarization, come together to form a flat, circular pattern resembling a rosette. This pattern then consolidates into a spherical three-dimensional structure with a central cavity filled with fluid. The KV emerges from the DFCs (dorsal forerunner cells), a cluster derived from a group of 20 to 30 dorsal surface epithelial cells controlled by Nodal signaling, which is located in the region adjacent to the embryonic shield (Cooper and D'amico, 1996). The DFC cluster moves towards the vegetal pole in a collective cell migration process (Amack and Yost, 2004; Essner et al., 2005; Oteíza et al., 2008; Matsui et al., 2015; Gokey et al., 2016; Lin et al., 2017). Subsequently, DFCs become polarized into a bottle-shaped structure through compaction to form a rosette-like structure, and the nascent lumen is visible at 2 somite stage (ss) (Oteíza et al., 2008). Lumen expansion occurs through a fluid secretion mechanism dependent on Myo1d (Saydmohammed et al., 2018), Rab11 (Rathbun et al., 2020), and CFTR (Navis et al., 2013; Roxo-rosa et al., 2015). Meanwhile, ciliogenesis takes place, in which a single cilium forms and elongates from the apical surface of each KV cell to extend into the lumen (Essner et al., 2005; Callol-massot and Izpisu, 2006; Kreiling et al., 2007; Von Der Hardt et al., 2007; Kim et al., 2017), and cilia motility progressively increases (Yuan et al., 2015b; Ferreira and Vermot, 2017; Tavares et al., 2017). Simultaneously, the KV must undergo an asymmetric cell shape rearrangement along the anteroposterior axis, where the anterior cells become thin and elongated, and the posterior cells become flattened and wide (Wang et al., 2011; Dasgupta et al., 2018). Such KV reshape is crucial for establishing an uneven distribution of cilia, constraining more ciliated cells on the anterior side. This remodeling ensures the production of an asymmetric counterclockwise fluid, which ultimately leads to the degradation of *dand5* on the left side (Kreiling et al., 2007; Sampaio et al., 2014; Maerker et al., 2021b) in the breaking of symmetry event. KV reshaping has been shown to be dependent on notochord-induced cytoskeletal rearrangements and extracellular matrix (ECM) accumulation and function of the Rho kinase gene *rock2b* and *non-muscle myosin II*, independent of lumen expansion. Sanematsu et al., (2021) recently investigated the pressure and shear stress generated by tailbud cells on the KV reshaping as the KV travels through the tailbud tissue from 2 ss to 8 ss, revealing notable velocity gradients surrounding the KV. These observations suggest that the tailbud tissue exerts mechanical drag forces on KV during the 2-4 ss and 4-6 ss stages and aids in the KV reshaping process.

Numerous studies have been conducted in zebrafish to examine cell movement, with a particular focus on posterior elongation (Lawton et al., 2013; Mongera et al., 2018; Das et al., 2019; Banavar et al., 2021). These studies examined the mechanical characteristics of zebrafish tail elongation, which complements the widely acknowledged involvement of morphogen gradients in this process (Das et al., 2019). The underlying mechanisms driving these morphogenetic changes involve a fluid-solid transition, with the mesodermal progenitor zone located in the posterior region of the tailbud displaying fluid-like tissue behavior while the presomitic mesoderm (PSM) behaves as a solid (Mongera et al., 2018; Banavar et al., 2021). Other studies have also focused on the exit of somite precursors from the tailbud (Fior et al., 2012b; O'Neill and Thorpe, 2013; Manning and Kimelman, 2015; Goto et al., 2017). Somite precursors originate from a dorsal tailbud population of neuromesodermal progenitor cells that commit to mesoderm fate and move ventrally towards the maturation zone (MZ) where cells become migratory (Kanki and Ho, 1997; Martin and Kimelman, 2012). MZ cells generate cell flows towards the PSM, where cell motility decreases to form somites (Kanki and Ho, 1997; Lawton et al., 2013; Banavar et al., 2021).

Ikeda et al., (2022) identified the fate and newly acquired function of KV-derived cells in axial muscles and notochord after they complete their initial role in LRO; however, the potential additional role of the KV in the tailbud remains unexplored, despite the proximity of the KV to the tailbud population. Our recent findings suggest that the KV may play a crucial role in tailbud movements, as we observed that a population of tailbud cells, including somite precursors, migrate asymmetrically towards the anterior side of the embryo in response to the proximity of the KV. These asymmetries are lost in the absence of Dand5, leading to symmetrical somite integration and altered *myoD* expression, indicating a new function for Dand5, in addition to its role in restricting Nodal to the left side of the LPM. Here, we aimed to examine the presence of the spheroid structure of the KV as a player in promoting tailbud movements besides being the bearer of *dand5* expression. We hypothesized that the KV could exert mechanical forces in the tailbud cell population as it travels through it. To test this, we generated embryos without KV, evaluated the behavior of the previously described tailbud population, and assessed somite morphology. We report that in the absence of the KV, the Non KV sox17:GFP^{+} cells do not move towards the anterior side of the embryo, and *myoD* expression is substantially reduced and in some more severe cases completely absent. Thus, we propose that the KV besides being the LRO in zebrafish, also plays a role in the initiation of tailbud cell movements crucial for proper somite development.

Materials and Methods

Zebrafish lines and embryo manipulation

The zebrafish strain used in this study was the transgenic line Tg(sox17:GFP)^{s870Tg}, as previously described by Sakaguchi et al., (2006). Adult zebrafish were housed in a recirculating water treatment system maintained at 28.0°C, pH 7, and 950 µS/m conductivity under a 10-hour dark/14-hour light cycle. Pair mating was used to obtain fertilized eggs, which were collected and staged according to standard protocols (Kimmel et al., 1995; Dahm and Nüsslein-Volhard, 2002). Embryos were cultured in E3 medium at 28.0°C, which consisted of 5 mM NaCl, 0.17 mM KCl, 0.33 mM CaCl2, 0.33 mM MgSO4, and 0.0001% methylene blue during the early stages of development.

Live imaging

For live imaging of sox17:GFP^{+} cells in whole zebrafish embryos, 10 ss embryos were mounted in 1% LMA (low melting agarose) in a petri dish with the dorsal side facing the objective and fully submerged in E3. Images of the KV and adjacent cells were acquired using a Praire Ultima two-photon system mounted on an Olympus BX60 upright microscope. Z-stacks were obtained at 2 µm intervals at 28°C and time cycles of 3 and 6 min for 3-6 hours.

DFCs laser ablation

The protocol for the laser ablation of DFCs was adapted from Essner et al. (2005). The embryos were mounted in agarose wells in glass-bottom dishes, with the shield region facing the bottom of the dish. The DFCs were detected by sox17:GFP and ablated from Tg(sox17:GFP) embryos between 75-80% epiboly stages (Figure 3.1) using a nitrogen laser-pumped dye laser (Micropoint Photonic Instruments) connected to an Andor Revolution Spinning Disk Confocal Microscope (Andor Technology). After ablation, the embryos were released into an agarose bottom-coated dish, fully submerged in E3 medium, and raised to 14 ss. The embryos were then fixed in 4% PFA ON and stored either in PBS 1x at 4 °C or 100% MeOH at -20 °C.

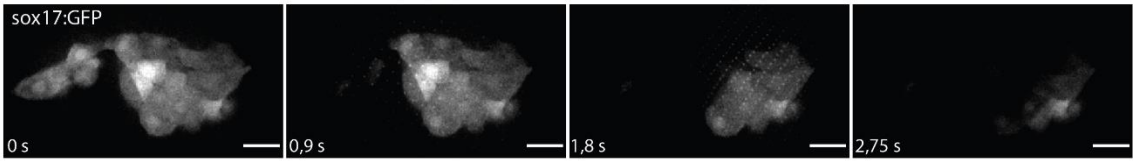

Figure 3.1. Snapshots of the laser ablation procedure targeting DFCs shown by sox17:GFP. The elapsed time is expressed in seconds (s). Scale bar = 20 µm.

Immunostaining and *in situ* Hybridization

Whole-mount immunostaining was performed as previously described (Lopes et al., 2010) using the following antibodies: anti-acetylated α-tubulin (1:300; Sigma), anti-GFP (1:500; Invitrogen), anti-rabbit Alexa Fluor 488 (Invitrogen; 1:500) and anti-mouse Alexa Fluor 647 (Invitrogen; 1:500). The DFC-ablated 14 ss embryos were mounted in 1% LMA, with the tail facing the bottom of the glass-bottom dish, and images were acquired using a Zeiss LSM 980 Airyscan confocal microscope. Double *myoD* and *dand5* (Hashimoto et al., 2004a) whole-mount *in situ* hybridization was performed as previously described (Thisse and Thisse, 2014). The embryos were photographed using a Zeiss Axio Imager Z2 upright microscope. Gene expression for double-staining *myoD* and *dand5* was scored and analyzed by Fisher's exact test using Prism 8 (GraphPad).

Image analysis

The FIJI/ImageJ software (Schindelin et al., 2012) was initially used to process the datasets. Subsequently, Imaris v9.8.1 (Bitplane) was used to create accelerated 3D movies and render Z-stacks of live-imaged sox17:GFP^{+} cells. To acquire KV 3D surfaces, manual drawing was performed on every slice, where KV cells were consistently observable. Immunostained Tg(sox17:GFP) DFC-ablated embryos and controls were processed in FIJI and the presence of the KV and location of sox17:GFP^{+} cells was performed using IMARIS.

Results

The Kupffer's vesicle organ drives anterior migration of NKSTCs

We previously showed that the KV is near a 'posterior cluster' of NKSTCs. We also showed that Dand5 plays a role in tailbud cell movement, in addition to its role in LR establishment. We have described that as the KV approaches the cluster, it causes the cells to move alternately towards the anterior side from the left or right side, suggesting that the KV may drive the departure of NKSTCs from the posterior cluster.

To investigate the 3D dynamics of this process, we rendered the KV into a surface and We observed the KV passage over the cluster from both left and right views (N=12) (Figure 9). Our

observations showed that the KV first approach to the posterior cluster seemed to push the cells to detach from the cluster and begin anterior migration. Subsequently, the KV passeed over the remaining cells of the cluster, progressively detaching more cells that moved towards the anterior side (Supplementary Video 3.1; Figure 3.2). Our results support the conclusion that the KV provides not only signaling cues, but also mechanical cues that promote the anterior migration of tailbud cells.

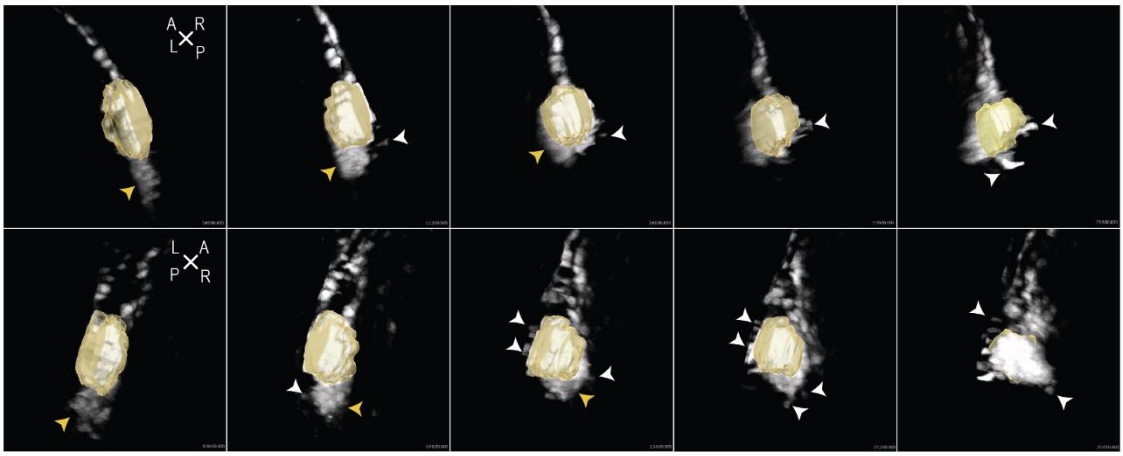

Figure 3.2. Time-lapse live imaging snapshots of the KV and NKSTCs, showing 3D lateral views of the posterior cluster and KV from 10 ss as the KV travels through the tailbud**.** Left, yellow arrowheads; right, white arrowheads. The KV surface is highlighted in yellow. The axes are indicated as A (anterior), P (posterior), L (left), and R (right), and the elapsed time is shown in h-min format at the bottom right.

Absence of the KV affects somite precursors and *myoD* expression

To investigate the contribution of the KV to the somite precursor population of cells in the tailbud, we planned an experiment to delete the KV cells. We performed laser ablation of the KV precursors, the DFCs, in Tg(sox17:GFP) embryos. DFCs were targeted at 75-80% epiboly for more effective ablation (Essner et al., 2005)(Figure 3.3A-B). Ablation was confirmed by acquiring both Tg(sox17:GFP) and brightfield z-stacks, which revealed the absence of GFP fluorescence and a suggestive wound at the ablation site, given that DFCs are located superficially (Figure 3.3B).

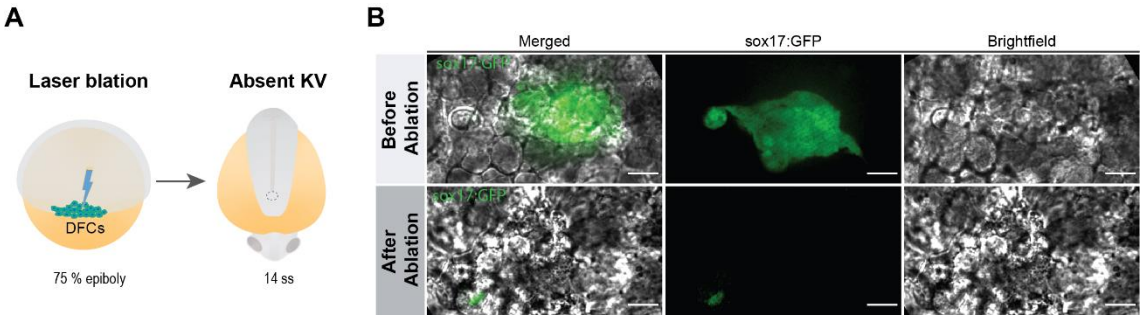

Figure 3.3. Generating embryos without the KV. **(A)** Schematic representation of the setup used to produce embryos without the KV. DFC-targeted ablation was performed at 75-80% epiboly stage using *Tg(sox17:GFP)* embryos. The embryos were released and raised to 14 ss. **(B)** A z-plane showing the presence of DFCs before ablation and their absence after ablation. DFCs are shown in green by sox17:GFP and the surrounding tissue by brightfield imaging. Scale bar = 20 µm.

The DFC-ablated embryos were raised to 14 ss, a stage at which left-sided asymmetries were observed in the position of the NKSTCs. The absence of the KV was also confirmed by acetylated α-tubulin staining, which revealed lack of KV cilia at the tailbud (Figure 10D). 80% of the embryos lacked any structure resembling the KV, despite showing one or two cells with longer and thicker cilia that resembled KV cilia. In contrast, the remaining embryos showed a small defective KV, as evidenced by the presence of only a few longer cilia (Figure 10D). This suggested defective DFCs laser ablation, in which a few cells were missed. Despite this variability, we observed that the overall NKSTC population in embryos lacking a functional KV was very destabilized. We observed that NKSTCs were absent, reduced in a small cluster, or confined to the posterior side, and were not displayed in an aggregate state. Thus, NKSTCs in DFC-ablated embryos did not show more anterior positions as those observed in the controls (Figure 10D). Since we previously reported that the majority of NKSTCs are somite precursors, this finding suggests that somite precursors are not only influenced by the Dand5 cues at the KV but are also affected by the absence of the KV, which results in somite precursor cell absence or its lack of movement towards the anterior side of the embryo.

To evaluate the role of the KV in somite morphology and specification, we performed double in situ hybridization for *myoD* and *dand5* at 14 ss in DFC-ablated embryos. The detection of *dand5* expression was used to confirm the absence of a functional KV. We observed that *dand5* expression was absent in all DFC-ablated embryos, as opposed to the controls, suggesting the lack of a KV (Figure 10E,F). Most interesting, in 71% of the DFC-ablated embryos, we observed defective *myoD* expression in the somites, where *myoD* expression was either absent from the posterior side of the embryo or faintly stained at the adaxial cells, or *myoD* expression was

completely absent (Figure 10E,F). In contrast, the remaining 29% of the DFC-ablated embryos showed no defects in *myoD* expression despite the absence of *dand5* expression, indicating that they developed without a functional KV (Figure 10E,F). Furthermore, the *myoD* expression pattern in the DFC-ablated embryos significantly differed from that in controls, where *myoD* expression was not defective (p-value = 0.0006) (Figure 10F). Thus, we conclude that the KV is involved in somite specification because of the observed defects in *myoD* expression in embryos lacking a functional KV.

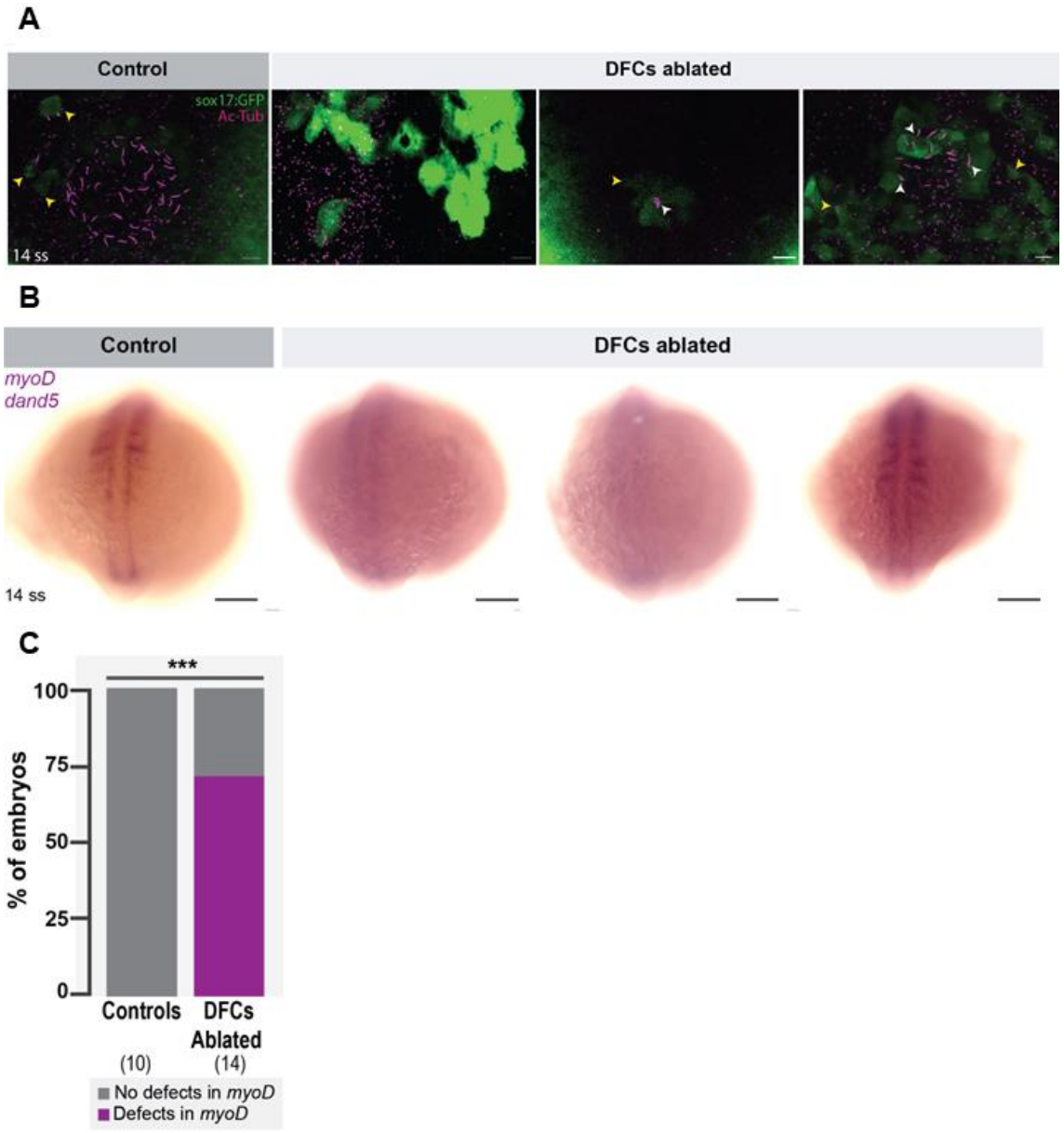

Figure 3.4. The role of the KV on tailbud cells. **(A)** Maximum intensity projections of 14 ss *Tg(sox17:GFP)*, control, and DFC-ablated embryos. sox17:GFP is shown in green and acetylated α-tubulin (AcTub) in magenta. Scale bar = 10 µm. **(B)** Whole-mount *in situ* hybridization for *myoD* and *dand5* expression in 14 ss controls and DFC-ablated embryos. **(C)** Quantification of the differences in *myoD* expression patterns between control and DFC-ablated embryos. Fisher's exact test was used for statistical analysis. *** corresponds to a p-value <0,0005. Scale bar = 100 µm. The top is anterior, and the bottom is posterior. N is shown in parentheses.

Discussion

The KV: A multifunctional organ in zebrafish embryonic development?

Here, we report that the zebrafish LRO, the KV, provides signaling cues and possibly additional mechanical cues that promote the anterior migration of tailbud cells. We also demonstrated that KV plays a role in somite specification during embryonic development.

We described that from 10 ss onwards, the presence of the KV appears to impact a population of tailbud cells. These cells transition from an aggregate to a migratory state upon KV collision, subsequently traveling anteriorly and contributing to the somites. While we only focused on a small population from the mesodermal progenitor zone, the NKSTCs, we reason that all cells near the KV may receive KV-derived cues to move.

Our findings strongly support the hypothesis that the mechanical properties of the KV may facilitate morphogenetic movements in the zebrafish tailbud. However, further studies are required to fully corroborate our observations, including live imaging studies of DFC-ablated Tg(sox17:GFP) embryos. Moreover, to validate the mechanical role of the KV in tailbud cell movement, it is crucial to explore the mechanical interactions between the KV and tailbud cells. Specifically, studying the pressure exerted by the KV on tailbud cells and how it affects tailbud cell flows would provide valuable insights into this process. Tailbud mechanical interactions have been studied to analyze the pressure and shear stress exerted by tailbud cells on KV cells and how they contribute to the reshaping of the KV (Sanematsu et al., 2021). A similar strategy can be applied to investigate tailbud cell flows in the presence *vs.* absence of the KV. This approach can uncover a new role for the KV beyond its known function as the zebrafish LRO. This hypothesis is supported by the fact that the KV lasts longer than the period required for LR axis establishment (Ikeda et al., 2022a).

Our study provides preliminary evidence that the KV is important for somite specification. We demonstrated that *myoD* expression was defective in the somites of DFC-ablated embryos, indicating that the KV provides important information for this process. Furthermore, MyoD is a myogenic regulator factor (MRF) that plays a key role in commitment to myogenic fate, along with Myf5 and Mrf4 (Devoto et al., 1996; Pownall et al., 2002). Thus, our findings suggest that the KV is involved in regulating myogenic fate determination during somite specification.

To fully understand the impact of the KV on the developing zebrafish embryo, it is important to evaluate somite morphology in the absence of the KV. Essner et al., 2005 conducted a study in

which they produced embryos without the KV to investigate its role in LR asymmetry. Here, they established the KV as the zebrafish LRO (Essner et al. 2005). However, beyond Essner et al.'s study and our own, there have been no further reports on generating zebrafish embryos lacking the KV. While Essner et al. observed that the absence of the KV only affected laterality, their assessment of morphology was limited to the expression pattern of LR markers, heart situs, and *ntl* expression as a measure of notochord integrity. Therefore, additional studies are required to fully elucidate the role of the KV in somite development.

Ikeda et al., (2022) reported that after the collapse of the KV, epithelial cells transition into mesenchymal cells and migrate into nearby mesodermal progenitors, including the presomitic mesoderm and the chordoneural hinge. Upon integration, the progeny of KV-derived epithelial cells express specific mesodermal differentiation markers and eventually develop into mature cell populations, such as the axial muscles and notochordal sheath, through normal developmental pathways. Although some KV-derived cells may contribute to somite formation, it is unlikely that their absence alone significantly affects the development of these structures in the absence of the KV. Therefore, it is probable that a mechanical or signaling cue originating from the KV is necessary to properly influence somite and muscle specification during zebrafish development. To better understand the interplay between mechanical and molecular mechanisms derived from the KV that contribute to somite specification and tailbud cell flows, a comprehensive analysis of the major signaling pathways governing the tailbud, such as the Wnt, FGF, Shh, and BMP pathways is needed.

The physical presence of the KV can be seen as an obstacle to the flow of cells that leave the tailbud to the PSM. In this scenario cells that migrate medially (in the midline axis) will have more resistance to travel offered by the KV cells, than those migrating more laterally. Wee postulate that such differences in the mechanical properties may impact on somite mediolateral specification and make cells different according to their migratory mechanical experiences during migration. Mechanical properties like shear stress and even some squeezing may be important players in cell fate that need more experimental studies in this context.

Conclusions

Our observations suggest that the zebrafish LRO, the KV, plays an important role in somite specification during embryonic development. While this finding provides preliminary evidence of the involvement of KV in regulating myogenic fate determination during somite specification,

further research is required to fully validate the mechanical role of KV in tailbud cell movement and investigate the interactions between KV and tailbud cells. Nonetheless, this study sheds light on the importance of KVs in somite specification and emphasizes the need for more comprehensive investigations in this area.

The absence of the KV in zebrafish embryos is summarized in a schematic illustration presented in Figure 3.5. This illustration provides a visual representation of the main findings discussed in this study and emphasizes the importance of the KV in embryonic development.

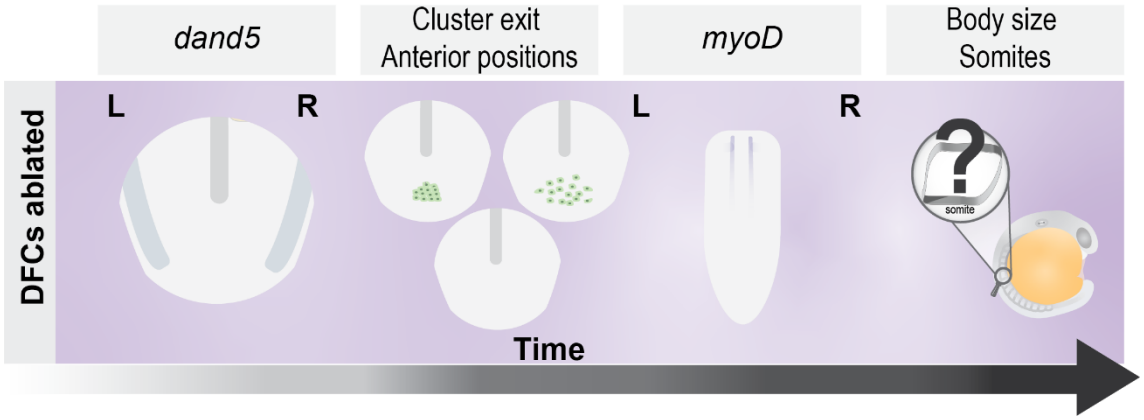

Figure 3.5. Schematic illustration of the key findings of this study. In embryos where DFCs are ablated, *dand5* expression is absent because of the absence of the KV. The NKSTC population is destabilized, which can manifest as the absence of NKSTCs posterior to the notochord, or the presence of a small cell aggregate or dispersed NKTCs. Additionally, DFC-ablated embryos exhibit reduced or completely absent posterior *myoD* expression. More studies are required to evaluate the effect of absent KVs on somite morphology.

References

Amack, J. D., and Yost, H. J. (2004). The T box transcription factor no tail in ciliated cells controls zebrafish left-right asymmetry. Current biology 14, 685–690.

Banavar, S. P., Carn, E. K., and Rowghanian, P. (2021). Mechanical control of tissue shape and morphogenetic flows during vertebrate body axis elongation. Scientific Reports, 1–14. doi: 10.1038/s41598-021-87672-3.

Callol-massot, C., and Izpisu, J. C. (2006). Regulation of primary cilia formation and left-right patterning in zebrafish by a noncanonical Wnt signaling mediator , duboraya. 38, 1316–1322. doi: 10.1038/ng1892.

Collignon, J., Varlet, I., and Robertson, E. J. (1996). Relationship between asymmetric nodal expression and the direction of embryonic turning. Nature 381, 155–158. doi: 10.1038/381155a0.

Cooper, M. S., and D'amico, L. A. (1996). A cluster of noninvoluting endocytic cells at the margin of the zebrafish blastoderm marks the site of embryonic shield formation. Developmental biology 180, 184–198.

Dahm, R., and Nüsslein-Volhard, C. (2002). Zebrafish: A practical approach. Oxford University Press doi: 10.1017/S0016672303216384.

Das, D., Jülich, D., Schwendinger-Schreck, J., Guillon, E., Lawton, A. K., Dray, N., et al. (2019). Organization of embryonic morphogenesis via mechanical information. Developmental cell 49, 829–839.

Dasgupta, A., Merkel, M., Clark, M. J., Jacob, A. E., Dawson, J. E., Manning, M. L., et al. (2018). Cell volume changes contribute to epithelial morphogenesis in zebrafish Kupffer's vesicle. eLife 7, e30963. doi: 10.7554/eLife.30963.

Devoto, S. H., Melançon, E., Eisen, J. S., and Westerfield, M. (1996). Identification of separate slow and fast muscle precursor cells in vivo, prior to somite formation. Development 122, 3371–3380.

Essner, J. J., Amack, J. D., Nyholm, M. K., Harris, E. B., and Yost, H. J. (2005). Kupffer's vesicle is a ciliated organ of asymmetry in the zebrafish embryo that initiates left-right development of the brain, heart and gut. Development 132 (6), 1247–1260. doi: https://doi.org/10.1242/dev.01663.

Essner, J. J., Branford, W. W., Zhang, J., and Yost, H. J. (2000). Mesendoderm and left-right brain , heart and gut development are differentially regulated by pitx2 isoforms. 1093, 1081–1093.

Ferreira, R. R., and Vermot, J. (2017). The balancing roles of mechanical forces during left-right patterning and asymmetric morphogenesis. Mechanisms of Development 144, 71–80. doi: 10.1016/j.mod.2016.11.001.

Fior, R., Maxwell, A. A., Ma, T. P., Vezzaro, A., Moens, C. B., Amacher, S. L., et al. (2012). The differentiation and movement of presomitic mesoderm progenitor cells are controlled by Mesogenin 1. Development 139, 4656–4665.

Gokey, J. J., Ji, Y., Tay, H. G., Litts, B., and Amack, J. D. (2016). Kupffer's vesicle size threshold for robust left-right patterning of the zebrafish embryo. Developmental Dynamics 245, 22–33. doi: 10.1002/dvdy.24355.

Goto, H., Kimmey, S. C., Row, R. H., Matus, D. Q., and Martin, B. L. (2017). FGF and canonical Wnt signaling cooperate to induce paraxial mesoderm from tailbud neuromesodermal progenitors through regulation of a two-step epithelial to mesenchymal transition. Development 144, 1412–1424.

Hashimoto, H., Rebagliati, M., Ahmad, N., Muraoka, O., Kurokawa, T., Hibi, M., et al. (2004). The Cerberus/Dan-family protein Charon is a negative regulator of Nodal signaling during left-right patterning in zebrafish. Development 131, 1741–1753. doi: 10.1242/dev.01070.

Hojo, M., Takashima, S., Kobayashi, D., Sumeragi, A., Shimada, A., Tsukahara, T., et al. (2007). Right-elevated expression of charon is regulated by fluid flow in medaka Kupffer ' s vesicle. 395–405. doi: 10.1111/j.1440-169x.2007.00937.x.

Ikeda, T., Inamori, K., Kawanishi, T., and Takeda, H. (2022). Reemployment of Kupffer's vesicle cells into axial and paraxial mesoderm via transdifferentiation. Development, Growth & Differentiation 64, 163–177.

Kanki, J. P., and Ho, R. K. (1997). The development of the posterior body in zebrafish. Development 124, 881–893.

Kim, J., Bae, S., Lee, H. S., Park, J., and Kim, K. (2017). Claudin5a is required for proper inflation of Kupffer ' s vesicle lumen and organ laterality. 1–18.

Kimmel, C. B., Ballard, W. W., Kimmel, S. R., Ullmann, B., and Schilling, T. F. (1995). Stages of embryonic development of the zebrafish. Developmental Dynamics 203, 253–310. doi: 10.1002/aja.1002030302.

Kreiling, J. A., Prabhat, Williams, G., and Creton, R. (2007). Analysis of Kupffer's vesicle in zebrafish embryos using a cave automated virtual environment. Developmental Dynamics 236, 1963–1969. doi: 10.1002/dvdy.21191.

Lawton, A. K., Nandi, A., Stulberg, M. J., Dray, N., Sneddon, M. W., Pontius, W., et al. (2013). Regulated tissue fluidity steers zebrafish body elongation. Development 140, 573–582.

Levin, M., Johnson, R. L., Sterna, C. D., Kuehn, M., and Tabin, C. (1995). A molecular pathway determining left-right asymmetry in chick embryogenesis. Cell 82, 803–814. doi: 10.1016/0092-8674(95)90477-8.

Lin, C., Tsai, M., Liu, Y., Lu, Y., Chen, Y., Lai, Y., et al. (2017). Klf8 regulates left-right asymmetric patterning through modulation of Kupffer ' s vesicle morphogenesis and spaw expression. 1–14. doi: 10.1186/s12929-017-0351-y.

Lopes, S. S., Lourenco, R., Pacheco, L., Moreno, N., Kreiling, J., and Saude, L. (2010). Notch signalling regulates left-right asymmetry through ciliary length control. Development 137, 3625–3632. doi: 10.1242/dev.054452.

Maerker, M., Getwan, M., Dowdle, M. E., McSheene, J. C., Gonzalez, V., Pelliccia, J. L., et al. (2021). Bicc1 and Dicer regulate left-right patterning through post-transcriptional control of the Nodal inhibitor Dand5. Nature Communications 12, 5482. doi: 10.1038/s41467-021-25464-z.

Manning, A. J., and Kimelman, D. (2015). Tbx16 and Msgn1 are required to establish directional cell migration of zebra fi sh mesodermal progenitors. Developmental Biology 406, 172–185. doi: 10.1016/j.ydbio.2015.09.001.

Martin, B. L., and Kimelman, D. (2012). Canonical Wnt signaling dynamically controls multiple stem cell fate decisions during vertebrate body formation. Developmental cell 22, 223–232.

Matsui, T., Ishikawa, H., and Bessho, Y. (2015). Cell collectivity regulation within migrating cell cluster during Kupffer's vesicle formation in zebrafish. Frontiers in cell and developmental biology 3, 27. doi: 10.3389/fcell.2015.00027.

Mongera, A., Rowghanian, P., Gustafson, H. J., Shelton, E., Kealhofer, D. A., Carn, E. K., et al. (2018). vertebrate body axis elongation. Nature. doi: 10.1038/s41586-018-0479-2.

Navis, A., Marjoram, L., and Bagnat, M. (2013). Cftr controls lumen expansion and function of Kupffer ' s vesicle in zebrafish. 1712, 1703–1712. doi: 10.1242/dev.091819.

O'Neill, K., and Thorpe, C. (2013). BMP signaling and spadetail regulate exit of muscle precursors from the zebrafish tailbud. Developmental biology 375, 117–127.

Oteíza, P., Köppen, M., Concha, M. L., and Heisenberg, C.-P. (2008). Origin and shaping of the laterality organ in zebrafish. Development (Cambridge, England) 135, 2807–13. doi: 10.1242/dev.022228.

Pownall, M. E., Gustafsson, M. K., and Emerson Jr, C. P. (2002). Myogenic regulatory factors and the specification of muscle progenitors in vertebrate embryos. Annual review of cell and developmental biology 18, 747–783.

Rathbun, L. I., Colicino, E. G., Manikas, J., O'Connell, J., Krishnan, N., Reilly, N. S., et al. (2020). Cytokinetic bridge triggers de novo lumen formation in vivo. Nature communications 11, 1269.

Roxo-rosa, M., Jacinto, R., Sampaio, P., and Lopes, S. S. (2015). The zebrafish Kupffer ' s vesicle as a model system for the molecular mechanisms by which the lack of Polycystin-2 leads to stimulation of CFTR. 1356–1366. doi: 10.1242/bio.014076.

Sakaguchi, T., Kikuchi, Y., Kuroiwa, A., Takeda, H., and Stainier, D. Y. R. (2006). The yolk syncytial layer regulates myocardial migration by influencing extracellular matrix assembly in zebrafish. Development 133, 4063–4072. doi: doi.org/10.1242/dev.02581.

Sampaio, P., Ferreira, R. R., Guerrero, A., Pintado, P., Tavares, B., Amaro, J., et al. (2014). Left-right organizer flow dynamics: how much cilia activity reliably yields laterality? Developmental cell 29, 716–728.

Sanematsu, P. C., Erdemci-Tandogan, G., Patel, H., Retzlaff, E. M., Amack, J. D., and Manning, M. L. (2021). 3D viscoelastic drag forces contribute to cell shape changes during organogenesis in the zebrafish embryo. Cells & Development 168, 203718. doi: https://doi.org/10.1016/j.cdev.2021.203718.

Saydmohammed, M., Yagi, H., Calderon, M., Clark, M. J., Feinstein, T., Sun, M., et al. (2018). Vertebrate myosin 1d regulates left–right organizer morphogenesis and laterality. Nature Communications 9, 3381.

Schindelin, J., Arganda-Carreras, I., Frise, E., Kaynig, V., Longair, M., Pietzsch, T., et al. (2012). Fiji: an open-source platform for biological-image analysis. Nature methods 9, 676–682.

Schweickert, A., Weber, T., Beyer, T., Vick, P., Bogusch, S., Feistel, K., et al. (2007). Report Cilia-Driven Leftward Flow Determines Laterality in Xenopus. 60–66. doi: 10.1016/j.cub.2006.10.067.

Tavares, B., Jacinto, R., Sampaio, P., Pestana, S., Pinto, A., Vaz, A., et al. (2017). Notch/Her12 signalling modulates, motile/immotile cilia ratio downstream of Foxj1a in zebrafish left-right organizer. Elife 6, e25165.

Thisse, B., and Thisse, C. (2014). "In situ hybridization on whole-mount zebrafish embryos and young larvae," in In situ hybridization protocols (Springer), 53–67.

Von Der Hardt, S., Bakkers, J., Inbal, A., Carvalho, L., Solnica-Krezel, L., Heisenberg, C.-P., et al. (2007). The Bmp gradient of the zebrafish gastrula guides migrating lateral cells by regulating cell-cell adhesion. Current Biology 17, 475–487.

Wang, G., Cadwallader, A. B., Jang, D. S., Tsang, M., Yost, H. J., and Amack, J. D. (2011). The Rho kinase Rock2b establishes anteroposterior asymmetry of the ciliated Kupffer ' s vesicle in zebrafish. 54, 45–54. doi: 10.1242/dev.052985.

Yuan, S., Zhao, L., Brueckner, M., and Sun, Z. (2015). Intraciliary calcium oscillations initiate vertebrate left-right asymmetry. Current biology 25, 556–567.

Supplementary Material

Supplementary videos

Supplementary Video 3.1. KV passes through the posterior NKSTCs cluster. 3D reconstruction from a time-lapse of two-photon z-stacks of a 10 ss *Tg*(*sox17:GFP*) embryo. The KV 3D surface (yellow) was created using Imaris (Bitplane). On the left side, the KV passes through the cluster from the dorsal view, at the center, and to the right from the left- and right-side views.

CHAPTER 4:

Spatial and Temporal Analysis of *dand5* mRNA Transcripts in Zebrafish Kupffer's Vesicle Using Single-Molecule Fluorescence *in situ* Hybridization (smFISH)

Spatial and Temporal Analysis of *dand5* mRNA Transcripts in Zebrafish Kupffer's Vesicle Using Single-Molecule Fluorescence *in situ* Hybridization (smFISH)

Catarina Bota[1], Susana S. Lopes[1]

1 iNOVA4Health, NOVA Medical School|Faculdade de Ciências Médicas, NMS|FCM, Universidade Nova de Lisboa; Lisboa, Portugal.

Abstract

Symmetry breaking at the left-right organizer (LRO) is a crucial process in establishing proper left-right asymmetry in vertebrate development. The LRO, also known as Kupffer's vesicle, is a monociliated structure in zebrafish that generates a highly regulated counterclockwise fluid flow. Although the mechanism of fluid flow detection in LROs is not fully understood, current evidence suggests that the initial response to fluid flow sensing is the influx of calcium ions. Asymmetric flow leads to the mRNA degradation of the nodal inhibitor *dand5* gene on the left side of the mice LRO, which is thought to remove the Dand5-Nodal inhibition in a left-sided manner. This suppression present in WT embryos allows nodal/*spaw* expression to be sustained only on the left side of the lateral plate mesoderm (LPM), making nodal/*spaw* the first asymmetrically expressed gene in the LPM. Recent studies in mouse and frog have suggested that Bicc1, a member of the BicC family of RNA-binding proteins, mediates the destabilization and translation inhibition of *dand5* on the left side via the 3'-UTR of *dand5*. However, the study of left-sided *dand5* mRNA decay has been limited by the lack of spatial resolution in RNA quantification methods. Previous studies have not been able to quantify the number of *dand5* mRNA transcripts on each side of the zebrafish KV over time, and the left-right asymmetry in *dand5* expression was only detected at 8 ss using traditional in situ hybridization methods, which have limited resolution. To address this gap, we used single-molecule fluorescence in situ hybridization (smFISH) to quantify the number of *dand5* mRNA transcripts in 3D in the KV over time. Our results show that *dand5* asymmetry is already established at 6 ss, which is 1 h earlier than previously reported, and primarily occurs on the anterior side of the KV. In summary, our study provides new insights into *dand5* asymmetric expression in zebrafish and highlights the importance of using high-resolution RNA quantification methods to fully understand the spatiotemporal dynamics of gene expression.

Keywords: *dand5*, zebrafish, kupffer's vesicle, symmetry breaking, smFISH

Introduction

Symmetry breaking at the left-right organizer during vertebrate development is a crucial process that establishes proper left-right asymmetry in the body. The asymmetric molecular signals generated at the LRO are transferred to the left side of the lateral plate mesoderm (LPM) activating an asymmetric cascade of gene expression. This leads to the precise patterning of asymmetric internal organs, such as the heart (extensively reviewed in (Grimes and Burdine, 2017a; Schweickert et al., 2017; Zinski et al., 2017). Understanding symmetry breaking is important for developmental studies and for understanding congenital disorders related to left-right asymmetry (Sutherland and Ware, 2009; Deng et al., 2014; Campione and Brand, 2018; Grimes, 2019b; Pinto et al., 2021).

The Left-Right organizer in zebrafish, also known as Kupffer's vesicle (KV), is a transient fluid-filled monociliated organ that develops at the posterior end of the notochord during the early segmentation period (Amack and Yost, 2004; Essner et al., 2005). The KV originates from a group of cells close to the embryonic shield called dorsal forerunner cells (DFCs) (Cooper and D'Amico, 1996). The motile cilia in the Kupffer's vesicle (KV) of zebrafish generate a counterclockwise fluid flow (Essner et al., 2005; Kramer-Zucker, 2005; Supatto et al., 2008) that is highly regulated (Sampaio et al., 2014; Tavares et al., 2017). Although the precise mechanism of fluid flow detection in LROs is not yet fully understood, current evidence suggests that the initial response to fluid flow sensing is an influx of calcium ions (Yuan et al., 2015b), which is related to the ciliary function of the polycystin complex, *pkd1l1* and *pkd2* (Pennekamp et al., 2002; Schottenfeld et al., 2007; Field et al., 2011a; Kamura et al., 2011; Yoshiba et al., 2012; England et al., 2017; Roxo-Rosa and Lopes, 2019).

As observed in mice and frogs (Schweickert et al., 2010; Nakamura et al., 2012), it is currently thought that the asymmetric flow targets the repression of the nodal inhibitor *dand5* gene on the left side of the KV, which removes the Dand5-Southpaw (Spaw) inhibition (Sampaio et al., 2014). *spaw,* the zebrafish nodal in LR, is also symmetrically expressed in peri-KV cells. Suppressing this Dand5-Spaw inhibition allows differential *spaw* expression on the left side of the lateral plate mesoderm (LPM), since the Spaw protein can reach the LPM and promote its own expression, making it the first gene to be asymmetrically expressed in the LPM (Long et al., 2003). Nakamura et al., (2012) first established in mice models that the destabilization of *dand5* mRNA on the left side of the LRO was flow-dependent, specifically targeting the 3'UTR region of *Dand5*. Additional recent studies in mice and *Xenopus* have revealed that the destabilization and translation inhibition of *dand5* on the left side is mediated by Bicc1, a member of the BicC family

of RNA-binding proteins, which acts through the 3'-UTR of *dand5* (Maerker et al., 2021b; Minegishi et al., 2021b). The mechanism by which Bicc1 interacts with the 3'-UTR of *dand5* in zebrafish is yet to be determined. Nevertheless, evidence from studies in mouse, frog, and zebrafish suggests that Bicc1, along with Dicer1 (an endonuclease enzyme critical for the biosynthesis of microRNAs) and Pkd2, contributes to the repression of *dand5* (Maerker et al., 2021b).

According to our flow studies on the zebrafish LRO (Sampaio et al., 2022), which are currently at peer-revision stage, the most productive flow period is at 4-6 ss. However, the first detection of L<R asymmetry in *dand5* expression using traditional in situ hybridization was only at 8 ss (Lopes et al., 2010), which may reflect the limitations of this older method in resolving mRNA transcripts at the cellular level. Furthermore, the number of *dand5* mRNA transcripts on the left and right sides of the KV over time has not been quantified in previous studies because the true quantitative methods used for *dand5* expression lack spatial resolution, such as RT-qPCR (Jacinto, 2018; Jacinto et al., 2021) and RNA-seq (White et al., 2017). Additionally, it remains unclear whether cells exposed to high flow velocities are the first to initiate these events and cause *dand5* mRNA reduction of expression. To date, no 3D evaluations of the dynamics of *dand5* transcripts over time have been conducted at the KV or at any LRO.

To address this, we used single-molecule fluorescence in situ hybridization (smFISH) to quantify the number of *dand5* mRNA transcripts in KV. SmFISH is a powerful technique that allows visualization and quantification of individual mRNA molecules within a cell, as described by Raj et al., (2008). This method uses multiple small antisense oligonucleotide probes, each approximately 15-20 nucleotides in length. These probes are designed to complement target RNA sequences and are conjugated to a fluorescent dye. The multiple probes work together to produce an additive fluorescence signal, making detecting the target RNA transcripts easier. This allows for the imaging, localization, and counting of transcripts, providing valuable insights into 3D mRNA localization at the organelle level (Raj et al., 2008; Tingey et al., 2022). The protocol has been adapted to zebrafish embryos (Oka and Sato, 2015; Keskin et al., 2018; Lord et al., 2021) but has never been applied in studies using tissue-deep structures such as the KV or in the LR field. Our goal was to use and optimize smFISH protocols to detect RNA transcripts in 3D Zebrafish LRO. Therefore, we needed to fine-tune various parameters, such as the probe design, imaging conditions, and analysis algorithms, to achieve the best sensitivity, specificity, and resolution. We evaluated the number of cytoplasmic transcripts on both the left and right sides of KV and compared them over time. Our results show the first detection of right-sided asymmetry at 6 ss and provide new insights into the temporal dynamics of *dand5* mRNA

expression on both the anterior and posterior sides of the KV by showing that *dand5* mRNA decay occurs primarily at the anterior side of the KV.

Materials and Methods

Zebrafish lines and embryo manipulation

The zebrafish strains used in this study were wild-type (AB strain, ZFIN), transgenic Tg(sox17:GFP)^{s870Tg} (Sakaguchi et al., 2006), Tg(βactin:HRAS-EGFP) ^{vu119Tg} (Cooper et al., 2005), and mutant *dand5*$^{a204/a204}$ (Montague et al., 2018a). Adult zebrafish were maintained in a recirculating water system at 28.0°C, pH 7, and 950 µS/m conductivity under a 10-hour dark/14-hour light cycle. Mating in pairs resulted in the collection of eggs, which were staged according to previously established protocols (Kimmel et al., 1995; Dahm and Nüsslein-Volhard, 2002). Embryos were then grown in E3 medium (consisting of 5 mM NaCl, 0.17 mM KCl, 0.33 mM CaCl2, 0.33 mM MgSO4 and 0.0001% methylene blue) at 28.0°C.

smFISH probe synthesis

Probes for single-molecule fluorescent *in situ* hybridization (smFISH) targeting the coding, 5-'UTR, and 3-'UTR regions of the zebrafish *dand5* gene were designed using Stellaris Probe Designer. The probes had an oligo length of 18-22 base pairs and a minimum spacing of two nucleotides. Forty-one probes specific to *dand5* were ordered from IDT (Table 1).

Table 1 - smFISH probes designed for *dand5*

Name	Sequence
dand5_probes_01	gcggttcaaggtttcgtt
dand5_probes_02	agccgacctgaaaagtca
dand5_probes_03	gcgccaattgttgtgact
dand5_probes_04	gctgaaatgcattgcgcg
dand5_probes_05	gccacgtgtcggtgaaat
dand5_probes_06	ccggaggattcaaagtct
dand5_probes_07	acaggttcgtctggtcca
dand5_probes_08	acaattcggacagatccc
dand5_probes_09	ccggcgcagaaaatgagg
dand5_probes_10	cggcacatgactaacggc
dand5_probes_11	gcctcgacttggtgaatt
dand5_probes_12	ggccaagaacgcgggaaa
dand5_probes_13	gctatgggtcaggattgc
dand5_probes_14	cactgctgctcacctgag

dand5_probes_15	atctcgagcccttgtttc
dand5_probes_16	ttgtgcaccactttcttc
dand5_probes_17	tgcctctttttttcgctc
dand5_probes_18	gggattgatgcgcagagc
dand5_probes_19	gctctgtttgttcatgtc
dand5_probes_20	tgtaaagggaactgcggc
dand5_probes_21	tgaacggtcaccgtctca
dand5_probes_22	gcactgaccgtagcagag
dand5_probes_23	gctggagggcacgaacat
dand5_probes_24	actgcgctttctgttgtc
dand5_probes_25	aggtgcaggagcacggag
dand5_probes_26	cctcaacgatcaggacgc
dand5_probes_27	gctgctggtttcacactt
dand5_probes_28	gttctgaactttggcctc
dand5_probes_29	gcaatgcctttacgattt
dand5_probes_30	ttttccactgatgtgcgt
dand5_probes_31	tattattgtcacgcgccc
dand5_probes_32	ggctcctcttatcacttt
dand5_probes_33	ggtgtgccgactttattt
dand5_probes_34	agagatgcagagaggggc
dand5_probes_35	tctgcacagaaaggtcgt
dand5_probes_36	cacacacacacacacaca
dand5_probes_37	cacacacacacacacaca
dand5_probes_38	gtcacacacacacacaca
dand5_probes_39	tagccattagatgtggct
dand5_probes_40	atatttcggccacttaca
dand5_probes_41	acgtttcctgtttgcagg

The procedure for creating labeled ddUTP and smFISH probes was adapted from that described by Gaspar et al. (2017). Amino-11-ddUTP was reconstituted to a concentration of 10 mM in 0.1 M NaHCO3 (pH 8.3), while the Atto565 NHS ester dye was reconstituted to 20 mM in anhydrous DMSO. 20 µL of the dye was mixed with 20 µL of the amino-ddUTP and the mixture was incubated in the dark at room temperature for three hours on a rotating platform. The reaction was stopped by adding 1 M Tris-HCl (pH 7.4) to a final concentration of 10 mM, and the mixture was stored in 10 µL aliquots at -20°C. A working aliquot was diluted to 1 mM with nuclease-free water (Invitrogen).

Oligos were resuspended in 100 µL of TE buffer (10 mM TRIS and 1 mM EDTA) per well, pooled (100 µL each), and diluted to a concentration of 200 mM. Labeling of the pooled oligos with dye-coupled ddUTP was performed using a reaction mix of 5 µL oligos, 5 µL of 1 mM dye-ddUTP, 5 µL of 5x TdT buffer (Thermo Scientific), 0.6 µL TdT enzyme (Thermo Scientific), and 1.4 µL of

nuclease-free water. The mixture was then incubated ON at 37°C in a thermocycler with a heated lid. Next, the labeled oligos were purified using a Zymo Oligo Clean & Concentrator kit (D4060) and eluted in 25 µL of nuclease-free water. Finally, probe concentration was measured using a NanoDrop 2000 spectrophotometer (Thermo Fisher Scientific).

smFISH staining protocol

The smFISH staining protocol for zebrafish embryos was adapted from Oka and Sato (2015, and Lord et al. (2021). First, the embryos were fixed in 4% paraformaldehyde (PFA) at 4°C ON, with ten embryos per Eppendorf tube. Next, the embryos were dehydrated after a quick wash in PBSTw (1x PBS + 0.1% Tween 20). The first step involved a 5-min wash in 50% MeOH and 50% PBSTW RT, followed by a 5-min wash in 100% MeOH. The embryos were then stored at -20°C until staining. On the first day of the protocol, the embryos were rehydrated in a series of MeOH and PBSTw solutions (50% and 100% PBSTw) before the manual removal of the chorion. The embryos were then incubated for 30 min at 30°C in 300 µL of pre-hybridization buffer (10% formamide, 2x SSC, 0.1% TritonX-100, 0.02% BSA, and 2 mM ribonucleoside-vanadyl complex (NEB)). This was followed by ON incubation in the dark at 30°C with probes diluted 1:100 in 100 µL hybridization buffer (10% dextran sulfate dissolved in pre-hybridization buffer). Sox17:GFP^{+} and Bactin:HRAS-EGFP^{+} embryos were also incubated with anti-GFP (1:500; Invitrogen) diluted in hybridization buffer with the probes. After staining, the embryos were washed twice for 30 min each at 30°C in a hybridization washing solution (10% formamide, 2x SSC, and 0.1% Triton X-100), followed by a brief rinse in a solution of 2x SSC and 0.1% Tween-20, and incubated for 20 min at 30°C in 0.2X SSC. Embryos were then incubated with DAPI for 15 min at RT in the dark, followed by two washes in 2x SSC and 0.1% Tween-20 for 5 min each. When performing immunostaining, before the DAPI incubation, the embryos were incubated for 2 h at room temperature in the dark with the anti-rabbit Alexa Fluor 488 secondary antibody (Invitrogen, 1:500), followed by six washes with PBSTw for 5 min each. If not mounted immediately, embryos were stored in 2x SSC at 4°C in the dark.

smFISH imaging

Embryos were kept in 2x SSC and deyolked by hand using tweezers. They were mounted on a glass slide with the dorsal side facing upward and flattened using a coverslip secured with vacuum grease. Imaging of the embryos was performed using a Zeiss LSM-980 Airyscan Confocal Microscope equipped with Airyscan SR detectors and controlled by Zen software version 3.3. Z-stack acquisition was achieved using a 40X water immersion objective and a 1.8x zoom factor, with images obtained at 0.18 µm intervals. Raw datasets were processed using the Airyscan

mode in the Zen software, with the processing filter adjusted to 0.5 above the software's recommended value.

Image 3D analysis and quantifications

The 3D datasets were analyzed using IMARIS v. 9.8.2 (Bitplane) software (Figure 1)**.** First, the axes were aligned with the notochord, which was visible in the DAPI channel, by rotating the image freely and applying the "Free Rotate" image processing setting to the desired angle. A surface representation of the KV was generated by manually tracing it in the AF 488 channel. This was done using the 'Isoline' drawing mode and tracing every other optical slice. The surface representation of the KV was used to extract various parameters, including the Volume, Area, Sphericity, and Ellipticity. This surface was then applied as a mask to the Atto565 and DAPI channels to eliminate voxels outside the surface effectively. This step resulted in masked channels containing only the fluorescence information of the KV. Next, an automatic detection setting was applied to the masked DAPI channel to create a surface representation of the nuclei. These surfaces were then used to mask the already masked Atto565 channel for the KV; however, the voxels inside the nuclei were set to zero. The aim was to quantify the number of cytoplasmic *dand5* mRNA transcripts and remove any non-specific nuclear staining of the probes. This was necessary because even cells outside the KV showed nucleic staining with the *dand5* probes. To achieve this goal, the KV was divided into two regions of interest (ROIs), the left and right sides, using a double-masked Atto565 channel. Automatic spot detection was applied to these ROIs using an estimated diameter of 0.3 µm and background subtraction. The filter range for spot detection was limited to detecting only individual spots. The number of detected spots and average distance to their nearest neighbors were extracted from both sides of the KV. To quantify the anterior and posterior number of transcripts, the center of the KV was estimated and marked by an individual spot. Then, an XZ clipping plane was added, showing only the anterior or posterior side. This allowed us to select only the spots on either the anterior or posterior side, being able to extract anterior and posterior parameters for both sides of the KV. To quantify the number of cells in the KV, the nuclei were detected using a spot detector with an estimated diameter of 7-8 µm. The detection was finalized manually to account for cases in which nuclei surface detection failed to separate the contiguous nuclei. A YZ clipping plane was added to measure both the left and right sides of the KV, and anterior and posterior measurements were obtained by setting the YZ and XZ clipping planes in a 90°display of the KV.

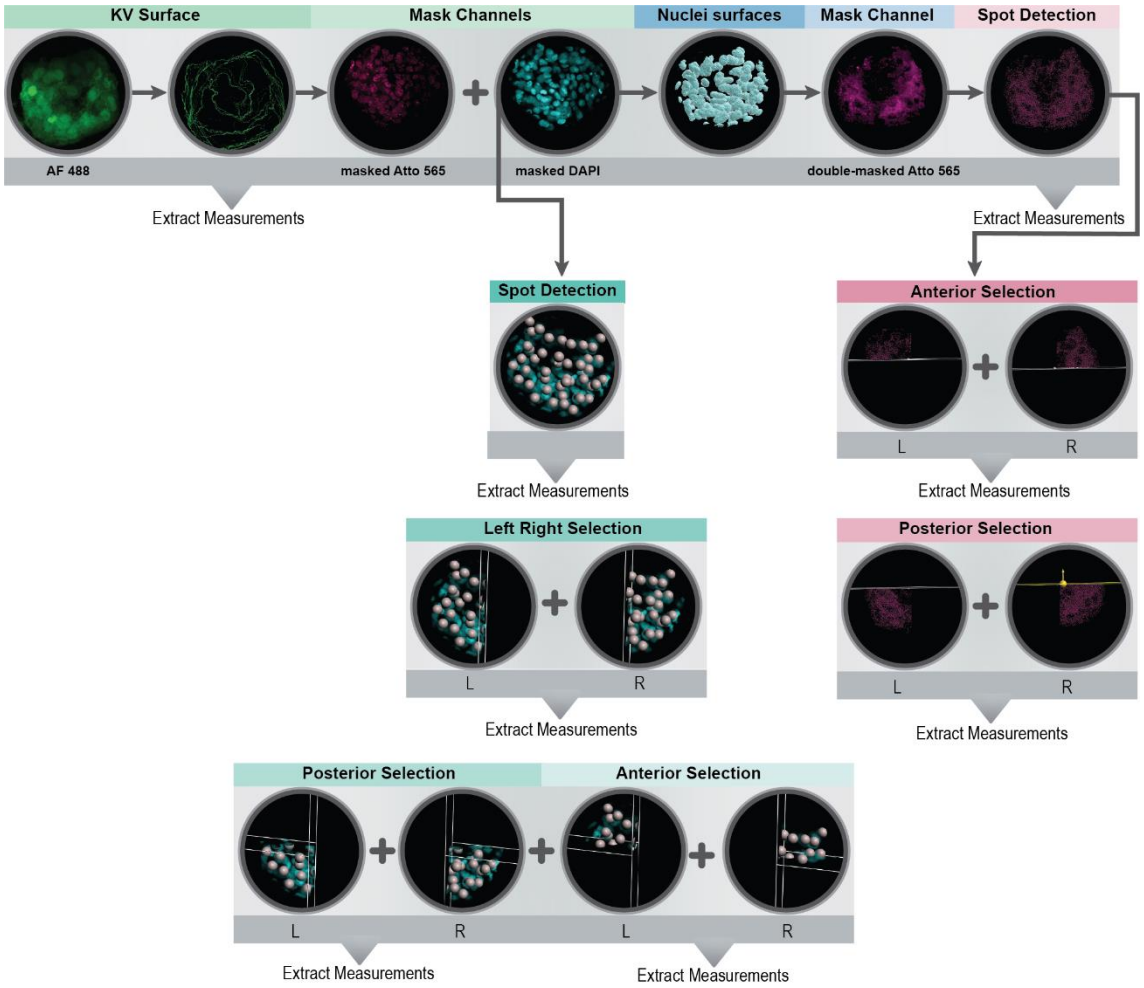

Figure 4.1. Protocol used for 3D analysis and quantification of wholemount SmFISH for *dand5* in zebrafish embryos. The process involves generating a 3D surface representation of the KV using manual tracing and extracting various parameters, such as volume, area, sphericity, and ellipticity. Surface representation was used to mask voxels outside the structure in the Atto565 and DAPI channels. The DAPI channel was used to create a surface representation of the nuclei, which was then used to mask the Atto565 channel and to remove voxels inside the surfaces. The KV was divided into two regions of interest for the automatic detection of cytoplasmic mRNA transcripts, and the number of cells in the KV was estimated by detecting nuclei by spot detection. The center of the KV was marked to quantify the anterior and posterior number of transcripts, and clipping planes were added to measure the left and right sides and the anterior and posterior of the KV to quantify both anterior and posterior transcripts and nuclei on the left and right sides.

Results

Detection of single transcripts of *dand5* mRNA by smFISH

We initially tested the smFISH protocol by combining it with membrane antibodies that were found to be incompatible with the conditions required for smFISH, such as overnight incubation at 30 °C. As a result, the first images acquired were restricted to DAPI and the *dand5* conjugated probes with Atto565 (Figure 4.2A).

Using the smFISH protocol, we detected cytoplasmic *dand5* mRNA transcripts, as expected, in the posterior end of the notochord, indicating the KV region. However, we also observed bright dots in the nucleus of every cell stained with DAPI, suggesting nonspecific staining by some of the *dand5* probes designed (Figure 4.2A). To confirm this, we applied the protocol to 8 ss *dand5* homozygous embryos that show no expression by traditional *in situ* hybridization (Figure 4.2B). Although we observed a residual cytoplasmic signal at the KV, consistent with deficient levels of *dand5* mRNA, we also observed the same nonspecific staining in the nucleus of every cell, as in WT embryos. These results confirmed the lack of specificity of some of the *dand5* probes designed, likely due to hybridization with other regions of the zebrafish genome. Probe specificity was confirmed by blasting the probes sequences against the zebrafish genome. We found that every probe showed some degree of overlap with other chromosomes of the zebrafish genome; especially, those designed against the 3'-UTR were the most problematic.

Nevertheless, we used the designed probes for their specific *dand5* mRNA staining and good additive fluorescence signal in the cytoplasm of KV cells, with no non-specific staining observed in other cell types. However, establishing a 3D analysis protocol was challenging due to the need for cell membranes and KV delimitation. To overcome this, we tested an anti-GFP antibody combined with the smFISH protocol in Tg(β-actin:HRAS-EGFP) embryos at 8 ss (Figure 4.2C). However, while the anti-GFP antibody produced clear membrane staining, all cell membranes were stained and had a low fluorescence signal at the depth of the KV, making it unsuitable for defining a 3D analysis protocol with automatic setup for spot detection. Finally, we tested the protocol using Tg(sox17:GFP) embryos, and observed successful staining with an anti-GFP antibody. KV staining was highly specific, and we successfully performed this protocol for embryos at 3 ss, 5 ss, 6 ss, 7 ss, and 8 ss (Figure 4.3). With a clear delimitation of the KV and nuclei, as visualized by DAPI staining, we optimized the protocol for analyzing cytoplasmic *dand5* mRNA transcripts.

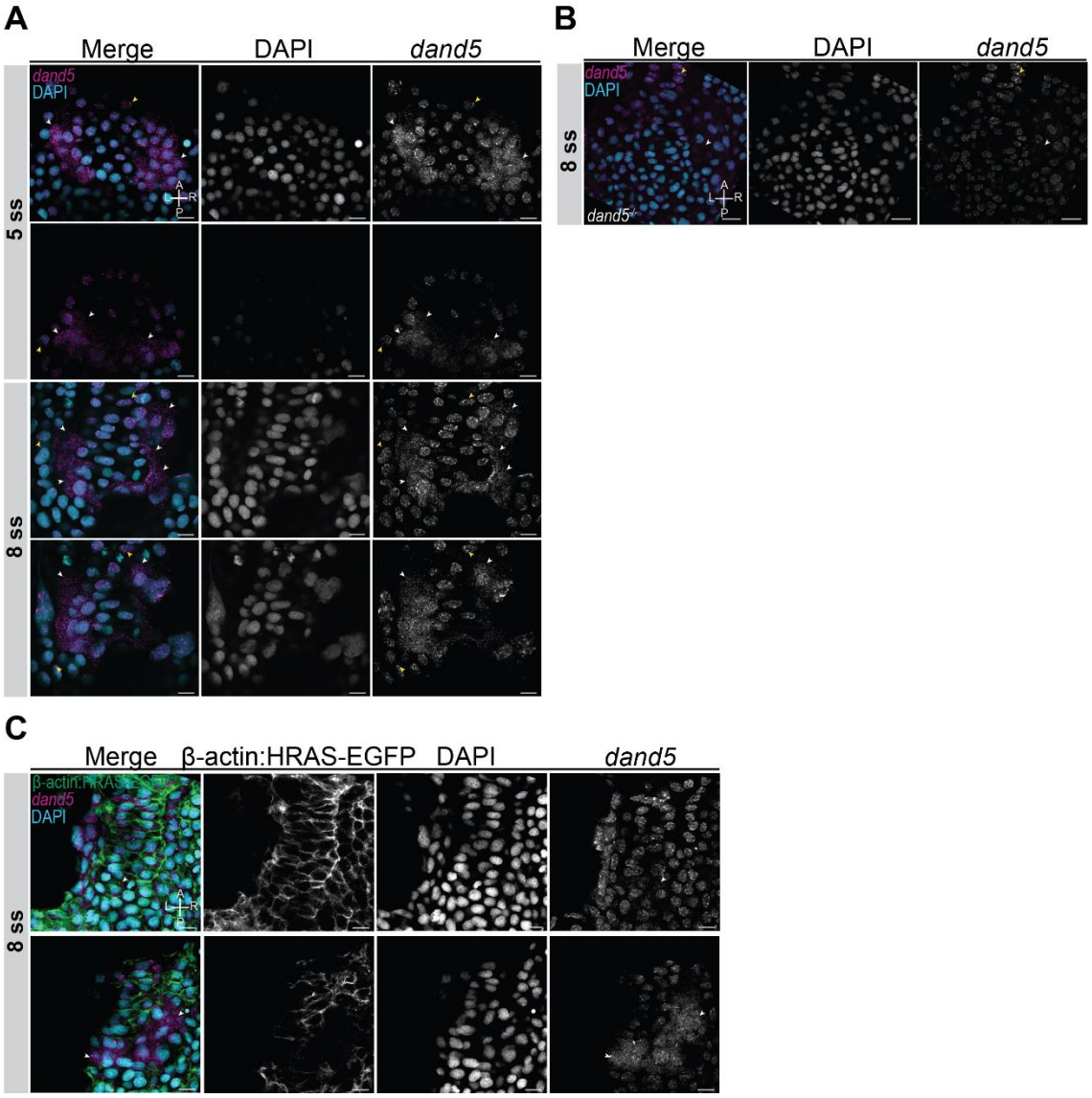

Figure 4.2. Detection and validation of *dand5* mRNA transcripts in zebrafish embryos using smFISH. **(A)** Two different z-planes of 5 and 8 ss embryos stained for *dand5* mRNA via probes conjufated with the dye Atto565 (magenta) and DAPI (cyan) demonstrate the sensitivity of the smFISH protocol. **(B)** Validation of the specificity of the designed *dand5* probes in the cytoplasm using smFISH in an 8 ss *dand5*$^{-/-}$ embryo. **(C)** Co-staining of *Tg(β-actin:HRAS-EGFP)* 8 ss embryo with *dand5* mRNA (magenta), GFP (green) and DAPI (cyan). White arrowheads indicate single cytoplasmic molecules of the *dand5* mRNA. Yellow arrowheads indicate non-specific nuclear staining. Scale bar = 10 µm.

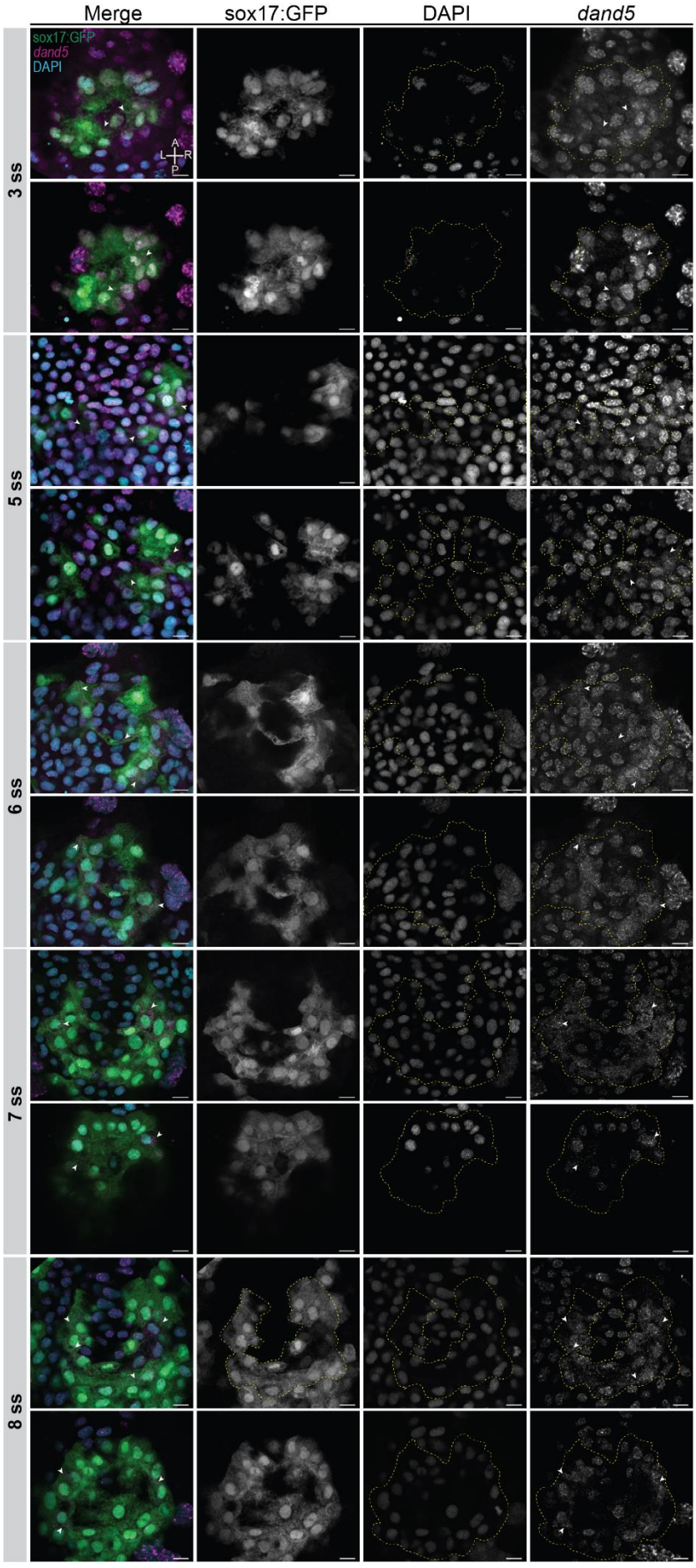
Merge
sox17:GFP
DAPI
dand5
sox17:GFP
dand5
DAPI
A
L
R
P
3 ss
5 ss
6 ss
7 ss
8 ss

Figure 4.3. Validation of SmFISH protocol for subsequent 3D segmentation of the zebrafish KV using Tg(sox17:GFP) embryos. Magenta shows *dand5* mRNA, green shows sox17:GFP, and cyan shows DAPI. Two z-planes are shown for each developmental stages 3 ss, 5 ss, 6 ss, 7 ss, and 8 ss. The specific co-staining of sox17:GFP^{+} cells allows for the accurate identification of the KV boundary (yellow dashed line), making it possible to analyze the number and distribution of *dand5* mRNA transcripts in this region. White arrowheads indicate individual cytoplasmic *dand5* mRNA transcripts. Scale bar = 10 µm.

Detection of earlier *dand5* anterior asymmetry

We established a protocol for the 3D detection of *dand5* mRNA transcripts by combining Tg(sox17:GFP) embryos with the smFISH technique, enabling us to delimit the KV. To eliminate non-specific hybridization with the nuclei of cells, we used the DAPI channel to mask the *dand5* Atto 565 channel and to remove the nucleic signal. Our analysis focused on the dynamics of cytoplasmic *dand5* mRNA transcripts. We evaluated the time course from 3 to 8 ss and detected the total number of spots on the left and right sides of the KV at each developmental stage (Figure 4.4A and C). We performed the same protocol on 8 ss *dand5*$^{-/-}$ embryos to validate the spot-detection algorithm (Fig. 4.4B).

We found symmetric expression of *dand5* in both 3 and 5 ss (Figure 4.4C). At 6 ss, we detected a right-sided asymmetry (p-value = 0.0012) that persisted throughout 7 ss (p-value = 0.0015) and 8 ss (p-value = 0.0347), making it the earliest *dand5* L<R asymmetric expression ever reported (Figure 4.4C). We also compared the number of detected transcripts on the left and right anterior sides of the KV from 3-8 ss and found that *dand5* expression was symmetrical at 3 and 5 ss, but a right-sided anterior asymmetry was established at 6 ss (p-value = 0.0378) and sustained at 7 ss (p-value = 0.0467) and 8 ss (p-value = 0.0197) (Figure 4.4D). However, we only found a right-sided posterior asymmetry in the number of *dand5* mRNA transcripts at 6 ss (p-value = 0.0392; Figure 4.4E). These results suggest that *dand5* asymmetry is established at 6 ss, which is 1 h earlier than that previously reported (Lopes et al., 2010). We also found that left-sided *dand5* mRNA decay is mainly restricted to the anterior region of the KV, where flow velocities are higher (Sampaio et al., 2022), suggesting that the anterior cells are the first to perceive the flow, and where the machinery behind *dand5* mRNA decay is first activated. This is supported by a report of larger anterior left intraciliary calcium oscillations (Yuan et al., 2015b). Current knowledge suggests that the initial response to fluid-flow sensing is the influx of calcium ions.

To compare the dynamics of total *dand5* transcript numbers in the KV, we analyzed developmental stages and observed a lower number of transcripts at 3 ss, which increased at 5

ss (p-value = 0.0156) and showed a downward trend at 6 ss, followed by an increase through 7 to 8 ss (Figure 4.4F). Previous studies have reported that *dand5* expression peaks between 14-19 ss (White et al., 2017). To further analyze the spatial distribution of *dand5* mRNA transcripts, we measured the average distance to the nearest neighbor and found larger values on the left side at 8 ss (p-value = 0.0283) (Figure 4.4G). When expanding this analysis to the 5 nearest neighbors, we found larger distances on the left side at both 6 ss (p-value = 0.0297) and 8 ss (p-value = 0.0185) (Figure 4.4H). We concluded that this is a sequential process; as the number of transcripts decreased on the left side, the distance between them increased.

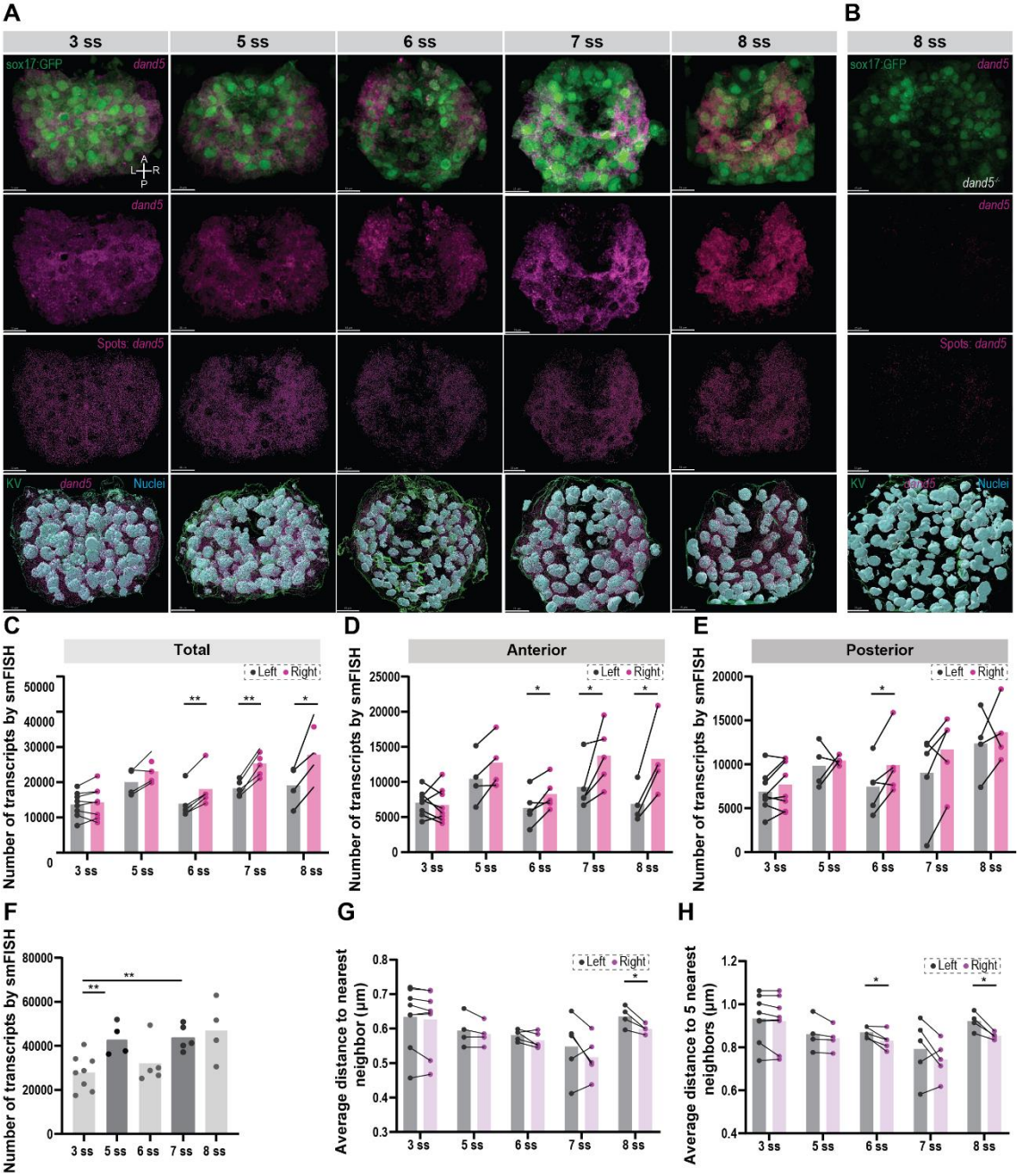

Figure 4.4. 3D smFISH and spatial analysis of *dand5* mRNA transcripts in the KV. **(A)** Time-course 3D analysis of *dand5* mRNA transcripts by smFISH in Tg(sox17:GFP) embryos at 3, 5, 6, 7, and 8 somite stage (ss). 3D representations of *dand5* mRNA (magenta), nuclei (cyan), and sox17:GFP (green) are shown. The KV surface (green) was used to mask both the *dand5*-Atto 565 and DAPI channels to remove nuclear staining. Spot detection was used to detect *the dand5* cytoplasmic transcripts. Axes are indicated. Scale bar = 15 μm. **(B)** The spot detection algorithm was validated in 8 ss *dand5*$^{-/-}$ embryos raised on the *Tg(sox17:GFP)* background. **(C-E)** Quantification of differences in the number of *dand5* mRNA transcripts detected on the left and right sides of the KV; total number **(C)**, at the anterior **(D)**, and posterior **(E)** sides of the KV. Gray and magenta represent the left and right sides, respectively. **(F)** Quantification of the differences in the total number of dand5 transcripts among 3ss, 5 ss, 6 ss, 7 ss and 8 ss. **(G-H)** Quantification of differences in the average distance to the nearest neighbor. **(G)** and the five nearest neighbors **(H)** between the left and right sides at 3, 5 ss, 6ss, 7, and 8 ss. Gray and purple colors represent the left and right sides, respectively. Paired and unpaired t-tests were used. The bars represent the mean values, and the dots represent individual embryos. Asterisks denote statistical significance: * corresponds to a p-value < 0.05, and ** indicates a p-value < 0.005.

Next, we aimed to determine whether differences in Kupffer's vesicle (KV) shape or the number of cells comprising the KV could account for the asymmetry in *dand5* mRNA transcript numbers between the left and right sides of the KV as well as the overall reduction in transcript numbers at 6 ss. We assessed the KV surface via sox17:GFP staining and measured the number of cells and sphericity at various developmental stages. Our analysis revealed no significant differences in KV sphericity or the total number of cells comprising the KV across the developmental stages studied (Figure 4.5A-C). However, we observed a significant decrease in the number of cells on the left side of the KV at 6 ss (p-value = 0.0036). At the same time, no such asymmetry was observed at the other developmental stages (Figure 4.5D). We hypothesize that this asymmetry is not directly related to the *dand5* asymmetry. However, this could have contributed to the overall reduction in transcript numbers. We speculate that this asymmetry in cell number may be due to the rearrangement of cells that occurs in the KV between 4-6 ss, which facilitates the optimal 3D shape for more ciliated cells at the anterior side of the KV (Wang et al., 2012).

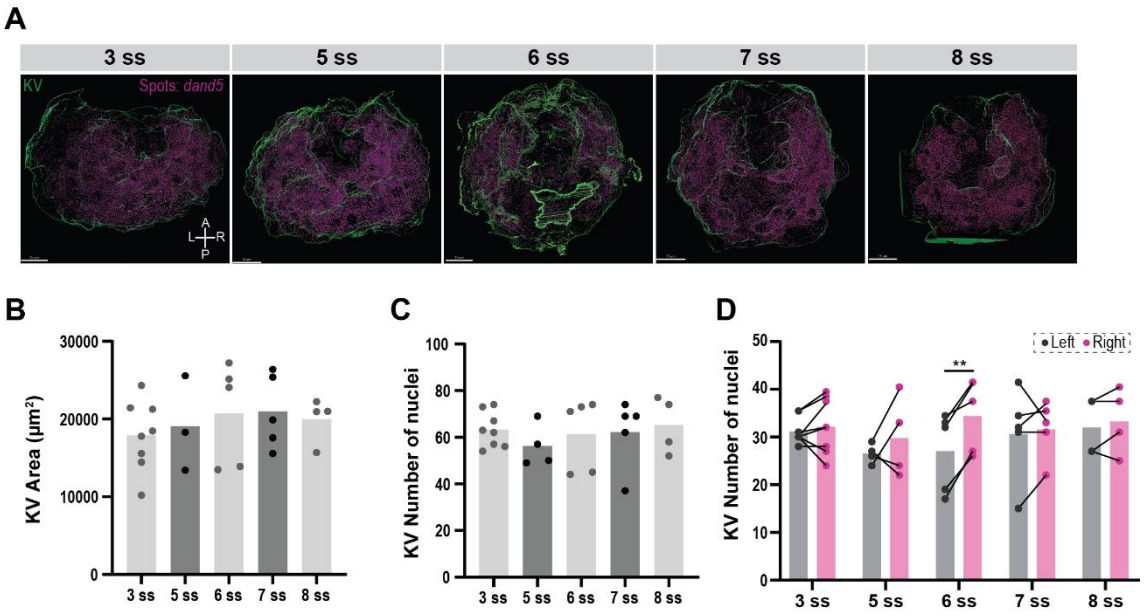

Figure 4.5. Kupffer's vesicle (KV) 3D structure and cell characteristics. **(A)** Time-course 3D analysis of the KV surface and *dand5* mRNA expression by smFISH in *Tg(sox17:GFP)* embryos at 3, 5, 6, 7, and 8 ss. 3D representations of *dand5* mRNA (magenta) and sox17:GFP (green) are shown. **(B)** Comparison of the KV area (µm^2) from 3 to 8 ss. **(C)** Total number of cells in the KV, as determined by the number of detected nuclei from 3 to 8 ss. **(D)** Differences in the number of cells on the right and left sides of KV. Gray and magenta represent the left and right side, respectively. Paired and unpaired t-tests were used to determine statistical significance. The bars represent the mean values and dots indicate individual embryos. Asterisks indicate statistical significance; ** indicates a p-value < 0.005.

Discussion

Here, we describe the implementation and optimization of a protocol to detect the asymmetrical expression of *dand5* in the KV of zebrafish embryos. We used SmFISH to detect single mRNA transcripts of *dand5* and tested various antibodies to define the cell membranes and KV boundaries for 3D analysis. We found that an anti-GFP antibody combined with smFISH in *Tg(sox17:GFP)* embryos produced highly specific staining of the KV, allowing us to optimize the protocol for analyzing cytoplasmic *dand5* mRNA transcripts in 3D.

Using this protocol, we detected a right-sided anterior asymmetry in *dand5* expression at 6 ss, which was one hour earlier than previously reported (Lopes et al., 2010). We also found that left-sided *dand5* mRNA reduction mainly occurs in the anterior region of the KV, where flow velocities are higher (Sampaio et al., 2022), suggesting that the left anterior cells are the first to perceive the flow, which is where we suggest the machinery behind *dand5* mRNA decay may be

activated in the first place. Our observations support the findings of Yuan et al. (2015), who showed that intraciliary calcium ion fluxes (ICOs) responsible for initiating LR development occur mainly in the cilia located in the anterior left quadrant of the KV. The authors also demonstrated that ICOs on the left side of the KV frequently trigger cytosolic calcium waves that propagate to KV-adjacent cells, culminating in a rapid calcium wave on the left that extends beyond the KV. Revealing cilia as the functional ion-signaling compartment connecting ciliary motility and flow to LR signaling, later corroborated by showing that non-motile cilia at the KV can translate biomechanical stimuli into calcium signals (Djenoune et al., 2023).

Our results showed a decrease in the number of cells on the left side of the KV at 6 ss; however, no such asymmetry was observed at other developmental stages. We hypothesized that this asymmetry is not directly related to *dand5* asymmetry but could have contributed to the overall reduction in transcript numbers. The asymmetry in cell numbers may be due to cell rearrangement in the KV between 4-6 ss. This rearrangement facilitates an optimal 3D shape for more ciliated cells on the anterior side of the KV, as suggested by Wang et al. (2012). Although this asymmetry is transient and probably the result of the KV cell rearrangements, it is possible that such rearrangements could aid the establishment of *dand5* asymmetry in the zebrafish LRO. The dynamics of LROs vary across species, and it is not known how Bicc1 interacts with the zebrafish *dand5* 3'-UTR to promote *dand5* left-sided decay. Overall, these results highlight the importance of understanding the complex processes involved in development and the potential impact of cell rearrangements on gene expression. Further research is needed to fully understand the mechanisms underlying this observation.

Although our results shed new light on the early establishment of *dand5* asymmetry in the KV, some technical challenges still need to be addressed to optimize our approach further. First, the design and combination of smFISH probes for *dand5* needs to be refined to avoid nuclear non-specific hybridization, which limited the analysis, in this case, to cytoplasmic mRNA. By testing probes for a conjugation that produce a strong fluorescence signal while preventing cross-hybridization in non-KV cell nuclei can enable the development of a specific set of probes for detecting nuclear mRNA as well. Additionally, by using probes of different colors, it is possible to label distinct segments within longer mRNA molecules. This technique enables the differentiation of intact mRNAs from those that are partially degraded or broken (Tingey et al., 2022) and provide insights into the dynamics of transcriptional repression versus post-transcriptional modifications of *dand5* on the left side of the KV. Intronic probes can also be designed to distinguish nascent transcripts from mature transcripts, which would test if transcription is affected in the anterior left-sided cells.

Image acquisition and analysis also require further optimization to maintain high sensitivity for single mRNA molecule detection while decreasing the time cost, which would allow more reproducibility and, therefore, more statistical significance.

Our study emphasizes the significance of employing high-resolution RNA quantification techniques to comprehensively study spatiotemporal gene expression patterns. SmFISH is a powerful technique for analyzing gene expression in individual cells. This method offers high sensitivity and specificity, allowing for the detection of low-abundance transcripts in complex tissues. Despite its advantages, smFISH can be time-consuming, especially when multiple channels are involved in image acquisition, and automated analysis of 2D images can be achieved using various methods (Stapel et al., 2016; Maynard et al., 2020; Bouilhol et al., 2022; Imbert et al., 2022). However, the automation of 3D analysis is still challenging owing to the diverse demands of membrane, nuclear, and single RNA dot detection, which are specific to each dataset and are affected by tissue/structure complexity and properties. Although software such as IMARIS can be used for 3D automation, the process relies heavily on user input. Recently, Keseroglu et al., (2023) published a protocol for quantifying mRNA transcripts by smFISH in the zebrafish PSM and tailbud using IMARIS, which is very similar to the one we showed here. This was published when we had already developed our own protocol, the fact that two different studies used the same approach highlights the limited available tools for quantifying single mRNA transcripts in complex structures in laboratories without dedicated bioinformatic and imaging facilities to help with the development of specific software for each dataset.

Furthermore, the cost and time required to perform smFISH on a single embryo can be substantial, making it difficult to obtain a large sample size for statistical analysis. Despite these limitations, smFISH remains a valuable tool for studying gene expression in the cell and developmental biology. Continuing developments in this field are likely to lead to more efficient and cost-effective data acquisition and analysis methods.

References

Campione, M., and Brand, T. (2018). Special Issue: Left-Right Asymmetry and Cardiac Morphogenesis. Journal of Cardiovascular Development and Disease 5, 40. doi: 10.3390/jcdd5030040.

Cooper, M. S., Szeto, D. P., Sommers-Herivel, G., Topczewski, J., Solnica-Krezel, L., Kang, H., et al. (2005). Visualizing morphogenesis in transgenic zebrafish embryos using BODIPY TR methyl

ester dye as a vital counterstain for GFP. Developmental dynamics: an official publication of the American Association of Anatomists 232, 359–368.

Dahm, R., and Nüsslein-Volhard, C. (2002). Zebrafish: A practical approach. Oxford University Press doi: 10.1017/S0016672303216384.

Deng, H., Xia, H., and Deng, S. (2014). Genetic basis of human left–right asymmetry disorders. Expert reviews in molecular medicine 16, e19.

Djenoune, L., Mahamdeh, M., Truong, T. V, Nguyen, C. T., Fraser, S. E., Brueckner, M., et al. (2023). Cilia function as calcium-mediated mechanosensors that instruct left-right asymmetry. Science 379, 71–78.

England, S. J., Campbell, P. C., Banerjee, S., Swanson, A. J., and Lewis, K. E. (2017). Identification and expression analysis of the complete family of zebrafish pkd genes. Frontiers in Cell and Developmental Biology 5, 5.

Essner, J. J., Amack, J. D., Nyholm, M. K., Harris, E. B., and Yost, H. J. (2005). Kupffer's vesicle is a ciliated organ of asymmetry in the zebrafish embryo that initiates left-right development of the brain, heart and gut. Development 132 (6), 1247–1260. doi: https://doi.org/10.1242/dev.01663.

Field, S., Riley, K.-L., Grimes, D. T., Hilton, H., Simon, M., Powles-Glover, N., et al. (2011). Pkd1l1 establishes left-right asymmetry and physically interacts with Pkd2. Development 138, 1131–1142. doi: 10.1242/dev.058149.

Grimes, D. T. (2019). Making and breaking symmetry in development , growth and disease. doi: 10.1242/dev.170985.

Grimes, D. T., and Burdine, R. D. (2017). Left-Right Patterning: Breaking Symmetry to Asymmetric Morphogenesis. Trends in Genetics 33, 616–628. doi: 10.1016/j.tig.2017.06.004.

Imbert, A., Ouyang, W., Safieddine, A., Coleno, E., Zimmer, C., Bertrand, E., et al. (2022). FISH-quant v2: a scalable and modular tool for smFISH image analysis. Rna 28, 786–795.

Jacinto, A. R. M. (2018). PKD2-dependent sensing mechanism in Kupffer's vesicle: how it affects the left-right axis establishment in zebrafish.

Jacinto, R., Sampaio, P., Roxo-Rosa, M., Pestana, S., and Lopes, S. S. (2021). Pkd2 affects cilia length and impacts LR flow dynamics and dand5. Frontiers in Cell and Developmental Biology 9, 624531.

Kamura, K., Kobayashi, D., Uehara, Y., Koshida, S., Iijima, N., Kudo, A., et al. (2011). Pkd1l1 complexes with Pkd2 on motile cilia and functions to establish the left-right axis. Development 138, 1121–1129. doi: 10.1242/dev.058271.

Keseroglu, K., Zinani, O. Q. H., and Özbudak, E. M. (2023). Using single-molecule fluorescence in situ hybridization and immunohistochemistry to count RNA molecules in single cells in zebrafish embryos. STAR Protocols 4, 102020. doi: https://doi.org/10.1016/j.xpro.2022.102020.

Keskin, S., Devakanmalai, G. S., Kwon, S. Bin, Vu, H. T., Hong, Q., Lee, Y. Y., et al. (2018). Noise in the vertebrate segmentation clock is boosted by time delays but tamed by notch signaling. Cell reports 23, 2175–2185.

Kimmel, C. B., Ballard, W. W., Kimmel, S. R., Ullmann, B., and Schilling, T. F. (1995). Stages of embryonic development of the zebrafish. Developmental Dynamics 203, 253–310. doi: 10.1002/aja.1002030302.

Kramer-Zucker, A. G. (2005). Cilia-driven fluid flow in the zebrafish pronephros, brain and Kupffer's vesicle is required for normal organogenesis. Development 132, 1907–1921. doi: 10.1242/dev.01772.

Long, S., Ahmad, N., and Rebagliati, M. (2003). The zebrafish nodal-related gene southpaw is required for visceral and diencephalic left-right asymmetry. Development 130, 2303–2316.

Lopes, S. S., Lourenco, R., Pacheco, L., Moreno, N., Kreiling, J., and Saude, L. (2010). Notch signalling regulates left-right asymmetry through ciliary length control. Development 137, 3625–3632. doi: 10.1242/dev.054452.

Lord, N. D., Carte, A. N., Abitua, P. B., and Schier, A. F. (2021). The pattern of nodal morphogen signaling is shaped by co-receptor expression. Elife 10, e54894.

Maerker, M., Getwan, M., Dowdle, M. E., McSheene, J. C., Gonzalez, V., Pelliccia, J. L., et al. (2021). Bicc1 and Dicer regulate left-right patterning through post-transcriptional control of the Nodal inhibitor Dand5. Nature Communications 12, 5482. doi: 10.1038/s41467-021-25464-z.

Maynard, K. R., Tippani, M., Takahashi, Y., Phan, B. N., Hyde, T. M., Jaffe, A. E., et al. (2020). dotdotdot: an automated approach to quantify multiplex single molecule fluorescent in situ hybridization (smFISH) images in complex tissues. Nucleic Acids Research 48, e66–e66. doi: 10.1093/nar/gkaa312.

Minegishi, K., Rothé, B., Komatsu, K. R., Ono, H., Ikawa, Y., Nishimura, H., et al. (2021). Fluid flow-induced left-right asymmetric decay of Dand5 mRNA in the mouse embryo requires a Bicc1-Ccr4

RNA degradation complex. Nature Communications 12, 4071. doi: 10.1038/s41467-021-24295-2.

Montague, T. G., Gagnon, J. A., and Schier, A. F. (2018). Conserved regulation of Nodal-mediated left-right patterning in zebrafish and mouse. Development 145, dev171090.

Nakamura, T., Saito, D., Kawasumi, A., Shinohara, K., Asai, Y., Takaoka, K., et al. (2012). Fluid flow and interlinked feedback loops establish left–right asymmetric decay of Cerl2 mRNA. Nature communications 3, 1322.

Oka, Y., and Sato, T. N. (2015). Whole-mount single molecule FISH method for zebrafish embryo. Scientific reports 5, 1–8.

Pennekamp, P., Karcher, C., Fischer, A., Schweickert, A., Skryabin, B., Horst, J., et al. (2002). The ion channel polycystin-2 is required for left-right axis determination in mice. Current Biology 12, 938–943. doi: 10.1016/S0960-9822(02)00869-2.

Pinto, A. L., Rasteiro, M., Bota, C., Pestana, S., Sampaio, P., Hogg, C., et al. (2021). Zebrafish motile cilia as a model for primary ciliary dyskinesia. International Journal of Molecular Sciences 22, 8361.

Raj, A., Van Den Bogaard, P., Rifkin, S. A., Van Oudenaarden, A., and Tyagi, S. (2008). Imaging individual mRNA molecules using multiple singly labeled probes. Nature methods 5, 877–879.

Roxo-Rosa, M., and Lopes, S. S. (2019). “The zebrafish kupffer’s vesicle: a special organ in a model organism to study human diseases,” in Zebrafish in Biomedical Research (IntechOpen).

Sakaguchi, T., Kikuchi, Y., Kuroiwa, A., Takeda, H., and Stainier, D. Y. R. (2006). The yolk syncytial layer regulates myocardial migration by influencing extracellular matrix assembly in zebrafish. Development 133, 4063–4072. doi: doi.org/10.1242/dev.02581.

Sampaio, P., Ferreira, R. R., Guerrero, A., Pintado, P., Tavares, B., Amaro, J., et al. (2014). Left-right organizer flow dynamics: how much cilia activity reliably yields laterality? Developmental cell 29, 716–728.

Sampaio, P., Pestana, S., Guerrero, A., Telley, I. A., Smith, D. J., and Lopes, S. S. (2022). Fluid extraction from the left-right organizer uncovers mechanical properties needed for symmetry breaking. bioRxiv, 2004–2022.

Schottenfeld, J., Sullivan-brown, J., and Burdine, R. D. (2007). Zebrafish curly up encodes a Pkd2 ortholog that restricts left-side-specific expression of southpaw. Development 134, 1605–1615. doi: 10.1242/dev.02827.

Schweickert, A., Ott, T., Kurz, S., Tingler, M., Maerker, M., Fuhl, F., et al. (2017). Vertebrate Left-Right Asymmetry: What Can Nodal Cascade Gene Expression Patterns Tell Us? Journal of Cardiovascular Development and Disease 5, 1. doi: 10.3390/jcdd5010001.

Schweickert, A., Vick, P., Getwan, M., Weber, T., Schneider, I., Eberhardt, M., et al. (2010). The nodal inhibitor Coco is a critical target of leftward flow in Xenopus. Current Biology 20, 738–743.

Stapel, L. C., Lombardot, B., Broaddus, C., Kainmueller, D., Jug, F., Myers, E. W., et al. (2016). Automated detection and quantification of single RNAs at cellular resolution in zebrafish embryos. Development 143, 540–546.

Supatto, W., Fraser, S. E., and Vermot, J. (2008). An All-Optical Approach for Probing Microscopic Flows in Living Embryos. Biophysical Journal 95, L29–L31. doi: 10.1529/biophysj.108.137786.

Sutherland, M. J., and Ware, S. M. (2009). Disorders of left-right asymmetry: Heterotaxy and situs inversus. American Journal of Medical Genetics, Part C: Seminars in Medical Genetics 151, 307–317. doi: 10.1002/ajmg.c.30228.

Tavares, B., Jacinto, R., Sampaio, P., Pestana, S., Pinto, A., Vaz, A., et al. (2017). Notch/Her12 signalling modulates, motile/immotile cilia ratio downstream of Foxj1a in zebrafish left-right organizer. Elife 6, e25165.

Tingey, M., Schnell, S. J., Yu, W., Saredy, J., Junod, S., Patel, D., et al. (2022). Technologies Enabling Single-Molecule Super-Resolution Imaging of mRNA. Cells 11, 3079.

Wang, G., Manning, M. L., and Amack, J. D. (2012). Regional cell shape changes control form and function of Kupffer ' s vesicle in the zebrafish embryo. Developmental Biology 370, 52–62. doi: 10.1016/j.ydbio.2012.07.019.

White, R. J., Collins, J. E., Sealy, I. M., Wali, N., Dooley, C. M., Digby, Z., et al. (2017). A high-resolution mRNA expression time course of embryonic development in zebrafish. eLife, 1–32.

Yoshiba, S., Shiratori, H., Kuo, I. Y., Kawasumi, A., Shinohara, K., Nonaka, S., et al. (2012). Cilia at the node of mouse embryos sense fluid flow for left-right determination via Pkd2. Science 338, 226–231.

Yuan, S., Zhao, L., Brueckner, M., and Sun, Z. (2015). Intraciliary calcium oscillations initiate vertebrate left-right asymmetry. Current biology 25, 556–567.

Zinski, J., Tajer, B., and Mullins, M. C. (2017). TGF-β Family Signaling in Early Vertebrate Development. Cold Spring Harbor Perspectives in Biology, a033274.

CHAPTER 5:

Discussion

General Discussion

During my PhD project, I conducted research on a population of tailbud cells in zebrafish embryos, which set my studies apart from those of my lab who focused on KV cilia or motile cilia generated fluid flow. Our focus was on the behavior of a specific population of tailbud cells located in close proximity to the KV in zebrafish embryos. Our findings revealed that these cells display left-sided asymmetries in both number and position, and that these asymmetries are influenced by manipulation of the LR cascade, such as the lack of *dand5* expression in KV cells. Through cell tracing, we identified that these cells are mainly somite precursors, which also display left-sided asymmetry in number when incorporated into symmetrical somites.

Additionally, our investigations uncovered a previously unreported role of Dand5, encoded by the first asymmetric gene in the LR patterning mechanism, in affecting the number of cells exiting the tailbud towards the anterior side of the embryo, as well as in regulating normal *myoD* LR fluctuations during somitogenesis. Furthermore, our studies also shed light on the impact of the absence of the KV on the position of the referred tailbud mesodermal population, as we found that the KV may be involved in triggering the migration of these cells to the PSM. Therefore, we uncovered a previously unknown role of the KV in tailbud cell movements with unreported effects on myogenesis specification.

Finally, we have implemented a new *in situ* hybridization protocol in zebrafish with a higher resolution to better understand the spatial and temporal dynamics of the left-sided decrease in *dand5* expression during symmetry breaking using smFISH. This technique allowed us to discover earlier asymmetric expression patterns of *dand5* mRNA at the anterior left pole of the KV, conciliating previous studies on flow mechanics with mRNA dynamics.

In vivo LR behaviors of somite precursors

The close proximity of somite precursors to both the LRO and LPM has led to the suggestion that these structures may be exposed to asymmetrical signals during embryonic development. Furthermore, because symmetrical and asymmetrical structures are formed using similar molecular cues, protective mechanisms have been proposed (Grimes, 2019a) and demonstrated (Kawakami et al., 2005; Vermot and Pourquié, 2005) to shield symmetrical structures from asymmetric LR signals. Consequently, known and potentially unknown mechanisms are in place to ensure somite symmetry by counteracting LR cues and developmental noise at various

checkpoints during embryo patterning (Holley et al., 2000; Jiang et al., 2000; Lewis, 2003; Kawakami et al., 2005; Horikawa et al., 2006; Lewis et al., 2009; Delaune et al., 2012; Keskin et al., 2018; Grimes, 2019a).

In this study, we found *in vivo* evidence of LR asymmetries in somite precursors in zebrafish embryos. We identified a group of tailbud cells called NKSTCs, which displayed LR asymmetries in cell number and migration patterns. Our results demonstrated that most NKSTCs contributed to somites with a left-sided bias. Additionally, these cells responded to lack of LR cues by losing their migratory asymmetries and exhibiting symmetrical somite incorporation in the absence of Dand5. While fate-map studies confirmed left-sided asymmetry in somite integration at 24 hpf, as expected, WT embryos still developed symmetrical somites, suggesting the presence of a counteracting mechanism to ensure symmetrical somite formation.

Our study only quantified a restricted population of tailbud cells, as we relied on the inadvertent labeling of a few somite precursors by the Tg(sox17:GFP) line. To test if our results were not dependent on the referred transgenic line, we investigated whether a visible asymmetry in tailbud exit could be confirmed when following the overall population of somite precursors exiting the tailbud region. Photoconverting an area of cells posterior to the same plane as the KV, we were able to trace a larger population of tailbud cells, which still exhibited LR asymmetries, albeit to a minor degree. To test whether the previously reported Retinoic Acid buffering mechanism is responsible for the lack of translation of the observed LR asymmetries into asymmetric somites, it would be interesting to examine the behavior of NKSTCs in embryos with reduced RA levels. One approach could involve overexpressing *cyp2a1* to decrease RA levels in zebrafish embryos. Based on our hypothesis, we predict that NKSTCs would acquire even more asymmetric positions in embryos with reduced RA levels, potentially leading to more asymmetrical somite integration. Previous studies have demonstrated that a lack of RA signaling can result in an asymmetric increase in the latest-formed somites on the left side (Kawakami et al., 2005).

Developmental noise in somitogenesis and myogenesis downstream of Dand5

It was previously thought that the asymmetry in somite development only occurred when RA signaling was lost, exposing the PSM molecular LR prepatterns. However, a recent study by Naganathan et al. (2022) challenged this view by demonstrating that the initial somite lengths

are imprecise. However, imprecisions lack left or right bias and are adjusted through 3D somite deformations. This suggests that the mechanisms underlying somite length and symmetry are more complex than previously thought and highlights the presence of developmental noise. In addition, the study reveals another fine-tuning mechanism that ensures somite symmetry, which relies on mechanical forces, such as somite surface tension, external stresses from neighboring tissues, and convergent extension within somites.

We have also reported noise in somite specification and commitment to myogenesis, specifically in the expression of *myoD* in WT embryos. Interestingly, our observations revealed that *myoD* expression fluctuates and is not perfectly bilaterally aligned in 50% of WT embryos. This leads to one side of the embryo exhibiting an additional presumptive somite marked by *myoD* expression. However, we found that Dand5, a secreted protein encoded by the first known asymmetric gene, is responsible for generating some asymmetry in presumptive somites from 13 to 15 ss. Furthermore, when we analyzed *dand5*$^{-/-}$ embryos, we found that *myoD* expression was consistently symmetric, indicating that Dand5 causes fluctuations in left-right asymmetry during myogenic differentiation.

Although this study did not explore the mechanism by which Dand5 impacts *myoD* expression, prior research indicates that *dand5* is expressed during the segmentation period from 1-25 ss, with its highest expression levels occurring between 14-19 ss (White et al., 2017), when embryonic asymmetry has already been established (Long et al., 2003). Furthermore, *dand5* expression is limited to KV-derived cells(Ikeda et al., 2022a), indicating that its effect is non-cell-autonomous. These observations suggest that Dand5, secreted by KV cells, may play a crucial role in myogenesis, as well as in breaking embryonic symmetry.

In zebrafish, *myf5* and *myoD* mRNAs are initiated de novo by slow and fast muscle precursors, generating each successive somite as the AP axis forms and extends (Coutelle et al., 2001). *myoD* expression is first detected at 75% epiboly, closer to the organizer, and begins in adaxial cells on each side of the future notochord before somite formation. After somite formation, *myoD* is expressed bilaterally in the posterior region of the somites (Weinberg et al., 1996). The regular expression of *myf5* and *myoD* in adaxial slow muscle precursors is dependent on Shh (Coutelle et al., 2001), whereas Tbx16 plays a crucial role in the Fgf-driven expression of MRFs in the PSM, independently inducing both *myf5* and *myoD*, as long as Fgf signaling remains active (Osborn et al., 2020). Moreover, Ntl binds directly to *myoD* regulatory elements and promotes dorsal midline in cooperation with Tbx16 (Osborn et al., 2020).

While it remains unclear how Dand5 function could directly or indirectly interact with the players involved in regulating *myoD* expression, other studies have shown that *dand5* expression is dependent on the presence of the Ntl protein (Hashimoto et al., 2004a; Amack et al., 2007; Gourronc et al., 2007). Moreover, a T-box-rich region has been identified near the *dand5* transcription start site (Gourronc et al., 2007). To fully understand the underlying mechanisms governing this particular phenotype as well as the extent of Dand5 interaction with myogenic differentiation and somite specification, it is necessary to conduct a more comprehensive evaluation of the expression patterns of key genes, such as *myf5*, *tbx16*, *shh*, and *ntl*, along with clock genes, in the absence of *dand5* expression.

Dand5 function on tailbud cell movement and embryo tail length

Our study revealed that *dand5*$^{-/-}$ embryos exhibited reduced tailbud cell migration from the posterior cluster, and subsequently a lower number of photoconverted cells was detected in somites at 24 hpf. Furthermore, we correlated these findings with the smaller somite size observed in *dand5*$^{-/-}$ embryos, which was proportional to their shorter body length. Although the observed effects due to Dand5 deficiency were transient, our results indicate that *dand5* plays a role in somite formation during embryonic development.

Located at the caudal end of the vertebrate embryo axis, the tailbud is a cluster of highly motile cells that contributes to the continuous elongation of the caudal body by providing a steady supply of cells to the extending axial tissues. This organizing center contains neural, notochord, somitic, and endothelial precursors (Narayanan et al., 2021).

The anterior dorsal medial domain of the tailbud continuously supplies a flux of cells, exhibiting a high global order (Lawton et al., 2013). Some of these cells migrate through the dorsal medial zone to the posterior zone, which serves as the maturation zone for the PSM cells. During this migration, there is a transition from ordered to disordered cell flow, which is further characterized by disordered cell motility in the posterior zone (Das et al., 2017). In our movies we observed the KV cells act as more solid-state organ pushing through the surrounding cells. Meanwhile, cells in the anterior region exhibit more directed movements, aiming to exit the posterior zone and integrate into the left and right sides of the PSM as observed by (Das et al., 2017; Narayanan et al., 2021).

Previous studies have suggested that somite size is regulated by the movement of cells through the PSM (Fior et al., 2012). The differentiation and migration of mesoderm progenitor cells from

the tailbud to the PSM are controlled by the expression of tbx16 and msgn1 (Fior et al., 2012a; Yabe and Takada, 2012; Manning and Kimelman, 2015), as reducing cell flows in the absence of these genes may result in smaller somites (Fior et al., 2012).Additionally, *tbx16* and *msgn1* mutants have been shown to exhibit deficient exit from the mesodermal progenitor zone due to unproductive lamellipodia and consequently randomized motility without directed migration over long distances and no consistent directed movement towards the anterior side (Manning and Kimelman, 2015).

It is currently unclear whether dand5 homozygous mutant cells have fewer lamellipodia or if their lamellipodia are not consistently positioned to facilitate directed cell movement, despite the observed decrease in migratory tailbud cells. Further investigations are required to determine the underlying mechanisms responsible for this phenomenon. Examining the cytoskeletal organization and the localization of key signaling molecules involved in cell migration could provide insights into the molecular pathways disrupted in these cells. Additionally, thoroughly live imaging studies of *dand5*$^{-/-}$ tailbud cells could reveal whether their lamellipodia are not consistently positioned and contribute to the observed decrease in directed cell movement. Overall, further research is needed to fully understand the cellular and molecular mechanisms underlying the role of Dand5 in tailbud cell migration during zebrafish embryonic development.

Several signaling cues, including BMP, Wnt, Fgf, and Nodal, regulate the flow of cells in the tailbud (Lawton et al., 2013; O'Neill and Thorpe, 2013; Das et al., 2017; Goto et al., 2017). In zebrafish, mesodermal commitment from the neuromesodermal population is induced by cooperative signaling of Wnt and Fgf, leading to the positive regulation of *tbx16* and *msgn1* (Goto et al., 2017). Proper levels of BMP signaling are crucial for cell exit from the tailbud and differentiation into tail somites, with excessive BMP levels inhibiting cell exit (O'Neill and Thorpe, 2013). Similarly, Nodal signaling is also proposed to be essential for tailbud cell exit, as *oep;tbx16* mutants lack somites, but do not by inhibiting BMP signaling (Griffin and Kimelman, 2002; O'Neill and Thorpe, 2013).

Since Dand5 is capable of inhibiting all three Nodal proteins (Sqnt, Cyc, and Spaw) in zebrafish, as well as weakly inhibiting BMP (Hashimoto et al., 2004a). To investigate the inhibitory effect of Dand5 on tailbud cell movement, we have formulated two hypotheses that potentially regulate cell exit from the tailbud by suppressing either Nodal or BMP signaling. First, Dand5 might specifically inhibit BMP signaling in cells located near the KV and KV-derived cells, where *dand5* expression persists. This could assist in maintaining optimal levels of BMP signaling and

working alongside *chordin* and *noggin* to regulate cell exit from the tailbud (Dal-Pra et al., 2006; Von Der Hardt et al., 2007).

On the other hand, the absence of Dand5 in *dand5*$^{-/-}$ embryos, triggers early *spaw* expression both in peri-KV cells and the LPM (Montague et al., 2018a), which could affect the induction of somite precursors to leave the tailbud, causing an acceleration of initial cell flow into the PSM and a reduction in the number of cells remaining in the tailbud niche. This, in turn, might lead to altered cell flow patterns in the tailbud, potentially disrupting the proper differentiation of cells into tail somites. Remarkably, inhibition Nodal signaling in endodermal cells was shown to slow migration velocity but increases persistence, as demonstrated by Woo et al., (2012). Nodal signaling affects actin dynamics via the small GTPase Rac1 and induces expression of the Rac activator *prex1*.

Consequently, these findings suggest that Dand5 regulates the balance of signaling cues in the tailbud, even if only transiently. However, embryos and larvae appear to have a mechanism that compensates for changes in the number of cells in the tailbud. This mechanism may conceal the impact of Dand5 on adult fish.

Notably, Wnt and FGF signaling pathways also regulate how tailbud cells movement at the ordered to disordered state transition. When Wnt signaling is inhibited or reduced, cell flows in the posterior zone become more ordered and vortices of stable cell flows form. This causes an asymmetric distribution of cells between the left and right halves of the PSM, described by the flow pattern losing its bilateral symmetry (Lawton et al., 2013). However, the authors did not specify whether this asymmetry was randomized or side-biased and it is not clear how Dand5 could be involved in Wnt inhibition, as it is not reported in zebrafish (Hashimoto et al., 2004a) unlike Dand5 in the Xenopus, which regulates Wnt signaling (Schweickert et al., 2010).

The impact of the KV on tailbud movements

Our findings indicate that in zebrafish, the KV, the LRO, provides signaling and potentially mechanical cues that facilitate the anterior migration of tailbud cells. Moreover, our findings suggest that the KV is involved in somite specification during embryonic development. Specifically, we observed that the KV affects a subset of tailbud cells from 10 ss onwards, causing them to transition from an aggregated to a migratory state and ultimately contributing to the formation of somites. In the absence of the KV, these cells seemed to lose their cues to move anteriorly or even fail to form aggregates. Although our study focused on a specific population

of mesodermal progenitor cells, NKSTCs, we suspect that neighboring cells close to the KV may also receive cues for promoting movement.

To further validate our observations, we suggest investigating the mechanical interactions between KV and tailbud cells is crucial to confirm the role of KV in tailbud cell movement. Specifically, assessing the pressure exerted by the KV on tailbud cells and its impact on cell flows would offer valuable insights into this process. Previous research has shown that the pressure and shear stress of tailbud cells influence the KV reshaping process as they move through the tailbud tissue from 2 to 8 ss (Sanematsu et al., 2021). In particular, the authors observed velocity gradients surrounding the KV, indicating that the tailbud tissue applies mechanical drag forces on the basal side of KV cells during the 2-4 ss and 4-6 ss stages, which facilitates the KV reshaping process. Therefore, it is reasonable to assume that the KV itself exerts mechanical forces on the surrounding tailbud cells. Although previous studies have investigated the pressure and shear stress generated by tailbud cells on the KV, our proposed approach of examining the mechanical interactions between the KV and tailbud cells takes the opposite perspective. However, these two approaches can be complementary, as they provide a more complete understanding of the mechanical forces at play during tailbud cell movement and KV reshaping. By examining the pressure exerted by the KV on tailbud cells, we can better understand the role of the KV in initiating and directing tailbud cell movement. Thus, understanding the mechanical interactions between the KV and tailbud cells can reveal an additional link between LR symmetry and asymmetry in developing embryos.

Furthermore, to explore the full extent of KV's involvement in tailbud cell movement, it is also necessary to perform live-imaging studies on DFC-ablated embryos and compare cell flows in the presence and absence of the KV. Such a comparative approach could reveal new roles for the KV beyond its established function as the zebrafish LRO. Supporting this idea is the observation that the KV persists longer than is necessary to establish LR asymmetry (Ikeda et al., 2022a). Moreover, observations suggest that NKSTCs lose their movement ability when the KV is absent, indicating that the KV plays a crucial role in regulating tailbud cell movements. This may have implications for the formation of somites from tailbud cells, which require the coordinated action of the wavefront and segmental clock. However, the absence of the ‘posterior cluster’ in DFC-ablated embryos remains unclear.

From a signaling perspective, our observations have confirmed that the KV, where *dand5* is expressed, significantly contributes to tailbud cell movements. The absence of Dand5 leads to reduced cell migration towards the anterior side and loss of left-side asymmetry. This suggests

that signaling pathways in the vicinity of the KV, such as Wnt, Fgf, and BMP, may also be compromised by its absence. Therefore, it is crucial to evaluate the activity of these signaling pathways in the absence of the KV to fully understand their role in tailbud cell movement. In addition, *spaw* expression in both the region where the KV is located and in the LPM should be assessed, as Nodal signaling is also important for tailbud movement and somite formation (Griffin and Kimelman, 2002). A previous study that generated embryos without the KV through laser ablation only assessed *lefty2* on the anterior side of the LPM and *lefty1* in the brain as measures of molecular disruption of laterality (Essner et al., 2005). Thus, a more comprehensive assessment of molecular disruption is necessary to fully understand the role of the KV in laterality determination and the signaling pathways involved.

Furthermore, it is essential to examine the expression of *spaw* in both the region where the KV is expected to form and in the LPM, as Nodal signaling also plays a role in tailbud movement and somite formation (Griffin and Kimelman, 2002). Therefore, a more comprehensive analysis of *spaw* expression in the relevant regions is important to establish the extent to which it is important for both tailbud movements and somite specification. It is worth noting that previous studies investigating defects in KV morphogenesis have primarily focused on the resulting impact on laterality. In contrast, potential effects on the tailbud cell movements have not been thoroughly explored. While laterality is undoubtedly a critical aspect of KV function, a more comprehensive analysis of the potential impact on other developmental processes, such as tailbud movement, would be beneficial to fully understand the overall consequences of KV morphogenesis defects. Therefore, our work highlighted the need for future studies to investigate the potential effects of KV defects on various developmental processes beyond laterality determination.

The KV and myogenesis

In addition to its role in laterality determination, we have also uncovered evidence suggesting that the KV may play a critical role in myogenic commitment. Specifically, our findings demonstrate that DFC-ablated embryos exhibited defective *myoD* expression in both the somites and adaxial cells, indicating that the KV provides crucial information for this developmental process. As reported by Essner et al., (2005) DFCs-ablated exhibited a lack of *ntl* gene expression in DFCs, while adjacent mesoderm cells displayed WT *ntl* expression. Given that *myoD* expression has been shown to be dependent on the Ntl protein (Osborn et al., 2020), one

might expect that normal notochord expression would correspond to unaffected *myoD* expression. These results suggest that the KV may provide additional cues or signaling pathways that are critical for myogenic commitment beyond those upstream of *ntl* expression. Further investigations are needed to fully elucidate the complex mechanisms underlying myogenesis and the role of the KV in this process by evaluating both Fgf and Tbx16 levels on embryos lacking a KV.

dand5 asymmetric expression

Studies in mouse, *Xenopus*, and zebrafish have shown that the asymmetric directional flow results in the right-sided expression of *dand5*, which is initially expressed bilaterally in the cells of the LRO (Hashimoto et al., 2004b; Marques et al., 2004; Schweickert et al., 2010; Nakamura et al., 2012; Sampaio et al., 2014). The decrease in *dand5* expression on the left side, is thought to dowregulate Dand5 secretion by the KV left sided cells towards the left tailbud and LPM. Dand5 which is a potent Nodal inhibitor, thereby releases the Dand5-Nodal repression on the left side, leading to subsequent *nodal mRNA* expression only on the left LPM.

The decrease in *dand5* expression at the KV cells is thought to result from the repression or decay of *dand5* mRNA on the left side, which expression is destabilized by the flow (Nakamura et al., 2012). Recently, Katoh et al., (2023), showed that in mice *Dand5* degradation was elicited in cells where repeated calcium transients occurred. They showed that optical tweezer mechanical stimulation on crown cell cilia acted via Pkd2 channels. This recent work highlights that *dand5* mRNA may be degraded in cells that are constantly stimulated by flow. Our own laboratory flow studies on the zebrafish KV have shown that the most sensitive flow period is at 4-6 somite stages, with higher flow velocities on the anterior side of the KV (Sampaio et al., 2022). This suggests that the anterior cells may be the first to perceive the flow. However, the lack of spatial resolution in techniques used to evaluate dand5 expression has not allowed for a thorough analysis to investigate whether these anterior cells are the first in which dand5 transcript levels decrease.

In this thesis, we report the earliest KV asymmetry in *dand5* expression in zebrafish at 6 ss using smFISH. This is one hour earlier than previously reported, at 8 ss (Lopes et al., 2010), and has been established for more than a decade as the timing from which *dand5* levels on the left side are reduced in a flow-dependent manner (Sampaio et al., 2014). This discrepancy may be due to the limitations of standard *in situ* hybridization for resolving mRNA transcripts at the cellular level. Furthermore, the number of *dand5* mRNA transcripts on the left and right sides of the KV

over time has not been quantified because the traditional quantification mechanisms used for *dand5* expression lack spatial resolution, such as RT-qPCR (Jacinto, 2018; Jacinto et al., 2021) and RNA-seq (White et al., 2017). More relevant, we showed that a left-sided decrease in *dand5* mRNA levels primarily occurs in the anterior region of the KV, where flow velocities are the highest, as reported by Sampaio et al. (2022). This observation suggests that the left anterior cells are the ones that are most stimulated by the flow, and therefore where the machinery responsible for the dand5 mRNA decrease is initially activated. Our findings are consistent with the current understanding that molecular asymmetries originate in the anterior region of the KV, particularly on the left anterior side that experiences the most robust flow. For instance, Yuan et al., (2015) demonstrated that the onset of flow triggers Pkd2-dependent asymmetric ICOs in the anterior left quadrant of the KV at the 1-4 somite stages, resulting in secondary calcium waves in the surrounding mesendodermal cells. The cumulative effect of these calcium transients leads to a stable elevation of mesendodermal calcium in the left domain beyond the KV, which persists until 6-10 ss. Furthermore, Francescatto et al. (2010) reported that the activation of CaMKII in the left anterior KV cells reaches its peak between 10 and 12 ss, indicating that calcium fluxes triggered by ICOs could target CaMKII. Therefore, we propose that the left anterior quadrant of the KV, in a flow-dependent manner, determines a potential mRNA decay of *dand5* on the left anterior region of the KV.

Recent studies have shown that Bicc1 recognizes a specific sequence motif in the first 200 nucleotides of the 3'-UTR of *Dand5* mRNA (Minegishi et al., 2021b), and a segment of approximately 139 nucleotides in the proximal 3'-UTR of *dand5* in *Xenopus* LRO (Maerker et al., 2021b). In addition, evidence suggests that Dicer1, an endonuclease enzyme critical for the biosynthesis of microRNAs, and Pkd2 contribute to the left-sided decrease of *dand5* in mouse, Xenopus, and zebrafish (Maerker et al., 2021b). Mouse *Dicer* mutants and Xenopus *dicer1* morphants showed compromised left-sided downregulation of *dand5* mRNA levels during the post-flow stages. Similarly, no left-sided *dand5* decrease was observed in 10 ss *MZ dicer* mutants in zebrafish, suggesting a specific role for Dicer in *dand5* regulation.

In zebrafish, the specific interaction between Bicc1 and the 3'-UTR of *dand5* has not been characterized, and there is a lack of studies examining the nucleotide sequences required within the 3'-UTR of *dand5,* perhaps because there are no such consensus sequences as in mice. A study by Bouvrette et al., (2010) found *bicc1* expression at motile ciliated structures, such as the hindbrain and developing pronephric ducts, at 14 ss. Therefore, it is reasonable to expect that *bicc1* may also be expressed in the KV or DFCs at earlier stages. Additionally, studies have shown that the depletion of *bicc1* in zebrafish embryos results in the development of kidney cysts

(Bouvrette et al., 2010), a phenotype akin to the absence of Pkd2, a critical player in detecting directional flow in LR patterning. However, the *pkd2-bicc1-dicer* module appears to function similarly in mouse, *Xenopus*, and zebrafish (Maerker et al., 2021b). The exact mechanism by which these proteins cooperate to regulate miRNAs to mediate the left-sided decrease in *dand5* expression remains unclear. Furthermore, although conserved miR-133 binding sites in the *bicc1* 3'-UTR have been predicted to hybridize in human, mouse, and *Xenopus* sequences, this has not been the case in zebrafish. Dicer1 is an endoribonuclease that plays a critical role in the biosynthesis of miRNAs by cleaving long mRNA molecules into pre-miRNAs (Wienholds et al., 2003). In zebrafish, Dicer1 binds to the accessory protein TARBP2, although Dicer alone has been shown to have significant pre-miRNA processing activity (Li et al., 2019). Indeed, depletion of overall miRNA synthesis, such as in *MZdicer* mutants used in (Maerker et al., 2021b), can result in cumulative defects that may obscure the specific role of certain miRNAs. For example, miR-430 regulates both the agonist *squint* and antagonist *lefty2* of the Nodal signaling pathway in zebrafish, thereby contributing to the robustness and precision of endoderm and DFC specification (Choi et al., 2007). However, in *MZdicer*$^{-/-}$ embryos, where the overall miRNA synthesis is disrupted, the balancing effect of miR-430 is lost (Choi et al., 2007). Thus, targeted manipulation of Dicer expression or activity in the LRO and/or at specific time points could provide more insights into its role in the regulation of *dand5* expression and LR patterning in response to fluid flow.

Alternatively, Dicer may promote the decrease in *dand5* mRNA levels through miRNA-independent mechanisms, which have been described in the literature. For instance, in zebrafish, Dicer has been found to generate tRNA-derived fragments, which are small non-coding RNAs but are not highly expressed during development (Soares et al., 2015). Moreover, Dicer has been shown to be involved in transcriptional regulation and RNA processing by interacting with RNA polymerase II (RNAPII) and chromatin at multiple human loci (White et al., 2014). In Drosophila melanogaster, the absence of Dicer-2 alters the behavior of RNAPII in the promoter-proximal regions of several genes (Cernilogar et al., 2011). Additionally, Dicer regulates the alternative cleavage of polyadenylation (APA) in human cells, where nuclear Dicer-induced heterochromatin slows down RNAPII and promotes proximal cleavage of APA site recognition (Neve et al., 2016).

The synthesis of miRNAs involves the nuclear processing of primary transcripts (pri-miRNAs) by a complex of Drosha associated with Dgcr8 to form pre-miRNAs, which are then processed by Dicer in the cytoplasm (Li et al., 2019). Therefore, to determine whether miRNAs modulate the

decrease in *dand5* expression on the left side, it is necessary to assess *dand5* expression in the post-flow stages in embryos depleted of both Drosha and Dgcr8.

Currently, it is unclear whether the decrease in *dand5* expression on left-sided cells is due to mRNA destabilization or if it can be transcriptionally regulated. In *Xenopus*, it has been proposed that the timing of *dand5* asymmetry indicates that mere post-transcriptional mRNA decay may not be sufficient to reduce Dand5 protein levels (Maerker et al., 2021b), suggesting the involvement of additional mechanisms in repression. The asymmetry of *dand5* mRNA is most prominent during the late neurula stage when *nodal1* is already expressed in the left LPM (Schweickert et al., 2010). In zebrafish, our report of the establishment of *dand5* asymmetry as early as 6 ss is compatible with *dand5* mRNA decay, as *spaw* is first asymmetrically expressed in the LPM from 10-12 ss (Long et al., 2003). To test this hypothesis, we suggest the use of smFISH to generate probes of different colors labelling distinct segments within *dand5* mRNA molecules. This technique enables the differentiation of intact mRNAs from those that are partially degraded or broken (Tingey et al., 2022) and would provide insights into the dynamics of transcriptional repression versus post-transcriptional modifications of *dand5* on the left side of the KV.

Alternatively, the presence of nascent mRNAs, which indicates ongoing transcription, has not been evaluated in previous studies. Therefore, one approach to address this question is to design intronic *dand5* smFISH probes that hybridize to the only intron present in the genomic *dand5* sequence. By detecting nascent mRNAs, we can determine whether *dand5* expression is regulated at the mRNA level. These experiments will provide knowledge into the mechanism of *dand5* asymmetry and contribute to a better understanding of LR development.

Understanding the molecular mechanisms underlying the establishment of asymmetry in *dand5* expression is critical because this is the first known gene in which its asymmetric expression is dependent on cilia-driven asymmetric fluid flow. As *dand5* is initially expressed symmetrically, identifying the factors responsible for its asymmetric expression would allow us to narrow down the search for upstream players mediating the symmetry-breaking event. This, in turn, would provide valuable insights into the overall process of laterality determination in vertebrates.

References

Amack, J. D., Wang, X., and Yost, H. J. (2007). Two T-box genes play independent and cooperative roles to regulate morphogenesis of ciliated Kupffer's vesicle in zebrafish. Developmental biology 310, 196–210.

Bouvrette, D. J., Sittaramane, V., Heidel, J. R., Chandrasekhar, A., and Bryda, E. C. (2010). Knockdown of bicaudal C in zebrafish (Danio rerio) causes cystic kidneys: a nonmammalian model of polycystic kidney disease. Comparative medicine 60, 96–106.

Cernilogar, F. M., Onorati, M. C., Kothe, G. O., Burroughs, A. M., Parsi, K. M., Breiling, A., et al. (2011). Chromatin-associated RNA interference components contribute to transcriptional regulation in Drosophila. Nature 480, 391–395.

Choi, W.-Y., Giraldez, A. J., and Schier, A. F. (2007). Target protectors reveal dampening and balancing of Nodal agonist and antagonist by miR-430. Science 318, 271–274.

Coutelle, O., Blagden, C. S., Hampson, R., Halai, C., Rigby, P. W. J., and Hughes, S. M. (2001). Hedgehog signalling is required for maintenance of myf5 and myoD expression and timely terminal differentiation in zebrafish adaxial myogenesis. Developmental biology 236, 136–150.

Dal-Pra, S., Fürthauer, M., Van-Celst, J., Thisse, B., and Thisse, C. (2006). Noggin1 and Follistatin-like2 function redundantly to Chordin to antagonize BMP activity. Developmental biology 298, 514–526.

Das, D., Chatti, V., Emonet, T., and Holley, S. A. (2017). Patterned disordered cell motion ensures vertebral column symmetry. Developmental cell 42, 170–180.

Delaune, E. A., François, P., Shih, N. P., and Amacher, S. L. (2012). Single-cell-resolution imaging of the impact of Notch signaling and mitosis on segmentation clock dynamics. Developmental cell 23, 995–1005.

Essner, J. J., Amack, J. D., Nyholm, M. K., Harris, E. B., and Yost, H. J. (2005). Kupffer's vesicle is a ciliated organ of asymmetry in the zebrafish embryo that initiates left-right development of the brain, heart and gut. Development 132 (6), 1247–1260. doi: https://doi.org/10.1242/dev.01663.

Fior, R., Maxwell, A. A., Ma, T. P., Vezzaro, A., Moens, C. B., Amacher, S. L., et al. (2012). The differentiation and movement of presomitic mesoderm progenitor cells are controlled by Mesogenin 1. 4665, 4656–4665. doi: 10.1242/dev.078923.

Francescatto, L., Rothschild, S. C., Myers, A. L., and Tombes, R. M. (2010). The activation of membrane targeted CaMK-II in the zebrafish Kupffer's vesicle is required for left-right asymmetry. Development 137, 2753–2762.

Goto, H., Kimmey, S. C., Row, R. H., Matus, D. Q., and Martin, B. L. (2017). FGF and canonical Wnt signaling cooperate to induce paraxial mesoderm from tailbud neuromesodermal progenitors through regulation of a two-step epithelial to mesenchymal transition. Development 144, 1412–1424.

Gourronc, F., Ahmad, N., Nedza, N., Eggleston, T., and Rebagliati, M. (2007). Nodal activity around Kupffer's vesicle depends on the T-box transcription factors notail and spadetail and on

notch signaling. Developmental dynamics: an official publication of the American Association of Anatomists 236, 2131–2146.

Griffin, K. J. P., and Kimelman, D. (2002). One-Eyed Pinhead and Spadetail are essential for heart and somite formation. Nature Cell Biology 4, 821–825.

Grimes, D. T. (2019). Making and breaking symmetry in development, growth and disease. Development 146, dev170985.

Hashimoto, H., Rebagliati, M., Ahmad, N., Muraoka, O., Kurokawa, T., Hibi, M., et al. (2004). The Cerberus/Dan-family protein Charon is a negative regulator of Nodal signaling during left-right patterning in zebrafish. Development 131, 1741–1753. doi: 10.1242/dev.01070.

Holley, S. A., Geisler, R., and Nüsslein-Volhard, C. (2000). Control of her1 expression during zebrafish somitogenesis by a delta-dependent oscillator and an independent wave-front activity. Genes & development 14, 1678–1690.

Horikawa, K., Ishimatsu, K., Yoshimoto, E., Kondo, S., and Takeda, H. (2006). Noise-resistant and synchronized oscillation of the segmentation clock. Nature 441, 719–723.

Ikeda, T., Inamori, K., Kawanishi, T., and Takeda, H. (2022). Reemployment of Kupffer's vesicle cells into axial and paraxial mesoderm via transdifferentiation. Development, Growth & Differentiation 64, 163–177.

Jacinto, A. R. M. (2018). PKD2-dependent sensing mechanism in Kupffer's vesicle: how it affects the left-right axis establishment in zebrafish.

Jacinto, R., Sampaio, P., Roxo-Rosa, M., Pestana, S., and Lopes, S. S. (2021). Pkd2 affects cilia length and impacts LR flow dynamics and dand5. Frontiers in Cell and Developmental Biology 9, 624531.

Jiang, Y.-J., Aerne, B. L., Smithers, L., Haddon, C., Ish-Horowicz, D., and Lewis, J. (2000). Notch signalling and the synchronization of the somite segmentation clock. Nature 408, 475–479.

Katoh, T. A., Omori, T., Mizuno, K., Sai, X., Minegishi, K., Ikawa, Y., et al. (2023). Immotile cilia mechanically sense the direction of fluid flow for left-right determination. Science 379, 66–71. doi: 10.1126/science.abq8148.

Kawakami, Y., Raya, Á., Raya, R. M., Rodríguez-Esteban, C., and Belmonte, J. C. I. (2005). Retinoic acid signalling links left–right asymmetric patterning and bilaterally symmetric somitogenesis in the zebrafish embryo. Nature 435, 165–171. doi: 10.1038/nature03512.

Keskin, S., Devakanmalai, G. S., Kwon, S. Bin, Vu, H. T., Hong, Q., Lee, Y. Y., et al. (2018). Noise in the vertebrate segmentation clock is boosted by time delays but tamed by notch signaling. Cell reports 23, 2175–2185.

Lawton, A. K., Nandi, A., Stulberg, M. J., Dray, N., Sneddon, M. W., Pontius, W., et al. (2013). Regulated tissue fluidity steers zebrafish body elongation. Development 140, 573–582.

Lewis, J. (2003). Autoinhibition with Transcriptional Delay: A Simple Mechanism for the Zebrafish Somitogenesis Oscillator. Current Biology 13, 1398–1408. doi: https://doi.org/10.1016/S0960-9822(03)00534-7.

Lewis, J., Hanisch, A., and Holder, M. (2009). Notch signaling, the segmentation clock, and the patterning of vertebrate somites. Journal of biology 8, 1–7.

Li, P., Tian, Q., Hu, M., Li, W., Zhang, X., and Zeng, Y. (2019). Cloning, expression, and characterization of the zebrafish Dicer and Drosha enzymes. Biochemical and Biophysical Research Communications 514, 200–204. doi: https://doi.org/10.1016/j.bbrc.2019.04.122.

Long, S., Ahmad, N., and Rebagliati, M. (2003). The zebrafish nodal-related gene southpaw is required for visceral and diencephalic left-right asymmetry. Development 130, 2303–2316.

Lopes, S. S., Lourenco, R., Pacheco, L., Moreno, N., Kreiling, J., and Saude, L. (2010). Notch signalling regulates left-right asymmetry through ciliary length control. Development 137, 3625–3632. doi: 10.1242/dev.054452.

Maerker, M., Getwan, M., Dowdle, M. E., McSheene, J. C., Gonzalez, V., Pelliccia, J. L., et al. (2021). Bicc1 and Dicer regulate left-right patterning through post-transcriptional control of the Nodal inhibitor Dand5. Nature Communications 12, 5482. doi: 10.1038/s41467-021-25464-z.

Manning, A. J., and Kimelman, D. (2015). Tbx16 and Msgn1 are required to establish directional cell migration of zebra fi sh mesodermal progenitors. Developmental Biology 406, 172–185. doi: 10.1016/j.ydbio.2015.09.001.

Marques, S., Borges, A. C., Silva, A. C., Freitas, S., Cordenonsi, M., and Belo, J. A. (2004). The activity of the Nodal antagonist Cerl-2 in the mouse node is required for correct L/R body axis. Genes & development 18, 2342–2347.

Minegishi, K., Rothé, B., Komatsu, K. R., Ono, H., Ikawa, Y., Nishimura, H., et al. (2021). Fluid flow-induced left-right asymmetric decay of Dand5 mRNA in the mouse embryo requires a Bicc1-Ccr4 RNA degradation complex. Nature Communications 12, 4071. doi: 10.1038/s41467-021-24295-2.

Montague, T. G., Gagnon, J. A., and Schier, A. F. (2018). Conserved regulation of Nodal-mediated left-right patterning in zebrafish and mouse. Development 145, dev171090.

Naganathan, S. R., Popović, M., and Oates, A. C. (2022). Left–right symmetry of zebrafish embryos requires somite surface tension. Nature 605, 516–521.

Nakamura, T., Saito, D., Kawasumi, A., Shinohara, K., Asai, Y., Takaoka, K., et al. (2012). Fluid flow and interlinked feedback loops establish left–right asymmetric decay of Cerl2 mRNA. Nature communications 3, 1322.

Narayanan, R., Mendieta-Serrano, M. A., and Saunders, T. E. (2021). The role of cellular active stresses in shaping the zebrafish body axis. Current Opinion in Cell Biology 73, 69–77. doi: https://doi.org/10.1016/j.ceb.2021.06.002.

Neve, J., Burger, K., Li, W., Hoque, M., Patel, R., Tian, B., et al. (2016). Subcellular RNA profiling links splicing and nuclear DICER1 to alternative cleavage and polyadenylation. Genome research 26, 24–35.

O'Neill, K., and Thorpe, C. (2013). BMP signaling and spadetail regulate exit of muscle precursors from the zebrafish tailbud. Developmental biology 375, 117–127.

Osborn, D. P. S., Li, K., Cutty, S. J., Nelson, A. C., Wardle, F. C., Hinits, Y., et al. (2020). Fgf-driven Tbx protein activities directly induce myf5 and myod to initiate zebrafish myogenesis. Development 147, dev184689. doi: 10.1242/dev.184689.

Sampaio, P., Ferreira, R. R., Guerrero, A., Pintado, P., Tavares, B., Amaro, J., et al. (2014). Left-right organizer flow dynamics: how much cilia activity reliably yields laterality? Developmental cell 29, 716–728.

Sampaio, P., Pestana, S., Guerrero, A., Telley, I. A., Smith, D. J., and Lopes, S. S. (2022). Fluid extraction from the left-right organizer uncovers mechanical properties needed for symmetry breaking. bioRxiv, 2004–2022.

Sanematsu, P. C., Erdemci-Tandogan, G., Patel, H., Retzlaff, E. M., Amack, J. D., and Manning, M. L. (2021). 3D viscoelastic drag forces contribute to cell shape changes during organogenesis in the zebrafish embryo. Cells & Development 168, 203718. doi: https://doi.org/10.1016/j.cdev.2021.203718.

Schweickert, A., Vick, P., Getwan, M., Weber, T., Schneider, I., Eberhardt, M., et al. (2010). The nodal inhibitor Coco is a critical target of leftward flow in Xenopus. Current Biology 20, 738–743.

Soares, A. R., Fernandes, N., Reverendo, M., Araújo, H. R., Oliveira, J. L., Moura, G. M. R., et al. (2015). Conserved and highly expressed tRNA derived fragments in zebrafish. BMC molecular biology 16, 1–16.

Tingey, M., Schnell, S. J., Yu, W., Saredy, J., Junod, S., Patel, D., et al. (2022). Technologies Enabling Single-Molecule Super-Resolution Imaging of mRNA. Cells 11, 3079.

Vermot, J., and Pourquié, O. (2005). Retinoic acid coordinates somitogenesis and left–right patterning in vertebrate embryos. Nature 435, 215–220.

Von Der Hardt, S., Bakkers, J., Inbal, A., Carvalho, L., Solnica-Krezel, L., Heisenberg, C.-P., et al. (2007). The Bmp gradient of the zebrafish gastrula guides migrating lateral cells by regulating cell-cell adhesion. Current Biology 17, 475–487.

Weinberg, E. S., Allende, M. L., Kelly, C. S., Abdelhamid, A., Murakami, T., Andermann, P., et al. (1996). Developmental regulation of zebrafish MyoD in wild-type, no tail and spadetail embryos. Development 122, 271–280. doi: 10.1242/dev.122.1.271.

White, E., Schlackow, M., Kamieniarz-Gdula, K., Proudfoot, N. J., and Gullerova, M. (2014). Human nuclear Dicer restricts the deleterious accumulation of endogenous double-stranded RNA. Nature structural & molecular biology 21, 552–559.

White, R. J., Collins, J. E., Sealy, I. M., Wali, N., Dooley, C. M., Digby, Z., et al. (2017). A high-resolution mRNA expression time course of embryonic development in zebrafish. eLife, 1–32.

Wienholds, E., Koudijs, M. J., van Eeden, F. J. M., Cuppen, E., and Plasterk, R. H. A. (2003). The microRNA-producing enzyme Dicer1 is essential for zebrafish development. Nature genetics 35, 217–218.

Woo, S., Housley, M. P., Weiner, O. D., and Stainier, D. Y. R. (2012). Nodal signaling regulates endodermal cell motility and actin dynamics via Rac1 and Prex1. Journal of Cell Biology 198, 941–952. doi: 10.1083/jcb.201203012.

Yabe, T., and Takada, S. (2012). Mesogenin causes embryonic mesoderm progenitors to differentiate during development of zebrafish tail somites. Developmental Biology 370, 213–222. doi: 10.1016/j.ydbio.2012.07.029.

Yuan, S., Zhao, L., Brueckner, M., and Sun, Z. (2015). Intraciliary calcium oscillations initiate vertebrate left-right asymmetry. Current biology 25, 556–567.